
Electronic Thesis and Dissertation Repository

4-19-2011 12:00 AM

Fabrication, Modification and Application of Visible Light Responsive TiO₂ Nanotubes

Tayirjan Taylor Isimjan, *The University of Western Ontario*

Supervisor: Dr.Ajay Ray, *The University of Western Ontario*

Joint Supervisor: Dr.Rohani, *The University of Western Ontario*

A thesis submitted in partial fulfillment of the requirements for the Doctor of Philosophy degree in Chemical and Biochemical Engineering

© Tayirjan Taylor Isimjan 2011

Follow this and additional works at: <https://ir.lib.uwo.ca/etd>

 Part of the [Other Chemical Engineering Commons](#)

Recommended Citation

Isimjan, Tayirjan Taylor, "Fabrication, Modification and Application of Visible Light Responsive TiO₂ Nanotubes" (2011). *Electronic Thesis and Dissertation Repository*. 146.
<https://ir.lib.uwo.ca/etd/146>

This Dissertation/Thesis is brought to you for free and open access by Scholarship@Western. It has been accepted for inclusion in Electronic Thesis and Dissertation Repository by an authorized administrator of Scholarship@Western. For more information, please contact wlsadmin@uwo.ca.

Fabrication, Modification and Application of Visible Light Responsive TiO₂ Nanotubes

(Spine title: Visible Light Responsive TiO₂ Nanotubes)

(Thesis format: Integrated-Article)

By

Tayirjan T. Isimjan

Graduate Program in Engineering Science
Department of Chemical and Biochemical Engineering

A thesis submitted in partial fulfillment of
the requirements for the degree of Doctor of Philosophy

School of Graduate and Postdoctoral Studies
The University of Western Ontario
London, Ontario, Canada

© Tayirjan T. Isimjan 2011

THE UNIVERSITY OF WESTERN ONTARIO
SCHOOL OF GRADUATE AND POSTDOCTORAL STUDIES

CERTIFICATE OF EXAMINATION

Supervisors

Dr. Ajay Ray

Dr. Sohrab Rohani

Examiners

Dr. Cynthia M. Goh

Dr. Shahzad Barghi

Dr. Hugo de Lasa

Dr. Mahi Singh

The thesis by

Tayirjan T. Isimjan

entitled:

Fabrication, Modification and Application of TiO₂ Nanotubes

is accepted in partial fulfillment of the
requirements for the degree of
Doctor of Philosophy

Date 2011 April 19

Pauline Barmby
Chair of the Thesis Examination Board

Abstract

The highly ordered TiO₂ nanotube arrays have demonstrated remarkable properties that include solar cells, hydrogen sensors, drug eluting surfaces, hydrogen generation, and water purification along with numerous other applications. Built upon a suitable fabrication approach that enable significant differences in reproducibility as well as the large scale production with low cost plus investigation of the effective way to increase its visible light response so that create environmental friendly alternative energy sources were the motivations of this work, Since the field has grown so rapidly as to make it difficult to summarize the scope of all related work, some key aspects on this field have been discussed and then mainly focus on the work that has been done during my Ph.D study. This Ph.D work focuses on the most challenging issues: 1) improves the tune quality of highly ordered TiO₂ nanotubes by reproducible manner as well as reduces the cost of fabrication. 2) Investigates the different methods of modification in order to increase photo response of the materials in visible light region. 3) Explore the surface superhydrophobic property of fluorinated TiO₂ nanotubes layer. Following progresses have been made towards the target.

An innovative technique of sonication assisted fabrication of highly ordered TiO₂ nanotubes in reproducible manner was proposed and the expensive platinum cathode was replaced by titanium by which the fabrication cost was reduced.

A one-step method for the fabrication of Fe–C–N-codoped TiO₂ nanotubes by electrochemical anodization is reported. A maximum photocurrent efficiency of 2.7% was achieved.

Highly ordered nitrogen-doped titanium dioxide (N-doped TiO₂) nanotube array films with enhanced photo conversion efficiency were reported and the conditions were optimized. The optimized experiment resulted in 7.42% PCE which was within 95% confidence interval of the predicted value by the model.

The structural and photo catalytic properties of Pt/ZIF-8 loaded TiO₂ nanotubes (TiO₂ NTs) are investigated and compared to Pt/TiO₂ NTs. The Pt/ZIF-8 loaded TiO₂ NTs has shown 18.6% oxidation towards phenol in 2 hours under visible light.

Finally, a simple process of tailoring the surface wettability of TiO₂ nanotube array surface was proposed by which any desirable degree of hydrophobicity between 100° to 170° can be achieved.

Key words: Highly ordered TiO₂ nanotubes, Anodization, Annealing, Ti cathode, Photoelectrochemical water splitting efficiency for hydrogen generation, Doping, Loading, photodegradation efficiency, superhydrophobic surface, self-assembly.

Co-Authorship

Chapter 3: A version of this chapter was published as: Tayirjan T. Isimjan, D.-Q Yang, Sohrab Rohani and Ajay K. Ray. An Innovative Approach to Synthesize Highly-Ordered TiO₂ Nanotubes Journal of Nanoscience and Nanotechnology 2011, 11: 1079-1083.

Chapter 4: A paper based on the chapter has been submitted to the following journal: International journal of hydrogen energy as: Tayirjan T. Isimjan, Sohrab Rohani and Ajay K. Ray. Fabrication of Highly Ordered and Efficient TiO₂ Nanotubes by Using Ti as Cathode.

Chapter 5: A version of this chapter was published as: Tayirjan T. Isimjan, Ahmed E. Ruby, Sohrab Rohani, and Ajay K. Ray. Fabrication of highly-ordered and visible-light responsive Fe-C-N-codoped TiO₂ nanotubes. Nanotechnology 2010, 21: 055706.

Chapter 6: A paper based on the chapter will be submitted to a journal as: Tayirjan T. Isimjan, Milana Trifkovic, Ajay K Ray and Sohrab Rohani. Optimization of Photoelectrochemical Water Splitting Efficiency for Hydrogen Generation of N-doped TiO₂ Nanotubes.

Chapter 7: A version of this chapter was published as: Tayirjan T. Isimjan, Hossein Kazemian, Sohrab Rohani and Ajay K. Ray. Photocatalytic activities of Pt/ZIF-8 loaded highly ordered TiO₂ nanotubes. Journal of Material Chemistry 2010, 20: 10241-10245.

Chapter 8: A paper based on the chapter has been submitted to Material Science and Engineering A as: Tayirjan. T. Isimjan, Zhu Yan, D.-Q Yang, Sohrab Rohani, Ajay K. Ray. A new approach of tailoring wetting properties of TiO₂ nanotubular surfaces.

To

My Parents (Ismayil Talip and Hanzohra Keyum), my wife (Karima Matniyaz) and my three little angles (Tumaris, Tungnur and Totiya)

Acknowledgments

It is a pleasure to thank to my supervisors Dr. Sohrab Rohani and Dr. Ajay Ray who made this work possible. Special thanks must go to their recommendations and endless help throughout this study.

I am also grateful to technical staffs, Fate Hashem, Christ Vandilar, Brian Dennis and Souheil Afara for their technical support.

Special thanks to Dr. Hossein Kazemian, Dr. Milana Trifkovic, Dr. Derry Yung, Dr. Shahzad Barghi, Dr. Paul Charpentier, Dr. Jose Herrera, Dr. Kibret Mequaninit, Dr. Lars, Rahmanm, Dr. Madhumita Ray and Dr. Feng Zhou Zhang for their help and constructive advises during my PhD studies at Western. Special thanks also go to my dear friend Gordon Black for his support on the manuscript preparations and encouragements.

I also enjoyed working with my colleagues in both Dr. Rohani and Dr. Ajay Ray's lab.

My deepest appreciation and sincere gratitude are extended to my wife, my daughters and my relatives for their unconditional love and support. Without them, I would have never been able to reach this point.

Thanks for Heavenly Father to all his blessing and the things that he has given to me which I did not deserve. He has kept my mind free from worry and filled it with love and joy. He has protected me and my family on his mighty hand. He is always with me every step along the way so that I can always fill his existence. With him everything is possible and everything works for good. All the glories belong to him.

Table of Contents

Title page.....	i
Certificate of Examination.....	ii
Abstract.....	iii
Co-authorship.....	v
Acknowledgments.....	vi
Table of Contents.....	vii
List of Tables	xv
List of Figures.....	xvii
List of Abbreviations and Symbols.....	xxiii
Chapter 1: Introduction.....	1
1.1 Objective of the Chapter.....	2
1.2 Fabrication Methods of TiO ₂ nanotubes.....	2
1.3 Challenges.....	3
1.4 Research Objectives.....	4
1.5 Approach and Methodology.....	5
1.6 Thesis Organization.....	6
1.7 Major Contributions.....	8
1.8 References.....	11
Chapter 2: Literature Review.....	12
1.1 Introduction.....	13

2.2 Fabrication of highly ordered TiO ₂ nanotubes.....	14
2.3 Modification of highly ordered TiO ₂ nanotubes.....	15
2.3.1 Doping.....	16
2.3.1.1 Metal doping.....	18
2.3.1.2 Non-metal doping.....	21
2.3.2 Sensitization.....	23
2.3.2.1 Inorganic Sensitization.....	24
2.3.2.2 Organic Sensitization	25
2.3.2.3 Dye Sensitization.....	26
2.3.2.3.1 Organic dye sensitization.....	26
2.3.2.3.2 Conjugated polymer sensitization.....	30
2.4 Photo-electrochemical properties.....	33
2.5 Efficiency measurement.....	38
2.5.1 Photo conversion efficiency (PCE).....	38
2.5.2 Quantum efficiency (IPCE).....	40
2.5.3 Absorbed photo to current conversion efficiency (APCE).....	41
2.6 Application.....	41
2.6.1 Solar cell.....	41
2.6.2 Solid-state dye sensitized solar cells.....	43
2.6.3 Water splitting.....	43
2.6.4 Degradation of Organics.....	44
2.7 References.....	46
Chapter 3: An Innovative Approach to Synthesize Highly-Ordered TiO ₂ Nanotubes.....	55
3.1 Abstract.....	56

3.2 Introduction.....	57
3.3 Experimental.....	59
3.4 Results and Discussion.....	60
3.4.1 Surface analysis.....	61
3.4.2 XRD result and thickness analysis.....	64
3.5 Conclusions.....	67
3.6 References.....	68
Chapter 4: Fabrication of Highly Ordered and Efficient TiO ₂ Nanotubes by Using Ti as Cathode.....	
4.1 Abstract.....	71
4.2 Introduction.....	72
4.3 Material and methods.....	74
4.4 Results and discussion.....	75
4.4.1 Potentiostatic current transients and oxide film formation.....	75
4.4.2 SEM images.....	76
4.4.3 Roughness factor.....	77
4.4.4 XRD pattern.....	80
4.4.5 Photoelectrochemical water splitting efficiency (PCE).....	81
4.5 Conclusions.....	83
4.6 References.....	84
Chapter 5: Fabrication of highly-ordered and visible-light responsive Fe-C-N-codoped TiO ₂ nanotubes.....	
5.1 Abstract.....	87
5.2 Introduction.....	88

5.3 Experimental.....	90
5.3.1 Preparation of TiO ₂ nanotubes.....	90
5.3.2 Photoelectrochemical characterization.....	92
5.4 Results and discussion.....	93
5.4.1 FE-SEM images of TiO ₂ nanotubes.....	93
5.4.2 UV-vis and XRD results.....	94
5.4.3 XPS and EDX results.....	96
5.4.4 Photo conversion efficiency.....	99
5.5 Conclusions.....	101
5.6 References.....	103
Chapter 6: Optimization of Photoelectrochemical Water Splitting Efficiency for	
Hydrogen Generation of N-doped TiO ₂ Nanotubes.....	
6.1 Abstract.....	106
6.2 Introduction.....	107
6.3 Experimental.....	111
6.3.1 Preparation of TiO ₂ nanotubes.....	111
6.3.2 N-doping.....	111
6.3.3 Analytical methods.....	112
6.4 Design of Experiment (DOE).....	113
6.5 Results and Discussion.....	114
6.5.1 Preparation and Characterization.....	114
6.5.1.1 SEM images.....	114
6.5.1.2 XPD patterns.....	115
6.5.1.3 Photoelectrochemical water splitting efficiency (PCE).....	116

6.5.1.4 XPS results.....	119
6.5.1.5 UV-vis results.....	121
6.5.2 Design of Experiment and Optimization.....	122
6.5.2.1 Design of Experiment (DOE).....	122
6.5.2.2 Optimization.....	126
6.6 Conclusions.....	127
6.7 References.....	128
Chapter 7: Photocatalytic Activities of Pt/ZIF-8 loaded Highly Ordered TiO ₂	
Nanotubes.....	131
7.1 Abstract.....	132
7.2 Introduction.....	133
7.3 Experimental.....	135
7.3.1 Preparation of TiO ₂ nanotubes.....	135
7.3.2 Preparation of ZIF-8 loaded TiO ₂ nanotubes.....	136
7.3.3 Pt deposition.....	137
7.3.4 Photo degradation.....	138
7.3.5 Analytical methods.....	138
7.4 Results and Discussion.....	139
7.5 Conclusions.....	146
7.6 References.....	148
Chapter 8: A New Approach of Tailoring Wetting Properties of TiO ₂ Nanotubular	
Surfaces.....	151
8.1 Abstract.....	152
8.2 Introduction.....	153

8.3 Materials and methods.....	154
8.4 Results and Discussion.....	156
8.4.1 XRD Results.....	156
8.4.2 SEM Results.....	157
8.4.3 XPS Results.....	159
8.4.4 Contact angle.....	162
8.5 Conclusions.....	166
8.6 References.....	167
Chapter 9: Conclusions and Recommendations.....	169
9.1 Fabrication of highly ordered TiO ₂ nanotubes.....	170
9.1.1 Conclusions.....	170
9.1.2 Limitations.....	171
9.1.3 Further Work.....	172
9.2 Modification of highly ordered TiO ₂ nanotubes.....	172
9.2.1 Conclusions.....	173
9.2.1.1 Fe-C-N codoped TiO ₂ nanotubes.....	173
9.2.1.2 PCE optimization of N-doped TiO ₂ nanotubes.....	173
9.2.1.3 Pt/ZIF-8-loaded TiO ₂ nanotubes composite.....	173
9.2.2 Limitations.....	174
9.2.3 Future work.....	174
9.3 Application of TiO ₂ nanotubes	175
9.3.1 Conclusions.....	175
9.3.2 Limitations.....	176

9.3.3 Future works.....	176
Appendices.....	177
Appendix A for Chapter 3.....	178
Appendix B for Chapter 4.....	184
Appendix C for chapter 6.....	189
Appendix D for chapter 7.....	197
Appendix E for copy rights permission of figures used.....	205
Curriculum Vitae.....	226

List of Figures

Figure 1-1: Two-electrode electrochemical cell in which the Ti samples are anodize.....	3
Figure 1-4: Outline of the research in the thesis.....	8
Figure 2-1: Figure 2-1: Results of the first-step anodization: (a) the SEM image of the Ti surface outside the anodization region (inset is the EDX); (b) the Ti surface after the removal of the nanotube layer (inset is the EDX); (c) the SEM image of the nanotube layer generated in the first-step anodization (inset was obtained when the sample was titled by 45° from the incident electron beam); (d) the bottom side of the nanotube layer that shed from the Ti foil; (e) the Ti foil surface exposed after the ultrasonic removal of a nanotube layer fabricated with an insufficiently aged electrolyte.....	14
Figure 2-2: Schematic for self-organized regular arrays of anodic TiO ₂ nanotubes.....	15
Figure 2-3: Schematic diagram to illustrate the photoexcitation process under visible light of metal-doped TiO ₂ : (a) Ti _{1-x} V _x O ₂ ; (b) Ti _{1-x} Fe _x O ₂ ; (c) Ti _{1-x} Cr _x O ₂	17
Figure 2-4: Structure of N3.....	27
Figure 2-5: Structure of chlorophyll-c1.....	28
Figure 2-6: Cyanidin-3-glucoside.....	29
Figure 2-7: Porphyrin dye.....	29
Figure 2-8: Chemical structure of the repeating units of HTM polymers.....	32
Figure 2-9: The different reactions accruing in the TiO ₂ /dye surface.....	33
Figure 2-10: Structure of the porphyrin sensitizers.....	36
Figure 2-11: Branched A and B approaches to chromophore antenna system.....	36

Figure 2-12: m-ZnTCPP on the surface of TiO ₂ or ZnO.....	38
Figure 2-13: Set-up for PCE measurement.....	40
Figure 2-14: Homemade photocell for hydrogen generation under sunlight. (1) TiO ₂ nanotube arrays anode, (2) Pt wire spiral cathode, (3) gas burette, (4) multimeter for voltage, (5) multimeter for current, (6) focus lens, (7) battery, (8) voltage adjust button.....	44
Figure 2-15: The photoactivation mechanism of TiO ₂	45
Figure 3-1: Removal of the nanowires layer by sonication and fabrication of highly-ordered titanium nanotube arrays.....	61
Figure 3-2: FE SEM images of the surfaces of Ti samples anodized in glycerol - 5% water - 3% NH ₄ F solution at 30V at 4 hrs. (a) top view of as-prepared, (b) cross-section of as-prepared, (c) top view of annealed and sonicated, (d) cross-section of annealed and sonicated, and (e) higher magnification of top view of annealed and sonicated sample...	62
Figure 3-3: XRD pattern for samples from different treatments.....	64
Figure 3-4: The wall thickness and diameter of TiO ₂ nanotubes as a function of the preparation time.....	65
Figure 3-5: The thickness of TiO ₂ layers as a function of preparation time.....	66
Figure 4-1: Current-time response of Ti samples anodized using Ti cathodes in ethylene glycol electrolytes for 3 hours, 1cm distance between anode and cathode: (a) voltage vs. time(b) current vs. time.....	76

Figure 4-2: SEM images of TiO ₂ nanotubes fabricated under condition of 1cm between cathode and anode, 20 V constant voltage and 3 h anodization time. a) before sonication, b) after sonication, c) larger magnitude image and d) cross-section.....	77
Figure 4-3: XRD results of TiO ₂ nanotubes fabricated under the condition of 1cm between cathode and anode, 40 V constant voltage and 3 hour anodization.....	80
Figure 4-4: Photo conversion efficiency (PCE) under UV illumination of a photoelectrochemical cell comprised of a TiO ₂ nanotubes array photoanode, Ag/AgCl as reference and Pt counter electrode. (a) Photocurrent vs. external voltage (b) Photo conversion efficiency vs. external voltage.....	82
Figure 5-1: SEM images of Fe-C-N-codoped TiO ₂ nanotubes.....	94
Figure 5-2: UV-vis of TiO ₂ nanotubes.....	95
Figure 5-3: XRD patterns of TiO ₂ nanotubes.....	96
Figure 5-4: XPS results of Fe-C-N codoped TiO ₂ nanotubes.....	97
Figure 5-5: EDX results of TiO ₂ nanotubes: a) Fe-C-N-codoped and b) un-doped.....	99
Figure 5-6: Photo current and photocurrent efficiency diagrams of TiO ₂ nanotubes. a) photo current b) photo conversion efficiency.....	101
Figure 6-1: SEM images of the TiO ₂ nanotube surfaces a) Before N-doping, b) N-doping at 350oC for 6h c) N-doping at 600oC for 6h.....	115
Figure 6-2: XRD patterns of N-doped TiO ₂ nanotubes.....	116
Figure 6-3: Photo current and photoelectron conversion efficiency as a function of measured potential bias vs/AgCl reference electrode of N-doped TiO ₂ nanotubes arrays under optimized condition.....	117

Figure 6-4: High-resolution XPS spectra of optimized sample: a) N 1s, b) O 1s region and c) Ti2p	119
Figure 6-5: UV-vis spectrum of TiO ₂ nanotubes and Optimized sample.....	121
Figure 6-6: Accuracy of the model prediction.....	124
Figure 6-7: Effect of Rate of heating and Temperature on response (Time=3.95h).....	124
Figure 6-8: Effect of Time and Temperature on response (Heating rate=20°C/h).....	125
Figure 6-9: Optimization results (Time=2h).....	127
Figure 7-1: (a) The single crystal of X-ray structure of ZIF-8: ZnN ₄ is shown in blue polyhedra, and the links in ball-and-stick presentation. The yellow ball indicates space in the cage. H atoms are omitted for clarity (C, black; N, green). (b) ORTEP diagram of the asymmetric unit of the ZIF-8 framework.....	134
Figure 7-2: Top view SEM micrograph : (a) unloaded TiO ₂ nanotubes. (b) Pt/ZIF-8 loaded TiO ₂ nanotubes. (c) larger magnitude of Pt/ZIF-8 loaded TiO ₂ nanotubes. (d) EDX results of Pt/ZIF-8 loaded TiO ₂ nanotubes.....	140
Figure 7-3: XRD results of Pt/TiO ₂ NTs, Pt/ZIF-8 loaded TiO ₂ nanotubes and ZIF-8...141	141
Figure 7-4: UV absorption spectra of Pt/ZIF loaded TiO ₂ nanotubes and Pt/TiO ₂ nanotubes.....	142
Figure 7-5: Band gap measurement of Pt/ZIF loaded TiO ₂ nanotubes and Pt/TiO ₂ nanotubes.....	143
Figure 7-6: Schematic illustration of photo oxidation mechanism of Pt promoted TiO ₂ semiconductors.....	144

Figure 7-7: Photo degradation of Pt/ZIF loaded TiO ₂ nanotubes, Pt/TiO ₂ nanotubes and control.....	146
Figure 8-1: XRD patterns for TiO ₂ nanotubes surface at 25°C and after annealing for 3hours at 550°C.....	157
Figure 8-2: SEM images of TiO ₂ nanotubes surfaces, tube length and water contact angle after different anodization time: a) 0 hour, b) 0.5 hour, c) 1.0 hour, d) 1.5 hour, e) 3.0 hours, f) 5.0 hours, g) 7.0 hours, h) 20 hours.....	158
Figure 8-3: The cross-section of TiO ₂ nanotubes surface as a function of the anodization time.....	159
Figure 8-4: XPS results of PTES functionalized TiO ₂ nanotubes surface, a) wide-scan spectrum, b) C 1s spectrum, c) F 1s spectrum, d) Ti 2p spectrum.....	160
Figure 8-5: Fluorine content of super hydrophobic TiO ₂ nanotubes surfaces versus different annealing times.....	161
Figure 8-6: Water contact angles measured of the TiO ₂ nanotubes surface after modification with PTES advancing (circles), static (squares), receding (triangles) and slide (black squares) water contact angles are plotted as a function of the anodization time of Ti foil in ethylene glycol solution.....	162
Figure 8-7: Wetting states of TiO ₂ layers: (a) Wenzler (b) Cassie-Baxter (c) Combined.....	163
Figure A-1: FE SEM images of the surfaces of Ti samples anodized in glycerol - 5% water - 3% NH ₄ F solution at 30V at 3 hrs. (a) top view of as-prepared, (b) cross-section	

of as-prepared, (c) top view of annealed and sonicated, (d) cross-section of annealed and sonicated, and (e) lower magnification of top view of annealed and sonicated sample.. 178

Figure A-2: FE SEM images of the surfaces of Ti samples anodized in glycerol - 5% water - 3% NH₄F solution at 30V at 5 hrs. (a) top view of as-prepared, (b) cross-section of as-prepared, (c) top view of annealed and sonicated, (d) cross-section of annealed and sonicated, and (e) lower magnification of top view of annealed and sonicated sample.....179

Figure A-3: FE SEM images of the surfaces of Ti samples anodized in glycerol - 5% water - 3% NH₄F solution at 30V at 6 hrs. (a) top view of as-prepared, (b) cross-section of as-prepared, (c) top view of annealed and sonicated, (d) cross-section of annealed and sonicated, and (e) lower magnification of top view of annealed and sonicated sample.....180

Figure A-4: FE SEM images of the surfaces of Ti samples anodized in glycerol - 5% water - 3% NH₄F solution at 30V at 7 hrs. (a) top view of as-prepared, (b) cross-section of as-prepared, (c) top view of annealed and sonicated, (d) cross-section of annealed and sonicated, and (e) lower magnification of top view of annealed and sonicated sample..181

Figure A-5: FE SEM images of the surfaces of Ti samples anodized in glycerol - 5% water - 3% NH₄F solution at 30V at 13 hrs. (a) top view of as-prepared, (b) cross-section of as-prepared, (c) top view of annealed and sonicated, (d) cross-section of annealed and sonicated, and (e) Lower magnification of top view of annealed and sonicated sample.....182

Figure A-6: FE SEM images of the surfaces of Ti samples anodized in glycerol - 5% water - 3% NH₄F solution at 30V at 20 hrs. (a) top view of as-prepared, (b) cross-section

of as-prepared, (c) top view of annealed and sonicated, (d) cross-section of annealed and sonicated, and (e) lower magnification of top view of annealed and sonicated sample.. 183

Figure B-1: SEM images of TiO₂ nanotubes fabricated under condition of 1cm between cathode and anode, 20 V constant voltage and 3 h anodization time. (a) top view of lower magnitude image (b) top view of higher magnitude image (c) cross-section..... 184

Figure B-2: SEM images of TiO₂ nanotubes fabricated under condition of 1cm between cathode and anode, 30 V constant voltage and 3 h anodization time. (a) top view of lower magnitude image (b) top view of higher magnitude image (c) cross-section..... 185

Figure B-3: SEM images of TiO₂ nanotubes fabricated under condition of 1cm between cathode and anode, 40 V constant voltage and 3 h anodization time. (a) top view of lower magnitude image (b) top view of higher magnitude image (c) cross-section..... 185

Figure B-4: SEM images of TiO₂ nanotubes fabricated under condition of 2cm between cathode and anode, 20 V constant voltage and 3 h anodization time (a) top view of lower magnitude image (b) top view of higher magnitude image (c) cross-section..... 186

Figure B-5: FE SEM images of the surfaces of Ti samples anodized in glycerol - 5% water - 3% NH₄F solution at 30V at 13 hrs. (a) top view of as-prepared, (b) cross-section of as-prepared, (c) top view of annealed and sonicated, (d) cross-section of annealed and sonicated, and (e) lower magnification of top view of annealed and sonicated sample.. 186

Figure B-6: SEM images of TiO₂ nanotubes fabricated under condition of 2cm between cathode and anode, 40 V constant voltage and 3 h anodization time (a) top view of lower magnitude image (b) top view of higher magnitude image (c) cross-section..... 187

Figure B-7: SEM images of TiO ₂ nanotubes fabricated under condition of 3cm between cathode and anode, 20 V constant voltage and 3 h anodization time (a) top view of lower magnitude image (b) top view of higher magnitude image (c) cross-section.....	187
Figure B-8: SEM images of TiO ₂ nanotubes fabricated under condition of 3cm between cathode and anode, 30 V constant voltage and 3 h anodization time (a) top view of lower magnitude image (b) top view of higher magnitude image (c) cross-section.....	188
Figure B-9: SEM images of TiO ₂ nanotubes fabricated under condition of 3cm between cathode and anode, 40 V constant voltage and 3 h anodization time (a) top view of lower magnitude image (b) top view of higher magnitude image (c) cross-section.....	188
Figure C 1: UV-vis of sample 2.....	189
Figure C 2: UV-vis of sample 3.....	189
Figure C 3: UV-vis of sample 4.....	190
Figure C 4: UV-vis of sample 5.....	190
Figure C 5: UV-vis of sample 6.....	191
Figure C 6: UV-vis of sample 7.....	191
Figure C 7: UV-vis of sample 8.....	192
Figure C 8: UV-vis of sample 9.....	192
Figure C 9: UV-vis of sample 10.....	193
Figure C 10: UV-vis of sample 11.....	193
Figure C 11: UV-vis of sample 12.....	194
Figure C 12: UV-vis of sample 13.....	194
Figure C 13: UV-vis of sample 14.....	195
Figure C 14 UV-vis of sample 15.....	195

Figure C 15 UV-vis of sample 16.....	196
Figure D 1: Synthesis of ZIF-8 Nanocrystals Capped with Neutral 2-Methylimidazole.....	197
Figure D 2: Cross section of the set-up used for photocatalytic tests: (1) Solar simulator; (2) Black box; (3) Reactor ; (4) Sample holder; (5) Stirrer bar; (6) Sample.....	198
Figure D 3: SEM micrographs of TiO ₂ nanotubes samples: (a) Cross-section of unloaded TiO ₂ nanotubes, (b) top view of unloaded TiO ₂ nanotubes at larger magnitude, (c) pore size and wall thickness of unloaded TiO ₂ nanotubes, (d) Pt/ZIF-8 loaded TiO ₂ nanotubes, (e) Pt loaded TiO ₂ nanotubes.....	201
Figure D 4: EDX results of Pt loaded TiO ₂ nanotubes.....	202
Figure D 5: Calibration curve for phenol.....	203

List of Tables

Table 4-1: Summary of the nanotube wall thickness, tube diameter, BET and length obtained at different voltages as well as different distances for a 3 h anodization in an ethylene glycol electrolyte containing 0.38 wt% NH ₄ F and 1.79 vol% H ₂ O.....	78
Table 6-1: PCE of TiO ₂ nanotubes were annealed at different conditions under N ₂ flow (250ml/min).....	119
Table 6-2: Factors and Response.....	122
Table 6-3: ANOVA Table.....	123

List of Scheme

Scheme 1-1: Outline of the research in thesis.....	8
Scheme 6-1: The six hours heating-treatment of the samples with heating rate of 10°C/min and 25°C/min.....	112
Scheme 7-1: Photo degradation of phenol.....	145

List of Abbreviations and Symbols

Analytical Instruments

SEM	Scanning Electron Microscopy
EDX	Energy dispersive X-ray
FE-SEM	Field Emission Scanning Electron Microscopy
XPS	X-ray Photo-electron Spectroscopy
XRD	X-ray diffraction
UV-vis	Ultraviolet visible light
HPLC	High performance liquid chromatography

Chemicals

N3 dye	(cis-di(thiocyanato)-bis(2,20-bipyridyl-4,40-dicarboxylate))ruthenium(II) dye
C ₂ H ₆ O ₂	Ethylene glycol
NH ₄ F	Ammonium fluoride
K ₃ [Fe(CN) ₆]	Potassium ferricyanide
H ₂ PtCl ₆	Chloroplatinic acid
PTES	1H,1H,2H,2H-perfluorooctyltriethoxysilane
HF	Hydrofluoric acid
<i>p</i> ZnTCPP	<i>para</i> Zinc-substituted porphyrin

Symbols

ANOVA	Analysis of variance model
DOE	Design of experiment
PCE	Water splitting Photoelectrochemical efficiency
IPCE	Incident Photon to Current conversion Efficiency
LHE	Light harvest efficiency
ϕ_{inj}	Electron injection efficiency
η	Efficiency of the Solar Cell
Abs	Absorption
Γ	Surface coverage (mol/cm ²)
AM 1.5	Air Mass Solar Spectrum [100 mW/m ²]
VB	Valance band
CB	Conduction band
E_g	Band gap (eV)
ΔE	Finite energy demand (eV)
E_{mean}	Applied potential (V)
DSSC	Dye Sensitized Solar Cell(s)
NTs	Nanotubes
J_{ph}	Current density (A/m ²)
L	Nanotube Length (nm)

W	Nanotube Wall Thickness (nm)
D	Nanotube Inner Diameter (nm)
G	Geometric roughness
<i>Ti 2p</i>	XPS signal of titanium due to an electron in a p-type orbital
<i>O1s</i>	XPS signal of oxygen due to an electron in a s-type orbital
<i>N1s</i>	XPS signal of nitrogen due to an electron in a s-type orbital
<i>C1s</i>	XPS signal of carbon due to an electron in a s-type orbital
<i>F1s</i>	XPS signal of fluorine due to an electron in a s-type orbital
<i>wt.%</i>	Weight %
μm	Micrometer [10^{-6} m]
<i>nm</i>	Nanometer [10^{-9} m]
<i>ff</i>	Fill Factor
I_{sc}	Short Circuit Current (A)
V_{oc}	Open Circuit Voltage (V)
I_s	Incident light intensity (mW/cm^2)

Chapter 1

Introduction

1.1 Objective of the Chapter

Titanium oxide nanotubes (TiO₂ NTs) present and potential value to applications such as self cleaning¹, solar cells², water splitting³, and wastewater treatment⁴ are largely due to its photocatalytic effect. Since TiO₂ is only active as a photocatalyst in near-UV light, much research was focused on modifying TiO₂ nanotubes to enhance their photocatalytic efficiency in the visible light spectrum. By doping⁵ or sensitization with various dyes⁶, much recent progress has been made, modifying properties to accomplish this. However, fabrication of highly ordered, reproducible and cost effective TiO₂ nanotubes is always a challenge in this field. Furthermore, the doping and coating techniques also need to be improved.

This chapter provides a comprehensive overview of the research on fabrication and application of titanium dioxide nanotubes (TiO₂ NTs). The challenges in this area are discussed along with most significant achievements of this work including the application. The final part of the chapter describes the objectives and the structure of this thesis work.

1.2 Fabrication Methods of TiO₂ NTs

The polished Ti foil was anodized in an electrolyte solution in a well-insulated bath for certain time at certain voltage using a DC power supply. The anodization current was monitored with a computer. After the anodization step, the sample was washed with distilled water and acetone and then dried with pressure air. Anatase TiO₂ nanotubes were made by annealing the as-anodized samples at 550°C for 3 hours under air atmosphere⁷.

The electrochemical anodization experiments were performed in a conventional two-electrode cell (Figure 1-1). A platinum foil (10mm×20mm) was used as a counter electrode and a titanium sheet served as a working electrode. The Ti sheet was pressed between a set of O-rings in the sample holder. The Pt wire was located on the back side of the sample as the electrical contact, and then fixed in the electrochemical cell with an active anode area exposed to the electrolyte. During the process, the anode and cathode were positioned adjacent to one another by a predetermined separation distance. All anodization experiments were performed potentiostatically, under constant applied voltage, at room temperature. The electrochemical anodization was carried out by using a source meter interfaced to a computer⁸.

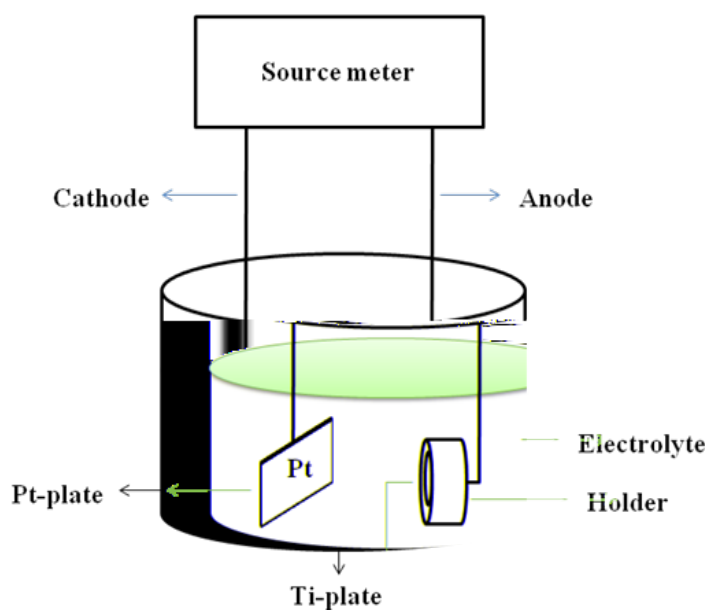


Figure 1-1: Two-electrode electrochemical cell in which the Ti samples are anodize

1.3 Challenges

Since the first report of the highly ordered TiO₂ nanotube arrays by Gong et al.⁹ The

field has grown very rapidly due to the better charge transfer ability and larger accessible surface area compare to the TiO₂ nanoparticles. As discussed above, despite the potential for expanded application of TiO₂ NTs, major problems remaining in this area are:

1) Although nanotubes with lengths of up to several hundreds of micrometers have been reported ¹⁰ due to the delicate balance between growing, etching and dissolving rates of nanotubes, it is very difficult to control the morphology of the nanotubes and reproduce them in the same fashion.

2) It is well-known that platinum is a precious metal and is scarcely available and platinum foil is used as a counter electrode in the anodization process. It creates a limitation on large scale production as well as the applications.

3) TiO₂ has a large band gap (3.2eV) and it is only active as photo-catalysis under UV light; however, doping different elements into the TiO₂ crystal lattice will change the band gap and active the crystal lattice under visible light. In general, most of doping process requires very harsh conditions, such as high temperature, high pressure, and expensive equipment that results in an overall costly process. Although dye sensitization offers the advantages of lower cost and convenience in process over doping, the temperature sensitivity, poor adhesion at low temperature and easy to be oxidized properties limit its usefulness.

1.4 Research Objectives

Aiming at the major concerns in the area of TiO₂ nanotubes, the general objectives of this thesis are:

- to develop effective fabrication methods in such a way that the fabricated TiO₂ nanotubes are not only reproducible but also highly ordered.

- to investigate alternative replacement for the Pt cathode
- to investigate and develop efficient doping process for activating TiO₂ nanotubes under visible light.

Specific objectives are addressed as follows:

- Develop a sonication-assisted fabrication process and understand the mechanism.
- Replace Pt with Ti and fabricate TiO₂ nanotubes.
- Optimize nitrogen doping process of TiO₂ nanotubes while maintaining the tubular structure.

- Investigate photo-degradation property of ZIF-8 coated TiO₂ nano-composite.
- Investigate wettability of TiO₂ nanotubes by changing the surface morphology

1.5 Approach and Methodology

In order to achieve the above general and specific objectives, the following approaches were implemented in the thesis.

- Highly ordered TiO₂ nanotubes will be fabricated by a comprehensive method, including establishment of sonication assisted process and changing the cathode to titanium plus characterization of by SEM, UV-vis and XRD pattern.

- Design of Experiment (DOE) study will be used to determine the relationship between temperature, heating rate and annealing time affect on photo conversion efficiency (PCE). The PCE is also called as photoelectrochemical water splitting

efficiency during the process of Nitrogen doping. The N-doped TiO₂ nanotubes will be characterized by SEM, UV-vis and XPS

- Photocatalytic property of ZIF-8 loaded TiO₂ nanotubes will be investigated by growing ZIF-8 crystals using TiO₂ nanotubes as templates.

- Superhydrophobic surface property of TiO₂ nanotubes layers will be investigated by functionalizing surface with fluorine compounds and the surface roughness can be altered by changing the anodization time. The surface will be characterized by contact angle measurement and atomic force microscopy (AFM).

1.6 Thesis Organization

The thesis is written in an article-integrated format as specified by the School of Postgraduate Studies at the University of Western Ontario.

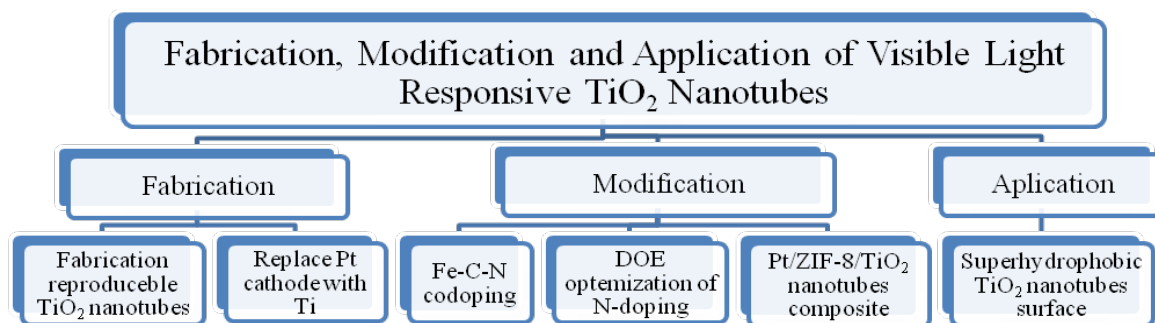
In this thesis, we have investigated issues from fabrication to activation and then applications of highly ordered TiO₂ nanotubes. This thesis consists of three sections.

1) Section 1 on fabrication has two chapters. Chapter 1 describes an innovative route that demonstrates fabrication of reproducible highly-ordered TiO₂ nanostructures. This technique can be extended to fabricate reproducible well-ordered TiO₂ nanotubes of a large area on other metals. Chapter 2 describes the electrochemical fabrication of TiO₂ nanotube arrays with high photoconversion efficiency by using Ti as a cathode which shows promising results to replace the conventionally used and comparatively expensive Pt cathode.

2) Section 2 on the activation of TiO₂ nanotubes contains chapters 3 through 5.

Chapter 3 describes an efficient and one-step method for the fabrication of Fe–C–N-codoped TiO₂ nanotubes. The SEM results showed that the average tube diameter, wall thickness and tube length are 70 nm, 20 nm and 2.4 μm respectively. The doped TiO₂ nanotubes exhibited the maximum photocurrent efficiency of 2.7%. Chapter 4 deals with optimization of the N₂ doping process by which the maximum photoconversion efficiency of 7.4% was obtained. This is comparable with the DOE (Design of Experiment) result of 7.2%. This work has potential application in photocatalytic water purification. Chapter 5 describes the newer photocatalyst Pt/ZIF-8 (zeolitic imidazolate framework) loaded TiO₂ nanotubes. The resulting composite exhibits 18.6% of phenol oxidation under visible light within 2 hours. These types of materials have the potential of serving as an effective photocatalyst for water purification.

3) The third and final section on application contains chapter 6 in which a facile electrochemical oxidation process has been applied to make TiO₂ nanotube-based superhydrophobic surfaces. The wettability can be altered by simply changing the anodization time. The results provide new insights into how to vary the wettability of superhydrophobic surfaces. These types of materials may have potential applications in coating and gene delivery. The outline of the research in thesis is shown in Scheme 1-1.



Scheme 1-1: Outline of the research in thesis

1.7 Major Contributions

1) Highly ordered TiO_2 nanotubes were fabricated in a reproducible manner and the expensive Pt metal was replaced with Ti foil. The results in this work suggest the following important implications:

- It is extremely difficult to fabricate highly ordered and uniformly covered TiO_2 nanotubes just by one step anodization because the tubes are easily bundled together if the anodization time was not controlled precisely. Due to the different surface roughness of samples before anodization, reproducing the same result in nano-level is almost impossible.
- Not all metals can be used as a replacement for Pt due to the cathode stability during the anodization.

Significance: These studies are important to overcome bundling problem which occurs quite often during the fabrication of TiO_2 nanotubes as well as the big step towards large scale production of inexpensive, reproducible and highly ordered TiO_2

nanotubes.

2) A Fe-C-N codoped TiO₂ nanotube array was prepared by a simple solution doping method. The photo conversion efficiency (PCE) of N-doped TiO₂ nanotubes was also optimized in order to obtain the best photo response and the photocatalytic property of Pt/ZIF-8/TiO₂ nanotubes composite was investigated as well. The specific findings are listed below:

- An optimized result of PCE (7.4%) was obtained under visible light by changing some parameters such as temperature, heating rate and annealing time under N₂ atmosphere.
- Fe-C-N was codoped into the TiO₂ nanotube lattice through the solution doping process which decreased the band gap of TiO₂.
- Highly visible light responsive Pt/ZIF-8/TiO₂ nano-composite was fabricated and 18% of phenol degradation under visible light was obtained. This result implicates that visible light responsive TiO₂ based photocatalysts can be achieved by incorporating highly porous materials within the TiO₂ nanotubes.

Significance: The modification results found in the present work provide evidence for activation of highly ordered TiO₂ nanotubes by simple and inexpensive processes. The conditions that were applied to obtain the optimized result from DOE also can be used as the standard conditions to achieve higher PCE.

3) As prepared, TiO₂ nanotubes layer shows a superhydrophilic wetting behavior which has 0° contact angle. The layer becomes superhydrophobic after modifying with

1H,1H,2H,2H-perfluorooctyltriethoxysilane (PTES). We demonstrated how to change the surface characteristics of the TiO₂ nanotube layers in order to achieve any desirable degree of hydrophobicity from hydrophilic to superhydrophobic.

- Surface wettability can be altered by changing the surface roughness followed by modification with low surface energy fluorine compounds.

Significance: This research on TiO₂ nanotubes based superhydrophobic material might eventually lead to industrial applications due to the following advantages. First of all, it has self cleaning property. In addition, it is corrosion resistance. Furthermore, the TiO₂ nanotube layer will not come off easily.

1.8 References

- (1) Song, Y. -.; Schmidt-Stein, F.; Berger, S.; Schmuki, P. *Small* **2010**, *6*, 1180-1184.
- (2) Nah, Y. -.; Paramasivam, I.; Schmuki, P. *ChemPhysChem* **2010**, *11*, 2698-2713.
- (3) Rani, S.; Roy, S. C.; Paulose, M.; Varghese, O. K.; Mor, G. K.; Kim, S.; Yoriya, S.; Latempa, T. J.; Grimes, C. A. *Physical Chemistry Chemical Physics* **2010**, *12*, 2780-2800.
- (4) Okour, Y.; Shon, H. K.; El Saliby, I. J.; Naidu, R.; Kim, J. B.; Kim, J. -. *Bioresour. Technol.* **2010**, *101*, 1453-1458.
- (5) Mor, G. K.; Varghese, O. K.; Paulose, M.; Shankar, K.; Grimes, C. A. *Solar Energy Mater. Solar Cells* **2006**, *90*, 2011-2075.
- (6) Roy, P.; Kim, D.; Lee, K.; Spiecker, E.; Schmuki, P. *Nanoscale* **2010**, *2*, 45-59.
- (7) Isimjan, T. T.; Kazemian, H.; Rohani, S.; Ray, A. K. *Journal of Materials Chemistry* **2010**, *20*, 10241-10245.
- (8) Isimjan, T. T.; Ruby, A. E.; Rohani, S.; Ray, A. K. *Nanotechnology* **2010**, *21*.
- (9) Albu, S. P.; Ghicov, A.; Macak, J. M.; Schmuki, P. *Physica Status Solidi - Rapid Research Letetrs* **2007**, *1*, R65-R67.
- (10) Gong, D.; Grimes, C. A.; Varghese, O. K.; Hu, W.; Singh, R. S.; Chen, Z.; Dickey, E. *C. J. Mater. Res.* **2001**, *16*, 3331-3334.

Chapter 2

Literature Review

1.1 Introduction

In recent years, growing attention has been paid to the design and fabrication of fine-structured metal oxides on the nanoscale and microscale because of their uniquely promising properties and applications. Among the structured metal oxides, TiO_2 in particular has been extensively studied and put to use in microporous membranes, dye-sensitized solar cells, humidity chemical sensors, water-splitting electronic devices, and hydrogen storage and sensing solutions among others¹. Its role as an environmentally-friendly photocatalyst has also seen wide application to environmental problems such as treatment of wastewater and purification of polluted aqueous systems². Titanium oxide's photocatalytic role could be expanded even more broadly if it were not so limited by its large bandgap ($E_g = 3.2$ eV) which requires near-UV light (λ shorter than 380 nm) to activate. In order to prepare the nanostructure and microstructures of TiO_2 , various approaches have been reported such as the sol-gel process³, pyrolysis⁴, electron beam evaporation⁵, chemical vapor deposition⁶, atomic-layer deposition⁷, and the hydrothermal process⁸. Of these, methods involving application of TiO_2 powder to aqueous solutions create the problem of suspensions that are very difficult and costly to separate out by filtration. By contrast, a solid array of TiO_2 nanotubes grown directly on titanium plates offers the possibility of a more robust and economical solution by not only eliminating the above problem, but even being reusable after photocatalytic reactions.

2.2 Fabrication of highly ordered TiO₂ nanotubes

Many applications of TiO₂ nanotube arrays strongly demand smooth topography and orderly arrangement, e.g., dye sensitized solar cells (DSSCs) and hydrogen storage. In this regard, a lot of work has been done on improving the morphology of the TiO₂ nanotube arrays. Among them the two-step anodization of a Ti foil is the most convenient and economical method. Normally, after first time anodizing, Ti usually gives rise to TiO₂ nanotube arrays with rough top surfaces and poor alignment. However, a well-textured Ti surface was obtained after the removal of the nanotube layer generated in the first-step anodization. Then, the Ti foil that had experienced this pre-treatment was anodized again for the eventual growth of highly ordered TiO₂ nanotubes. The first anodized surface can be removed either by ultrasonic sonication⁹ (Figure 2-1) or using an adhesion tape¹⁰ (Figure 2-2).

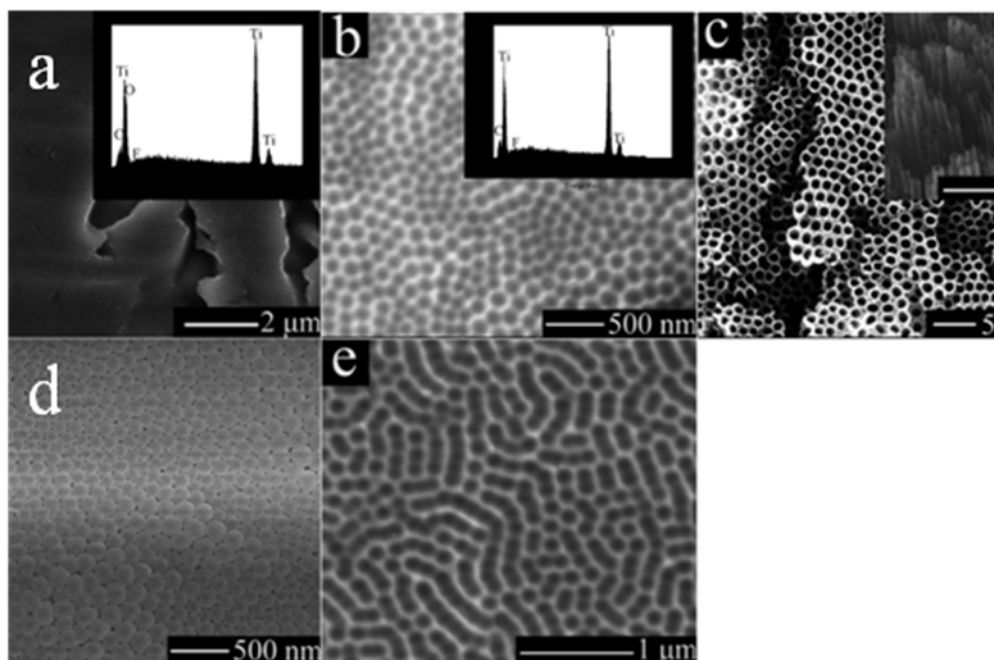


Figure 2-1: Results of the first-step anodization: (a) the SEM image of the Ti surface outside the anodization region (inset is the EDX); (b) the Ti surface after the removal of the nanotube layer (inset is the EDX); (c) the SEM image of the nanotube layer generated in the first-step anodization (inset was obtained when the sample was tilted by 45° from the incident electron beam); (d) the bottom side of the nanotube layer that shed from the Ti foil; (e) the Ti foil surface exposed after the ultrasonic removal of a nanotube layer fabricated with an insufficiently aged electrolyte⁹. Reprinted from Li, S.; Zhang, G.; Guo, D.; Yu, L.; Zhang, W. *Journal of Physical Chemistry C* **2009**, *113*, 12759-12765. Copyright (2009) with permission from American Chemical Society.

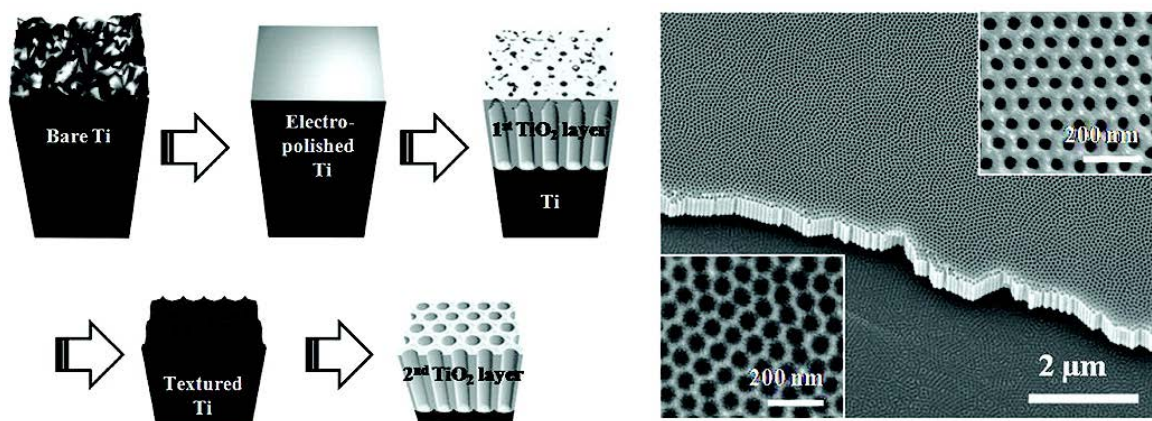


Figure 2-2: Schematic for self-organized regular arrays of anodic TiO₂ nanotubes¹⁰. Reprinted from Yeonmi, S.; Seonghoon, L. *Nano Letters* **2008**, *8*, 3171-3173. Copyright (2008) with permission from American Chemical Society.

Although using sonication is relatively better than using adhesion tape in order to avoid possible left over residue on the surface, it is not always easy to completely remove the TiO₂ nanotube layer which was fabricated by the first anodization step. For this reason, the second fabrication step becomes difficult.

2.3 Modification of highly ordered TiO₂ nanotubes

It is of great significance to prepare and develop unique TiO₂ nanotubes which can work efficiently even under broad-spectrum visible light irradiation while having a high mechanical and physical stability. By either doping or sensitization, it is possible to improve the optical sensitivity and activity of TiO₂ nanotubes in the visible light

spectrum.

2.3.1 Doping

The underlying electronic structure determines the optical response of materials, which are closely related to its chemical composition (chemical nature of the bonds between the atoms or ions), its atomic arrangement, and its physical dimension (confinement of carriers) for nanometer-sized materials. The chemical composition of TiO₂ can be altered by doping. Specifically, the metal (titanium) or the nonmetal (oxygen) component can be replaced in order to alter the material's optical properties. It is desirable to maintain the integrity of the crystal structure of the photocatalytic host material and to produce favorable changes in electronic structure. Small amount of a dopant usually improves the catalytic activity and visible light sensitivity by changing the band gap between conduction band (CB) and valance (VB) band of TiO₂, however the visible light sensitivity of the doped semiconductors appear to be a complex function of the dopant concentration, the energy level of the dopants, their oxidation states and the type of defects created in the host lattice. For example ¹, Photoexcitation for V-, Cr-, Mn-, and Fe-doped TiO₂ occurred via the t_{2g} level of the dopant. The visible light absorption for Mn- and Fe-doped TiO₂ was due to the optical transitions from the impurity band tail into the CB. The Mn (Fe) t_{2g} level was close to the VB and easily overlapped in highly impure media. The visible light absorption for the Cr-doped TiO₂ can be attributed to a donor

transition from the Cr t_{2g} level into the CB and the acceptor transition from the VB to the Cr t_{2g} level (Figure 2-3).

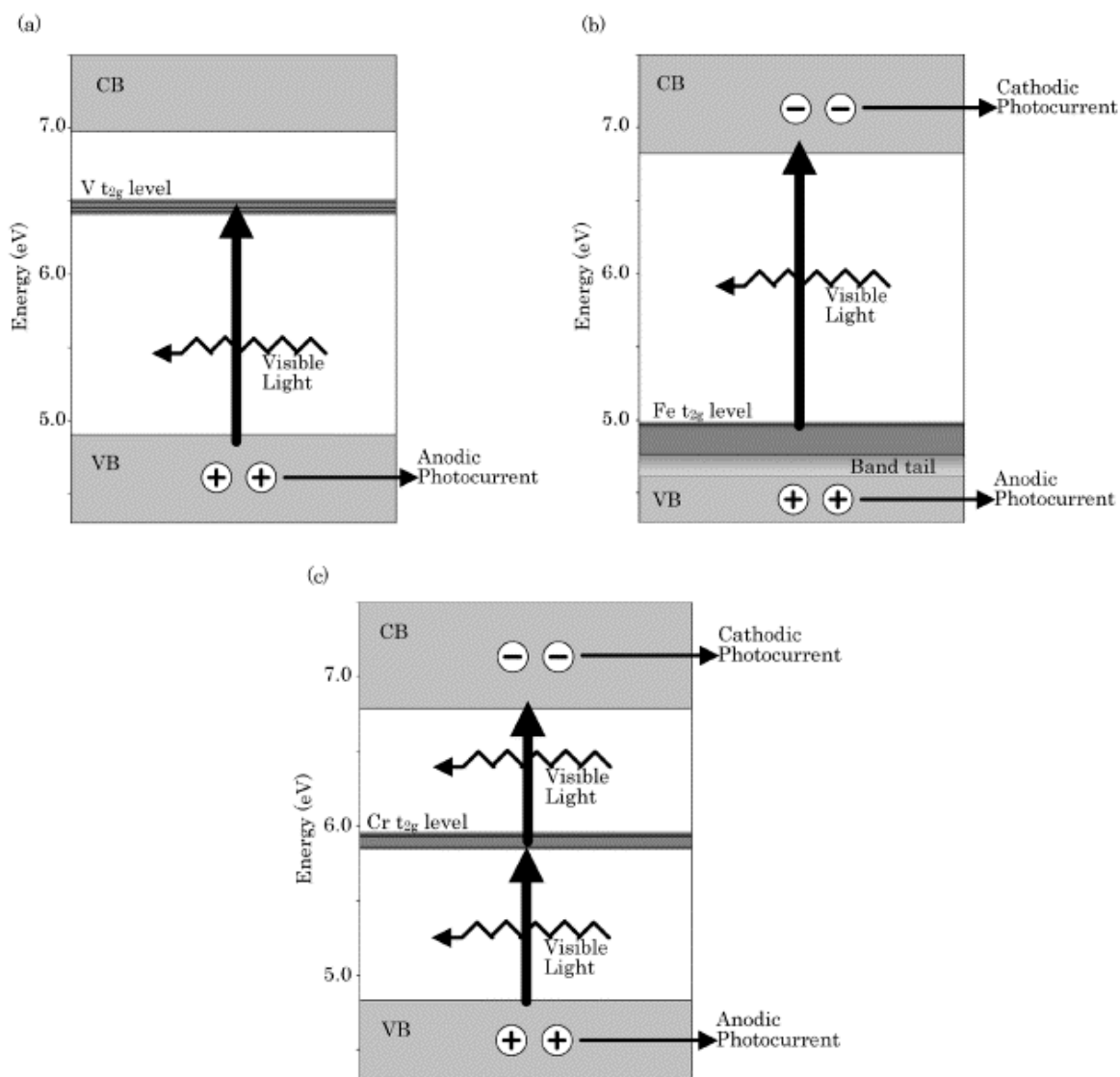


Figure 2-3: Schematic diagram to illustrate the photoexcitation process under visible light of metal-doped TiO_2 : (a) $\text{Ti}_{1-x}\text{V}_x\text{O}_2$; (b) $\text{Ti}_{1-x}\text{Fe}_x\text{O}_2$; (c) $\text{Ti}_{1-x}\text{Cr}_x\text{O}_2$ ¹. Reprinted from Chen, X.; Mao, S. S. *Chem. Rev.* **2007**, *107*, 2891-2959. Copyright (2007) with permission from American Chemical Society.

It appears easier to substitute the Ti^{4+} cation in TiO_2 with other transition metals, as it is more difficult to replace the O^{2-} anion with other anions due to differences in charge states and ionic radii. The small size of the nanoparticle is beneficial for the modification of the chemical composition of TiO_2 due to the higher tolerance of the structural distortion than that of nanotubes because of the inherent lattice strain in nanotubes.

2.3.1.1 Metal doping

Various metal elements such as Al, Nb, V, Cr, Mn, Co, Ni, Zr, Ru, Mo, W and Hf have been successfully doped into TiO_2 nanotubes by solution doping, sol-gel-hydrothermal method, ion implantation and hydrothermal method. The visible light response of TiO_2 nanotubes can be significantly expanded, if Ti alloys, rather than pure Ti, is used as a substrate for nanotube growth in an aqueous electrolyte.

Yu et al reported ¹¹ Fe-doped TiO_2 nanotube by impregnating-calcinations method using the hydrothermally prepared TiO_2 nanotubes as precursors and $\text{Fe}(\text{NO}_3)_3$ as dopant. The Fe-doping induces the shift of the absorption edge into the visible-light range with the narrowing the band gap and reducing the recombination of photo-generated electrons and holes. Others also reported Fe -doped visible-light sensitive TiO_2 nanotubes by solution doping¹². Highly ordered Fe-doped TiO_2 nanotube array films were fabricated directly by the electrochemical anodization of pure titanium in an HF electrolyte solution containing iron ions¹³.

Nb, V, Cr, Mn, Co doped TiO_2 nanotubes were prepared using solution chemical processing in order to control optical and electrical properties¹⁴. The Co-doped TiO_2

nanotube arrays have been synthesized by a sol-gel template method.¹⁵ Layers of TiO₂ nanotubes have been fabricated by electrochemical anodization of Ti. After annealing the tubes to an anatase structure Cr-doping was carried out on the surface of TiO₂ nanotubes by ion implantation at energy of 60 keV.¹⁶

TiO₂ nanotube arrays and W-doped (containing 3-wt% W) TiO₂ nanotube arrays were obtained using a direct anodization method.¹⁷ Liu et al described a new method for the preparation of Zr doped TiO₂ nanotube arrays by electrochemical method¹⁸. A series of Nd-TiO₂ powders have been prepared by the sol-gel technique with neodymium nitrate and tetra-n-butyl titanium as raw materials, and then Nd- TiO₂ nanotubes were fabricated by the hydrothermal method¹⁹

Doping of ruthenium by the ion exchange method to the hydrothermally synthesized TiO₂ nanotubes were found to be an effective photocatalyst which decolorizes methylene blue under visible light.²⁰

Pure TiO₂ nanotubes and TiO₂ nanotubes doped with Fe³⁺/Ni²⁺/Mn²⁺ ions were synthesized by the hydrothermal method. In this process, TiO₂ nanotubes were prepared synchronously with doping Fe³⁺/Ni²⁺/Mn²⁺ ions.²¹

Using TiO₂ alloy as substrate in anodization is the most efficient methods to dope metals and non metals into TiO₂ lattice. Ding and his coworkers reported²² anodic formation of Ti-Nb-O nanotubes on top of a Ti35Nb alloy, and in vitro bioactivity and stem cell response of the anodic nanotubes. Jang et al²³ investigated Ti-xNb alloys nanotubes using 1.0 M H₃PO₄ electrolyte containing 0.8 wt.% NaF and various

electrochemical methods. Ti-xHf (x=10%, 20%, 30% and 40%, mass fraction) alloys were prepared by arc melting, and the microstructure was controlled for 24 h at 1 000 °C in argon atmosphere. The formation of nanotube was conducted by anodizing on Ti-Hf alloys in 1.0 mol/L H₃PO₄ electrolytes with small amounts of NaF at room temperature.^{24, 25} Ti-Zr alloy nanotubes were fabricated by anodization in H₃PO₄ containing 0.5 wt.% NaF.²⁶

Self-organized TiO₂-MoO₃ composite oxide nano-tubes with tunable dimensions have been fabricated by anodization of a Ti-Mo alloy and these nano-tube layers exhibit a significantly enhanced electrochromic color contrast compared with plain TiO₂ nano-tubes.²⁷ Ti-W-doped TiO₂ nanotubes have been successfully fabricated using TiW alloy anodization²⁸. TiO₂-Nb₂O₅ nanotubes were grown on a Ti-Nb alloy (Ti45Nb) by anodization in a fluoride-containing electrolyte²⁹ Macak et al reported the fabrication of self-organized porous oxide-nanotube layers on the biomedical titanium alloys Ti-6Al-7Nb and Ti-6Al-4V by a simple electrochemical treatment.³⁰

The presence of metal ion dopants significantly influenced the photoreactivity, charge carrier recombination rates, and interfacial electron transfer rates of the resulting materials. Metal ion-doped TiO₂ prepared by ion implantation with various transition-metal ions such as V, Cr, Mn, Fe, and Ni was found to have a large shift in the absorption band toward the visible light region, with the order of the effectiveness in the red-shift being V > Cr > Mn > Fe > Ni¹.

2.3.1.2 Non-metal doping

There are four major methods for preparing non-metal-doped TiO₂ nanotubes such as: high temperature doping, chemical vapor deposition, flame annealing and solution doping through electrochemical anodization. Various nonmetal elements such as B, C, N, F, S and P have been successfully doped into TiO₂ nanomaterials by these methods. The high temperature treatment methods usually involve heating of a titanium nanotube precursor in presence of corresponding gas flow of doping elements for example N₂ can be doped into TiO₂ nanotubes by heating nanotubes under N₂ flow meanwhile in the process of the flame annealing flammable gas is used to anneal newly prepared TiO₂ nanotubes. This method is mostly used for C-doping. Solution doping is the most convenient process by which different non-metals can be doped through anodization.

To enhance the absorption in the visible region for TiO₂, C-doped TiO₂ nanomaterials have been obtained by heating titanium carbide or by annealing TiO₂ under CO gas flow at high temperatures (500-800°C) or by direct burning of a titanium metal sheet in a natural gas flame^{31, 32, 33}. Carbon also can be doped into TiO₂ lattes by plasma electrolysis.³⁴ Fan et al reported³⁵ C-doped TiO₂ nanotubes by solution method. It showed high degradation result of methylene blue compare to the result of non-doped TiO₂ nanotubes.

Chen and his coworkers fabricated photo responsive S-F-codoped TiO₂ nanotubes by one-step electrochemical anodization process to extend the photo-response of TiO₂ to the visible-light region.³⁶

F-doped TiO₂ nanotubes were prepared by impregnation method. Compared with pure TiO₂ nanotubes, the doping with F⁻ significantly enhanced the photocatalytic efficiency.³⁷

Chemical vapor deposition (CVD) was firstly used to simultaneously codope fluorine and boron into TiO₂ nanotubes anodized Ti in C₂H₂O₄ · 2H₂O + NH₄F electrolyte.³⁸

N-doping is the most popular area because N-doping is easier than doping any other non-metals, due to the differences in charge states and ionic radii. Visible-light-responsive N-doped TiO₂ nanotubes were synthesized via an environment-conscious solvothermal treatment of protonated TiO₂ nanotubes in an NH₄Cl/ethanol/water solution.³⁹ N-doped TiO₂ (anatase) with high visible light photo-activity was obtained by the thermal treatment of nanotube in an NH₃ flow.⁴⁰ N-doped TiO₂ nanotubes with high photocatalytic activity were prepared by the combination of sol-gel process with hydrothermal treatment.⁴¹ N-doped TiO₂ nanotubes were produced by anodization of a TiN alloy. The alloy was prepared to contain approximately 5 at.% of N from high-purity Ti and TiN powders using an arc-melting and consisted of a two-phase structure with different N-contents.⁴² N-doped TiO₂ nanotubes were prepared by a solution process and with an additional thermal treatment. Firstly, TiO₂ nanotubes were prepared by a hydrothermal chemical method and then the nanotubes were immersed into a 0.5 mol/L NH₃ solution for different periods. Finally, the resulting TiO₂ nanotubes were annealed at high temperature to complete the substitution of O by N.⁴³ Different thicknesses of the nanotubular layer architecture were formed by electrochemical anodization of Ti in

different fluoride-containing electrolytes; tube lengths were 500 nm, 2.5 μm , and 6.1 μm . As-formed nanotube layers were annealed to an anatase structure and treated in ammonia environment at 550 $^{\circ}\text{C}$ to achieve nitrogen doping.⁴⁴ N-doped TiO_2 nanomaterials have also been obtained by the following alternate means: heating TiO_2 under NH_3 flux at 500 $^{\circ}\text{C}$, calcination of the hydrolysis product of $\text{Ti}(\text{SO}_4)_2$ with ammonia as precipitator, decomposition of gas-phase TiCl_4 with an atmosphere microwave plasma torch, or by sputtering/ion-implanting techniques with nitrogen or N^{2+} gas flux⁴⁵.

Boron-doped TiO_2 nanotube arrays were produced by forming a nanotube-like TiO_2 film in an anodization process on a Ti sheet, followed by chemical vapor deposition treatment using trimethyl borate as the boron source with N_2 as the carrier gas, and was characterized by ESEM, XPS, XRD, and UV-vis methods.^{38, 46, 47, 48}

Titanium dioxide doped with phosphorus (P) was synthesized by anodization of Ti in the mixed acid electrolyte of H_3PO_4 and HF.^{49, 50}

S-doped TNT was successfully prepared using the solid-phase method at 350 $^{\circ}\text{C}$ under aerated conditions.⁵¹

2.3.2 Sensitization

When a photocurrent is generated with light energy less than that of the semiconductor band gap, the process is known as sensitization, and the light-absorbing dyes are referred to as sensitizers. TiO_2 is a semiconductor with a wide band gap and with optical absorption in the UV region (<400 nm). Any materials with a narrower band gap or absorption in the visible or infrared regime can be used as a sensitizer. These materials

include inorganic semiconductors with narrow band gaps: metals, organic dyes, and conjugated polymers. How efficiently the sensitized TiO_2 can interact with the light depends largely on how efficiently the sensitizer interacts with the light. A common and key step in the photosensitization of TiO_2 is the efficient charge transfer from the excited sensitizer to TiO_2 and the resulting charge separation. The match between the electronic structures of the sensitizer and TiO_2 plays a large role in this process, as does the structure of the interface, including the grain boundaries and bonding between the sensitizer and TiO_2 . Careful design is needed to avoid charge trapping and recombination which eventually harms the performance of sensitized TiO_2 ¹.

2.3.2.1 Inorganic Sensitization

The preparation method for these inorganic semiconductor sensitized TiO_2 nanomaterial systems is usually the sol-gel method. The sensitization of nanoporous TiO_2 by CdS, PbS, Ag_2S , Sb_2S_3 , and Bi_2S_3 has found that the relative positions of the energetic levels at the interface between the quantum size particles and TiO_2 can be optimized for efficient charge separation by using the size quantization effect, and that the photostability of the electrodes can be significantly enhanced by surface modification of the TiO_2 nanoparticles with CdS nanoparticles. Additionally, excitation of the sensitizer AgI on TiO_2 nanoparticles results in a stabilization of electron-hole pairs with a lifetime well beyond 100 and in electron migration from AgI to TiO_2 . Ag or Au nanoparticle-sensitized TiO_2 nanorods sustain a higher degree of conduction band electron accumulation than pure TiO_2 .

Xiong et al. fabricated TiO₂ nanotubes and nanofibers through a hydrothermal technique, and which were fabricated through a templating method. They demonstrated the doping of these two materials with PbS QDs (quantum dots) as well as the ability to control the size of the QDs, thus controlling the spectral absorption range.⁵²

Yin et al.⁵³ reported novel fabrication route for core/sheath/hetero-structure CdS/TiO₂ nanotube array using ac electrodeposition for application in photoelectrochemical cells. CdS/TiO₂ nanotube array was prepared by electrochemically depositing CdS directly into anodic TiO₂ from an electrolyte containing Cd²⁺ and S in dimethyl sulfoxide. Ag, Au, Pt nanoparticles supported on TiO₂ nanotubes were prepared by microwave assisted heating polyol process^{54,55}. The results show that Ag and Au nanoparticles were found to significantly enhance the photocatalytic activity of self-organized TiO₂ nanotubular array.

2.3.2.2 Organic Sensitization

Organic compounds have been widely employed as sensitizers for TiO₂ nanotubes to improve its optical properties, i.e., organic dyes and conjugated polymers. Organic dyes are usually transition metal complexes with low lying excited states, such as polypyridine complexes, phthalocyanine, and metalloporphyrins. The metal centers for the dyes include Ru(II), Zn(II), Mg(II), Fe(II), and Al(III), while the ligands include nitrogen heterocyclics with delocalized π or aromatic ring systems. Organic semiconductors such as conjugated polymers are interesting candidates for electronic devices based on molecular materials with their advantages of lower weight, high mechanical flexibility, and sometimes lower costs as compared to conventional electronics.

2.3.2.3 Dye Sensitization

These organic dyes are normally linked to TiO₂ nanoparticle surfaces via functional groups by various interactions between the dyes and the TiO₂ nanoparticle substrate: (a) covalent attachment by directly linking groups of interest or via linking agents, (b) electrostatic interactions via ion exchange, ion-pairing, or donor-acceptor interactions, (c) hydrogen bonding, (d) van der Waals forces, etc. The most preferable linkage is covalent attachment which can be achieved by reacting carboxylic and phosphonic acid derivatives with the hydroxyl groups to form esters, while amide linkages are obtained via the reaction of amine derivatives and dicyclohexyl carbodiimide on TiO₂. The most common and successful functional groups are based on carboxylic acids.

The mechanism of the dye sensitization of TiO₂ nanoparticles normally involves the excitation of the dye and the charge transfer from the dye to TiO₂ nanoparticles. As an efficient photosensitizer, the dye has to meet several requirements. First, the dye should have high absorption efficiency and a wide spectral range of coverage of light absorption in the visible, near-IR, and IR regions. Second, the excited states of the dye should have a long lifetime and a high quantum yield. Third, the dye should have matched electronic structures for the ground and excited states with TiO₂ nanoparticles to ensure the efficient charge transfer between them; that is, the energy level of the excited state should be well matched to the lower boundary of the conduction band of TiO₂ to minimize energetic losses during the electron-transfer reaction.

2.3.2.3.1 Organic dye sensitization

Dye-sensitized solar cells (DSSCs) have received considerable attention as a cost-effective alternative to conventional solar cells. One of main issues for the development of DSSCs is the design and synthesis of dyes that serve as light absorbers for energy conversion. Up to now, many different pure organic dyes and transition metal complexes have been evaluated as sensitizers. Among the wide variety of dyes, polypyridyl complexes of Ru with four pendant carboxyl groups, such as (cis-di(thiocyanato)-bis(2,20-bipyridyl-4,40-dicarboxylate))ruthenium(II) dye (Figure 2-4) (commercially known as N3), has become the most efficient and widely used dye.⁵⁶ However, the Ru dyes is getting very expensive because of the increasing price of Ru. Therefore, people start to look for the alternatives.

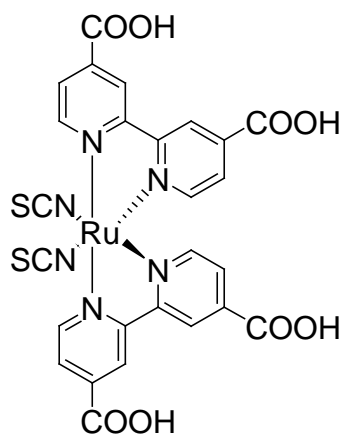


Figure 2-4: Structure of N3

Chlorophylls and their analogues (Figure 5) are attractive candidates for application in dye-sensitized solar cells since these molecules strongly absorb light, and have the

potential to provide pathways for long-range excitation transport.^{57, 58} Eighty to ninety percent of the excitations formed on light absorption are transferred to the reaction centre where charge separation occurs.

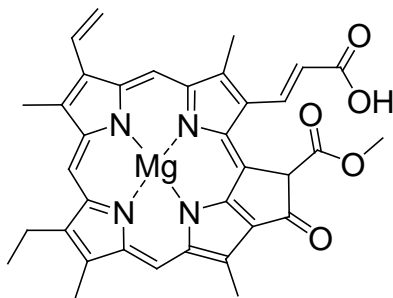


Figure 2-5: Structure of chlorophyll-c1

DSSCs sensitized with pure organic dyes (Figure 6) have relatively lower power conversion efficiencies than those sensitized with metal complexes. However, pure organic dyes have many advantages for their application in DSSCs, such as lower cost, higher absorption coefficient and easier control of redox potentials of LUMO and HOMO levels. Importantly, the highest power conversion efficiency of DSSCs with pure organic dyes has reached 8.0%, which is close to that (~10%) of DSSCs with metal complexes.⁶⁰

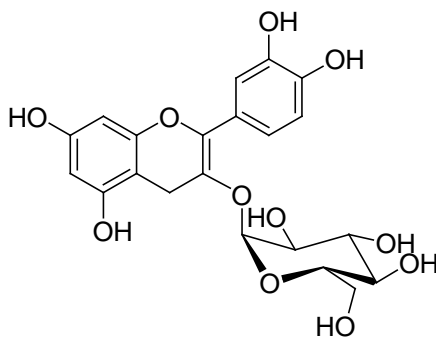


Figure 2-6: Cyanidin-3-glucoside

Porphyrin derivatives are of particular interest because of their improved stability as compared to chlorophylls. Of crucial importance is the realization of low-cost dye layers in which photons are efficiently harvested. Recent studies have shown that the lifetime of the excited states and the mutual arrangement of porphyrin dye (Figure 2-7) molecules play a key factor in realizing efficient light-harvesting.^{59, 62}

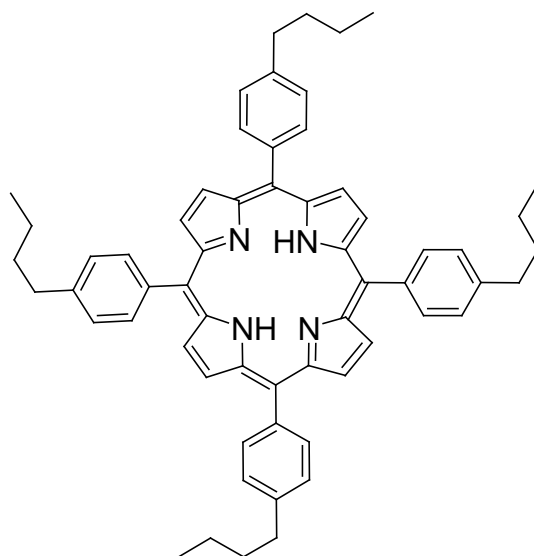


Figure 2-7: Porphyrin dye

However, the expensive elaborate deposition technique makes these layers commercially less attractive and could economically only be applied in a few dye materials.

2.3.2.3.2 Conjugated polymer sensitization

To improve the efficiency and increase the technological value of DSSC, there is a tendency to substitute some of materials which are used to make DSSC with polymers. For example, poly(ethylene terephthalate) based electrodes can substitute with glass electrodes improving the flexibility and impact resistance of a DSSC. Liquid electrolytes are volatile and may leak if the cell if it is not properly sealed. Their replacement by polymeric electrolytes not only solves this problem but also acts as a binder for the electrodes. More recently, intrinsically conducting polymers have been used as hole conducting materials in DSSC with promising results. Polymeric materials are less expensive, lighter, and consume less energy for their large scale production, making these cells more environmentally friendly.

Tripathy and coworkers⁶³ have discovered a way to produce plastic cells that the suspension coated on PET-ITO films required heating to 110 °C for <1 min which exhibits efficiencies higher than 5% at air mass 1.5 condition (AM 1.5), and the manufacturing cost could be as low as the lowest estimated cost for amorphous and crystalline silicon. In the same direction, a highly efficient flexible DSSC prepared on a conductive plastic film substrate was assembled using mechanically stable mesoporous amorphous TiO₂ films prepared at low temperature (100 °C) by hydrothermal treatment⁶⁴.

Houarner-Rassin and coworkers⁶⁵ have reported on the molecular wiring efficiency of a ruthenium polypyridine complex acting as a sensitizer connected to a poly(3-hexyl)thiophene chain acting as hole transporting material. The comparison of the photocurrent-photovoltage characteristics of the cells recorded under AM1.5 indicates a twofold improvement of the overall photoconversion efficiencies when the sensitizer is grafted to the hole transporting material relative to the reference system.

A scientifically interesting and promising approach to replace the liquid electrolyte in DSSC consists in the use of p-type semiconductors referred as hole transporting materials. In principle, all materials with p-type semiconducting behaviour capable of accepting holes from the dye cation are potential candidates to replace the liquid electrolyte in DSSC. Intrinsically-conducting polymers are well known as good hole transporting material, carrying current densities of several mA/cm².^{66, 67} Thus, these materials are potential candidates to use as HTM in solid-state DSSC (Figure 2-8).

Application of a spin-coated poly(4-undecyl-2,2'-bithiophene) layer on dye-sensitized TiO₂ has shown that it can act as an efficient charge mediator. Typical J-V values for flat TiO₂ film devices are $J_{sc} = 60 \mu\text{A}/\text{cm}^2$, and $V_{OC} = 0.65 \text{ V}$, which is comparable to values obtained with liquid electrolytes in the same geometrical configuration. The polymer is also able to sensitize the TiO₂ without a dye.⁶⁸

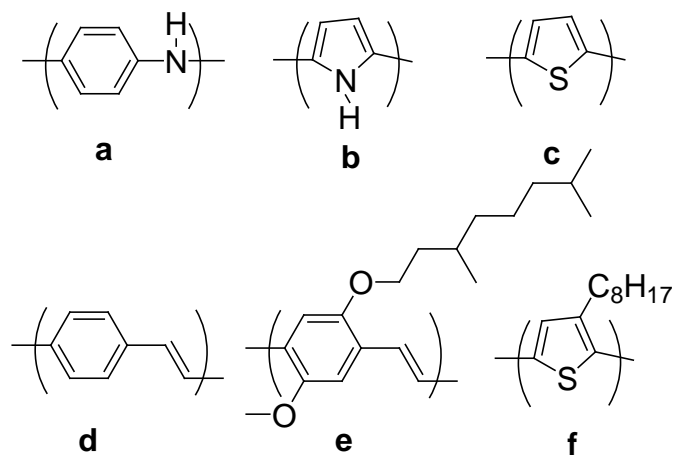


Figure 2-8: Chemical structure of the repeating units of HTM polymers

Rodolfo Espinosa and coworkers⁶⁹ have studied different condensed tannins extracted from the bark wastes of tropical wood trees as possible sensitizers of TiO₂. These natural polymers adhere strongly to TiO₂ even in aqueous solutions. The major drawback involved in developing “plastic” DSSC concerns the deposition of the TiO₂ film. That requires high annealing temperatures of around 450 °C for 30 min. This sintering step removes the binder and solvent, giving rise to an electrically-connected network of TiO₂ particles. However, with polymers, thermal treatment must be limited to 150 °C, because above this temperature the polymer undergoes thermal degradation, losing its transparency and becoming completely distorted. If polymer deposition on TiO₂ film is done at low temperature, this results in poor adhesion and thus reduced electrical contact between the particles and decreased dye adsorption. Another issue is that the low annealing temperature precludes the total elimination of organic residues from the surfactants commonly used in TiO₂ suspensions.^{70, 71, 72, 73, 74}

2.4 Photo-electrochemical properties

The IPCE of the photovoltaic cell can be expressed as the product of three key parameters which are shown in equation (2-1): the light harvesting efficiency (LHE), the electron-injection yield (ϕ_{inj}) and the electron collecting efficiency (η) in the external circuit.

$$IPCE \sim LHE \times \phi_{inj} \times \eta \quad (2-1)$$

The actual reactions that happen in the dye sensitized solar cell are as shown in Figure 2-9. CB is the conduction band; VB is the valence band; k_{fluor} is the rate constant of the fluorescence deactivation of the porphyrin excited state; k_{inj} is the rate constant of the photo induced electron transfer from the porphyrin excited state; k_{CR} is the rate constant of the charge recombination between the oxidized porphyrin and electrons in the CB; k_{reg} is the rate constant of the electron-transfer reaction between the oxidized porphyrin and the iodide in the electrolyte.

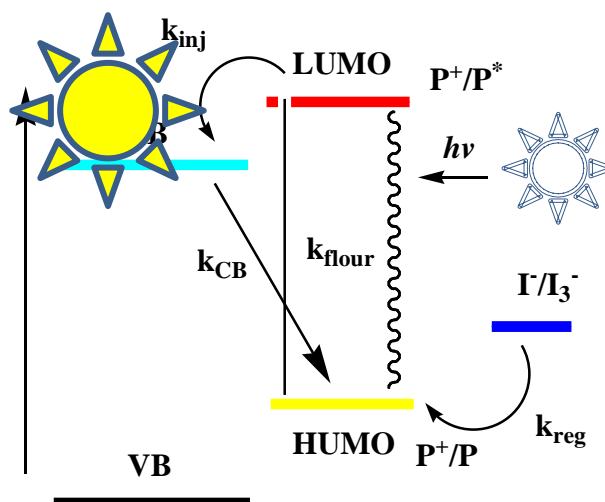


Figure 2-9: Different reactions accruing in the TiO₂/dye surface

The LHE is controlled by absorption (Abs) as shown in equations (2-2) and (2-3). Higher the absorption is better the LHE. Where Γ (mol/cm²) is the surface coverage of the sensitizer and σ (cm²/mol) is the molar cross section for absorption of monochromatic light.

$$\text{LHE} = 1 - 10^{-\text{Abs}} \quad (2-2)$$

$$\text{Abs} = \Gamma \sigma \quad (2-3)$$

The η term is essentially controlled by two parameters: (i) the rate of iodide oxidation by the oxidized porphyrin after electron injection (k_{reg}) and (ii) the rate of charge recombination (k_{CR}) of the oxidized porphyrin with the conduction band electrons. k_{reg} cannot be considered a limiting factor because the ground-state oxidation potentials of the porphyrins are more positive than those of the best dyes that yield very high IPCEs.⁷⁵ Durrant et al.⁷⁶ have recently reported that the rate of charge recombination between conduction band electrons and oxidized porphyrin sensitizers is in the range of several milliseconds. This rate is sufficiently slow to permit the regeneration of the ground state of the porphyrin by the iodide in solution. As a result, η is not the limiting factor for obtaining high IPCE.

The injection efficiency (ϕ_{inj}) directly depends on the electron-injection rate (k_{inj}). The residual fluorescence emission which was detected upon adsorption of the dye on TiO₂ suggests the electron injection yield is far from completed.⁷⁷ The radiative process competes with the electron injection, thus decreasing the branching ratio between these two deactivation channels (k_{fluor} versus k_{inj}). Marcus theory framework model⁷⁷ states that the

factors controlling the electron-transfer rate are: the free energy change, the reorganization energy associated with the interfacial electron transfer and the electronic coupling between the electron donor and the acceptor. The reorganization energy may not be a limiting factor for these sensitizers, since it is known not to be larger than that of ruthenium polypyridine complexes. The free energy associated with the electron injection may play a role in the rate of the electron injection, because the best porphyrin sensitizer has the highest excited-state oxidation potentials. The other factors which may affect the electron-transfer are position of functional groups for example ⁷⁷ (Figure 2-10): although **1** and **2** exhibit similar excited-state oxidation potentials and similar absorption and emission excited-state oxidation potentials and similar absorption and emission characteristics, they lead to very different IPCE values. Porphyrin **2** bears the COOH anchoring group directly on the p-aromatic core. This feature certainly allows for a stronger electronic interaction with TiO₂ compared to porphyrin**1**, in which the remote COOH groups are electronically decoupled from the porphyrin macrocycle. Porphyrin **3** has much higher IPCE than **4** due to the orientation and distance of the dye respect to TiO₂ surface. Interestingly, replacing of COOH to PO₃H₂ does not impact the IPCE ⁶².

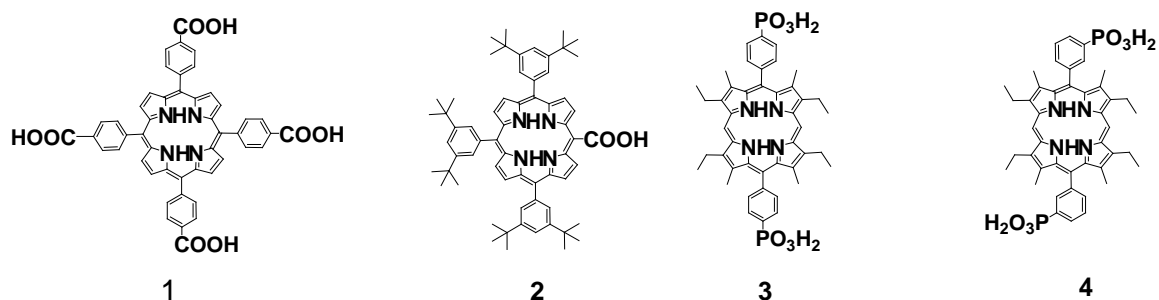


Figure 2-10: Structure of the porphyrin sensitizers

In addition, binding state and amounts of dye adsorbed are also important factors in IPCE⁶².

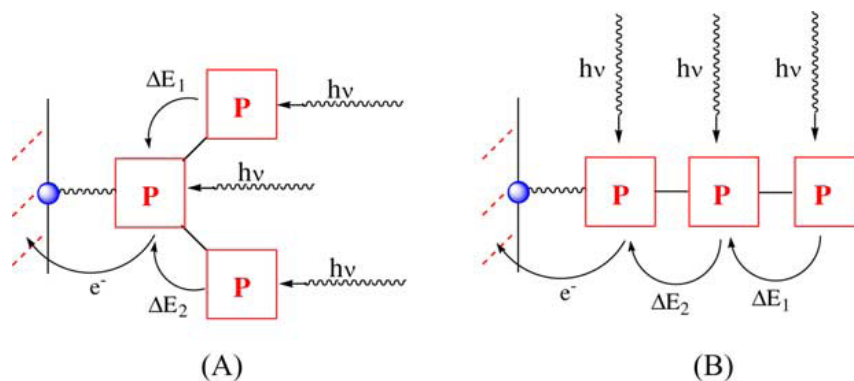


Figure 2-11: Branched A and B approaches to chromophore antenna system⁶². Reprinted from Campbell, W. M.; Burrell, A. K.; Officer, D. L.; Jolley, K. W. *Coordination Chemistry Reviews* **2004**, *248*, 1363-1379. Copy right (2004) with the permission from Elsevier

There are significant energy-related problems associated with multi-component chromophore systems. If a finite energy demand (ΔE) exists for each parallel transfer step, a branch design (Figure 2-11, A), utilizing parallel energy processes ($\Delta E_{\text{total}} = (1/\Delta E_1 + 1/\Delta E_2)^{-1}$), should be more energy efficient than the linear design (Figure 2-11, B) where all processes are in series and energy demands are additive ($\Delta E_{\text{total}} = \Delta E_1 + \Delta E_2$). In the case of the highly branched antenna system, however, a much larger surface area on the

SC will be occupied by each bound chromophoric array, compared to that of a linear array sensitizer. At saturation coverage, this would reduce any gain achieved from the antennae effect. From this point of view, the linear design would be superior to the branched one. In order to obtain the best result in linear array a full covered dye monolayer seems to be the best however, a monolayer of dye absorbs a few percentage of light because it occupies an area that is much larger than its optical cross section. Therefore, LHE of dye monolayer on TiO₂ surface is very low.

Rochford J. et al.⁷⁸ studied four *para*- and *meta*-Zn(II) tetra(carboxyphenyl)porphyrins in solution and bound to metal oxide (TiO₂, ZnO, and ZrO₂) nanoparticle films to determine the effect of the spacer length and anchoring group position on their photoelectrochemical and photophysical properties (Figure 2-11). Both COOH and COOEt₃NH derivatives were employed for the binding studies as well as solution studies. Solution phase electrochemistry studies were performed on the methyl ester derivatives (COOMe). In *m*-ZnTCPP, *m*-ZnTCP₂P, and *m*-ZnTC(PEP)P the anchoring groups are in meta position on the *meso*-phenyl rings. The meta substitution favored a planar binding mode to the metal oxide surfaces, as determined by a combination of studies that included IR, UV, and solar cell efficiencies on TiO₂. Fluorescence emission was studied on ZrO₂. All studies indicated that only *p*-ZnTCPP aggregated, suggesting close packing of the dye molecules on the semiconductor surface. Aggregation effects were not observed for the meta porphyrins. These observations are consistent with the work of others on *p*-ZnTCPP and *m*-ZnTCPP. The

photoelectrochemical behavior of the para- and meta-substituted porphyrin sensitizers suggests that the binding geometry, as well as the distance of the sensitizer from the metal oxide surface, dramatically influence their efficiencies. The greater efficiency of the rigid planar meta-substituted systems was explained in terms of a greater charge injection into the TiO_2 semiconductor from rings that lie flat, and closer, to the surface.

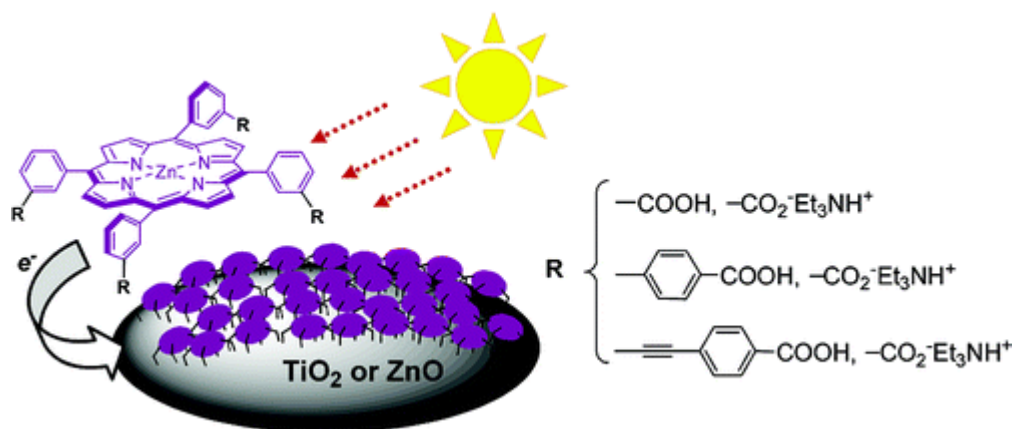


Figure 2-12: *m*-ZnTCPP on the surface of TiO_2 or ZnO ⁷⁸. Reprinted from Rochford, J.; Chu, D.; Hagfeldt, A.; Galoppini, E. *J. Am. Chem. Soc.* **2007**, *129*, 4655-4665. Copy right (2007) with the permission from American Chemical Society.

2.5 Efficiency measurement

There are three different efficiency measurement methods for evaluating the performance of photoelectrolysis cells such as: photoconversion efficiency (PCE), quantum efficiency (IPCE) and absorbed photo to current conversion efficiency (APCE).

2.5.1 Photo conversion efficiency (PCE)

The photo conversion efficiency of water electrolysis is calculated based on the following relation.⁷⁹

$$\eta = [J_{\text{ph}} \times (1.23 - E_{\text{app}}) \times 100\%] / I_0 \quad (2-4)$$

$$E_{\text{app}} = |E_{\text{means}} - E_{\text{oc}}| \quad (2-5)$$

Where J_{ph} (A/m^2) is the photocurrent density; E_{app} (V) is applied potential which can be obtained from eq. (2-5); E_{means} (V) is the potential applied to photo anode versus a reference electrode; E_{oc} (V) is the open circuit potential of photo anode under illumination; I_0 (W/m^2) is the intensity of incident light. Figure 2-13 shows the I-V measurement of as anodized TiO_2 nanotubes in 1M KOH solution as a function of potential applied to the photo anode with reference to a Ag/AgCl reference electrode. It is obvious that the photocurrent increases with increasing the applied potential to the anode. The photocurrents developed under illumination were compared with that in the dark. It shows that almost no current was developed in the dark. Based on the eq. (2-4) and (2-5), the photo conversion efficiency into hydrogen generation of annealed nanotubular arrays of TiO_2 in 1M KOH is plotted as a function of external potential applied to the photo anode.

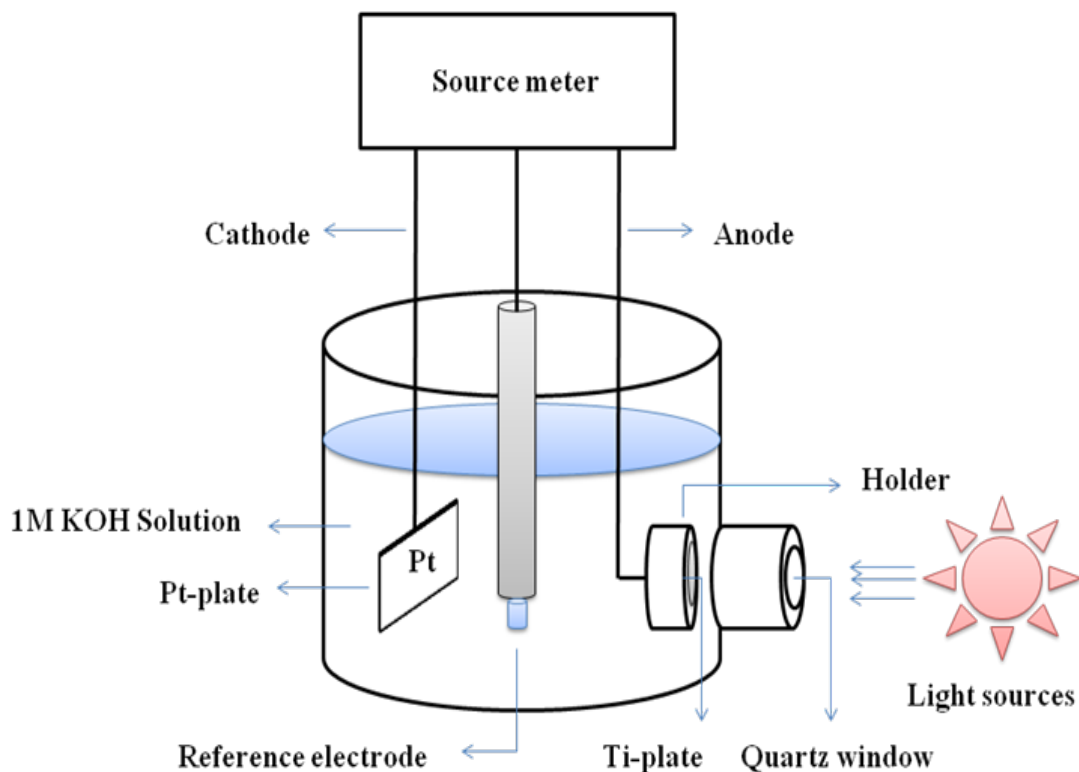


Figure 2-13: Set-up for PCE measurement

2.5.2 Quantum efficiency (IPCE)

IPCE is a measure of the effectiveness in converting photon's incident on the cell to photocurrent flowing between the working and counter electrodes. The IPCE can be calculated using equation (2-6).⁸⁰

$$\text{IPCE} = 1240 I_p(\lambda) / P(\lambda)\lambda \quad (2-6)$$

$I_p(\lambda)$ (A/m^2) is the photocurrent density at wavelength λ . $P(\lambda)$ (W/m^2) is power density at wavelength λ . IPCE also can be expressed as (2-1)

$$\text{IPCE} \sim \text{LHE} \times \phi_{\text{inj}} \times \eta \quad (2-1)$$

The light harvesting efficiency (LHE), the electron-injection yield (ϕ_{inj}) and the electron collecting efficiency (η) in the external circuit.

2.5.3 Absorbed photo to current conversion efficiency (APCE)

APCE also called the internal quantum efficiency and is defined as the number of electrons (or holes) collected per absorbed photon. It is calculated after considering the losses in incident photons like reflection, scattering, absorption, etc. APCE and IPCE are related by equation (2-7) ⁸¹

$$\text{APCE} = \text{IPCE} / \text{LHE} \quad (2-7)$$

$$\text{LHE} = 1 - 10^{-\text{Abs}} \quad (2-2)$$

2.6 Application

One of the most important research areas for future clean energy applications is to look for efficient materials for the production of electricity and/or hydrogen. The dye sensitized solar cell convert solar energy into electrical energy for solar cell applications. For example, an overall solar to current conversion efficiency of 10.6% has been reached by the group led by Gratzel with DSSC technology.⁸² TiO₂ nanotubes have been widely studied for water splitting and hydrogen production due to their suitable electronic band structure given the redox potential of water^{83, 84, 85}. Another application of TiO₂ nanotubes is the photocatalytic decomposition of various pollutants⁸⁶. Apart from above three major applications, the TiO₂ nanotubes surface can be used as antimicrobial⁸⁷ surfaces.

2.6.1 Solar cell

The dye-sensitized solar cell (DSSC) has attracted considerable interest because of the attractive properties, such as low production cost and low environmental impact during fabrication. However, a comparison with conventional solid-state junction devices made of

crystalline silicon indicates that the DSSC has a relatively low conversion efficiency of 10.6%. The overall efficiency (η) of the photovoltaic cell is calculated using equation (2-8) from the short circuit current density (J_{sc}), the open circuit photovoltage (V_{oc}), the fill factor (ff) and the intensity of incident light (I_s)

$$\eta = (J_{sc} V_{oc} ff)/I_s \quad (2-8)$$

Studies suggest that the possibility of fabricating highly efficient dye solar cells by increasing the length of the nanotube array on the negative electrode as the amount of the absorbed dye appears to be the limiting factor. A second key factor that impacts photoconversion efficiency is uniform dye absorption within the pores of the nanotube arrays. The nanotube array geometry has only one entrance, or exit, makes the prospect of pore filling by a liquid more challenging since the air may be trapped. A third factor for improvement is the ff , which is reduced with increasing series resistance. The series resistance will be increased, and hence ff reduced, with increasing barrier layer thickness, and poor contact between the barrier layer and FTO substrate. The barrier layer thickness can be reduced using a step-wise reduction in the anodization voltage⁸⁸, followed as needed by an acid rinse to further thin the barrier layer. Adhesion between the barrier layer and FTO substrate is a function of initial Ti film quality, in turn dependent upon deposition parameters. Finally, we note that the resistance of the FTO substrate increases at least one order of magnitude with the oxygen annealing step needed to crystallize the nanotube array. Modification of this annealing step should facilitate retention of the FTO-conducting properties thus increasing the ff .

2.6.2 Solid-state dye sensitized solar cells

TiO₂ nanomaterials can be an electron acceptor due to the n-type polarity. The charge neutrality on the dye being restored by a hole delivered by the complementary semiconductor inorganic^{89,90} or organic^{91,92} of p-type polarity. Normally, the conversion efficiency of solid-state dye sensitized solar cells is much lower than the corresponding common dye sensitized solar cell. Since the first report on this system in 1998, it is photovoltaic conversion efficiency has been improved considerably. The highest efficiency of 5.0% was recently achieved.⁹³

2.6.3 Water splitting

As one of the major applications of TiO₂ nanotubes the water splitting is the general term for a chemical reaction in which water is converted into oxygen and hydrogen⁹⁴. Water splitting is actively researched because demand for cheap hydrogen is expected to rise with the new hydrogen economy. A simple laboratory water splitting set-up shows in Figure 2-14.⁹⁵

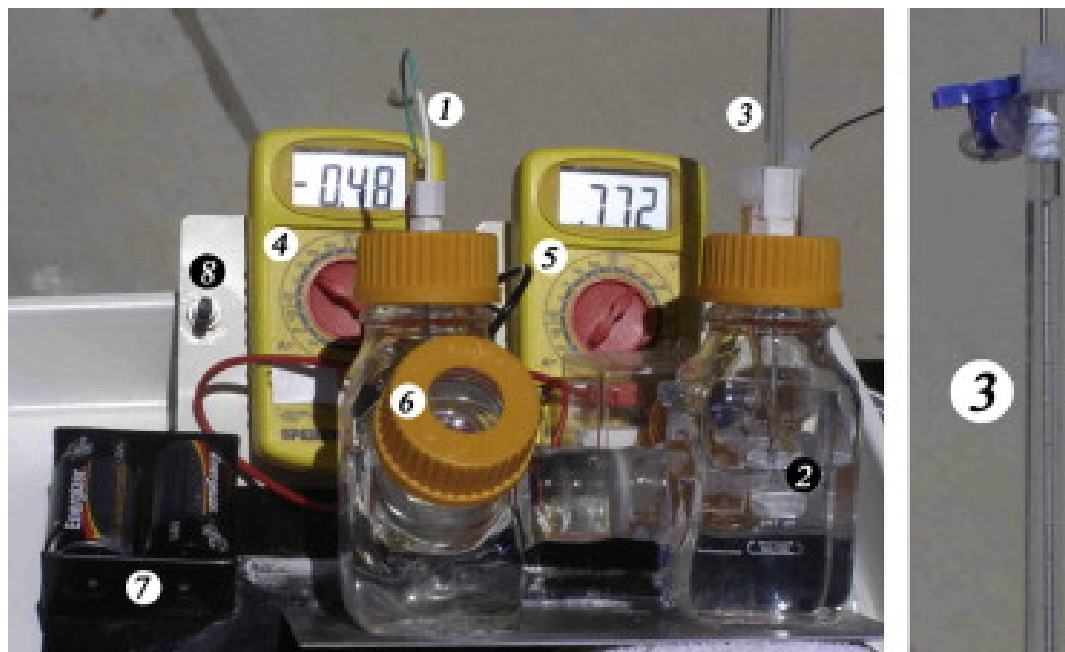


Figure 2-14: Homemade photocell for hydrogen generation under sunlight. (1) TiO₂ nanotube arrays anode, (2) Pt wire spiral cathode, (3) gas burette, (4) multimeter for voltage, (5) multimeter for current, (6) focus lens, (7) battery, (8) voltage adjust button.⁹⁵ Reprinted from Liu, Z., Pesic, B., Raja, K.S., Rangaraju, R.R., Misra, M. *International Journal of Hydrogen Energy* **2009**, *34*, 3250-3257. Copy right (2008) with the permission from Elsevier.

2.6.4 Degradation of Organics

Dye sensitized TiO₂ nanotubes oxidize organics into CO₂ and H₂O. Mechanism is showing blow (Figure 2-15)

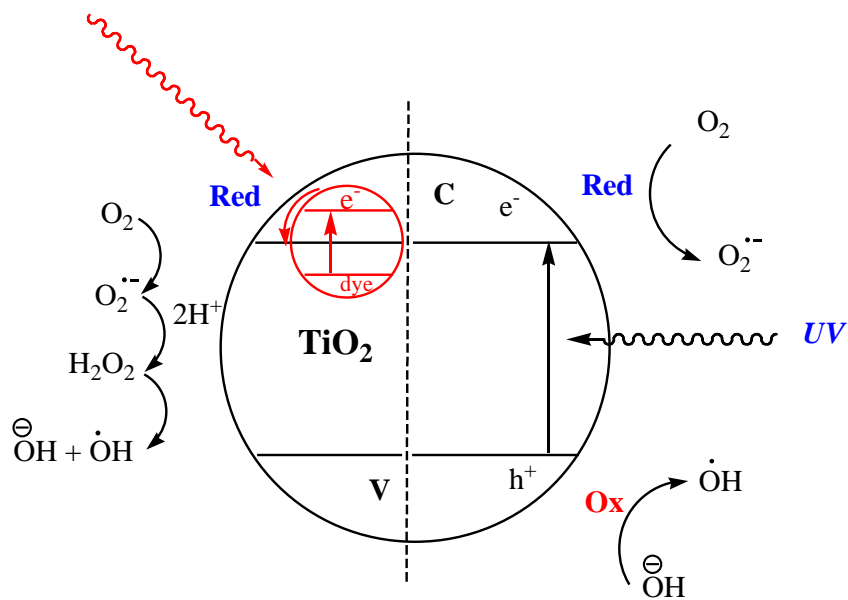


Figure 2-15: The photoactivation mechanism of TiO₂

These 1D TiO₂ nanotubes, with both internal and external surface areas being available for chemical reaction, are promising materials for surface functionalization. The integrated electrode (with TiO₂ nanotubes standing on the Ti surface) gives better stability and geometrical exposure to react better with the substrate compared to other TiO₂ architectures. Mohapatra et al.⁹⁶ reported the synthesis of highly disperse Pd nanoparticles on vertically oriented TiO₂ nanotube arrays (Pd/TiO₂). The catalytic activity of Pd/TiO₂ is tested for the decoloration of two organic dyes, viz., methyl red (MR) and methyl orange (MO).

2.7 References

- (1) Chen, X.; Mao, S. S. *Chem. Rev.* **2007**, *107*, 2891-2959.
- (2) Likodimos, V.; Dionysiou, D. D.; Falaras, P. *Re-views in Environmental Science and Biotechnology* **2010**, *9*, 87-94.
- (3) Arconada, N.; Durán, A.; Suárez, S.; Portela, R.; Coronado, J. M.; Sánchez, B.; Castro, Y. *Appl. Catal. B Environ.* **2009**, *86*, 1-7.
- (4) Campostrini, R.; Ischia, M.; Palmisano, L. *J Therm Anal Calor* **2003**, *71*, 1011-1021.
- (5) Eiamchai, P.; Chindaudom, P.; Pokaipisit, A.; Limsuwan, P. *Curr.Appl.Phys.* **2009**, *9*, 707-712.
- (6) Li Puma, G.; Bono, A.; Krishnaiah, D.; Collin, J. G. *J. Hazard. Mater.* **2008**, *157*, 209-219.
- (7) Rooth, M.; Quinlan, R. A.; Widenkvist, E.; Lu, J.; Grennberg, H.; Holloway, B. C.; Hårsta, A.; Jansson, U. *J. Cryst. Growth* **2009**, *311*, 373-377.
- (8) Doong, R. -.; Kao, I. -. *Recent Pat. Nanotechnol.* **2008**, *2*, 84-102.
- (9) Li, S.; Zhang, G.; Guo, D.; Yu, L.; Zhang, W. *Journal of Physical Chemistry C* **2009**, *113*, 12759-12765.
- (10) Yeonmi, S.; Seonghoon, L. *Nano Letters* **2008**, *8*, 3171-3173.
- (11) Yu, J.; Xiang, Q.; Zhou, M. *Applied Catalysis B: Environmental* **2009**, *90*, 595-602.
- (12) Sun, L.; Li, J.; Wang, C. L.; Li, S. F.; Chen, H. B.; Lin, C. J. *Solar Energy Mater. Solar Cells* **2009**, *93*, 1875-1880.

- (13) Li, J.; Yun, H.; Lin, C. -. In *In Investigations on the Fe-doped TiO₂ nanotube arrays as a photoanode for cathodic protection of stainless steel*; 2008; Vol. 3, pp 1-9.
- (14) Sekino, T.; Okamoto, T.; Kasuga, T.; Kusunose, T.; Nakayama, T.; Niihara, K. *Key Eng Mat* **2006**, 317-318, 251-254.
- (15) Huang, C.; Liu, X.; Liu, Y.; Wang, Y. *Chemical Physics Letters* **2006**, 432, 468-472.
- (16) Ghicov, A.; Schmidt, B.; Kunze, J.; Schmuki, P. *Chemical Physics Letters* **2007**, 433, 323-326.
- (17) Zhao, J.; Wang, X.; Kang, Y.; Xu, X.; Li, Y. *IEEE Photonics Technology Letters* **2008**, 20, 1213-1215.
- (18) Liu, H.; Liu, G.; Zhou, Q. *Journal of Solid State Chemistry* **2009**.
- (19) Xu, Y. -.; Chen, C.; Yang, X. -.; Li, X.; Wang, B. -. *Appl. Surf. Sci.* **2009**, 255, 8624-8628.
- (20) Khan, M. A.; Han, D. H.; Yang, O. -. *Appl. Surf. Sci.* **2009**, 255, 3687-3690.
- (21) Wang, M.; Song, G.; Li, J.; Miao, L.; Zhang, B. *Journal of University of Science and Technology Beijing: Mineral Metallurgy Materials (Eng Ed)* **2008**, 15, 644-648.
- (22) Ding, D.; Ning, C.; Huang, L.; Jin, F.; Hao, Y.; Bai, S.; Li, Y.; Li, M.; Mao, D. *Nanotechnology* **2009**, 20.
- (23) Jang, S. -.; Choe, H. -.; Ko, Y. -.; Brantley, W. A. *Thin Solid Films* **2009**, 517, 5038-5043.
- (24) Lee, K.; Kim, W. -.; Cho, J. -.; Eun, S. -.; Choe, H. -. *Transactions of Nonferrous Metals Society of China (English Edition)* **2009**, 19, 857-861.

- (25) Jeong, Y.-H.; Kim, W.-G.; Park, G.-H.; Choe, H.-C.; Ko, Y.-M. *Transactions of Nonferrous Metals Society of China (English Edition)* **2009**, *19*, 852-856.
- (26) Kim, W. -.; Choe, H. -.; Ko, Y. -.; Brantley, W. A. *Thin Solid Films* **2009**, *517*, 5033-5037.
- (27) Shrestha, N. K.; Nah, Y. -.; Tsuchiya, H.; Schmuki, P. *Chemical Communications* **2009**, 2008-2010.
- (28) Nah, Y. -.; Ghicov, A.; Kim, D.; Berger, S.; Schmuki, P. *J. Am. Chem. Soc.* **2008**, *130*, 16154-16155.
- (29) Ghicov, A.; Macak, J. M.; Tsuchiya, H.; Kunze, J.; Haeublein, V.; Frey, L.; Schmuki, P. *Nano Letters* **2006**, *6*, 1080-1082.
- (30) Macak, J. M.; Tsuchiya, H.; Taveira, L.; Ghicov, A.; Schmuki, P. *Journal of Biomedical Materials Research - Part A* **2005**, *75*, 928-933.
- (31) Dong, F.; Wang, H.; Wu, Z. *Journal of Physical Chemistry C* **2009**, *113*, 16717-16723.
- (32) Reddy, K. M.; Baruwati, B.; Jayalakshmi, M.; Rao, M. M.; Manorama, S. V. *Journal of Solid State Chemistry* **2005**, *178*, 3352-3358.
- (33) Wang, Q.; Jiang, Z.; Wang, Y.; Chen, D.; Yang, D. *Journal of Nanoparticle Research* **2009**, *11*, 375-384.
- (34) Shi, J.; Li, J.; Cai, Y. -. *Wuli Huaxue Xuebao/ Acta Physico - Chimica Sinica* **2008**, *24*, 1283-1286.
- (35) Fan, X. -.; Zhang, Y. -.; Xiao, P.; Hu, F.; Zhang, H. *Chinese Journal of Chemical Physics* **2007**, *20*, 753-758.

- (36) Chen, X.; Zhang, X.; Su, Y.; Lei, L. *Appl. Surf. Sci.* **2008**, *254*, 6693-6696.
- (37) Yu, Y.; Wu, H. -.; Zhu, B. -.; Wang, S. -.; Huang, W. -.; Wu, S. -.; Zhang, S. -. *Catalysis Letters* **2008**, *121*, 165-171.
- (38) Su, Y.; Zhang, X.; Han, S.; Chen, X.; Lei, L. *Electrochemistry Communications* **2007**, *9*, 2291-2298.
- (39) Jiang, Z.; Yang, F.; Luo, N.; Chu, B. T. T.; Sun, D.; Shi, H.; Xiao, T.; Edwards, P. P. *Chemical Communications* **2008**, 6372-6374.
- (40) Feng, C.-X.; Wang, Y.; Jin, Z.-S.; Zhang, S.-L. *Wuli Huaxue Xuebao/ Acta Physico - Chimica Sinica* **2008**, *24*, 633-638.
- (41) Chen, Y.; Zhang, S.; Yu, Y.; Wu, H.; Wang, S.; Zhu, B.; Huang, W.; Wu, S. *J. Dispersion Sci. Technol.* **2008**, *29*, 245-249.
- (42) Kim, D.; Fujimoto, S.; Schmuki, P.; Tsuchiya, H. *Electrochemistry Communications* **2008**, *10*, 910-913.
- (43) Langhuan, H.; Zhongxin, S.; Yingliang, L. *J Ceram Soc Jpn* **2007**, *115*, 28-31.
- (44) Macak, J. M.; Ghicov, A.; Hahn, R.; Tsuchiya, H.; Schmuki, P. *J. Mater. Res.* **2006**, *21*, 2824-2828. (45) Ghicov, A.; Aldabergenova, S.; Tsuchiya, H.; Schmuki, P. *Angewandte Chemie - International Edition* **2006**, *45*, 6993-6996.
- (45) Lu, N.; Zhao, H.; Li, J.; Quan, X.; Chen, S. *Separation and Purification Technology* **2008**, *62*, 668-673.
- (46) Su, Y.; Han, S.; Zhang, X.; Chen, X.; Lei, L. *Mater. Chem. Phys.* **2008**, *110*, 239-246.

- (47) Lu, N.; Quan, X.; Li, J.; Chen, S.; Yu, H.; Chen, G. *Journal of Physical Chemistry C* **2007**, *111*, 11836-11842.
- (48) Zhang, Y.; Fu, W.; Yang, H.; Liu, S.; Sun, P.; Yuan, M.; Ma, D.; Zhao, W.; Sui, Y.; Li, M.; Li, Y. *Thin Solid Films* **2009**, *518*, 99-103.
- (49) Chen, X.; Su, Y.; Zhang, X.; Lei, L. *Chinese Science Bulletin* **2008**, *53*, 1983-1987
- (50) Nishijima, K.; Fujisawa, Y.; Murakami, N.; Tsubota, T.; Ohno, T. *Applied Catalysis B: Environmental* **2008**, *84*, 584-590.
- (51) Xiong, C.; Ratanatawanate, C.; Balkus Jr., K. *ACS National Meeting Book of Abstracts* **2007**, *1*
- (52) Yin, Y.; Jin, Z.; Hou, F. *Nanotechnology* **2007**, *18*, 495608.
- (53) Bao, H. -.; Xu, Z. -.; Yin, H. -.; Zheng, Y. -.; Chen, W. -. *Chinese Journal of Inorganic Chemistry* **2005**, *21*, 374-378.
- (54) Paramasivam, I.; Macak, J. M.; Schmuki, P. *Electrochemistry Communications* **2008**, *10*, 71-75.
- (55) Grätzel, M. *Journal of Photochemistry and Photobiology C: Photochemistry Reviews* **2003**, *4*, 145-153.
- (56) Campbell, W. M.; Burrell, A. K.; Officer, D. L.; Jolley, K. W. *Coordination Chemistry Reviews* **2004**, *248*, 817-833.
- (57) Amao, Y. *Curr.Nanosci.* **2008**, *4*, 45-52.
- (58) Amao, Y.; Takeuchi, Y. *Int J Hydrogen Energy* **2008**, *33*, 2845-2849.
- (59) Zhou, J.; Takeuchi, M.; Ray, A. K.; Anpo, M.; Zhao, X. S. *Journal of Colloid and*

Interface Science **2007**, *311*, 497-501.

- (60) Kroeze, J. E.; Savenije, T. J.; Warman, J. M. *J.Photochem.Photobiol.A Chem.* **2002**, *148*, 49-55.
- (61) Campbell, W. M.; Burrell, A. K.; Officer, D. L.; Jolley, K. W. *Coordination Chemistry Reviews* **2004**, *248*, 1363-1379.
- (62) (1) Hao, Y.; Yang, M.; Yu, C.; Cai, S.; Liu, M.; Fan, L.; Li, Y. *Solar Energy Mater. Solar Cells* **1998**, *56*, 75-84.
- (63) Zhang, D.; Yoshida, T.; Minoura, H. *Advanced Materials* **2003**, *15*, 814-817.
- (64) Houarner-Rassin, C.; Blart, E.; Buvat, P.; Odobel, F. *Photochem.Photobiol.Sci.* **2008**, *7*, 789-793.
- (65) Higgins, R. W. T.; Zaidi, N. A.; Monkman, A. P. *Advanced Funtional Materials* **2001**, *11*, 407-412.
- (66) Shaheen, S. E.; Brabec, C. J.; Sariciftci, N. S.; Padinger, F.; Fromherz, T.; Hummelen, J. C. *Applied Physics Letters* **2001**, *78*, 841-843.
- (67) Takahashi, K.; Takano, Y.; Yamaguchi, T.; Nakamura, J. -.; Yokoe, C.; Murata, K. *Synth Met* **2005**, *155*, 51-55.
- (68) Espinosa, R.; Zumeta, I.; Santana, J. L.; Martínez-Luzardo, F.; González, B.; Docteur, S.; Vigil, E. *Sol Energ Mater Sol Cells* **2005**, *85*, 359-369.
- (69) Boschloo, G.; Lindström, H.; Magnusson, E.; Holmberg, A.; Hagfeldt, A. *Journal of Photochemistry and Photobiology A: Chemistry* **2002**, *148*, 11-15.
- (70) De Paoli, M. -.; Nogueira, A. F.; Machado, D. A.; Longo, C. *Electrochimica Acta*

- 2001**, 46, 4243-4249.
- (71) Lindström, H.; Holmberg, A.; Magnusson, E.; Malmqvist, L.; Hagfeldt, A. *Journal of Photochemistry and Photobiology A: Chemistry* **2001**, 145, 107-112.
- (72) Longo, C.; Freitas, J.; De Paoli, M. -. *Journal of Photochemistry and Photobiology A: Chemistry* **2003**, 159, 33-39.
- (73) Longo, C.; Nogueira, A. F.; De Paoli, M. -.; Cachet, H. *Journal of Physical Chemistry B* **2002**, 106, 5925-5930.
- (74) Kalyanasundaram, K.; Grätzel, M. *Coord. Chem. Rev.* **1998**, 177, 347-414.
- (75) Palomares, E.; Clifford, J. N.; Haque, S. A.; Lutz, T.; Durrant, J. R. *Chem. Commun.* **2002**, 1464-1465.
- (76) Odobel, F.; Blart, E.; Lagrée, M.; Villieras, M.; Boujtita, H.; El Murr, N.; Caramori, S.; Bignozzi, C. A. *Journal of Materials Chemistry* **2003**, 13, 502-510.
- (77) Rochford, J.; Chu, D.; Hagfeldt, A.; Galoppini, E. *J. Am. Chem. Soc.* **2007**, 129, 4655-4665.
- (78) Khan, S. U. M.; Al-Shahry, M.; Ingler Jr., W. B. *Science* **2002**, 297, 2243-2245.
- (79) Shankar, K.; Mor, G. K.; Fitzgerald, A.; Grimes, C. A. *J. Phys. Chem. C.* **2007**, 111, 21-26.
- (80) Nazeeruddin, M. K.; Kay, A.; Rodicio, I.; Humphry-Baker, R.; Muller, E.; Liska, P.; Vlachopoulos, N.; Gratzel, M. *J. Am. Chem. Soc.* **1993**, 115, 6382-6390.
- (81) Grätzel, M. *J. Photochem. Photobiol., A* **2004**, 164, 3-14.
- (82) Zhang, Z.; Hossain, M. F.; Takahashi, T. *Int J Hydrogen Energy* **2010**, 35, 8528-8535.

- (83) Bai, J.; Li, J.; Liu, Y.; Zhou, B.; Cai, W. *Applied Catalysis B: Environmental* **2010**, *95*, 408-413.
- (84) Gong, J.; Lai, Y.; Lin, C. *Electrochim. Acta* **2010**, *55*, 4776-4782.
- (85) He, X.; Cai, Y.; Zhang, H.; Liang, C. *Journal of Materials Chemistry* **2011**, *21*, 475-480.
- (86) Díaz-Visurraga, J.; Meléndrez, M. F.; García, A.; Paulraj, M.; Cárdenas, G. *J. Appl. Polym. Sci.* **2010**, *116*, 3503-3515.
- (87) Pang, Q.; Leng, L.; Zhao, L.; Zhou, L.; Liang, C.; Lan, Y. *Mater. Chem. Phys.* **2011**, *125*, 612-616.
- (88) Cameron, P.J.; Peter, L.M.; Zakeeruddin, S.M.; Grätzel, M. *Coordination Chemistry Reviews* **2004**, *248*, 1447-1453.
- (89) Lee, H. J.; Chen, P.; Moon, S.-J.; Sauvage, F.; Sivula, K.; Bessho, T.; Gamelin, D. R.; Nazeeruddin, M. K. *Langmuir* **2009**, *25*, 7602-7608.
- (90) Chen, P.; Yum, J. H.; De Angelis, F.; Mosconi, E.; Fantacci, S.; Moon, S. -J.; Baker, R. H.; Grätzel, M. *Nano Letters* **2009**, *9*, 2487-2492.
- (91) Choi, H.; Baik, C.; Kang, S. O.; Ko, J.; Kang, M. S.; Nazeeruddin, M. K.; Grätzel, M. *Angewandte Chemie - International Edition* **2009**, *48*, 1701-1712.
- (92) Pattantyus-Abraham, A. G.; Kramer, I. J.; Barkhouse, A. R.; Wang, X.; Konstantatos, G.; Debnath, R.; Levina, L.; Raabe, I.; Nazeeruddin, M. K.; Grätzel, M.; Sargent, E. H. *ACS Nano* **2010**, *4*, 3374-3380.
- (93) Alam Khan, M.; Shaheer Akhtar, M.; Woo, S. I.; Yang, O. -B. *Catalysis*

Communications **2008**, *10*, 1-5

(94) Liu, Z., Pesic, B., Raja, K.S., Rangaraju, R.R., Misra, M. *International Journal of*

Hydrogen Energy **2009**, *34*, 3250-3257.

(95) Mohapatra, S.K.; Kondamudi, N.; Banerjee, S.; Misra, M. *Langmuir* **2008**, *24*,

11276-11281.

Chapter 3

An Innovative Approach to Synthesize Highly-Ordered TiO₂ Nanotubes

A version of this chapter was published as:

Tayirjan T. Isimjan, Sohrab Rohani, Ajay K. Ray. “An Innovative Approach to Synthesize Highly-Ordered TiO₂” *Journal of Nanoscience and Nanotechnology*. 2011, 11, 1079-1083.

3.1 Abstract

Although much progress has been achieved in the last few years for preparing ordered TiO₂ nanotubes by anodization, the resulting nanotubes still possess a broad pore size distribution and a rough top surface because of the uneven Ti substrate, in the absence of an electropolishing step. Herein, we describe a facile route to form highly ordered TiO₂ nanotubes with controlled dimensions. The proposed method uses sonication assisted fabrication and cleaning of TiO₂ nanotubes from electrochemical anodized Ti foil. The main processes involve three steps. (1) Electrochemical anodization of Ti foil in NH₄F electrolytes, (2) heat treatment of the TiO₂ nanostructures in a short period of time (approximately 30 min at 100°C) and (3) a mild sonication of TiO₂ nanostructures.

Keywords: TiO₂ nanotubes; TiO₂ nanowires; Anodization; Annealing; Sonication.

3.2 Introduction

Titanium dioxide based nanotubes have attracted much attention due to the potential applications in ultraviolet nanoelectronics^{1,2} and photonics³. Self-organized TiO₂ nanotube arrays not only have a large specific surface area but also their self-aligned nature leads to a significant enhancement of the performance when used in self-cleaning surface coating^{4,5}, photoelectrochemistry^{6,7}, dye-sensitized solar cells⁸, biomedical applications⁹⁻¹² and electrochromic devices¹³. The electronic and optical properties of the titanium dioxide nanotubes are largely dependent on their crystal structure, dimension, and morphology. In particular, one-dimensional titanium dioxide nanotubes with controlled morphology offer great potential in efficient assembly and performance of nanoscale devices due to quantum confinement of charge carriers in small dimensions¹⁴.

There have been various ways of fabricating highly ordered regular arrays of nanostructures in a controlled and reproducible way¹⁵⁻¹⁷. The main process still uses electrochemical anodizing of Ti metal in NH₄F electrolytes. Although much progress has been achieved in last few years for preparing of ordered TiO₂ nanotubes by anodizing, the TiO₂ nanotubes still possess a broad pore size distribution and a rough top surface because of an uneven Ti substrate, omitting an electropolishing step. In general, there is a delicate balance between the oxide growth rate, the etching rate and dissolving rate through etching reagent such as fluorine ion which needs to be maintained through anodization process when fabricating self-organized regular titanium dioxide nanotubes. The lattice mismatch between the grown metal oxide and the underlying metal plays a

key role in forming a curved oxide layer on the metal surface. Although nanotubes with lengths of up to several hundreds of micrometers have been reported¹⁸, due to the delicate balance between growing, etching and dissolving rates of nanotubes, it is very difficult to control the morphology of the nanotubes and reproduce them in the same fashion. After a critical anodization time, it is almost impossible to produce nanotubes because either the nanotubes grow too long and collapse creating debris surface or dissolve faster than being etched, and resulting in nanoporous structures. Recently, Seonghoon Lee and his coworkers reported the fabrication of the highly uniform and self-organized nanotubes by electro polishing and two-step anodization¹⁹. In their method, first, a flat Ti surface was achieved by electro polishing a bare Ti foil as purchased. Secondly, a well ordered structure was obtained through the first anodization step performed for 3 h at 30V. Finally, The TiO₂ nanotubular layer was removed by using an adhesive tape and then the highly ordered and self-organized TiO₂ nanotubes were fabricated by performing a second anodization step for 5 min under conditions identical to those in the first anodization step. Even though this technique resulted in highly ordered nanotubes, there were still some difficulties. For example, the method required very harsh electro polishing conditions such as a mixed solution of acid (60%), butanol, and ethanol (1:6:9 in volume) at 20 V and an operating temperature of -20°C for 5 min. In addition the TiO₂ nanotube layer cannot always be removed easily by tape; therefore, there were some parts of TiO₂ nanotube layer remaining. The remaining layers may result in an uneven surface. Overall, reproducing the highly uniform and self-organized surface by this method is not practical.

The highly ordered TiO₂ nanotube arrays are very important not only for the fundamental study of nanostructures but also for the realization of useful devices^{20, 21}. Herein, we describe a facile route to form highly ordered TiO₂ nanotubes with controlled dimensions. The proposed method uses sonication assisted fabrication and cleaning of TiO₂ nanotubes from electrochemical anodized Ti foil. The main processes involve three steps. (1) Electrochemical anodization of Ti foil in NH₄F electrolytes using a typical condition; (2) heat treatment of the TiO₂ nanostructures in a short period of time (approximately 30 min at 100 °C) and (3) a mild sonication of TiO₂ nanostructures.

3.3 Experimental

The Ti foil (0.8 mm thickness, 99.6 % purity) and all chemicals were purchased from Alfa-Aesar (Ward Hill, MA, USA). Prior to anodization, the titanium foil was cleaned by using distilled water and acetone. It was then dried off in air, etched in (3.4 M HF+5M HNO₃) for 30 s, rinsed with deionized water, dried with air and used immediately.

The polished Ti foil was anodized in an ethylene glycol (EG) solution containing NH₄F (0.38 wt%) and H₂O (1.79 wt%), and placed in a well-insulated bath for several hours at 30 V and at room temperature using a DC power supply. After the anodization, the sample was washed with distilled water and acetone and then dried off with air. In order to increase the adhesion force between TiO₂ layers with substrate, the prepared sample was annealed at 100°C for 30 min and then sonicated with 240W, 50/60 Hz ultrasonic cleaner (Crest Ultrasonics, Malaysia) for 30 sec.

The electrochemical anodization experiments were performed in a conventional

two-electrode cell. A platinum foil (10mm×20mm) was used as a counter electrode and a titanium sheet served as a working electrode. A Ti sheet of size 1 cm × 1 cm was pressed between a set of O-rings in the sample holder. The Pt wire was located on the back side of the sample as the electrical contact, and then fixed in the electrochemical cell with an active anode area of 0.9 cm² exposed to the electrolyte. During processing, the anode and cathode were parallel with a separation distance of 2 cm. All anodization experiments were performed potentiostatically, under constant applied voltage, at room temperature. The electrochemical anodization was carried out by using a source meter (Keithley 2602, MetricTest, Hayward, CA, USA) interfaced to a computer. The microstructural morphological features of all the samples were examined with a field emission scanning electron microscope (FE-SEM, Hitachi S-5000, Tokyo, Japan). The crystalline phases were recorded by X-ray diffraction using a powder X-ray diffractometer (Rigaku RINT 2500, Tokyo, Japan) with Cu K radiation ($\lambda = 1.54 \text{ \AA}$) at 40 kV and 50 mA with a scan rate of 0.05 °/s and a scan speed of 1 °/min over a 2 θ range from 20° to 90°. Final samples were cleaned by Crest Ultrasonics (Model No: 275 HTA).

3.4 Results and Discussion

Figure 3-1 shows a pictorial presentation of the innovative approach to remove the nanowires from the top layer of the nanotube arrays by sonication.

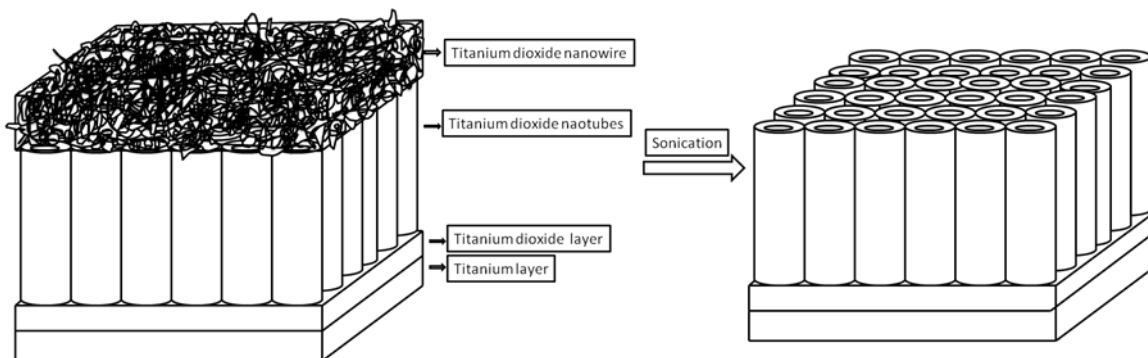


Figure 3-1: Removal of the nanowires layer by sonication and fabrication of highly-ordered titanium nanotube arrays

3.4.1 Surface analysis

Figure 3-2 shows a typical surface morphology of TiO_2 nanostructures in different processes as mentioned in previous section. The non-uniform surface topographical structure can be easily seen for as-prepared samples due to the rough surface of the Ti foil (Figure 3-2a). The SEM cross-section micrograph clearly indicates that the nanostructures formed on Ti metal surface can be composed of two layers (Figure 3-2b): the top layer (region) is very rough and contains low density nanowires with different length. The bottom layer, however, is composed of dense nanotubes with uniform length, the interface of two sections can be clearly seen in the SEM image (Figure 3-2b). The highly ordered nanotubes can be found in SEM image (see Figure 3-2c and 3-2d) after annealing and 30s of sonication. It is noticed that the two layers for as-prepared sample have changed into one layer in the cross-section image (Figure 3-2f), indicating that the top layer has been removed based on the fact of thickness decrease in the cross-section image of the sample experienced during annealing and mild sonication.

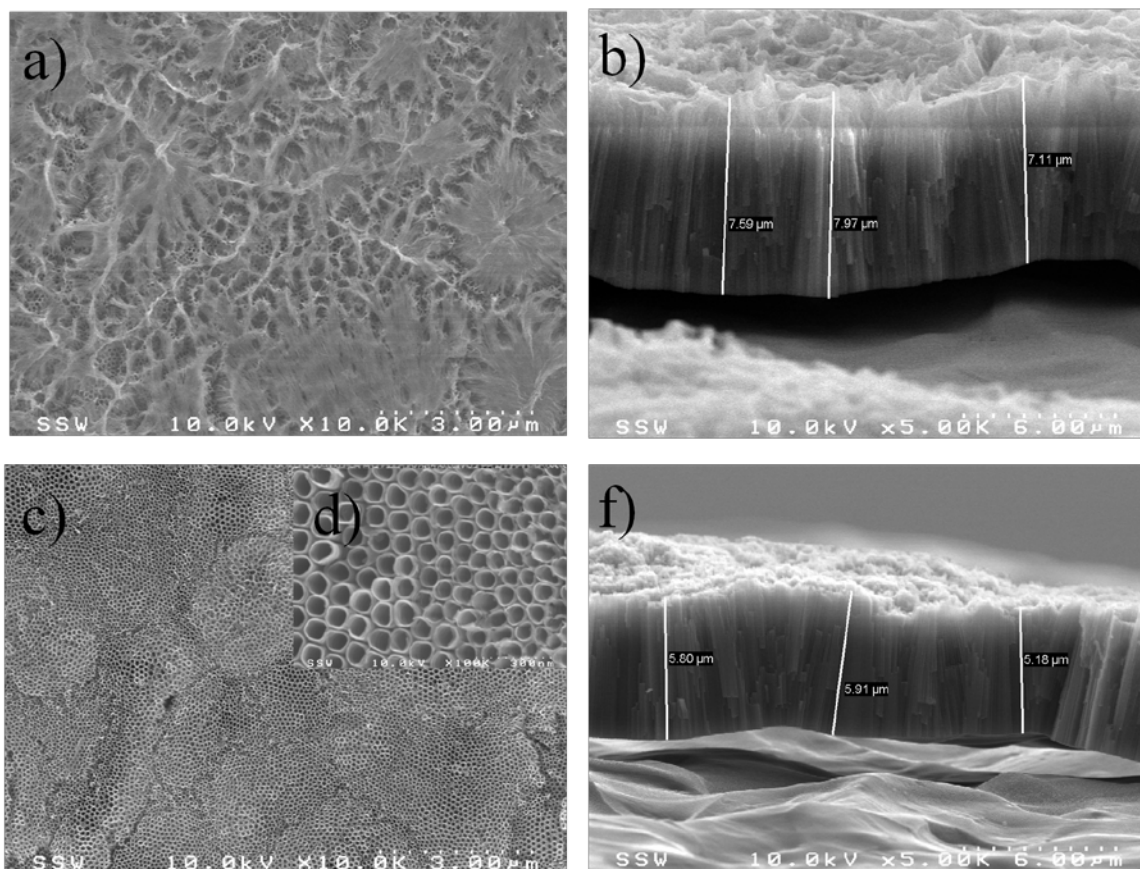


Figure 3-2: FE SEM images of the surfaces of Ti samples anodized in glycerol - 5% water - 3% NH₄F solution at 30V at 4 hrs. (a) top view of as-prepared, (b) cross-section of as-prepared, (c) top view of annealed and sonicated, (d) cross-section of annealed and sonicated, and (e) higher magnification of top view of annealed and sonicated sample

The formation TiO₂ nanotubes follow the widely accepted anodic aluminum oxide (AAO) mechanism²². Firstly, an oxide layer at Ti metal surface is formed when reacting with O²⁻ and OH⁻ at the anode; subsequently the anions diffuse into the oxide layer and continuously react with the metal beneath. Secondly, migration of Ti from the oxide/metal interface to metal/electrolyte interfaces under the electric field. Finally, the chemical dissolution of metal and oxide will proceed due to etching by fluoride ions and

substantially enhanced by the presence of H^+ ion²³. Ti-O bond also becomes weak under the applied electric field which causes the field dissolution of TiO_2 . Ti^{4+} goes into the electrolyte while the free O^{2-} ions diffuse across the oxide layer and react with Ti metal at the oxide/metal interface. Since the neutral electrolytes are used for the Ti anodization in this study, the chemical dissolution can be neglected. Therefore, instead of forming nonporous structure, the TiO_2 nanotubes grow high and then collapse to form nanowires.

The thickness of the as-prepared samples first increased slowly from about 6.0 μm at 3h (Figure 3-5) to 8.0 μm at 7h. It was followed by a rapid increase to reach approximately 13.6 μm at 20h. After sonication treatment, the tube length increased slowly from 5.3 μm to 6.4 μm and then stabilized around 6.7 μm at 7h. From the sonication results we can conclude that with anodizing at 30 V, the growth rate of the nanotubes reached a maximum value (approximately 6.7 μm). In other word, after reaching the maximum length around 6.7 μm , the nanotubes started to collapse to form nanowires. The thickness of TiO_2 layer before and after heat treatment was investigated. The results show that average thickness of as-prepared sample decreased by approximately 0.3 μm after heat treatment due to the changes of crystal structure from amorphous to anatase which was confirmed by XRD (Figure 3-3), hence a compact TiO_2 layer was formed.

3. 4.2 XRD result and thickness analysis

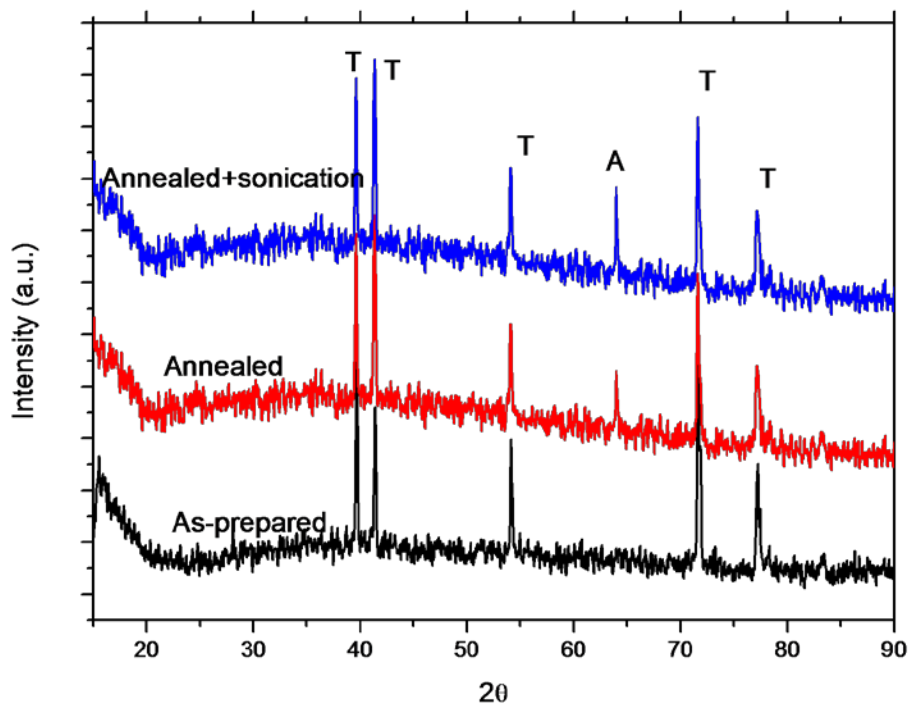


Figure 3-3: XRD pattern for samples from different treatments

The linear increase in the diameter of the TiO_2 nanotubes with anodization time, as shown in Figure 3-4, indicates the etching reaction of TiO_2 during anodization. The change in the thickness of the wall of TiO_2 nanotubes in Figure 3-4 indicates that the initial stage is linear etching, and is followed by reaching a balance between etching and oxidation.

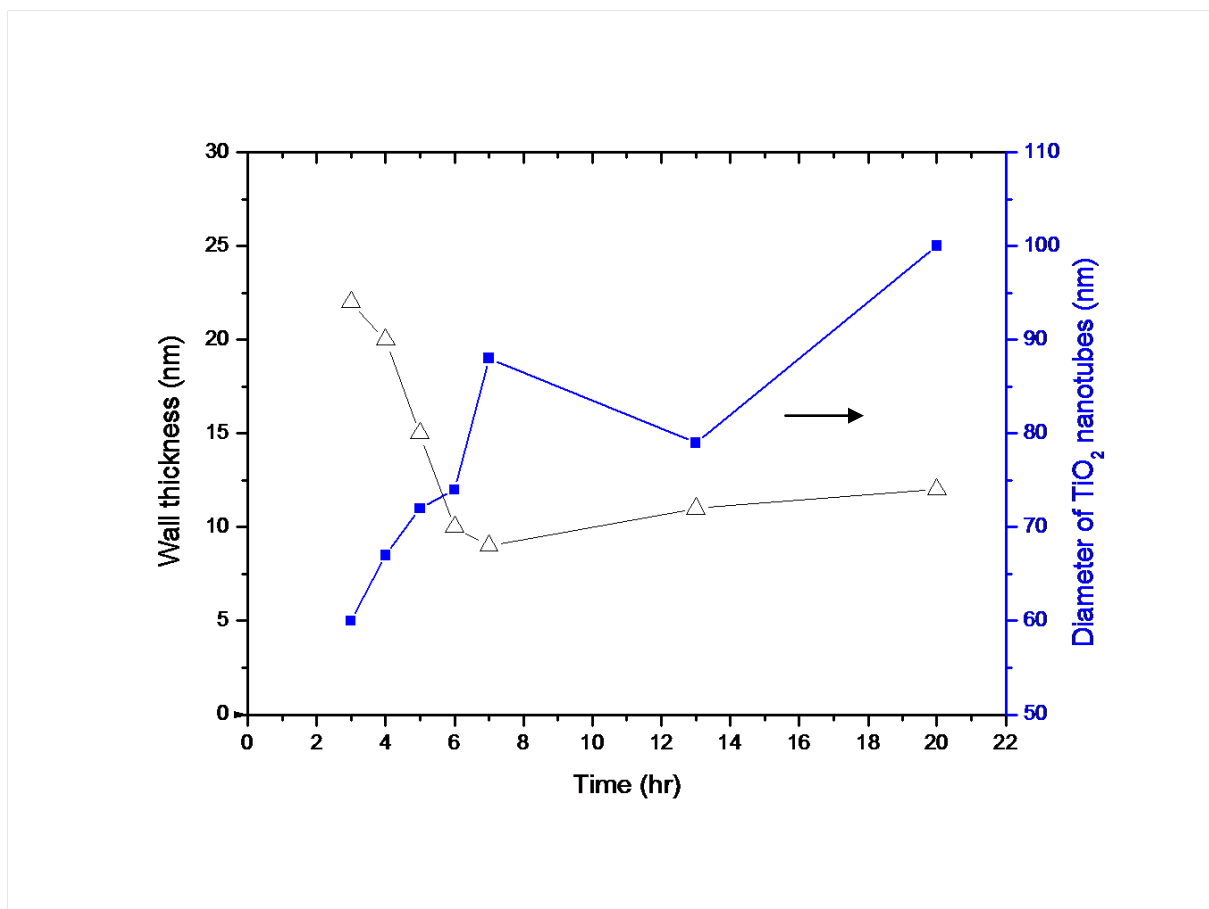


Figure 3-4: The wall thickness and diameter of TiO₂ nanotubes as a function of the preparation time

Figure 3-5 reveals that the length (as-prepared) of TiO₂ nanowire/nanotubes is almost a linear function of the etching time. The initial increase in nanotubes length (for example, up to 5 h), indicates that etching dominates the anodizing in the top layer.

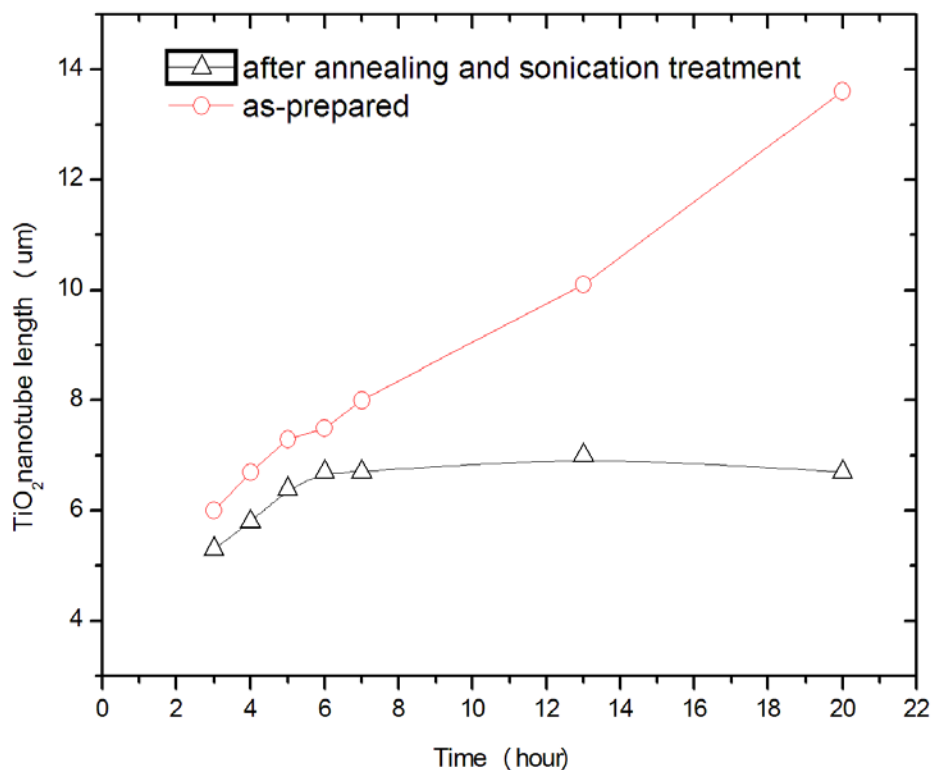


Figure 3-5: The length of TiO₂ layers as a function of preparation time

It is interesting to note that the removing of the top nanowire layer by mild sonication is only limited to the annealed TiO₂ nanostructures. In other words, the removing of the top layer is incomplete if one does not go through the annealing treatment for as-prepared TiO₂ nanostructures. We see a slight change in topography of annealing treated sample in comparison to the as prepared in XRD (Figure 3-3), similar to the published data²⁴. X-ray diffraction (XRD) measurements were carried out to investigate the crystal structures of TiO₂ nanotube layers, and their patterns. The results reveal that the as-prepared nanotube layers on the titanium substrate contain only the Ti substrate peaks, indicating that such

layers have an amorphous structure. After annealing at 100 °C in air for 30 min, very distinctive peak appeared around 65° indicating that some of the TiO₂ layers transform to the anatase resulting in a stronger adhesion between TiO₂ layers with Ti substrate compared to the as prepared sample. However, the majority of the TiO₂ layers still remained amorphous.

The peak intensity of anatase increased after treating the surface with sonication which was ascribed to an increase in the degree of crystallization. Another reason that can explain the removal of nanowires from the surface is the banding between nanotubes and nanowires due to the collapsing of nanotubes at one point of anodization. Therefore, the nanotube and nanowire are separated at that point after sonication. Therefore, in order to form highly-ordered nanotube arrays, it is very important to completely remove the top nanowires using annealing treatment sonication.

3.5 Conclusions

In summary, we were able to form highly ordered TiO₂ nanostructures by anodizing Ti foil in NH₄F electrolytes. The Ti surface has two layers: the top layer is TiO₂ nanowire and underneath is a highly ordered TiO₂ nanotubes array. The top layer can be completely removed by annealing and a mild sonication process to expose the highly ordered nanotube layer. The length of the retained uniform and highly ordered nanotubes is independent of the treatment time. The dimensions of the retained TiO₂ nanotubes can be well controlled. The process may be extended to other nanotubes preparation.

3.6 References

- (1) Lee, Y.; Yoo, J.; Park, D.; Kim, D. H.; Ju, B. K. *Appl. Phys. Lett.* **2005**, *86*, 1-3.
- (2) Shin, H.; Jeong, D.; Lee, J.; Sung, M. M.; Kim, J. *Adv Mater* **2004**, *16*, 1197-1200.
- (3) Anonymous. *In Proceedings of SPIE: Device and process technologies for MEMS, microelectronics and photonics III*; 2004; Vol. 5276.
- (4) Byrne, J. A.; Hamilton, J. W. J.; McMurray, T. A.; Dunlop, P. S. M.; Donaldson, V. J. A.; Rankin, J.; Dale, G.; Al Rousan, D. *In Titanium dioxide nanostructured coatings: Application in photocatalysis and sensors*; 2006; Vol. 1, pp 72-75.
- (1) Wagner, S. *Engineer* **2006**, *293*, 33-35.
- (2) Ghicov, A.; Schmuki, P. *Chemical Communications* **2009**, 2791-2808.
- (3) Wu, C.; Lei, L.; Zhu, X.; Yang, J.; Xie, Y. *Small* **2007**, *3*, 1518-1522.
- (4) Adachi, M.; Jiu, J.; Isoda, S. *Current Nanoscience* **2007**, *3*, 285-295.
- (5) Bavykin, D. V.; Walsh, F. C. *European Journal of Inorganic Chemistry* **2009**, 977-997.
- (6) Byrappa, K.; Ohara, S.; Adschiri, T. *Adv. Drug Deliv. Rev.* **2008**, *60*, 299-327.
- (7) Macak, J. M.; Tsuchiya, H.; Ghicov, A.; Yasuda, K.; Hahn, R.; Bauer, S.; Schmuki, P. *Current Opinion in Solid State and Materials Science* **2007**, *11*, 3-18.
- (8) Lanone, S.; Boczkowski, J. *Curr. Mol. Med.* **2006**, *6*, 651-663.
- (9) Ghicov, A.; Schmuki, P. *Chemical Communications* **2009**, 2791-2808.
- (10) Sidorov, A.; Mudd, D.; Sumanasekera, G.; Ouseph, P. J.; Jayanthi, C. S.; Wu, S. *Nanotechnology* **2009**, *20*, 055611.

- (11) Masuda, H.; Fukuda, K. *Science* **1995**, *268*, 1466-1468.
- (12) Li, J.; Papadopoulos, C.; Xu, J. M.; Moskovits, M. *Appl. Phys. Lett.* **1999**, *75*, 367-369.
- (13) Martin, C. R. *Science* **1994**, *266*, 1961-1966.
- (14) Albu, S. P.; Ghicov, A.; Macak, J. M.; Schmuki, P. *Physica Status Solidi - Rapid Research Letters* **2007**, *1*, R665-R673.
- (15) Yeonmi, S.; Seonghoon, L. *Nano Letters* **2008**, *8*, 3171-3173.
- (16) Zhang, G.; Huang, H.; Zhang, Y.; Chan, H. L. W.; Zhou, L. *Electrochem. Commun.* **2007**, *9*, 2854-2858.
- (17) Park, J. H.; Kim, S.; Bard, A. J. *Nano Lett.* **2006**, *6*, 24-28.
- (18) Gorokh, G.; Mozalev, A.; Solovei, D.; Khatko, V.; Llobet, E.; Correig, X. *Electrochim. Acta* **2006**, *52*, 1771-1780.
- (19) Liu, S.; Fu, W.; Yang, H.; Li, M.; Sun, P.; Luo, B.; Yu, Q.; Wei, R.; Yuan, M.; Zhang, Y.; Ma, D.; Li, Y.; Zou, G. *Journal of Physical Chemistry C* **2008**, *112*, 19852-19859.
- (20) Lin, D.; Ying, M.; Yuwei, W.; Yongtao, T.; Guotian, Y.; Xiaolin, J.; Guoxi, Cao. *Materials Letters* **2008**, *63*, 1598-1600.

Chapter 4

Photoelectrochemical Water Splitting for Hydrogen Generation on Highly Ordered TiO₂ Nanotubes Fabricated by Using Ti as Cathode

Tayirjan T. Isimjan, Sohrab Rohani*, Ajay K. Ray paper based on the chapter has been submitted to the following journal: International Journal of Hydrogen Energy

4.1 Abstract

Sonication assisted anodization of titanium in a fluorinated ethylene glycol and water electrolyte using Ti itself as a cathode was investigated. The prepared anodic film has a highly ordered nanotube-array surface architecture. The resulting TiO₂ nanotubes at potential 20V to 40V had various diameters (30 nm-100 nm), tube length (3 μm-12 μm) and wall thicknesses (6 nm-15 nm). The tube diameter and wall thickness were increased with the anodization time while the overall length of the nanotube arrays is controlled by the duration of the anodization time. In addition, apart from the anodization time, formation of nanotubes is governed by the distance and supplied voltages between the two electrodes, for a given electrolyte. The crystal structure and surface morphology of the annealed anodic films are investigated by XRD and SEM. The corresponding photoelectrochemical water splitting efficiency (PCE) was calculated under UV light. Our results showed a very high PCE under UV (315-400 nm, 100 mW/cm²) irradiation. The maximum value of PCE for hydrogen generation obtained was 29% which is one of the best results reported in literature ¹.

Key word: Anodization, TiO₂ nanotubes, Ti cathode, UV irradiation and photoelectrochemical water splitting efficiency.

4.2 Introduction

Since Gong et al.² reported the fabrication of vertically oriented, highly ordered TiO₂ nanotube arrays by potentiostatic anodization of titanium in an HF aqueous electrolyte, titanium dioxide nanotubes have attracted considerable interest due to unique and excellent properties in optics³, electronics⁴, photochemistry⁵ and biology⁶. Because of the high surface to volume ratio, as well as highly accessible surface area, TiO₂ nanotubes have great potential for various applications such as solar cell⁷, biosensor⁸, water purification⁹ and hydrogen generation¹⁰. Anodic oxidation is considered to be the most convenient and efficient method to generate highly ordered TiO₂ nanotubes in comparison to the hydrothermal treatment¹¹, template-assistant deposition¹² and electrospinning¹³.

Two types of electrolytes are used in the anodic oxidation: organic-based electrolytes and aqueous-based electrolytes. Since the aqueous electrolytes have lower electrical resistance compared to the organic electrolytes, the oxidation as well as etching speeds are faster than organic electrolytes; therefore, it is always difficult to get longer tube in aqueous electrolytes. The required voltages in aqueous electrolytes are lower but the quality of the tubes in terms of uniformity and surface to volume ratio is worse². On the other hand, organic electrolytes have high electrical resistance which slows down the ion transports, therefore; they require longer anodization times and higher voltages. Organic electrolytes result in highly ordered long tubes ranging from couple of micrometers to thousand micrometers¹⁴. Generally, TiO₂ nanotubes fabricated in organic electrolytes have higher photo conversion efficiency than aqueous based TiO₂ nanotubes. However, the tubes grown in organic electrolytes collapse easily and form nanowires bundles. In a

previous work ¹⁵, we reported that the surface layer of nanotubes can be completely removed by a mild sonication resulting in highly ordered TiO₂ nanotubes that hide under the bundles.

Since platinum foil is used as a counter electrode in the anodization process the process will be expensive for the large scale production. Therefore, much research is being focused on replacing the cathode material (Pt) with other materials. Recently, Allam et al. ¹⁶ reported the morphologies and optical properties of different cathode materials for TiO₂ nanotubes in both aqueous and organic electrolytes. It was revealed that some materials such as Fe, Co, Pd and C show promising results to replace the conventionally-used and expensive Pt cathode. However, the quality of the TiO₂ nanotubes was poor in most cases. Even though the Fe-cathode resulted in the highest photo conversion efficiency (PCE) 6.9% illuminated under 100 mW/cm² 315–400 nm, but cathode stability was a big concern in aqueous based electrolyte. However, no cathode loss was observed and the tubes quality was high in the terms of uniformity in organic based electrolyte. Moreover, no clogging with surface debris was observed. But the PCE of TiO₂ nanotubes was lower. The highest PCE under illumination with 100 mW/cm² was less than 6%.

In this work, we propose the use of Ti as cathode. We used sonication to assist fabrication of TiO₂ nanotubes under potentiostatic conditions in fluorinated ethylene glycol and 5% water. Under a range of anodizing conditions, we achieved highly ordered TiO₂ nanotubes. To the best of our knowledge, this is the first report on synthesizing highly ordered TiO₂ nanotubes in a reproducible manner by using Ti as a cathode with a photoelectrochemical water splitting efficiency (PCE) of 29% under UV(315-400 nm,

100 mW/cm²) irradiation. This PCE is one of the highest reported so far. No loss on cathode was detected.

4.3 Material and methods

The Ti foil (0.8 mm thickness, 99.6 % purity) and all chemicals were purchased from Alfa-Aesar (Ward Hill, MA, USA). Prior to anodization, the titanium foil was cleaned by using distilled water and acetone. It was then dried off in air, etched in 3.4 M HF plus 5M HNO₃ for 30 s, rinsed with deionized water, dried with air and used immediately.

The polished Ti foil was anodized in an ethylene glycol solution containing NH₄F (0.38 wt%) and H₂O (1.79 wt%), and placed in a well-insulated bath for several hours at 20~40V and at room temperature using a DC power supply (Keithley 2602, MetricTest, Hayward, CA). After the anodization, the sample was washed with distilled water and acetone and then dried off with air. In order to increase the adhesion force between TiO₂ layers with substrate, the prepared sample was annealed at 100 °C for 30 min and then sonicated for 30 s. The amorphous highly ordered TiO₂ nanotubes were crystallized by annealing in an oxygen atmosphere for 3 h at 550 °C with heating and cooling rates of 10 °C/min.

The electrochemical anodization experiments were performed in a conventional two-electrode cell. A Ti foil (10mm×20mm) was used as a counter electrode and a titanium sheet served as a working electrode. A Ti sheet of size 1 cm × 1 cm was pressed between a set of O-rings in the sample holder. A copper wire was located on the back side of the sample as the electrical contact, and then fixed in the electrochemical cell with an active anode area of 0.9 cm² exposed to the electrolyte. During processing, the anode and

cathode were parallel with a separation distance of 2 cm. All anodization experiments were performed potentiostatically, under constant applied voltage, at room temperature. The microstructural morphological features of all the samples were examined with a field emission scanning electron microscope (FE-SEM, Hitachi S-5000, Tokyo, Japan). The crystalline phases were characterized by X-ray diffraction using a powder X-ray diffractometer (Rigaku RINT 2500, Tokyo, Japan) with Cu K radiation ($\lambda = 1.54\text{\AA}$) at 40 kV and 50 mA with a scan rate of $0.05^\circ/\text{s}$ and a scan speed of $1^\circ/\text{min}$ over a 2θ range from 20° to 90° . Final samples were cleaned by Crest Ultrasonics (Model No: 275 HTA, Penang, Malaysia). UV lamp (Model: S480 S/N, Burlington, ON) was used as the UV light source ($\lambda = 365.5\text{ nm}$). The light intensity of $100\text{ mW}/\text{cm}^2$ was measured by UVX digital radiometer (E29004, UVP, Inc. Upland, C).

4.4 Results and discussion

4.4.1 Potentiostatic current transients and oxide film formation

Three simultaneously occurring processes happen during the formation of nanotube arrays in a fluoride containing electrolyte¹⁷: (1) field-assisted oxidation of Ti, (2) field-assisted dissolution of Ti metal, and (3) chemical dissolution of Ti and TiO_2 due to etching by fluoride ions.

In the beginning, the electric field forces oxygen ions to diffuse from cathode to anode producing an ionic current. The thickness of TiO_2 layer increases by the reaction between oxygen ions and the metal. This process of high-field ionic conduction is central to anodization. Since the electric resistance increases with the increase in the thickness and because the rate of oxide growth is proportional to the current density, higher current is generated by thinner TiO_2 layer¹⁸. Figure 1 shows three potentiostatic current-time

plots for a titanium electrode in ethylene glycol (EG) electrolytes under different voltages. During the first 60 s, the external voltage increases from 0 to the specific voltage and then stays that level for 3 h. In the first 60 s, the current will increase due to the increase of voltage and then decreases rapidly because of the sudden increase of the oxide layer. The current stabilizes for some period of time during the equilibrium state between oxidization and dissolution and then decreases slowly along with the increase of the thickness of TiO₂ layer (Figure 4-1b). It appears that a higher constant voltage results in a higher current.

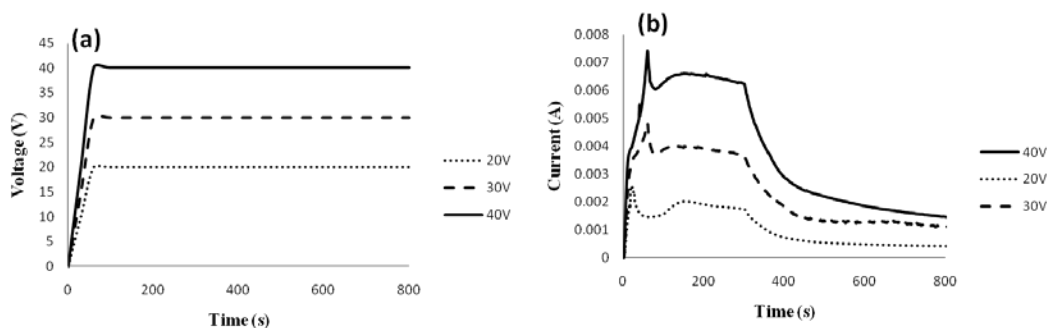


Figure 4-1: Current-time response of Ti samples anodized using Ti cathodes in ethylene glycol electrolytes for 3 hours, 1cm distance between anode and cathode: (a) voltage vs. time (b) current vs. time

4.4.2 SEM images

It is a challenge to fabricate highly ordered TiO₂ nanotubes as shown in Figure 4-2b due to the collapse of the tubes after certain period of anodization time (Figure 4-2a). The as-prepared samples were annealed at 100 °C for 0.3 h followed by sonication at room temperature for 30 s and then the highly ordered TiO₂ nanotubes appeared as shown in Figure 4-2c¹⁵. The tube length was also measured (Figure 4-2d). Besides, the proposed method leaves no surface debris clogging the nanotubes and ensuring a higher PCE due to higher surface exposure (Figure 4-2b and 4-2c). The morphology and dimension of the

nanotube arrays were found to be influenced by the anodizing voltage. The wall thickness ranging from 6.5 to 14.6 nm, tube length stretching from 3.3 to 11.6 μm and tube diameters from 41.5 to 92.4 nm were achieved by changing the anodization potential as well as the distance between the anode and cathode. They all increased with the increase of anodization voltage while the distance was kept constant. Overall, the higher PCEs were observed with the tubes that were anodized under a potential of 20V due to the smaller wall thickness¹⁸.

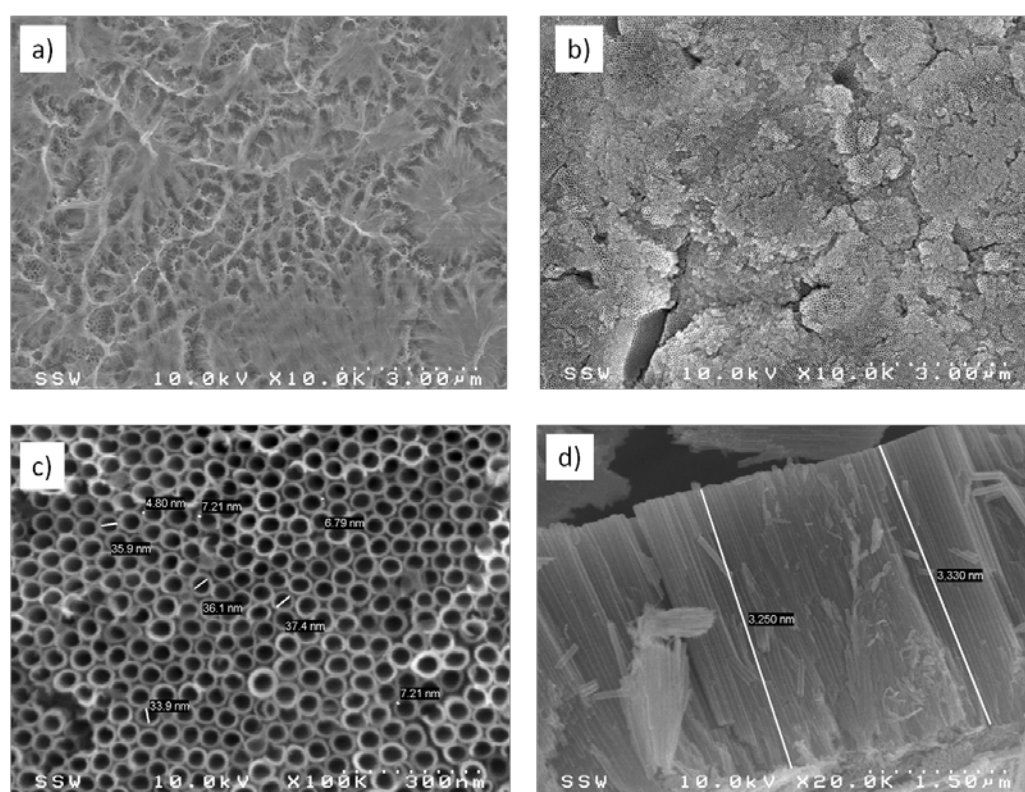


Figure 4-2: SEM images of TiO_2 nanotubes fabricated under condition of 1cm between cathode and anode, 20 V constant voltage and 3 h anodization time. a) before sonication, b) after sonication, c) larger magnitude image and d) cross-section

4.4.3 Roughness factor

The physical surface area of the film per unit projected area is defined as roughness factor which has a crucial significance in different applications such as sensing and

catalysis. The geometric roughness factor is calculated by the following equation assuming the surface (4-1) ¹⁹

$$G = \left[\frac{4\pi L(D+W)}{\sqrt{3}(D+2W)^2} \right] + 1 \quad (4-1)$$

where D is the inner diameter, W is the wall-thickness and L is the tube-length. Equation (4-1) assumes all surfaces of the nanotubes to be perfectly smooth. However, because of the fluctuations in voltage, the actual surface is not smooth. Table 1 shows geometric roughness factor for nanotubes with different geometries. It shows that higher surface area is more easily obtained at higher voltages which also correlate with the high photocurrent conversion efficiencies. Meanwhile, small pore size also results in better photo conversion efficiency despite of lower roughness factor due to high surface to volume ratio (Table 4-1).

Table 4-1: Summary of the nanotube wall thickness, tube diameter, aspect ratio, PCE% and length obtained at different voltages as well as different distances for a 3 h anodization in an ethylene glycol electrolyte containing 0.38 wt% NH₄F and 1.79 vol% H₂O

V	Distance cm	Average wall thickness (nm)	Average tube diameters (nm)	Average thickness (um)	Average roughness factor	Average aspect ratio	PCE (%)
20	1	6.5	41.5	3.3	388	61	28.7
30	1	7.1	59.9	5.7	506	77	20.7
40	1	12.6	72.8	11.6	750	118	22.8
20	2	5.6	46.2	2.8	321	49	27.7
30	2	6	49.2	5.3	568	87	23.8
40	2	14.6	92.4	10.9	574	90	28.5
20	3	5.4	49.7	2.3	252	38	28.9
30	3	9	60	5.5	454	71	27.9
40	3	10.3	72	8.7	607	94	27

It is well-established that the properties of the nanotube arrays are dependent upon their specific architecture, including length, wall thickness, wall roughness, pore diameter, and tube-to-tube spacing. The geometrical features of the nanotube arrays are controlled by a variety of parameters including anodization potential, electrolyte composition and properties thereof (conductivity, viscosity), as well as anodization time, distance between two electrode and temperature.

Supplied potential affects both the behavior of the electrochemical etching and the chemical dissolution due to the hydrolysis of titanium ions. With increasing voltage, the hydrolysis content increases and it, in turn, slows the rate of chemical dissolution. As shown in Table 4-1, longer nanotubes are formed at higher potential. For example, with a inter-electrodes distance of 1cm and with the increase from 20 V to 40 V, nanotube length increased from 3.3 μm to 11.6 μm ; wall thickness and tube diameter also increased from 6.5 nm to 12.6 nm and from 41.5 nm to 72.8 nm, respectively. However, at a specific applied voltage, the pore size was almost independent of distance between anode and cathode.

In general, the PCE depends on different factors such as the size, aspect ratio, roughness factor of the nanotube arrays and the annealing temperature, etc. All these factors together determine how much light can be trapped on the surface. The higher the amount of trapped light on the surface, the higher is the PCE. It is reported that the pore diameter of the nanotubes does not have significant effect on the PCE. Increasing the tube length, however, has positive effect on the PCE. The minimum aspect ratio around 3.0 is sufficient to trap most of the light. However, it has been observed that an increase in aspect ratio leads to poorer performance due to the larger dark currents and a decrease in nanotube quality²⁰. In our case, the lowest aspect ratio gave the highest PCE (28.9%).

However, the highest aspect ratio gave the second lowest PCE (22.8%). The PCE results show that roughness factor has negative effect on the PCE, due to the higher level of scattering as shown in Table 4-1.

4.4.4 XRD pattern

The XRD results of the sample fabricated at 40 V and 1cm separation distance between cathode and anode for 3 hours is shown in Figure 3. It has been reported²⁰ that the higher annealing temperature results in higher PCE, due to the increased crystallinity of the nanotube-walls with the reduction of the amorphous regions and grain boundaries. This will reduce the number of charge carrier recombination centers. However, above 600°C the PCE decreases because the nanotube-array architecture starts to collapse. In this regard, the annealing temperature of 550 °C was chosen in this work. After annealed at 550 °C for 3 h, the sample was mainly composed of anatase TiO₂ with a trace of rutile¹⁵. Linsebigler and his co-workers found that anatase has higher photocatalytic activity than rutile, whereas a mixture of anatase and rutile has higher photocatalytic activity than either anatase or rutile²¹.

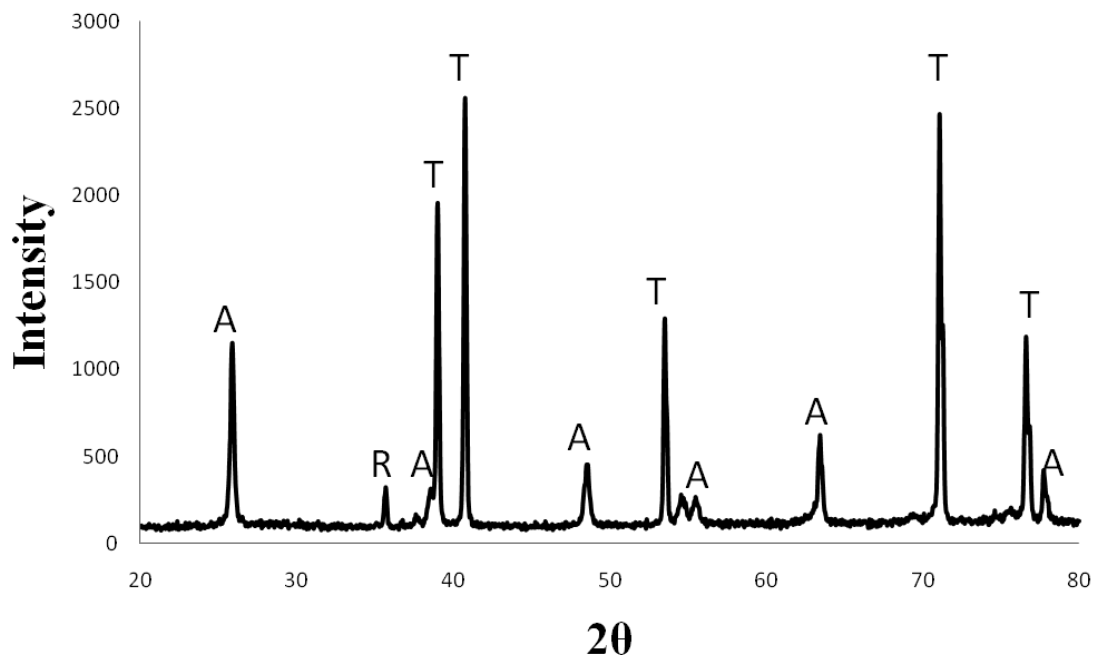


Figure 4-3: XRD results of TiO₂ nanotubes fabricated under the condition of 1cm between cathode and anode, 40 V constant voltage and 3 hour anodization .

4.4.5 Photoelectrochemical water splitting efficiency (PCE)

The PCE of TiO₂ nanotubes was measured by a three-electrode cell at room temperature under UV(100 mW/cm²) illumination in a 1M KOH solution²². The samples were annealed at 550 °C for 3 h in air. The annealing temperature is very crucial to the PCE because when tube length exceeds several microns, the majority of charge carriers are photogenerated in the TiO₂ nanotube wall, hence increasing crystallinity will significantly improve the photoelectrochemical properties of the TiO₂ nanotubes²³. However the annealing temperature cannot be increased above 600°C since TiO₂ nanotubes will be destroyed at high temperatures. The photo conversion efficiency of water electrolysis was calculated based on the following relations using equation (4-2):

$$\text{PCE} = [J_{\text{ph}}(1.23 - E_{\text{app}}) \times 100\%] / I_0 \quad (4-2)$$

$$E_{app} = |E_{means} - E_{oc}| \quad (4-3)$$

where J_{ph} is the photocurrent density; E_{app} is applied potential which can be obtained from equation (4-3); E_{means} is the potential applied to photo anode versus a reference electrode; E_{oc} is the open circuit potential of photo anode under illumination; I_0 is the intensity of incident light. Figure 4-4 (a) shows the photocurrent plots of as-anodized TiO₂ nanotubes in 1M KOH solution as a function of potential applied to the photo anode with reference to an Ag/AgCl reference electrode. The photocurrent increases with increasing the applied potential up to certain point and then decreases. Equations (4-2) and (3) give the photo conversion efficiency for hydrogen generation of annealed nanotubular arrays of TiO₂ in 1M KOH is plotted as a function of external potential applied to the photo anode as shown in Figure 4-4(b).

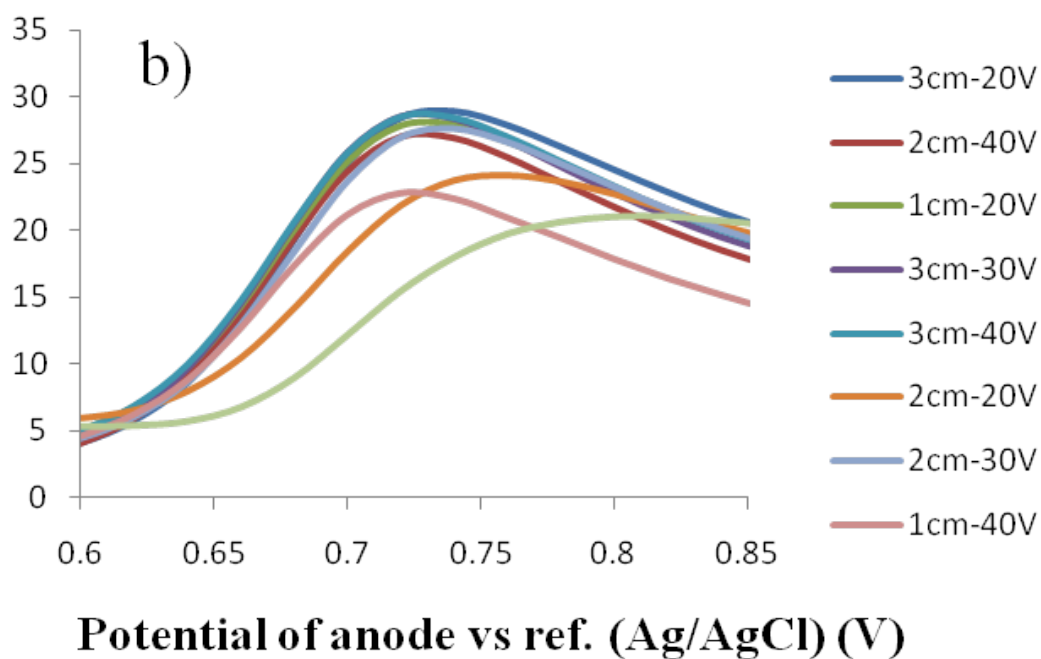
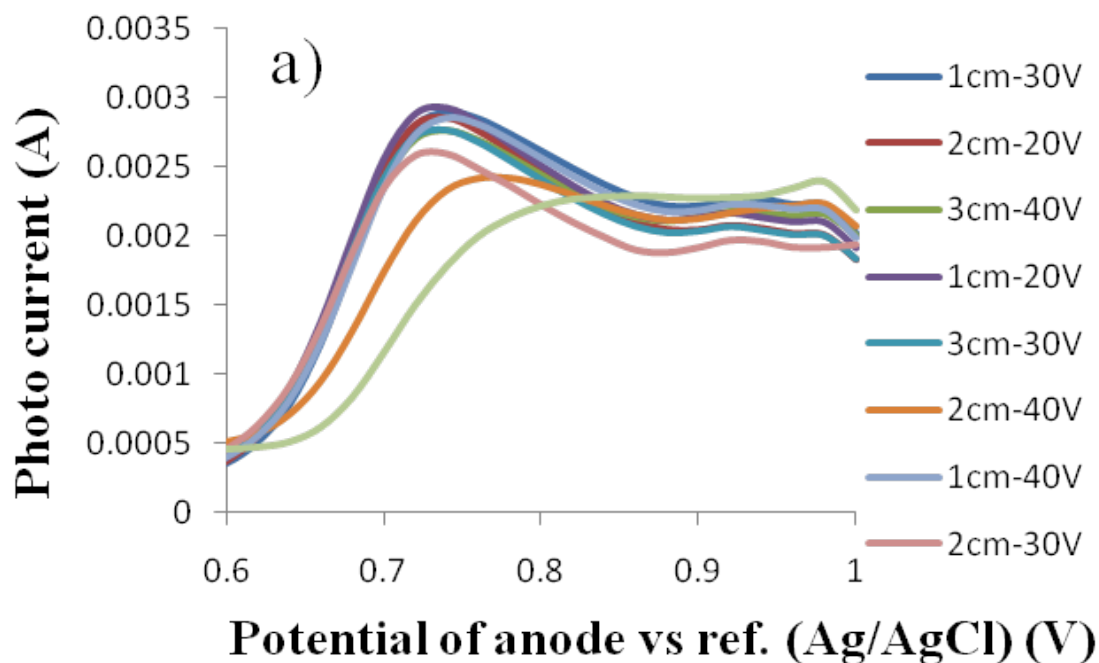


Figure 4-4: Photo conversion efficiency (PCE) under UV illumination of a photoelectrochemical cell comprising TiO_2 nanotube array photoanode, Ag/AgCl as reference and Pt counter electrode. (a) Photocurrent vs. external voltage (b) Photo conversion efficiency vs. external voltage

Figure 4-4 shows the photo current and corresponding photoconversion efficiency of the samples. Higher photo current corresponds to higher PCE. All TiO₂ nanotubes exhibit PCE greater than 20%. The TiO₂ nanotubes that were fabricated at 20 V show higher photocurrent and PCE followed by the TiO₂ nanotubes fabricated at 40 V and 30 V. A maximum photoconversion efficiency of 29% was obtained for nanotubes that were anodized under the condition of 3 cm distance between two electrodes, 20 V applied potential and 3 h annealing time. To the best of our knowledge, this is the highest reported photo conversion efficiency so far for TiO₂ nanotubes under UV illumination.

4.5 Conclusions

We have used Ti as a cathode material during the electrochemical fabrication of TiO₂ nanotube arrays in non-aqueous electrolytes. Ti showed promising results to replace the conventionally used and comparatively expensive Pt cathode. In terms of photo conversion efficiency, the highest PCE was achieved using Ti-cathode. Ti showed excellent stability in the EG electrolytes. The structure, morphology, and photoelectrochemical properties were studied in comparison to the nanotube arrays fabricated under different conditions such as: applied potential (20 V – 40 V) and distance between two electrodes (1 cm to 3 cm) with the same anodization time of 3 h. We show that highly ordered and strong photochemical responsive TiO₂ nanotubes can be fabricated simply by changing the distance between two electrodes and applied potential during the anodization. This work not only opens a new way to engineer titanium dioxide nanostructures but also offers a big step towards producing cheap TiO₂ nanotubes in large area.

4.6 References

- (1) F. Mura, A. Masci, M. Pasquali and A. Pozio, *Electrochim. Acta* 2010, **55**, 2246-2251.
- (2) (a) D. Gong, A. C. Grimes, K. O. Varghese, W. Hu, S. R. Singh, Z. Chen and C. E. Dickey, *J. Mater. Res.* 2001, **16**, 3331-3334. (b) J. M. Macak,; H. Tsuchiya; L. Taveira; S. Aldabergerova; P. Schmuki, *Angew. Chem. Int. Ed.* 2005, **44**, 7463-7465.
- (3) N. K. Allam, and M. A. El-Sayed, *J. Phys. Chem. C* 2010, **114**, 12024-12029.
- (4) Y. Ohsaki, N. Masaki, T. Kitamura, Y. Wada, T. Okamoto, T. Sekino, K. Niihara and S. Yanagida, *Phys. Chem. Chem. Phys.* 2005, **7**, 4157-4163.
- (5) Zhang, J.; Bang, J. H.; Tang, C.; Kamat, P. V. *ACS Nano* **2010**, *4*, 387-395.
- (6) Kang, Q.; Lu, Q. Z.; Liu, S. H.; Yang, L. X.; Wen, L. F.; Luo S. L.; Cai, Q. Y. *Biomaterials* **2010**, *31*, 3317-3326.
- (7) Kislyuk V. V.; Dimitriev, O. P. *J. Nanosci. Nanotechnol.* **2008**, *8*, 131-148.
- (8) Mun, K. S.; Alvarez, D.; Choi W.; Sailor, M. J. *ACS Nano* **2010**, *4*, 2070-2076.
- (9) Li, Q.; Mahendra, S.; Lyon, D. Y.; Brunet, L.; Liga, M. V.; Li D.; Alvarez, P. J. J. *Water Res.* **2008**, *42*, 4591-4602.
- (10) a) Gong, J.; Lai Y.; Lin, C. *Electrochim. Acta* **2010**, *55*, 4776-4782. b) Varghese, O. K.; Paulose, M.; Shankar, K.; Mor, G. K.; Grimes, C. A. *J. Nanoscience and Nanotechnology* **2005**, *5*, 1158-1165.
- (11) Torrente-Murciano, L.; Lapkin A. A.; Chadwick, D. *J. Mater. Chem.* **2010**, *20*, 6484-6489.
- (12) Yang, L.; Luo, S.; Cai Q.; Yao, S. *Chin. Sci. Bull.* **2010**, *55*, 331-338.

- (13) Qiu, Y.; Yu, J. *Solid State Commun* 2008, **148**, 556-558.
- (14) Paulose, M.; Prakasam, H. E.; Varghese, O. K.; Peng, L.; Popat, K. C.; Mor, G. K.; Desai, T. A. Grimes, C. A. *J. Phys. Chem. C* **2007**, *111*, 14992-14997.
- (15) Isimjan, T. T.; Yang, D. -Q.; Rohani, S.; Ray, A. K. *Journal of Nanoscience and Nanotechnology* **2011**, *11*, 1079-1083.
- (16) Allam, N. K. Grimes, C. A. *Solar Energy Materials & Solar Cells* **2008**, *92*, 1468– 1475.
- (17) Mor, G. K.; Varghese, O. K.; Paulose, M.; Mukherjee N.; Grimes, C. A. *J. Mater. Res.* **2003**, *18*, 2588-2593.
- (18) Grimes, C. A.; Mor, G. K. in *TiO₂ Nanotube Arrays Synthesis, Properties, and Applications*, ed. Springer, Dordrecht Heidelberg, London, New York , 1nd edn., 2008, ch1. pp. 3-4.
- (19) (a) Zhu, K.; Neale, N. R.; Miedaner A.; Frank, A. J. *Nano Lett.* **2007**, *7*, 69-74. (b) Shankar, K.; Mor, G. K.; Prakasam, H. E.; Yoriya, S.; Paulose, M.; Varghese O. K.; and Grimes, C. A. *Nanotechnology* **2007**, *18*, 065707.
- (20) Shankar, K.; Basham, J. I.; Allam, N. K.; Varghese, O. K.; Mor, G. K.; Feng, X. J.; Paulose, M.; Seabold, J. A.; Choi K. -S.; Grimes, C.A. *J. Phys. Chem. C* **2009**, *113*, 6327–6359.
- (21) Linsebigler, A. L.; Lu, G. Q.; Yates, J. T. *Chem. Rev.* **1995**, *95*, 735–758.
- (22) Isimjan, T. T.; Ruby, A. E.; Rohani S.; Ray, A. K. *Nanotechnology* **2010**, *21*, 055706.
- (23) Ong, K. G.; Varghese, O. K.; Mor G. K.; Grimes, C. A. *J. Nanosci. Nanotechnol.* **2005**, *5*, 1801-1808.

Chapter 5

Fabrication of highly-ordered and visible-light responsive

Fe-C-N-codoped TiO₂ nanotubes

A version of this chapter was published as:

Tayirjan T. Isimjan, Ahmed E. Ruby, Sohrab Rohani, Ajay K. Ray. Nanotechnology 2010, 21, 055706.

5.1 Abstract

A one step method for the fabrication of Fe-C-N-codoped TiO₂ nanotubes by electrochemical anodization is reported. The proposed method is both simple and efficient. The prepared samples were annealed at 550°C for 3 hours. The resulting nanotubes were characterized by SEM, XRD, XPS, EDX and UV-vis spectrophotometer. The results showed that the average tube diameter of the nanotubes was 70 nm and wall thickness was 20 nm and the average tube length was 2.4 μm. The doped TiO₂ nanotubes exhibited strong absorption in visible-light region. The maximum photocurrent efficiency measured under solar simulator was 2.7%.

Keywords: Titanium dioxide; Doping; Photocurrent efficiency; Photoelectrochemical; Hydrogen generation.

5.2 Introduction

In recent years, growing attention has been paid to the design and fabrication of fine-structured metal oxides on the nanoscale and microscale because of their unique potential applications. Among the structured metal oxides, TiO₂, in particular, has been extensively studied and put to use in microporous membranes¹, dye-sensitized solar cells², humidity chemical sensors³, water-splitting electronic devices, and hydrogen storage and sensing devices among others. Its role as an environmentally-friendly photocatalyst has also seen wide applications in dealing with environmental problems such as in the treatment of wastewater⁴. Titanium oxide's photocatalytic role could be expanded even more broadly if it were not so limited by its large bandgap ($E_g = 3.2$ eV) which requires near-UV light (λ shorter than 380 nm) for activation. For preparing the nanostructure and microstructures of TiO₂, various approaches have been reported such as the sol-gel process⁵, pyrolysis⁶, electron beam evaporation⁷, chemical vapor deposition⁸, atomic-layer deposition⁹, and the hydrothermal process¹⁰. Application of powder TiO₂ in aqueous solutions suffers from the problem of handling the suspensions. By contrast, a solid array of TiO₂ nanotubes grown directly on titanium plates offers the possibility of a more robust and economical solution by not only eliminating the above problem, but also being reusable after photocatalytic reactions. Thus, it is of great significance to prepare and develop unique TiO₂ nanotubes which can work efficiently even under broad-spectrum visible light irradiation while having a high mechanical and physical

stability. By either doping or dye sensitization, it is possible to improve the optical sensitivity and activity of TiO₂ nanotubes in the visible light spectrum. Doping of TiO₂ nanotubes with transition metal ions^{11, 12, 13} and non-metal ions¹⁴ using various doping approaches, have been reported. For example: ion implantation¹⁵, thermal annealing¹⁶ and Ti-alloys¹⁷, are among the reported doping techniques. It is well known that the electrochemically synthesized oxide films contain complicated anion species incorporated from the electrolyte. This phenomenon can be used to dope anion species into a TiO₂ nanotubular structure during anodization to significant levels (a few atomic %) by tailoring the electrolyte composition. Some research groups have demonstrated incorporation of non-metals such as F-P¹⁸, Si¹⁹, F-S²⁰, N²¹, B²² elements and metals such as Fe²³ and W²⁴ into a nanotubular structure during anodization. However, in the most of solution doping techniques, the electrolytes are aqueous based inorganic solution, therefore the resulting tubes have neither uniform structure no high density.

In this study, the Fe-C-N-codoped TiO₂ nanotubes were fabricated by a one-step electrochemical anodization process on titanium plate using 0.38% K₃Fe(CN)₆ in ethylene glycol solution as an electrolyte. The resulting nanotubes were not only highly organized but also had high density. This simple and efficient one-step process, includes both fabrication and Fe-C-N-codoping of TiO₂ nanotubes. The prepared samples were annealed in air at 350°C and 550°C, respectively, and characterized by SEM, XRD, XPS, EDX, and UV-vis spectrophotometer. The results showed that the average tube diameter of the nanotubes was 70 nm, wall thickness was 20 nm, length-to-diameter aspect ratio

was about 34, and the average tube length was 2.4 μm . The doped TiO_2 nanotubes exhibited strong absorption in the visible-light region.

5.3 Experimental

5.3.1 Preparation of TiO_2 nanotubes

The Ti foil (0.8 mm thickness, 99.6 % purity) and all chemicals were purchased from Alfa-Aser (Ward Hill, MA, USA). Prior to anodization, the titanium foil was cleaned by using distilled water and acetone. It was then dried off in air then etched in (3.4 M $\text{HF}+5\text{M HNO}_3$) for 30 s and immediately rinsed with deionized water, dried with air and used immediately.

The polished Ti foil was anodized in an ethylene glycol solution containing NH_4F (0.38 wt%) and H_2O (1.79 wt%) and placed in a well-insulated bath for 3 h at 30 V and at room temperature using a DC power supply. The textured Ti surface was obtained by removing the first anodized TiO_2 nanotubular layer with adhesion tape. Subsequently, the second anodization was performed for 3 h in a solution of glycol NH_4F (0.38 wt%), H_2O (1.79 wt%), and $\text{K}_3\text{Fe}(\text{CN})_6$ (0.38 wt%). The anodization current was monitored with a computer. After the second anodization step, the sample was washed with distilled water and acetone and then dried off with air. An anatase TiO_2 structure was made by annealing the as-anodized samples in air at 550 $^\circ\text{C}$ for 3 h at a heating rate of 10 $^\circ\text{C}/\text{min}$.

The electrochemical anodization experiments were performed in a conventional two-electrode cell. A platinum foil (10mm \times 20mm) was used as a counter electrode and a

titanium sheet served as a working electrode. A Ti sheet of size 1 cm × 1 cm was pressed between a set of O-rings in the sample holder. The Pt wire was located on the back side of the sample as the electrical contact, and then fixed in the electrochemical cell with an active anode area of 0.9 cm² exposed to the electrolyte. During processing, the anode and cathode were parallel with a separation distance of 2 cm. All anodization experiments were performed potentiostatically, under constant applied voltage, at room temperature. The electrochemical anodization was carried out by using a source meter (Keithley 2602) interfaced to a computer. The microstructural morphological features of all the samples were examined with a field emission scanning electron microscope (FE-SEM, Hitachi S-5000, Tokyo, Japan) equipped with an energy dispersive X-ray analyzer unit (EDXA). The elemental compositions of the samples were determined by EDX analysis. The crystalline phases were recorded by X-ray diffraction using a powder X-ray diffractometer (Rigaku RINT 2500, Tokyo, Japan) with Cu K radiation ($\lambda = 1.54\text{\AA}$) at 40 kV and 50 mA with a scan rate of 0.02 °/s and a scan speed of 1 °/min over a 2 θ range from 20° to 90°. The results in the elemental compositions were determined by X-ray photoelectron spectroscopy (XPS, Perkin Elmer, Waltham, MA, USA) and EDXA. The XPS analyses were carried out with a Kratos Axis Ultra spectrometer using a monochromatic Al K(alpha) source (15mA, 14kV). XPS can detect all elements except hydrogen and helium, probes the surface of the sample to a depth of 5-7 nanometres, and has detection limits ranging from 0.1 to 0.5 atomic percent depending on the element. The instrument work function was calibrated to give a binding energy (BE) of 83.96 eV for

the Au 4f_{7/2} line for metallic gold and the spectrometer dispersion was adjusted to give a BE of 932.62 eV for the Cu 2p_{3/2} line of metallic copper. The Kratos charge neutralizer system was used on all specimens. Survey scan analyses were carried out with an analysis area of 300 x 700 microns and pass energy of 160 eV. High resolution analyses were carried out with an analysis area of 300 x 700 microns and pass energy of 20 eV. Spectra have been charge corrected to the main line of the carbon 1s spectrum (adventitious carbon) set to 284.8 eV. Spectra were analysed using CasaXPS software (version 2.3.14). UV-vis diffuse reflectance absorption spectra were measured using a UV-VIS-NIR spectrophotometer.

5.3.2 Photoelectrochemical characterization

The photocurrent spectra were recorded by a home-made photoelectrochemical measurement system with using LPX150 Xe-lamp in the range of 250-600 nm. The electrochemical characterization was carried out by measuring the open circuit potential (OCP) of the sample under visible light illumination. The sample of the doped TiO₂ nanotube films electrode served as the working electrode, and a Pt sheet was used as the counter electrode. The testing electrolyte was 1M KOH solution. For the photopotential measurement, the sample was illuminated using a 150W high-pressure Xe lamp. The photopotential was obtained when the OCP reached a stable value under an illumination. A computer controlled power supply (Keithley 2602, Hayward, CA, USA) was employed to control the potential and record the photocurrent generated. A 300W solar simulator

was used as light sources. The light at the 100W power level was passed through a 400 nm cut filter which allowed wavelength only between 400-700 nm to be incident upon the photo-anode. The intensity of the light was measured by a radiation power and energy meter. The incidence light intensity on the sample is measured as 63 mW/cm^2 . The external potential was applied to the anode at a scan rate of 20 mV/sec under illumination and the photocurrent was recorded. The potential of the open circuit was measured by digital multimeter during the illumination.

5.4 Results and discussion

5.4.1 FE-SEM images of TiO₂ nanotubes

It was apparent from Figure 5-1 FESEM images that the nanotubes are open on the top and closed at the bottom. Although the surface is not very uniform, almost every tube grows straight and highly-ordered. The length, average tube outer diameter and wall thickness were 2.4 μm , 70 nm and 20, nm respectively, with a length-to-diameter aspect ratio of about 34. The tubes had no ripples on their walls and they were entirely smooth and clean over their length from SEM images.

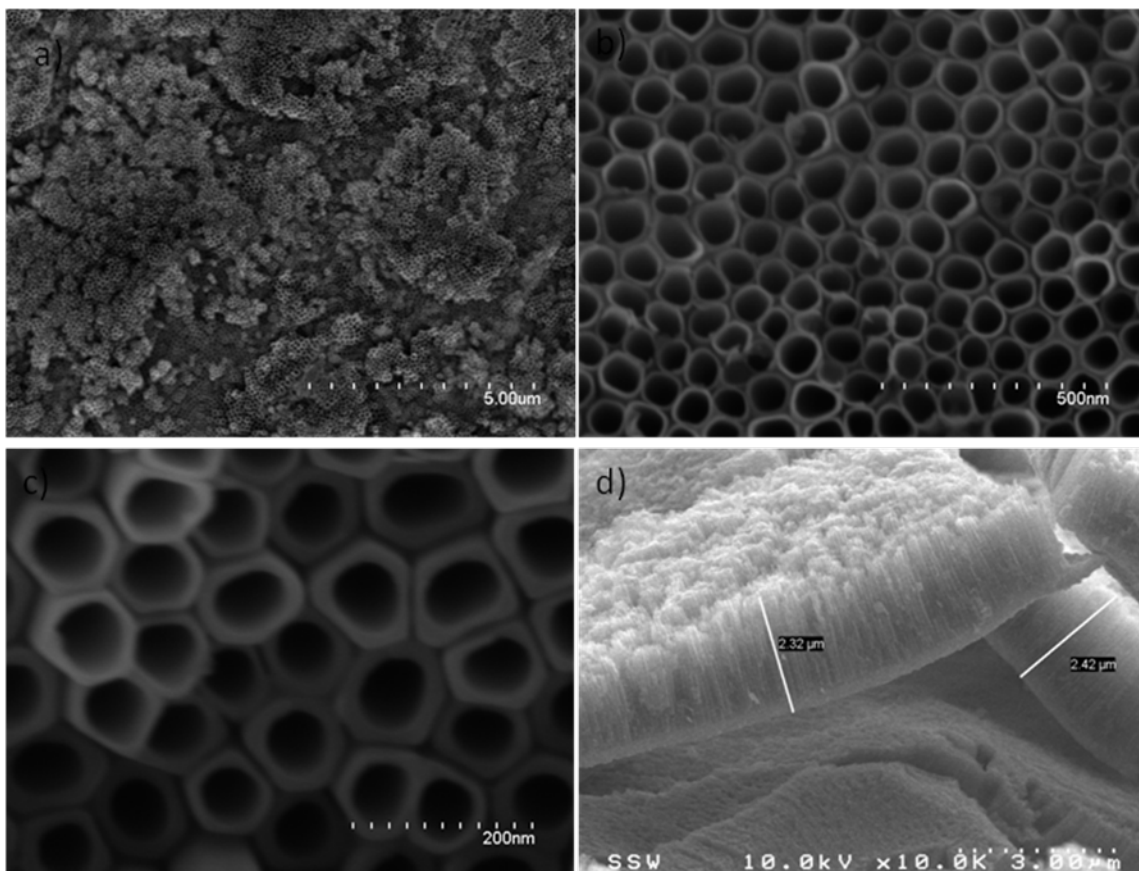


Figure 5-1: SEM images of Fe-C-N-codoped TiO₂ nanotubes

5.4.2 UV-vis and XRD results

The UV-vis diffuse reflectance absorption spectra of TiO₂ nanotubes are shown in Figure 5-2. There are some differences of absorbance response between as prepared, annealed at 350 °C and at 550°C of TiO₂ nanotubes. The absorbance response of as prepared TiO₂ nanotube exhibits lower absorption in visible light region, whereas the annealed TiO₂ nanotubes show a red-shift and stronger absorption in the range of wavelength from 350 to 600 nm. The absorbance responses can be explained in terms of surface color and crystalline structure of titanium

dioxide nanotubes. The color of annealed TiO₂ nanotube layer was blue with heat treatment at 350 °C and dark brown at 550 °C, respectively. However, the color of anodic TiO₂ nanotubes without heat treatment was light yellow which causes more absorption in the ultra violet region and reflection in visible light region than that of TiO₂ nanotube with heat treatment. In the case of TiO₂ film annealed at 350 °C as shown in Figure 5-2 (UV-vis), the absorption onset around 430 nm was observed. The TiO₂ nanotubes annealed at 350 °C (Figure 5-2) showed a slight red-shift which can be attributed mainly to the light absorption of blue color on titanium.

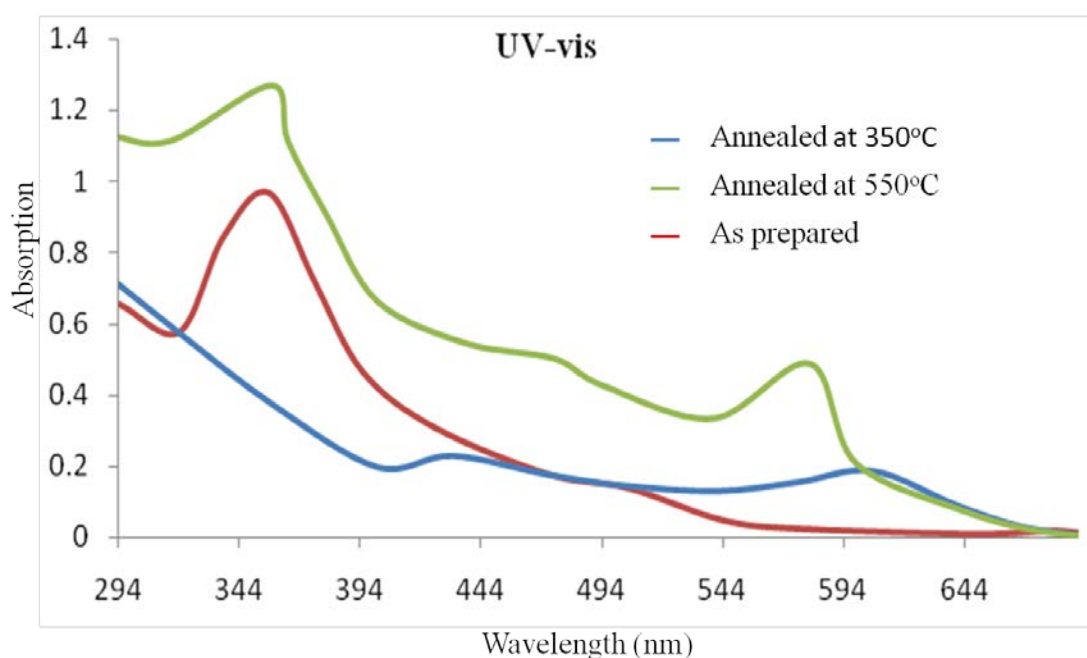


Figure 5-2: UV-vis of TiO₂ nanotubes

However, for TiO₂ film annealed at 550 °C, the position of the absorption onset was observed around 480 nm, as phase transition of anatase into rutile phase takes place and the rutile phase starts to form. The wavelength of 475 nm means that energy of band gaps for the anodic TiO₂ films annealed at 550 °C represent about 2.7 eV²⁶. The UV-vis

spectra in Figure 5-2 are consistent with the changes in crystalline structure observed with the X-ray diffractometer²⁷ in Figure 5-3.

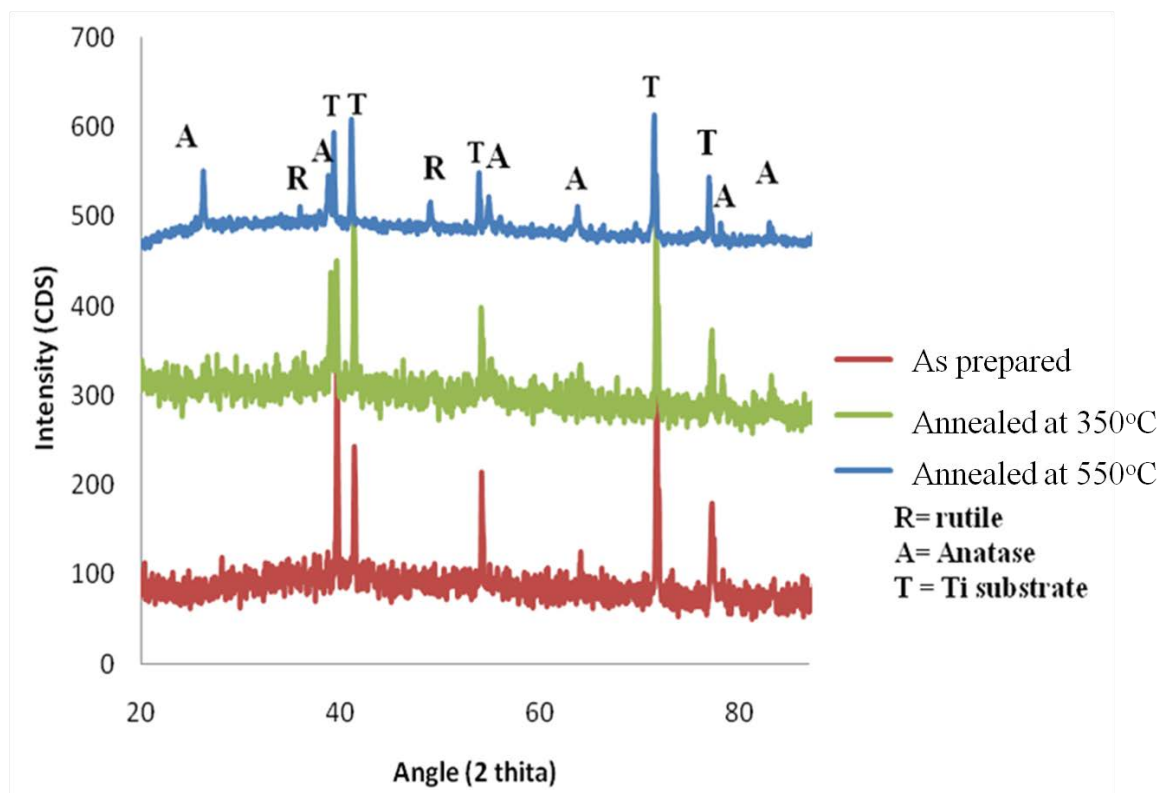
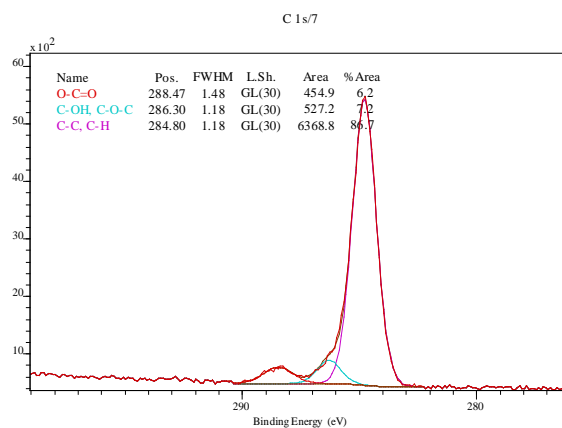
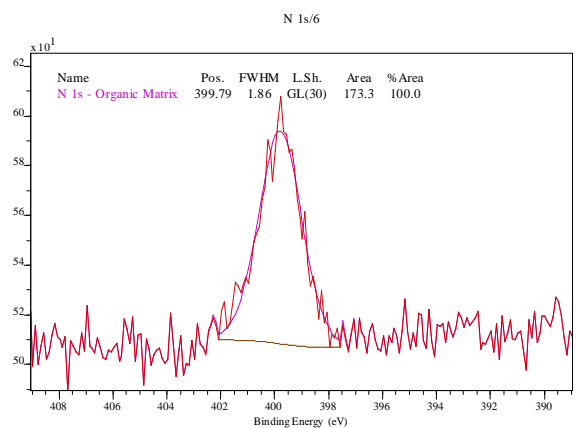
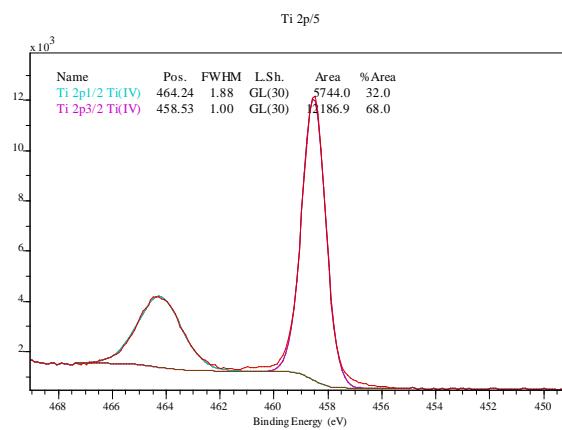
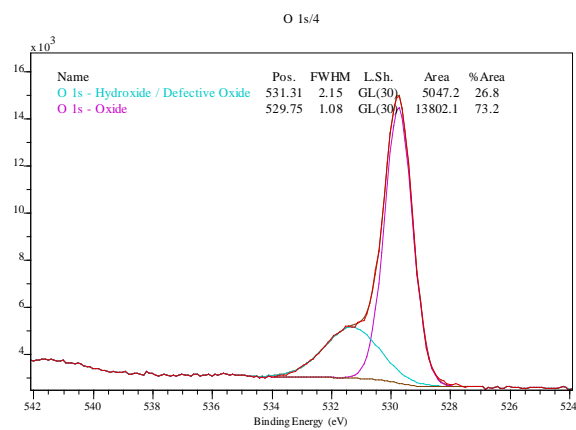
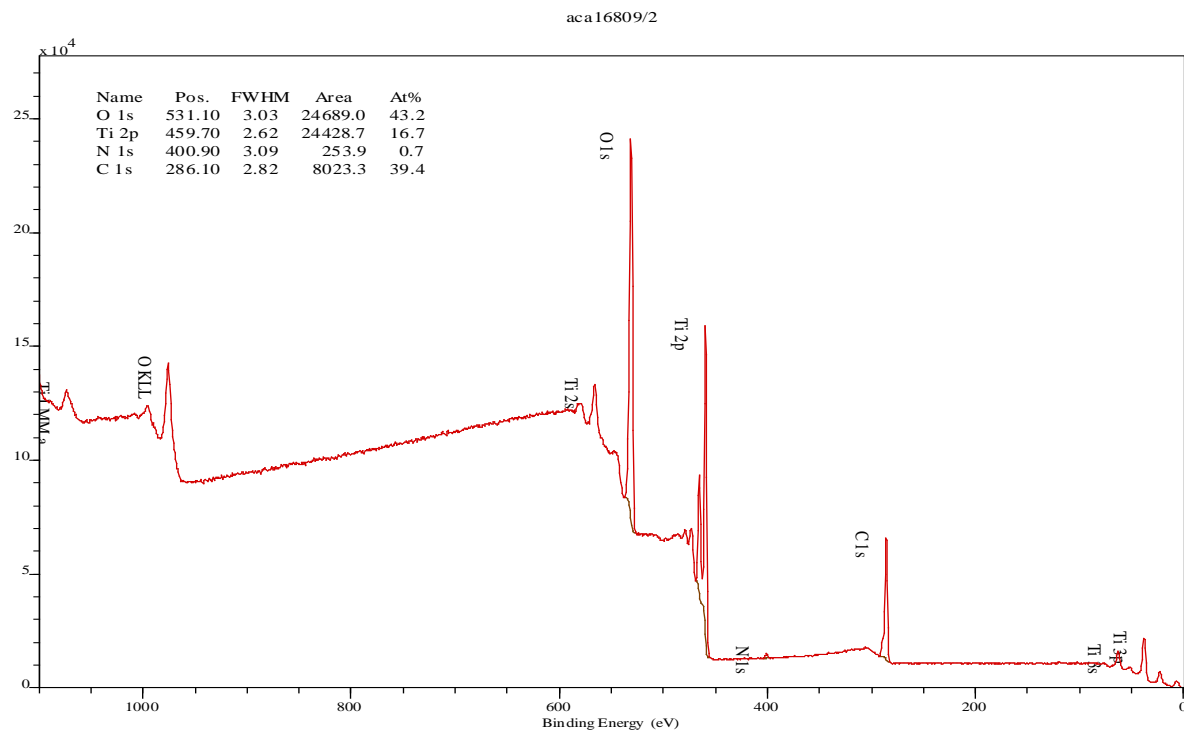


Figure 5-3: XRD patterns of TiO₂ nanotubes

5.4.3 XPS and EDX results

Investigation of the oxidation state of the Fe, C and N dopants were carried out by XPS. The Fe-C-N-codoped TiO₂ nanotube arrays contained Ti, O, N, and C. The binding energies of Ti 2p, O 1s, N 1s, and C 1s were 459.7, 531.0, 400.9 and 286.1 eV, respectively (Figure 5-4). Among them, C could be come from CN⁻, the residual carbon from the precursor solution and the adventitious hydrocarbon from the XPS instrument itself²⁸.



Surface Science Western

Figure 5-4: XPS results of Fe-C-N codoped TiO₂ nanotubes

The effectiveness of nitrogen doping into titanium nanotubes was confirmed by XPS spectra. As shown in Figure 5-4, a strong signal with its peak at 399.8 eV appears in the N 1s region and the content of nitrogen is about 0.7%. The state of nitrogen doped titania identified according to the binding energy of N 1s, can vary from 396 to 401 eV when different synthesis routes and nitrogen sources are employed. The difference in the binding energy of N 1s indicates different electron density around the N and hence variable chemical environments in the lattice structure of titanium where doped nitrogen is located. For nitrogen doped with the lower binding energy of around 396 eV, the β -state N atoms are generally accepted, namely the formation of a N–Ti–N structure in the titanium. On the other hand, the formation of O–Ti–N structure by partially substituting O atoms with N atoms can lead to higher binding energy of N 1s because of the smaller electronegativity of N compared to O, which corresponds to the state of doped nitrogen with the binding energy of around 400 eV. From the analysis above, the state of nitrogen doped in our case should be the lattice, namely the formation of N–Ti–O structure²¹.

The same technique was used to investigate the chemical compositions of C-doped TiO₂ annealed at 550 °C. Figure 3 shows the high-resolution spectra of C 1s in which the C 1s peaks can be fitted as three peaks at binding energies of 284.8 eV, 286.3 eV and 288.5 eV, implying three different chemical environments of carbon existing in the sample. The peak at around 284.8 eV was assigned to carbon adsorbed on the surface of the photo catalyst as a contaminant. While the peak at 286.3 eV was ascribed to the existence of C-O bonds, the peak was detected around 289 eV, suggesting carbonate

species. No obvious signals were detected around 281.5 eV and 283 eV showing that the amount of Ti-bonded carbon was very low^{29, 30}.

Since $K_3Fe(CN)_6$ is ionized to K^+ and $Fe(CN)_6^{3-}$ in the solution, it is obvious that trace amounts of Fe should be mixed to the titanium while C and N are doped. However, no appreciable signal related to Fe (281.5 eV) was observed by XPS, showing that the amount of Ti-bonded Fe was very low. Fortunately, EDX clearly shows Fe signals (Figure 5-5a) in comparison to the undoped TiO_2 nanotubes (Figure 5-5b). Therefore, according to the composition of N (0.7%), the Fe- composition can be estimated as $\sim 0.1\%$.

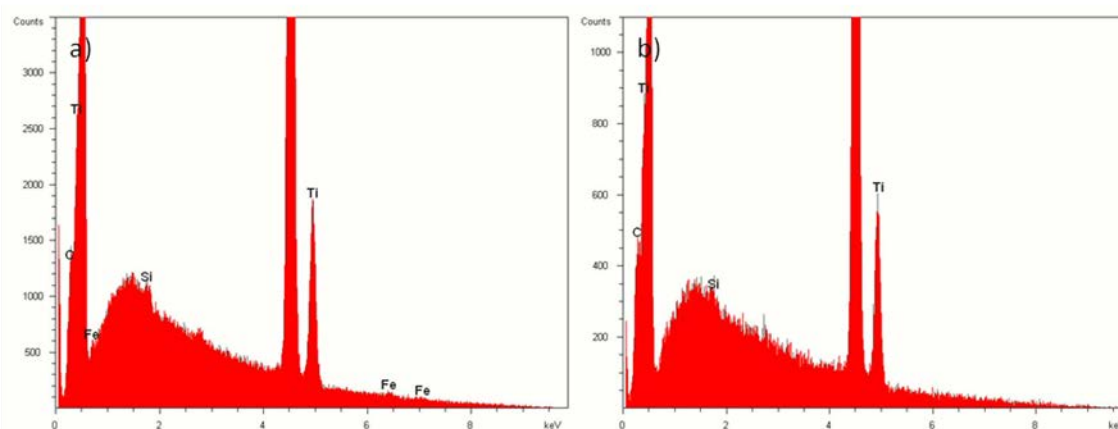


Figure 5-5: EDX results of TiO_2 nanotubes: a) Fe-C-N-codoped and b) undoped

5.4.4 Photo conversion efficiency

The photo conversion efficiency of water electrolysis is calculated based on the following relation³¹

$$PCE = \frac{I_{ph} \times (1.23 - E_{app}) \times 100\%}{I_0} \quad (1)$$

$$E_{app} = |E_{means} - E_{oc}| \quad (2)$$

Where J_{ph} is the photocurrent density; E_{app} is applied potential which can be obtained from eq. (2); E_{means} is the potential applied to photo anode versus a reference electrode; E_{oc} is the open circuit potential of photo anode under illumination; I_0 is the intensity of incident light. Figure 5-6 (a) shows the photocurrent and dark current plots of as anodized TiO_2 nanotubes in 1M KOH solution as a function of potential applied to the photo anode with reference to a Ag/AgCl reference electrode. It is obvious that the photocurrent increases with increasing the applied potential to the anode. The photocurrents developed under illumination were compared with that in the dark. It shows that almost no current was developed in the dark. Based on the eqs. (1) and (2), the photo conversion efficiency into hydrogen generation of annealed nanotubular arrays of TiO_2 in 1M KOH is plotted as a function of external potential applied to the photo anode as shown in Figur 5- 6(b). It is observed that the maximum photo conversion efficiency of TiO_2 nanotubular arrays annealed at $550^{\circ}C$ for 3h was 2.7% in 1M KOH; the maximum photocurrent was 1.06 mA under illumination power of 63 mW/cm^2 and the photo current without external potential was 0.56 mA. The best photo conversion efficiency into hydrogen generation of coped TiO_2 nanotube reported so far by Raja et al.²⁶ is around 4% in KOH.

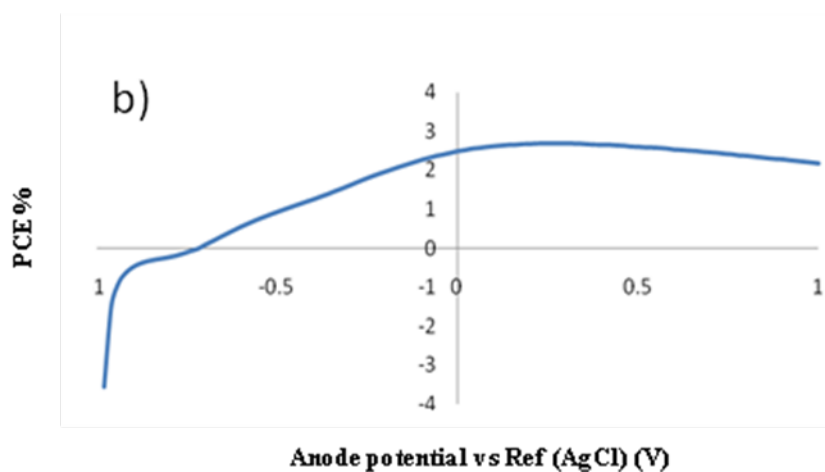
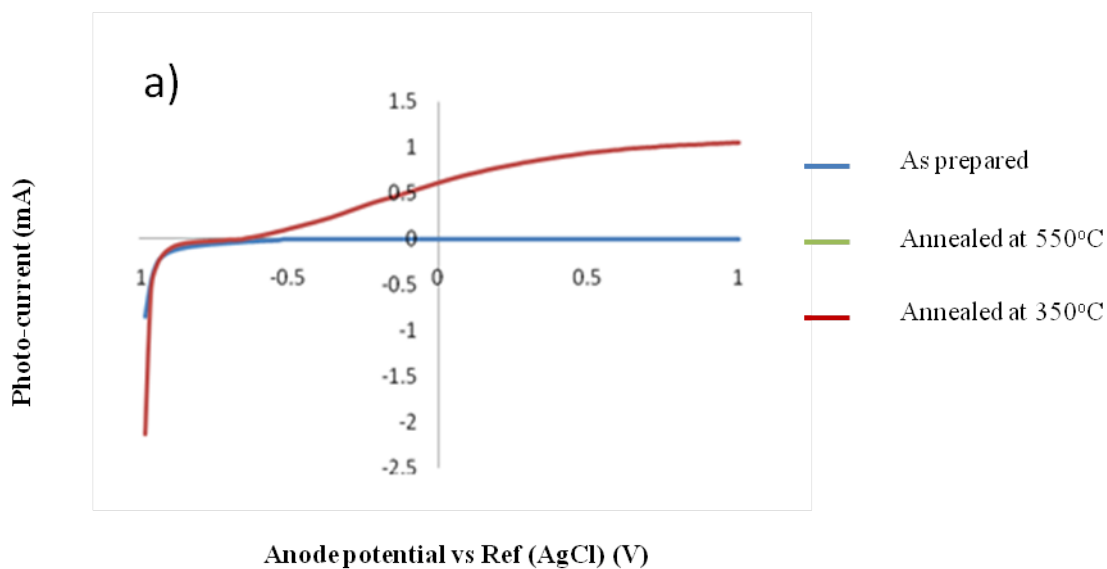


Figure 5-6: Photo current and photocurrent efficiency diagrams of TiO₂ nanotubes. a) photo current b) photo conversion efficiency

5.5 Conclusions

A new and simple modified anodization method was utilized to fabricate Fe-N-C doped and highly ordered TiO₂ nanotubes which exhibit strong visible light absorption and small band gap $E_g = 2.7$ eV. The enhancement of photo activity can be attributed to

not only the huge surface area of TiO_2 nanotube but also to possible band gap states created by addition of Fe, N and C into TiO_2 nanotube lattice during the anodization process. The resulting nanotubes exhibited the maximum photo conversion efficiency around 2.7% in 1M KOH.

5.6 References

- (1) Sharma, V. K.; Yngard, R. A.; Lin, Y. *Adv. Colloid Interface Sci.* **2009**, *145*, 83-96.
- (2) Thavasi, V.; Renugopalakrishnan, V.; Jose, R.; Ramakrishna, S. *Mater Sci Eng R Rep* **2009**, *63*, 81-99.
- (3) Dai, L. *Adv. Appl. Ceram.* **2008**, *107*, 177-189.
- (4) Chen, X.; Mao, S. S. *Chem. Rev.* **2007**, *107*, 2891-2959.
- (5) Arconada, N.; Durán, A.; Suárez, S.; Portela, R.; Coronado, J. M.; Sánchez, B.; Castro, Y. *Appl. Catal. B Environ.* **2009**, *86*, 1-7.
- (6) Campostrini, R.; Ischia, M.; Palmisano, L. *J Therm Anal Calor* **2003**, *71*, 1011-1021.
- (7) Eiamchai, P.; Chindaudom, P.; Pokaipisit, A.; Limsuwan, P. *Curr. Appl. Phys.* **2009**, *9*, 707-712.
- (8) Li Puma, G.; Bono, A.; Krishnaiah, D.; Collin, J. G. *J. Hazard. Mater.* **2008**, *157*, 209-219.
- (9) Rooth, M.; Quinlan, R. A.; Widenkvist, E.; Lu, J.; Grennberg, H.; Holloway, B. C.; Hårsta, A.; Jansson, U. *J. Cryst. Growth* **2009**, *311*, 373-377.
- (10) Doong, R.; Kao, I. *Recent Pat. Nanotechnol.* **2008**, *2*, 84-102.
- (11) Deng, L.; Wang, S.; Liu, D.; Zhu, B.; Huang, W.; Wu, S.; Zhang, S. *Catal Lett* **2009**, *129*, 513-518.
- (12) Zaleska, A. *Recent Pat. Eng.* **2008**, *2*, 157-164.
- (13) Pedraza-Avela, J. A.; López, R.; Martínez-Ortega, F.; Páez-Mozo, E. A.; Gómez, R. *J.*

- Nano. Res.* **2009**, *5*, 95-105.
- (14) Lei, L.; Su, Y.; Zhou, M.; Zhang, X.; Chen, X. *Mater. Res. Bull.* **2007**, *42*, 2230-2236.
- (15) Yamaki, T.; Umebayashi, T.; Sumita, T.; Yamamoto, S.; Maekawa, M.; Kawasuso, A.; Itoh, H. *Nucl Instrum Methods Phys Res Sect B* **2003**, *206*, 254-258.
- (16) Park, J.; Ryu, Y.; Kim, H.; Yu, C. *Nanotechnology* **2009**, *20*.
- (17) Li, Y.; Ding, D.; Bai, S.; Li, M.; Mao, D. In *In Titania nanostructures fabricated through anodization of Ti6Al4V alloy*; 2008 International Conference on Electronic Packaging Technology and High Density Packaging, ICEPT-HDP 2008; 2008; .
- (18) Chen, X.; Zhang, X.; Su, Y.; Lei, L. *Appl. Surf. Sci.* **2008**, *254*, 6693-6696.
- (19) Fahim, N. F.; Morks, M. F.; Sekino, T. *Electrochim. Acta* **2009**, *54*, 3255-3269.
- (20) Chen, X.; Su, Y.; Zhang, X.; Lei, L. *Chin. Sci. Bull.* **2008**, *53*, 1983-1987.
- (21) Liu, G.; Li, F.; Wang, D. -.; Tang, D. -.; Liu, C.; Ma, X.; Lu, G. Q.; Cheng, H. -. *Nanotechnology* **2008**, *19*.
- (22) Lu, N.; Zhao, H.; Li, J.; Quan, X.; Chen, S. *Sep. Purif. Technol.* **2008**, *62*, 668-673.
- (23) Li, J.; Yun, H.; Lin, C. -. In *In Investigations on the Fe-doped TiO2 nanotube arrays as a photoanode for cathodic protection of stainless steel*; Corrosion of Electronic Materials and Devices - 210th ECS Meeting; 2008; Vol. 3, pp 1-9.
- (24) Zhao, J.; Wang, X.; Kang, Y.; Xu, X.; Li, Y. *IEEE Photonics Technol Lett* **2008**, *20*, 1213-1215.
- (25) Yeonmi, S.; Seonghoon, L. *Nano Lett.* **2008**, *8*, 3171-3173.

- (26) Raja, K. S.; Mahajan, V. K.; Misra, M. *J. Power Sources* **2006**, *159*, 1258-1265.
- (27) Oh, H. J.; Lee, J. H.; Kim, Y. J.; Suh, S. J.; Lee, J. H.; Chi, C. S. *Applied Catalysis B, Environmental* **2008**, *84*, 142-147.
- (28) Chen, D.; Yang, D.; Wang, Q.; Jiang, Z. Y. *Ind. Eng. Chem. Res* **2006**, *45*, 4110-4118.
- (29) Chu, D.; Yuan, X.; Qin, G.; Xu, M.; Zheng, P.; Lu, J.; Zha, L. *J. Nanopart. Res.* **2008**, *10*, 357-363.
- (30) Huang, Y.; Ho, W.; Lee, S.; Zhang, L.; Li, G.; Yu, J. C. *Langmuir* **2008**, *24*, 3510-3516.
- (31) Licht, S. *Electrochemistry Communications* **2002**, *4*, 790-795.

Chapter 6

Optimization of Photoelectrochemical Water Splitting Efficiency for Hydrogen Generation of N-doped TiO₂ Nanotubes

A version of this chapter will be submitted to publication

6.1 Abstract

Highly ordered nitrogen-doped titanium dioxide (N-doped TiO₂) nanotube array films with enhanced photoelectrochemical water splitting efficiency for hydrogen generation (PCE) were fabricated by electrochemical anodization, followed by annealing under nitrogen atmosphere. Morphology, structure and composition of the N-doped TiO₂ nanotube array films were investigated by FESEM, XPS, UV-vis and XRD. The effect of annealing temperature, heating rate and annealing time on the morphology, structures, and photoelectrochemical property of the N-doped TiO₂ nanotube array films were investigated. A design of experiments (DOE) method was applied in order to minimize the number of experiments and obtain response surface and regression models for this system. From the modeling results, optimum values for the influential factors were obtained in order to achieve the maximum PCE. The optimized experiment resulted in 7.42% PCE which was within 95% confidence interval of the predicted value by the model.

Key words: Photoelectrochemical water splitting efficiency (PCE), TiO₂ nanotubes, Nitrogen doping, Design of experiments, Optimization

6.2 Introduction

TiO₂ nanotubes (NTs) are considered as one of the best alternative for photo-electrochemical materials. TiO₂ in particular has been extensively studied and put to use in microporous membranes¹, dye-sensitized solar cells², chemical sensors^{3, 4}, water-splitting electronic devices^{5,6,7}, and hydrogen storage^{8,9}. The large energy band gap (3.2 eV) is the main drawback back for optical response of these types of materials under visible light. The optical response of TiO₂ NTs is closely related to its chemical composition, atomic arrangement and physical dimension. These properties of TiO₂ NTs can be altered by doping in which either O or Ti is replaced by other elements. The various metal and non-metal have been doped into TiO₂ NTs lattice through solution doping¹⁰, hydrothermal method¹¹, ion-implantation¹² and flame annealing¹³. Among all other doping, N-doping is considered to be one of the most conventional methods due to easier substitution of O because of high electro negativity. Although the N-doped TiO₂ nanotubes arrays have shown to be the most effective at narrowing the band gap, the optical response of the materials is not always enhanced with increasing of nitrogen inside TiO₂ lattice. Based on their calculation Asahi et al.,¹⁴ believe that band gap narrowing will occur when nitrogen substitutes around 6% to 12% oxygen sites. In contrast, Okato et al.,¹⁵ claimed that high concentration of nitrogen inside TiO₂ lattice will not change the band gap. Some researchers also believe that the nitrogen can become a recombination centre for photo generated electron-hole pair^{16,17}. Obviously, this is the

area that needs further investigation. However, in practical application of view, finding the optimized condition for nitrogen doping by which the TiO_2 gains the best photo response becomes crucial.

Although there has been a lot of interest on N-doped TiO_2 nanoparticles and film, only few reports have been published on TiO_2 nanotubes. For example, Dong et al., reported that an highly ordered and N-doped TiO_2 NTs layer exhibits enhanced photocatalytic efficiency compared with their non-doped nanotubes according to the photocatalytic degradation of methyl orange under visible light irradiation¹⁸. Han et al., reported an enhanced energy-storage performance for Li ions when selectively doped with atomic N, $\text{TiO}_{2-x}\text{N}_x$ nanotubes were applied¹⁹. N-doped TiO_2 TNs as the photoanodes are used as cathodic protection materials of stainless steel²⁰. The main reason for TiO_2 nanotubes to have various applications because of following features: (1) scattering and absorption of visible light can be strongly enhanced because of the high length to diameter ratio. (2) The highly ordered TiO_2 nanotubes have much larger accessible surface area. (3) The 1D structure will facilitate electron transport along the longest direction.

Nitrogen can be doped into TiO_2 lattice through various methods²¹⁻²⁴. The calcinations of the TiO_2 nanotube arrays under the flow of NH_3 ^{25,26,27} was used as one of the conventional hydrothermal method. However, NH_3 is not only toxic but also destroys the nanotubular structure easily due to the high reactivity. In this regard, we used N_2 gas as source of nitrogen.

In the present work, an optimal condition of nitrogen doping of self-organized anodic TiO₂ NTs by thermal annealing under N₂ gas is explored. Since a specific nanostructuring is crucial for photolysis or photocatalytic applications, an optimal material architecture is required that limits recombination of photogenerated charge carriers. In this regard, our main focus is investigating the relationship between Photoelectrochemical water splitting efficiency (PCE) and amounts of nitrogen inside the lattice. The nitrogen doping process involves two steps. First of all, TiO₂ NTs were fabricated through anodization and then annealed under N₂ atmosphere with different heating rates, annealing times and temperatures. During the nitrogen doping under hydrothermal process, the integrity of the TiO₂ tubular structure remained unchanged. Although a considerable amount of work has been conducted in the field of TiO₂ NTs, very few published studies are available which use a thorough statistical approach to optimize the process and achieve specific targets in terms of photoelectrochemical water splitting efficiencies. DOE provides a method to first conduct a study in a systematic way with a small number of experiments, and second to statistically analyze and investigate the results with respect to correlations, or causality relationships between factors and responses. Optimal photoelectrochemical water splitting efficiencies were obtained by Design of Experiment (DOE) and the optimized theoretical result was evaluated by experiment. To the best of our knowledge, this is the first time report on the systematic optimization of photo response of N- doped TiO₂ NTs at nanoscale.

6.3 Experimental

6.3.1 Preparation of TiO₂ nanotubes^{28, 29}

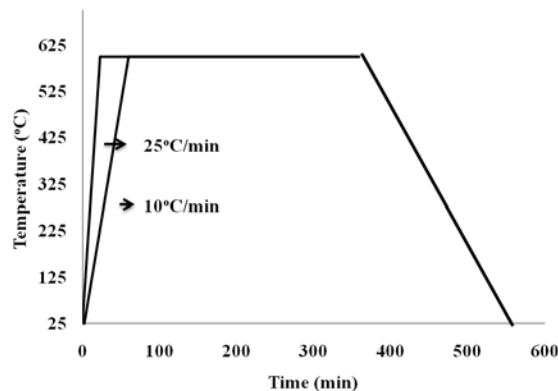
The Ti foil (0.8 mm thickness, 99.6 % purity) and all chemicals were purchased from Alfa-Aesar (Ward Hill, MA, USA). Prior to anodization, the titanium foil was cleaned by using distilled water and acetone. It was then dried off in air then etched in (3.4 M HF+5M HNO₃) for 30 s and immediately rinsed with deionized water, dried with air and used immediately.

The polished Ti foil was anodized in an ethylene glycol solution containing NH₄F (0.38 wt%) and H₂O (1.79 wt%), and placed in a well-insulated bath for several hours at 30 V and at room temperature using a DC power supply. After the anodization, the sample was washed with distilled water and acetone and then dried off with air. In order to increase the adhesion force between TiO₂ layers with substrate, the prepared sample was annealed at 100°C for 30 min and then sonicated for 30 sec.

6.3.2 N-doping

Thermal annealing was performed in pure N₂ gas. The samples were treated in a pipe furnace with a quartz glass tube with N₂ flow of 250 ml/min through the tube at 350°C to 600°C and duration of 2 to 6 hours. The TiO₂ nanotubes were gradually heated up at a rate of 10°C/min and 25°C/min from room temperature to the temperature of interest and then held at this temperature for the remaining time. Finally, the furnace was shut down

and the samples were cooled down to room temperature. Scheme 6-1 shows the details of heat-treatment scheme1.



Scheme 6-1: The heating-treatment of the samples with heating rate of 10°C/min and 25°C/min

6.3.3 Analytical methods

During processing, the anode and cathode were parallel with a separation distance of 2 cm. All anodization experiments were performed potentiostatically, under constant applied voltage, at room temperature. The electrochemical anodization was carried out by using a source meter (Keithley 2602) interfaced to a computer. The microstructural morphological features of all the samples were examined with a field emission scanning electron microscope (FE-SEM, Hitachi S-5000, Tokyo, Japan) equipped with an energy dispersive X-ray analyzer unit (EDXA). The crystalline phases were recorded by X-ray diffraction using a powder X-ray diffract meter (Rigaku RINT 2500, Tokyo, Japan) with Cu K radiation ($\lambda = 1.54\text{\AA}$) at 40 kV and 50 mA with a scan rate of 0.02 °/s and a scan speed of 1°/min over a 2θ range from 20° to 90°. The results in the elemental compositions

were determined by X-ray photoelectron spectroscopy (XPS, Perkin Elmer, Waltham, MA, USA) and EDXA. The XPS analyses were carried out with a Kratos Axis Ultra spectrometer using a monochromatic Al K(alpha) source (15mA, 14kV). A UV-vis spectrophotometer (Shimadzu 3600) equipped with diffuse reflectance cell was used to obtain UV spectrum.

6.4 Design of Experiment (DOE)

In order to estimate interaction and accordingly to estimate the shape of the response surface, the central composite design (CCD), which is one of the response surface method (RSM) was used in this study. In CCD, in addition to the “high” and “low” levels, center point and intermediate levels were also considered.

DOE methodology consisted of designing the experiments, obtaining the experimentally obtained responses, performing surface response analysis and modeling. The initial point of modeling is the computation of the effects. This effect list will suggest the appropriate model type with or without interaction. The models were estimated from regression analysis. For an k-run experimental design, the model for the experimental data can be described as follows:

$$y = b_0 + \sum_i^n b_1 X_i + \sum_i^n \sum_j^n b_2 X_i X_j + \sum_j^n b_3 X_j + e \quad (6-1)$$

where, y is response data for one of the outputs for an experiment, b_0 , b_1 , b_2 and b_3 are the model intercept, the matrix of the regression coefficients for individual factors,

and for two factor interaction, respectively. X_i and X_j are the matrixes of individual factor values for k runs and e is a vector of independent error from the experiment. The least squares regression technique was used to obtain the model coefficients.

Analysis of Variance Models (ANOVA) was used to check the selected model and examine the F tests on the regression coefficient. The F test provides information about eliminating the insignificant coefficients. Residual analysis, related diagnostics plots and calculation of model characteristics were used to verify the correctness of the model and ANOVA assumptions.

The regression model predicts the response values in a predefined range of factors. However, it is desirable to predict the model responses within real limitations and constraints for the factors and certain goals for the responses. In DOE analysis, this step is called optimization and it is based on the best-obtained regression model. In this study, it was attempted to achieve maximum values for PCE with respect to the predetermined influential factor. The graphical optimization was performed to find the best (optimal) factor levels to simultaneously satisfy all operational constraints.

6.5 Results and Discussion

6.5.1 Preparation and Characterization

6.5.1.1 SEM images

The TiO_2 nanotubes were fabricated under same conditions. The SEM images (Figure. 6-1) of the TiO_2 nanotube surfaces show that although both of N-doped surfaces

have more cracking compared to the un doped surface and the surface color was changed from light brown to dark blue, the TiO₂ tubular structures still remain the same in terms of average pore size (60 nm), wall thickness (10 nm) and tube length (4.4 μm). This can be explained by following; firstly, the annealing temperature is not high enough to convert the anatase crystal structure of TiO₂ nanotubes into rutile which may cause the surface distortion and eventually break the tube³⁰. Secondly, the level of N-doping was so low that there were not enough disturbance on the tubular structure. Normally, the highest annealing temperature should be lower than 650°C in ordered to keep the tubular structure. In this study, 600 °C was chosen as the highest temperature and results show that the tube structures were well maintained as shown in Figure 6-1.

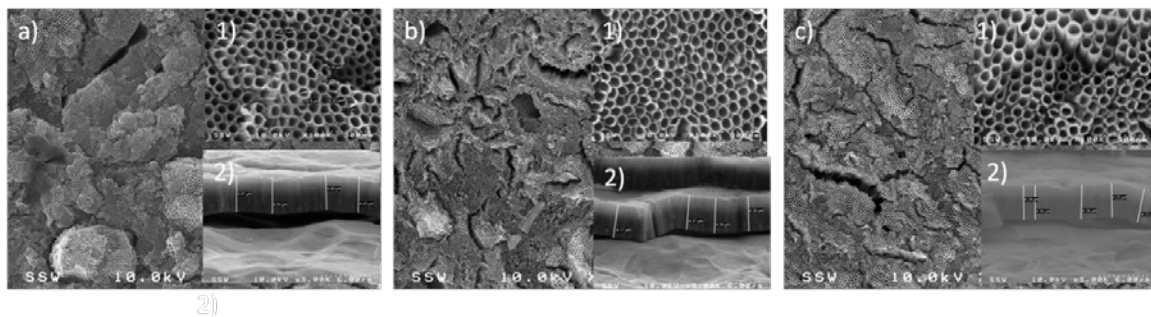


Figure 6-1: SEM images of the TiO₂ nanotube surfaces a) Before N-doping, b) N-doping at 350°C for 6h c) N-doping at 600°C for 6h

6.5.1.2 XRD patterns

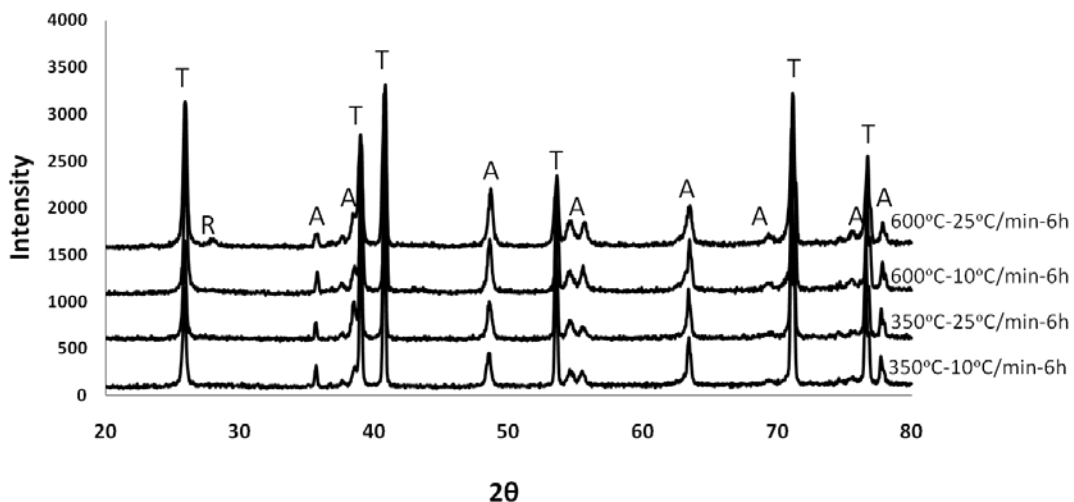


Figure 6-2: XRD patterns of N-doped TiO₂ nanotubes

The XRD patterns of TiO₂ nanotubes arrays are shown in Figure 6-2. The N-doping processes were under the nitrogen atmosphere. Only the XRD spectrums at the lowest and the highest temperatures, the longest annealing time and the lowest and the highest heading rates were selected due to the representative characters of these samples. Although there are no major differences between the samples which annealed at 350°C and 600°C and they are mostly in anatase form, the rutile form started forming at 600°C. Interestingly, the rutile forms only by incorporating the heating rate of 25°C/min, not 10°C/min because as the overall annealing time does not change, the sample stay longer at 600°C under quicker heating rate than that of slower.

6.5.1.3 Photoelectrochemical water splitting efficiency (PCE)

The PCE of TiO₂ nanotubes array was measured by three-electrode at room temperature under 400 nm cut-off filter with 150 mW/cm² illumination in a 1 M KOH solution. The photo conversion efficiency of water electrolysis was calculated based on

the following relations:

$$PCE = \frac{I_{ph} \times (1.23 - E_{app}) \times 100\%}{I_0} \quad (6-2)$$

$$E_{app} = |E_{means} - E_{oc}| \quad (6-3)$$

Where J_{ph} is the photocurrent density; E_{app} is applied potential which can be obtained from equation 6-3; E_{means} is the potential applied to photo anode versus a reference electrode; E_{oc} is the open circuit potential of photo anode under illumination; I_0 is the intensity of incident light. The PCE vs potential bias of optimized sample (at 567°C, heating rate of 17.6 and annealing time of 2h) is shown in Figure 6-3. The maximum PCE of 7.42 % was achieved under bias of 0.62V. The maximum PCE of the rest of the samples are shown in the Table 6-1.

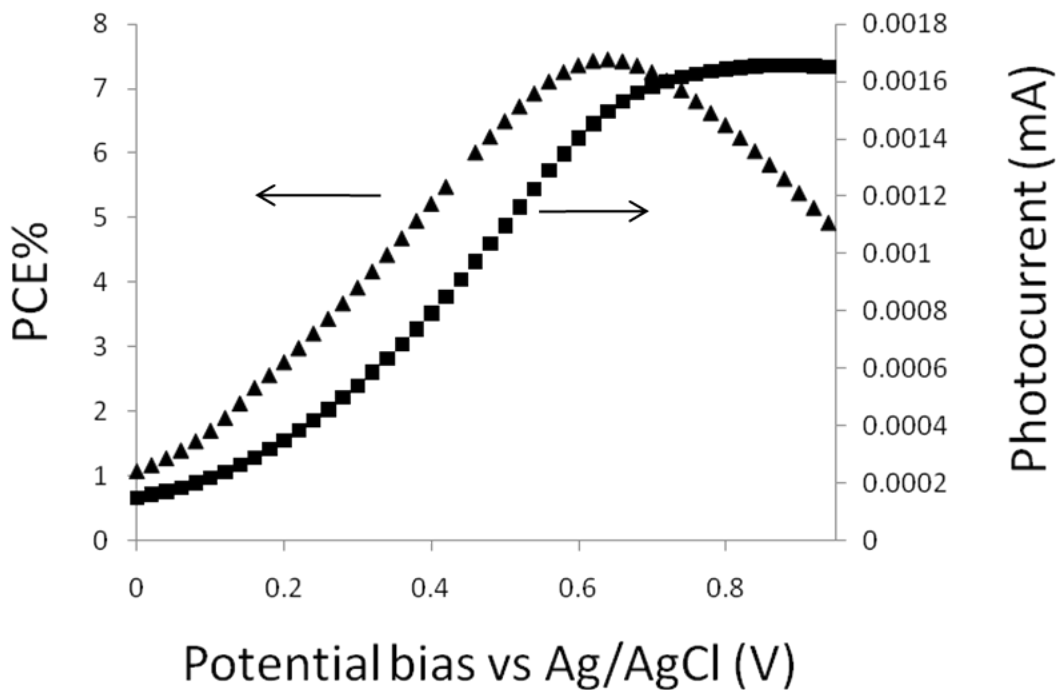


Figure 6-3: Photo current and photoelectron conversion efficiency as a function of measured potential bias vs/AgCl reference electrode of N-doped TiO₂ nanotube arrays

under optimized condition.

The samples were annealed at 350°C, 475°C and 600°C for 2 h, 4h and 6 h respectively under N₂ atmosphere through the nitrogen doping process. Table 1 shows the corresponding photoconversion efficiency of the all fourteen samples. It has been reported that when the nanotube length exceeds several microns, the great majority of the charge carriers are photogenerated in the nanotube walls³¹; hence, nanotube photoelectrochemical properties are significantly improved by increased crystallinity of the nanotube walls. The higher photoconversion efficiencies are obtained for nanotubes annealed at the higher temperatures. However there are two exceptions such as; the highest PCE (6.73%) was obtained at 350°C, heating rate 25°C/min and total 6h of annealing time and the second lowest PCE (2.76%) was appeared at 600°C, heating rate 25°C/min and total 6h of annealing time may be due to the following reasons. As we see from Figure 6-2 the crystallinities of the samples are not much different at 350°C and 600°C. However, when the higher heating rate was applied, the annealing time at specific temperatures was longer because the maximum temperature was reached faster. In the case of 350°C, the sample was at 350°C long enough so that the TiO₂ nanotube arrays were fully crystallized to anatase form as shown in Figure 6-2, which resulted in high PCE. In the case of the high final temperature of 600°C, the sample was exposed to high temperature of 600°C for longer time and consequently changed to rutile form therefore the efficiency may decrease.

Table 6-1: PCE of TiO₂ nanotubes were annealed at different conditions under N₂ flow (250 ml/min).

Run	Temperature (°C)	Heating rate (°C/min)	Time (hour)	Estimated band	
				gap (eV)	Maximum PCE (%)
1	600	25	6	2.40	2.76
2	475	25	4	2.20	5.5
3	350	17.5	4	2.49	5.91
4	600	10	6	3.02	4.5
5	350	10	6	2.38	2.42
6	350	10	2	~	3.76
7	350	25	2	2.29	4.48
8	475	10	4	2.48	4.88
9	600	25	2	2.18	6.38
10	475	17.5	4	2.85	6.69
11	350	25	6	2.07	6.83
12	475	17.5	6	2.25	5.16
13	600	17.5	4	2.27	5.01
14	600	10	2	2.33	5.72
15	567	17.6	2	2.03	7.42

6.5.1.4 XPS results

In order to investigate the amounts and the chemical states of nitrogen on surface the optimized sample XPS was performed. Since the N1s assignment of the XPS is still under debate, the characteristic peaks were labelled according to the recent publication³².

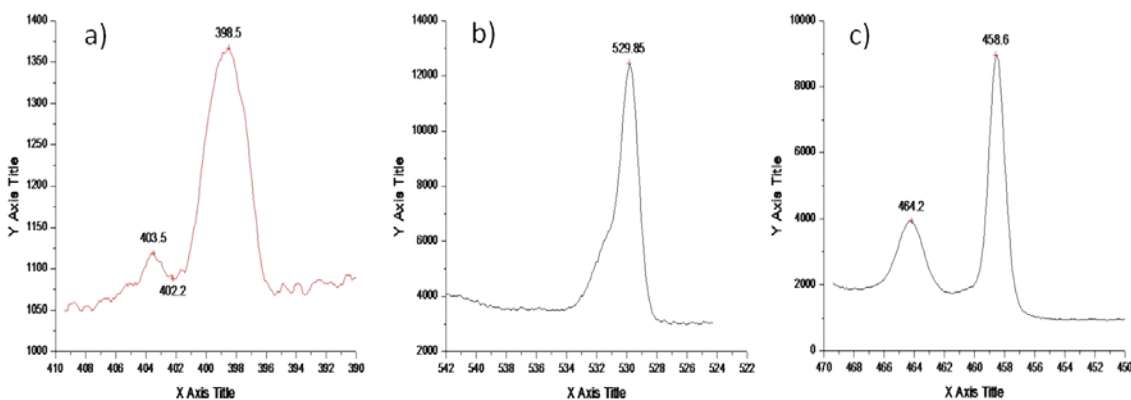


Figure 6-4: High-resolution XPS spectra of optimized sample: a) N 1s, b) O 1s region and c) Ti 2p

In general, the XPS spectrum of the TiO₂ single crystal exhibits Ti 2P_{3/2} peak at 458.7 eV and O 1s peak at 530.3 eV. After treatment with the optimized condition, the Ti 2P_{3/2} and O 1s peaks shifted to 458.6 eV and 529.85 eV, respectively (Figure 6-4b and 4c). The shifts are mainly because of the nitrogen doping which causes partial electron transformation from the N to the Ti and an increase of the electron density on Ti due to the lower electronegativity of nitrogen compared to oxygen. The state of nitrogen doped into TiO₂ lattice identified according to the binding energy of N 1s, can vary from 396 to 401 eV when different synthesis routes and nitrogen sources are employed^{33,34}. Although, there was no peaks around 396 eV observed, which is characteristic of N⁻³ and represents the Ti-N bonding, a signal with the binding energy of 398.5 eV appeared in N1s region and the content of nitrogen is 2.7 %. The signal at 398.5 eV can be ascribed to Ti-O-N or Ti-N-O oxynitride (Figure 6-4a). The other peak at 403.5 eV may represent adsorbed nitrogen. One should notice that since XPS is surface characterization technique, the amount of nitrogen showed in XPS only represents the nitrogen on the surface not the bulk.

6.5.1.5 UV-vis results

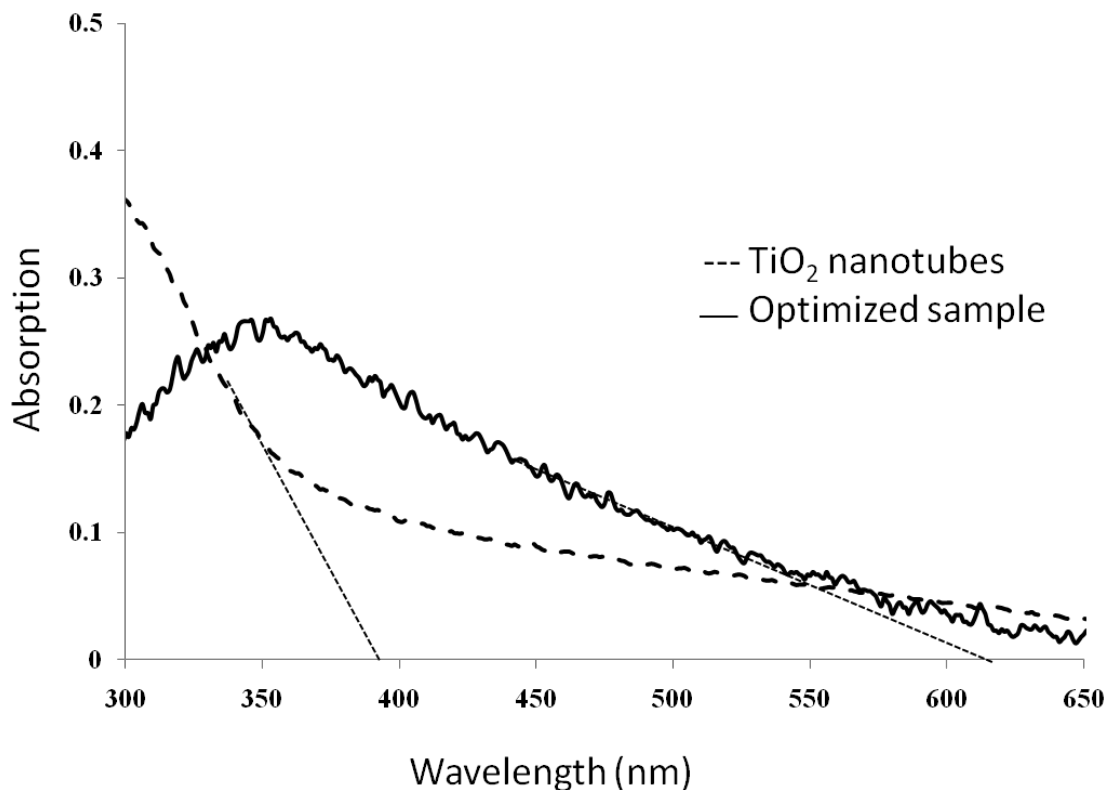


Figure 6-5: UV-vis spectrum of TiO₂ nanotubes and Optimized sample

All samples exhibit strong red shift in UV-vis spectrum. The band gap was estimated according to the literature³⁴. The band gaps were shown in Table1-1. In general, the optical absorption is a function of both film thickness and nitrogen concentration. The band gap which causes higher PCE was resulted by either mixing the nitrogen 2p states with O 2p states on the top of the valence band or the creation of the N-induced mid-gap level³⁵. There are three main external factors which can alter the crystallinity and amounts of nitrogen inside the TiO₂ lattice including temperature, heating rate and annealing time under constant nitrogen atmosphere. Although the band gap directly related to the PCE, it does not necessarily meant that smaller the band gaps the higher the

PCEs. For example the band gap 2.49 eV results in a PCE of 5.91% but the band gap of 2.33 eV shows PCE of 2.76 % (Table 6-1).

6.5.2 Design of Experiment and Optimization

6.5.2.1 Design of Experiment (DOE)

The experiments were performed according to the central composite design. The low and high values of studied process variables and are shown in Table 6-2.

Table 6-2.Factors and Response

	Parameter	Name	Units	Type	Range	
					Low	High
Factors	A	Temperature	°C	Numeric	350	600
	B	Heating Rate	°C/h	Numeric	10	25
	C	Time	h	Numeric	2	6
Response	Y	PCE	%	Numeric	N/A	

The most important objective of DOE methodology employed in this study was to find the most influential factors and use this information to determine the optimal experimental conditions in order to achieve maximum PCE.

The contribution of each factor and their interaction was determined by the statistical analysis, and can be determined by looking at the model equation in terms of coded factors shown below:

$$PCE = 6.43 + 0.33A + 0.70B - 0.38C - 1.07AB - 1.02AC - 0.13BC - 0.90A^2 - 1.17B^2 - 0.06C^2 \quad (3)$$

It was found that all the factors are significant; however factor B (Heating rate) is the

most influential factor on the studied response. The interaction between all factors has also considerable influence on the response.

The validity of the developed statistical model can be examined by ANOVA table, which is shown in Table 6-3.

Table 6-3: ANOVA Table

Source	Sum of Squares	Degree of Freedom	Mean Square	F Value	P-value
Model	21.74	9	2.42	1.85	0.2900
A	0.73	1	0.73	0.56	0.4965
B	3.29	1	3.29	2.52	0.1876
C	0.95	1	0.95	0.73	0.4408
AB	5.65	1	5.65	4.32	0.1061
AC	5.18	1	5.18	3.97	0.1173
BC	0.09	1	0.09	0.07	0.8117
A ²	2.01	1	2.01	1.54	0.2822
B ²	3.40	1	3.40	2.60	0.1820
C ²	8.10E-003	1	8.10E-003	6.20E-003	0.9410

The correctness of the model is also evident from Figure 6-6, which depicts predicted vs. experimental values for the studied response.

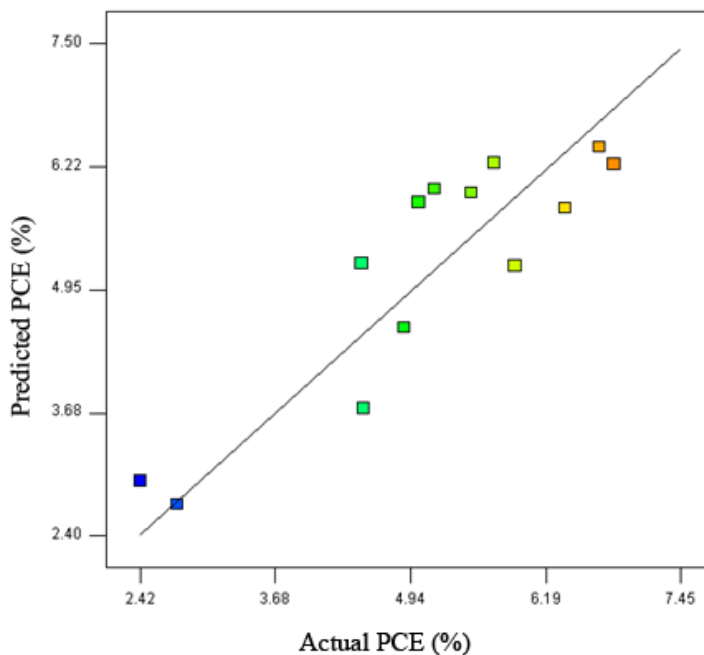


Figure 6-6: Accuracy of the model prediction

Figure 6-7 shows the surface response of two factors (temperature and heating rate) on the photo conversion efficiency.

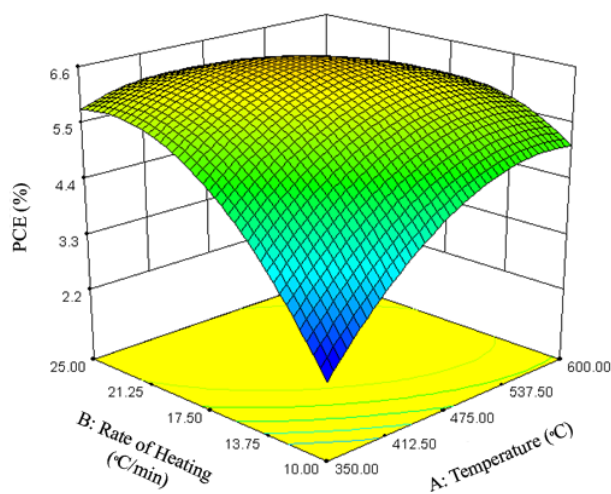


Figure 6-7: Effect of Rate of heating and Temperature on response (Time=3.95h)

From the surface plot, it can be seen that there is a non-linear relationship between the output and the two factors. The maximum photo conversion efficiency is found in the mid ranges for both factors.

Figure 6-8 shows the surface response of time and heating rate. From the plot it can be seen that both factors have opposite effect on the response at the low values and high values of its pre-specified range. At low values of temperature, increasing time results in the increase in photo conversion efficiency however, at high values of temperature this effect is negative.

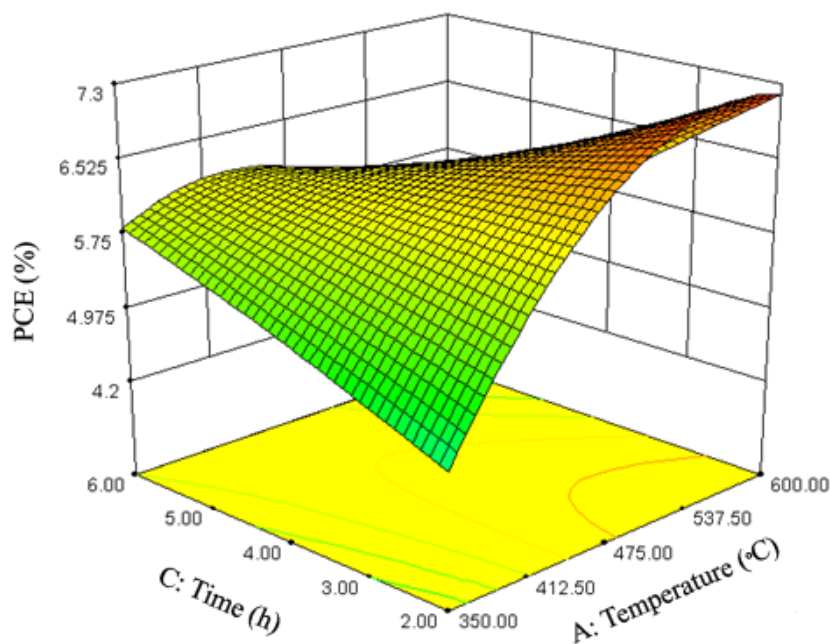


Figure 6-8: Effect of Time and Temperature on response (Heating rate=20°C/h)

Figure 6-8 shows the effect of temperature and time on hydrogen generation, respectively. Both figures show the values of photo conversion efficiency at three levels of two above-mentioned factors. It is obvious that both factors have opposite effect at the high and low values of the other factor (i.e., increasing temperature at the low level of time factor has a positive effect on PCE, however increasing temperature the high level of time factor decreases PCE). This can be attributed to the high interaction effect between

these factors, which can be noted from Equation 3.

6.5.2.2 Optimization

Thus far, the effect of three studied factors on the specified response was investigated. The results confirmed that one factor could influence the response in a positive way, while others could have an effect in a negative way. Although the output models provided some insights into the significance of the studied factors, as well as into the interactions between them, the optimal operational condition was still not obvious. Hence, an optimization of statistical results was needed. A graphical optimization method was used to obtain the optimal formulation. This method involved overlaying all model responses in the form of contour plots with specified constraints on inputs and desired goals. The target ranges based on typical requirements were set for each input, and the optimization was performed. In order to show the concept of optimization, the following optimization problem was chosen:

$$\begin{aligned} & \textit{target } Y - \textit{maximized} \\ & \textit{subject to } A, B, C \textit{ (within the specified range)} \end{aligned} \tag{4}$$

Figure 6-9 depicts the plot with the area in which the desired output can be obtained. The corresponding values of three studied factors are shown as well. The results were validated by performing three experiments using the formulation obtained from the statistical optimization and the optimal PCE obtained was 7.42%, which is within 95% confidence interval of the model.

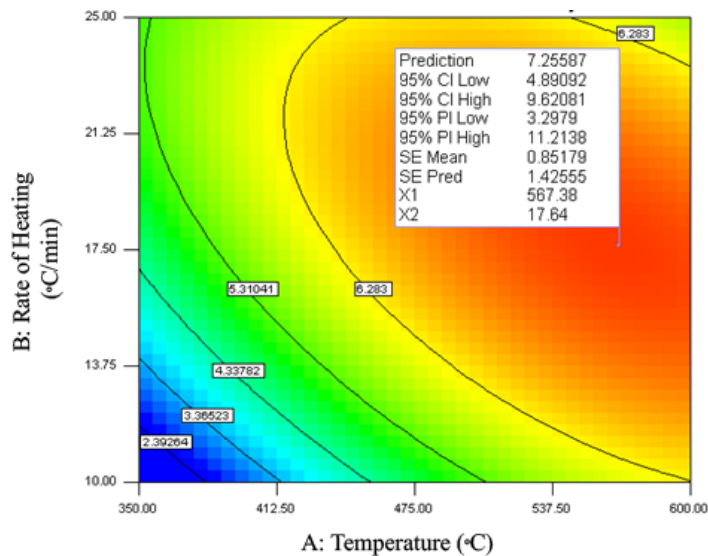


Figure 6-9: Optimization results (Time=2h)

6.6 Conclusions

In summary, we prepared N_2 doped, highly smooth and ordered TiO_2 NTs by two-step process and then annealed under N_2 atmosphere. The photoelectrochemical water splitting efficiencies (PCE) of the N_2 doped TiO_2 nanotubes under visible light were measured and used as the response for DOE optimization. The changing parameters are annealing temperatures, heating rates and annealing time respectively. The optima of these factors were determined based on the polynomial equations generated by response modelling and the optimal PCE was 7.26%. The optimal result was validated by performing real experiments using the formulation obtained from the statistical optimization and the average optimal PCE obtained was 7.42%, which is within 95% confidence interval of the model. The visible light active N- doped TiO_2 nanotubes has potential application on water purification.

6.7 References

- (1) Li, X. H.; Liu, W. M.; Li, H. L. *Applied Physics A: Materials Science and Processing* **2005**, *80*, 317-320.
- (2) Roy, P.; Kim, D.; Lee, K.; Spiecker, E.; Schmuki, P. *Nanoscale* **2010**, *2*, 45-59.
- (3) Lai, Y. -.; Huang, J. -.; Zhang, H. -.; Subramaniam, V. -.; Tang, Y. -.; Gong, D. -.; Sundar, L.; Sun, L.; Chen, Z.; Lin, C. -. *J. Hazard. Mater.* **2010**, *184*, 855-863.
- (4) Zheng, Q.; Zhou, B.; Bai, F.; Li, L.; Jin, Z.; Zhang, J.; Li, J.; Liu, Y.; Cai, W.; Zhu, X. *Adv Mater* **2008**, *20*, 1044-1049.
- (5) Zhang, Z.; Hossain, M. F.; Takahashi, T. *Int J Hydrogen Energy* **2010**, *35*, 8528-8535.
- (6) Allam, N. K.; Alamgir, F.; El-Sayed, M. A. *ACS Nano* **2010**, *4*, 5819-5826.
- (7) Gong, J.; Lai, Y.; Lin, C. *Electrochim. Acta* **2010**, *55*, 4776-4782.
- (8) Mishra, A.; Banerjee, S.; Mohapatra, S. K.; Graeve, O. A.; Misra, M. *Nanotechnology* **2008**, *19*.
- (9) Rather, S. -.; Mehraj-ud-din, N.; Zacharia, R.; Hwang, S. W.; Kim, A. R.; Nahm, K. S. *Int J Hydrogen Energy* **2009**, *34*, 961-966.
- (10) Yang, L.; Chen, B.; Luo, S.; Li, J.; Liu, R.; Cai, Q. *Environmental Science and Technology* **2010**, *44*, 7884-7889.
- (11) Wang, S.; Zhou, S. *J. Hazard. Mater.* **2011**, *185*, 77-85.
- (12) Ghicov, A.; Schmidt, B.; Kunze, J.; Schmuki, P. *Chemical Physics Letters* **2007**, *433*, 323-326.

- (13) Xu, C.; Shaban, Y. A.; Ingler Jr., W. B.; Khan, S. U. M. *Solar Energy Mater. Solar Cells* **2007**, *91*, 938-943.
- (14) Asahi, R.; Morikawa, T.; Ohwaki, T.; Aoki, K.; Taga, Y. *Science* **2001**, *293*, 269-271.
- (15) Okato, T.; Sakano, T.; Obara, M. *Physical Review B - Condensed Matter and Materials Physics* **2005**, *72*, 1-6.
- (16) Di Valentin, C.; Finazzi, E.; Pacchioni, G.; Selloni, A.; Livraghi, S.; Paganini, M. C.; Giamello, E. *Chem. Phys.* **2007**, *339*, 44-56.
- (17) DArienzo, M.; Siedl, N.; Sternig, A.; Scotti, R.; Morazzoni, F.; Bernardi, J.; Diwald, O. *Journal of Physical Chemistry C* **2010**, *114*, 18067-18072.
- (18) Dong, L.; Cao, G. -.; Ma, Y.; Jia, X. -.; Ye, G. -.; Guan, S. -. *Transactions of Nonferrous Metals Society of China (English Edition)* **2009**, *19*, 1583-1587.
- (19) Han, K. S.; Lee, J. W.; Kang, Y. M.; Lee, J. Y.; Kang, J. K. *Small* **2008**, *4*, 1682-1686.
- (20) Li, J.; Yun, H.; Lin, C. -. *J. Electrochem. Soc.* **2007**, *154*, C631-C636.
- (21) Shankar, K.; Tep, K. C.; Mor, G. K.; Grimes, C. A. *J. Phys. D* **2006**, *39*, 2361-2366.
- (22) Dong, F.; Zhao, W.; Wu, Z. *Nanotechnology* **2008**, *19*.
- (23) Ghicov, A.; Macak, J. M.; Tsuchiya, H.; Kunze, J.; Haeublein, V.; Frey, L.; Schmuki, P. *Nano Letters* **2006**, *6*, 1080-1082.
- (24) Ghicov, A.; Macak, J. M.; Tsuchiya, H.; Kunze, J.; Haeublein, V.; Kleber, S.; Schmuki, P. *Chemical Physics Letters* **2006**, *419*, 426-429.
- (25) Macak, J. M.; Ghicov, A.; Hahn, R.; Tsuchiya, H.; Schmuki, P. *J. Mater. Res.* **2006**, *21*, 2824-2828.

- (26) Vitiello, R. P.; Macak, J. M.; Ghicov, A.; Tsuchiya, H.; Dick, L. F. P.; Schmuki, P. *Electrochemistry Communications* **2006**, *8*, 544-548.
- (27) Wang, Y.; Feng, C.; Jin, Z.; Zhang, J.; Yang, J.; Zhang, S. *Journal of Molecular Catalysis A: Chemical* **2006**, *260*, 1-3.
- (28) Isimjan, T. T.; Kazemian, H.; Rohani, S.; Ray, A. K. *Journal of Materials Chemistry* **2010**, *20*, 10241-10245.
- (29) Isimjan, T. T.; Ruby, A. E.; Rohani, S.; Ray, A. K. *Nanotechnology* **2010**, *21*.
- (30) Quan, X.; Yang, S.; Ruan, X.; Zhao, H. *Environmental Science and Technology* **2005**, *39*, 3770-3775.
- (31) Ong, K. G.; Varghese, O. K.; Mor, G. K.; Grimes, C. A. *Journal of Nanoscience and Nanotechnology* **2005**, *5*, 1801-1808.
- (32) Wang, J.; Tafen, D. N.; Lewis, J. P.; Hong, Z.; Manivannan, A.; Zhi, M.; Li, M.; Wu, N. *J. Am. Chem. Soc.* **2009**, *131*, 12290-12297.
- (33) Liu, G.; Li, F.; Wang, D. -.; Tang, D. -.; Liu, C.; Ma, X.; Lu, G. Q.; Cheng, H. -. *Nanotechnology* **2008**, *19*, 345604.
- (34) Furrer, G.; Phillips, L. B.; Ulrich, K-U.; Pothig, R.; Casy, H. W. *Science* **2002**, *297*, 2243-2245.
- (35) Cong, Y.; Zhang, J.; Chen, F.; Anpo, M. *Journal of Physical Chemistry C* **2007**, *111*, 6976-6982.

Chapter 7

Photocatalytic activities of Pt/ZIF-8 loaded highly ordered TiO₂ nanotubes

A version of this chapter was published as:

Tayirjan T. Isimjan, Hossein Kazemian, Sohrab Rohani and Ajay K. Ray Photocatalytic activities of Pt/ZIF-8 loaded highly ordered TiO₂ nanotubes. *J. Mater. Chem.*, 2010, 20, 10241-10245

7.1 Abstract

The structural and photocatalytic properties of Pt/ZIF-8 (Zeolitic imidazolate frameworks) loaded TiO₂nanotubes (TiO₂ NTs) are investigated and compared to Pt/TiO₂ NTs. The loaded ZIF-8 nano crystallites were in the range of 20–40 nm and adhered well to the inner and outer lateral surfaces of the nanotubes. A uniform coverage of the ZIF-8 on the surfaces of TiO₂ NTs was observed by SEM. EDX results revealed 18.1% loading of ZIF-8 on the TiO₂ NTs. An increase in photocatalytic properties of ZIF-8 loaded TiO₂ NTs was observed by photodegradation of phenol in a 15 mL batch reactor. The resulting Pt/ZIF-8 loaded TiO₂ NTs composite were characterized by UV-vis, XRD and SEM.

Key words: ZIF-8, TiO₂ Nanotubes, Photo degradation, Pt deposition and Band gap.

7.2 Introduction

In recent years, TiO₂ nanotubes layer (TiO₂ NTs) s have attracted much attention due to their unique advantages over TiO₂ nanoparticles including larger surface-to-volume ratio, high charge transfer rate¹, and promising applications in commercial devices such as in solar cells^{2, 3, 4, 5}, sensors⁶ and water purification^{7, 8}, where the unique optical properties of TiO₂ NTs have been exploited.

To achieve higher efficiency, many researchers have improved TiO₂ NTs properties by doping with different materials or forming composite materials. Usually the modified TiO₂ NTs exhibit better performance under visible light than TiO₂ TNs. As a result of loading silica⁹, carbon nanotubes¹⁰, and zeolites¹¹ on TiO₂ NTs, higher photo catalytic efficiency and better pollutant harvesting ability were achieved. Among these, microporous zeolitic materials are attractive due to their unique uniform pores and channel sizes (3–8 Å), high surface area, high adsorption capacity, and hydrophobic and hydrophilic properties. Recently, Paramasivam et al.¹¹ have shown that under UV illumination, the ZSM-5 loaded TiO₂ NTs composites show an enhanced decay of organic pollutants up to 5.5% after 2h using a reactor with 2.7cm² surface area of TiO₂ NTs on the titanium plate .

Zeolitic imidazolate frameworks (ZIFs) that display zeolitic structural characteristics represent a rapidly growing family of organic molecular frameworks because of their high surface areas¹² and selective adsorption properties¹³. The structure of a ZIF closely

mimics the zeolitic frameworks, where the T–O–T bridges (T = Si, Al, P) in zeolites are replaced by M–Im–M bridges (M = Zn, Co, Cu). The T–O–T and M–Im–M bond angles are 145° . There is enormous potential for their applications ranging from gas storage^{14, 15} to catalysis^{16, 17}.

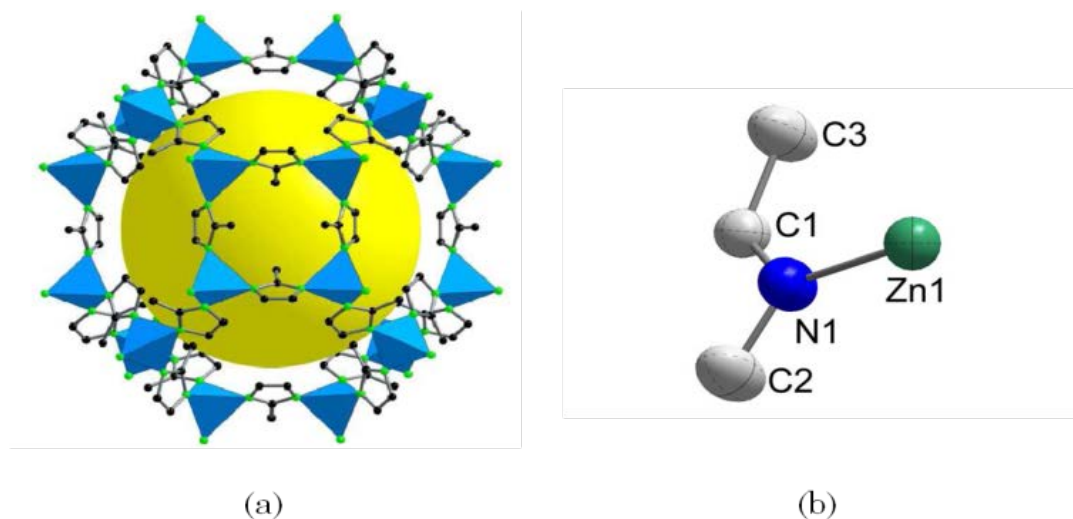


Figure 7-1: (a) The single crystal of X-ray structure of ZIF-8: ZnN₄ is shown in blue polyhedra, and the links in ball-and-stick presentation. The yellow ball indicates space in the cage. H atoms are omitted for clarity (C, black; N, green). (b) ORTEP diagram of the asymmetric unit of the ZIF-8 framework¹⁸. Reprinted from Banerjee, R.; Phan, A.; Wang, B.; Knobler, C.; Furukawa, H.; O’Keeffe, M.; Yaghi, O. M. *Science* **2008**, *319*, 939-943. Copy right (2008) with the permission from The American Association for the Advancement of Science.

We investigate the photo catalytic properties of ZIF-8 loaded TiO₂ NTs composite. In this work, 18.1% of ZIF-8 nano-particles were loaded on TiO₂ NTs (wall thickness: ~13 nm, pore size: ~70 nm, thickness of TiO₂ NTs layer: 5.5 μm as shown in Supplementary Information Figure S-3) using in-situ growth of ZIF-8 crystallites (Figure 7-1)^{12, 18} on the self-organized TiO₂ NTs layer.

The pore volume and surface area of prepared ZIF-8 were 0.32 cm³/g and 1100 m²/g (BET), respectively. The results are lower than reported in the literature (pore volume

0.662 cm³/g and surface area 1947 m²/g)¹². The objective was to combine the photocatalytic properties of TiO₂ with strong adsorbing properties of ZIF-8 to generate a composite material with enhanced photocatalytic characteristics including higher photocatalytic degradation rate as well as better visible light response comparing to TiO₂ NTs. In order to accelerate the electron transfer process¹⁹, Pt nanoparticles were loaded on the ZIF-8/TiO₂ NTs composite surface. The host-guest interactions between the TiO₂ NTs and ZIF-8 nanoparticles were characterized by means of SEM, EDX, XRD, UV-vis and photo degradation of organic pollutants. The 18.1% ZIF-8 loaded TiO₂ NTs composite material (please see the Supplementary Information) exhibited remarkable improvement in its optical and photo catalytic behaviors, showing strong visible light absorption as well as stronger degradation capabilities even under visible light in comparison to the ZSM-5 zeolite loaded TiO₂ NTs, which was shown to be active under UV illumination only¹¹. The TiO₂ NTs as a substrate for ZIF-8 provide well-defined geometry and improve the photo catalytic activity under visible light. TiO₂ NTs contain well ordered pores to confine ZIF-8 nanoparticles. To the best of our knowledge, the photo catalytic performance of ZIF loaded TiO₂ NTs has not been reported yet.

7.3 Experimental

7.3.1 Preparation of TiO₂ NTs

The TiO₂ NTs were prepared by means of the anodizing process that we have developed in our group and reported previously^{20,21}. The Ti foil (0.8 mm in thickness

and 99.6 % in purity) and all chemicals were purchased from Alfa-Aesar (Ward Hill, MA, USA). Prior to anodization, the titanium foil was cleaned using distilled water and acetone by means of ultrasonic bath. It was then dried off in air, etched in acid solution (i.e. 3.4 M HF and 5M HNO₃) for 30 s, rinsed with deionized water, dried in air and used immediately.

During the anodizing process, the anode and cathode were exactly parallel to each other with a distance of 2 cm. The polished Ti foil was anodized in an ethylene glycol solution containing NH₄F (0.38 wt%) and H₂O (1.79 wt%), and placed in a well-insulated bath for several hours at room temperature using a dc power supply. All anodization experiments were performed potentiostatically under constant applied voltage of 30V at room temperature. The electrochemical anodization was carried out by using a source meter (Keithley 2602, Metric Test, Hayward, CA, USA) interfaced to a computer. After the anodizing process, the sample was washed with distilled water and acetone and then air dried. In order to increase the adhesion force between TiO₂ nanotube layers with substrate, the prepared sample was further dried at 100°C for 30 min and then sonicated for 30 s in deionized water. An anatase TiO₂ structure was made by annealing the as-anodized samples in air atmosphere with a heating rate of 1°C/min from room temperature to 550°C and was kept at this temperature for 3 h.

7.3.2 Preparation of ZIF-8 loaded TiO₂ NTs

According to the literature²², a solution of Zn(NO₃)₂·6H₂O (0.2933 g, 0.987 mmol)

in 20 mL of methanol was rapidly poured into a solution of 2-methylimidazole in 20 mL of methanol under stirring with a magnetic bar, while the TiO₂ nanotubes disc were held vertically inside the glass reactor using a particularly designed PTFE holder. The mixture that was kept in room temperature without mixing was slowly turned turbid after 30 min, which indicated the starting point of ZIF-8 crystallization. The TiO₂ disc was removed after 15 h of reaction, washed carefully with fresh methanol in an ultrasonic bath for 30 min, then dried in air atmosphere at ambient temperature and the composite was activated at 170°C for 24 h. The produced ZIF-8 nanocrystals were also separated from the milky suspension by centrifugation. The resulting ZIF particles were washed with methanol and then dried at 60 °C in air. Finally, the ZIF nanoparticles were used for surface area measurement.

7.3.3 Pt deposition

Pt deposition on the surface of ZIF-8 loaded TiO₂ NTs was carried out by slight modification of an already reported procedure²³. ZIF-8 loaded TiO₂ NTs were immersed into diluted H₂PtCl₆ solution for 1 h and then immediately immersed in 0.002 M NaBH₄ solution for 30 min. The resulting Pt/ZIF-8 loaded TiO₂ NTs material was washed with water and dried under N₂ atmosphere at ambient temperature.

7.3.4 Photo degradation

Photocatalytic activity of the prepared composite was evaluated by phenol degradation in aqueous media under visible light illumination. The experiments were carried out in a 12 mL cylindrical reactor with an open top. The initial phenol concentration (C_0) was 52 ppm. The Pt/ZIF-8 loaded TiO_2 NTs were fixed in the middle of the reactor. The surface area of the plate which contained TiO_2 NTs was 1cm^2 . Before turning on the light illumination, the solution containing phenol and photocatalyst was stirred using a magnetic stirrer in a dark condition for 60 min in order to establish the absorption–desorption equilibrium. Then, the solution was irradiated with visible light (AM 1.5 filter, 100 mW/cm^2) at constant stirring speed. The first sample was taken out at the end of the dark absorption period, just before the light was turned on, in order to determine the actual and exact phenol concentration in the solution, which was considered as the phenol initial concentration (C_0). Sample portions of 0.2 mL were taken from the reactor every 30 min. Samples were analyzed by HPLC according to the standard procedure²⁴. The full chromatogram for each sample was recorded within the range of 0-5 min retention time. The retention time of phenol was of 2.57 min. Repeated tests were conducted to ensure the reproducibility.

7.3.5 Analytical methods

The micro-structural morphologies of all the TiO_2 NT samples were examined with a field emission scanning electron microscope (FE-SEM, Hitachi S-5000, Tokyo, Japan) equipped with an energy dispersive X-ray analyzer (EDX). The elemental compositions

of the TiO₂ NT samples were determined by EDX analysis. The crystallinity of the TiO₂ NT samples were measured by means of X-ray diffraction technique using a powder X-ray diffractometer (Rigaku RINT 2500, Tokyo, Japan) with Cu K radiation ($\lambda = 1.54\text{\AA}$) at 40 kV and 50 mA with a scan rate of 0.02 degrees per second over a 2θ ranges of 5° to 90°. Photo degradation was measured under the solar simulator (Sciencetech with AM 1.5 filter, London, ON, Canada), light intensity (100 mW/cm²). A mercury vapour lamp (Heraeus TQ 150 medium-pressure) was located axially and held in a quartz window. HPLC (Agilent Technologies 1200 series, Santa Clare, CA, USA) analysis was performed using a UV detector (218 nm) and C8 column with water/methanol/phosphoric acid (59/41/0.1%; v/v) as eluent at a flow rate of 1 mL/min. The BET surface areas and pore size distributions were determined using nitrogen adsorption–desorption isotherms by means of an ASAP2010 instrument (Micromeritics Instrument Corporation, Norcross, GA, USA). The pore size distributions were also calculated by the advanced Barrett–Joyner–Halenda (BJH) method using the adsorption-desorption branches of the isotherms. Prior to these measurements, the samples were degassed at 170 °C for 24 h in vacuum.

7.4 Results and Discussion

Figure 7-2(a) shows the top section view SEM images of the neat TiO₂ nanotubes layer after anodic growth. After the ZIF-8 loading process, in the case of ZIF-8 loaded sample, almost all the nanotubes were uniformly covered with ZIF-8 nano particles

(Figure 7-2c) with layers of tightly inter-grown ZIF-8 crystals with dimensions ranging from 20-40 nm as it shown in Figure 7-2(b). From the micrographs, one can see that the ZIF-8 crystallites are not only visible on the top but also inside the nanotubes. The ZIF-8 crystallites inside the nanotubes show very good adherence to the walls even after sonication. EDX spectrum that is shown in Figure 7- 2(d) clearly indicates the chemical analysis of the Pt/ZIF-8 loaded TiO₂ NTs. The percentage of Pt and Zn are around 1% and 5.2%, respectively from EDX. The chemical composition of ZIF-8 is Zn(2-methylimidazole)₂ and the corresponding molecular weight is 227.6 g/mol. Therefore, 5.2% Zn from EDX represents 18.1% ZIF-8 loading. For further details please refer to the Supplementary Information.

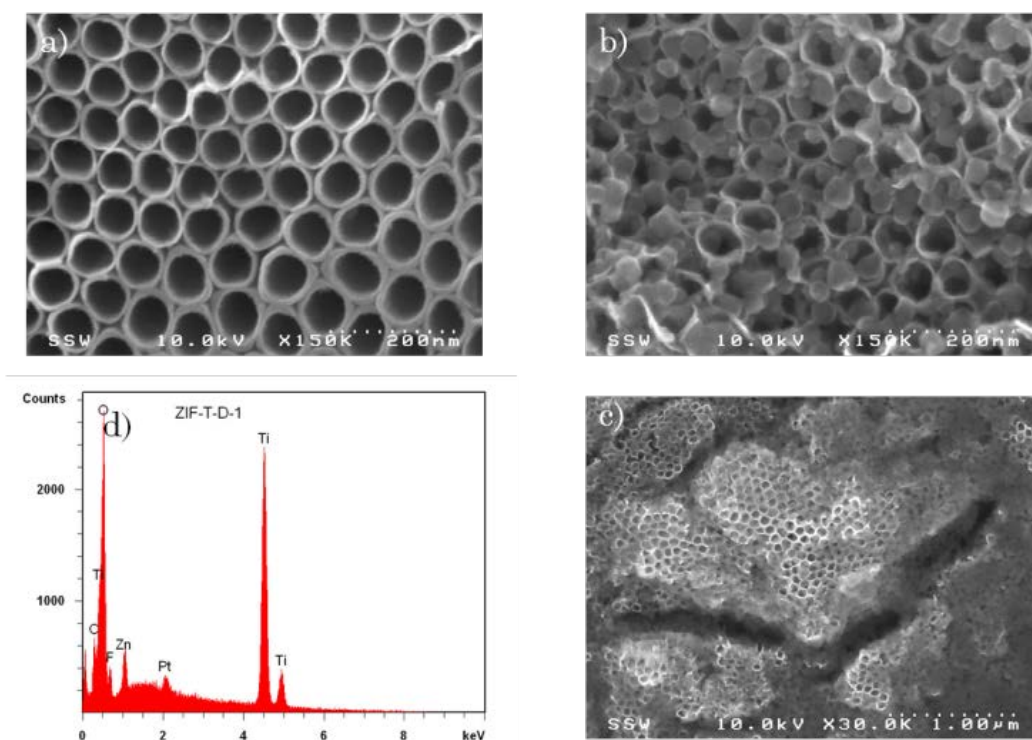


Figure 7-2: Top view SEM micrograph : (a) unloaded TiO_2 NTs. (b) Pt/ZIF-8 loaded TiO_2 NTs. (c) larger magnitude of Pt/ZIF-8 loaded TiO_2 NTs. (d) EDX results of Pt/ZIF-8 loaded TiO_2 NTs

Figure 7-3 shows the XRD patterns of as-prepared TiO_2 NTs (i.e. TiO_2 NTs arrays annealed at 550°C under air atmosphere for 3 h), as-synthesized ZIF-8 powders as well as the prepared composite material. The pattern that represents the 18.1% ZIF-8 loaded TiO_2 NTs sample, clearly exhibits ZIF-8 characteristic peaks at $2\theta = 7.2^\circ$, 7.5° , 17.9° and 26.9° which ascertains the presence of the ZIF-8 on the surface of the TiO_2 nanotubular skeleton. The characteristic peaks of ZIF-8 were slightly shifted due to the sample height displacement of ZIF-8 nanocrystals grown in the nanotube substrate compared to excess material collected as powder from the reactor bottom.

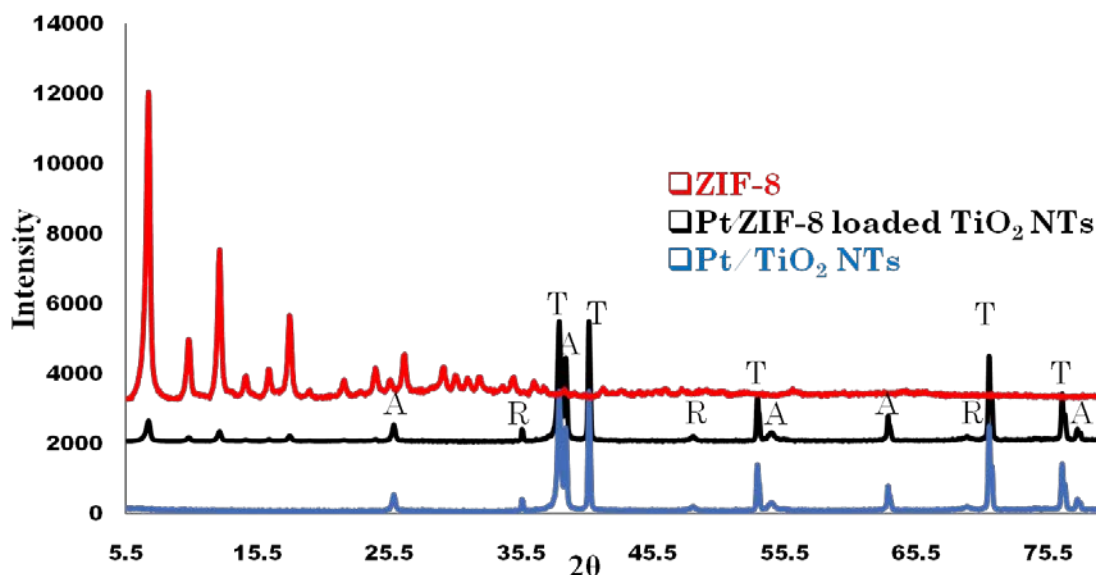


Figure 7-3: XRD results of Pt/ TiO_2 NTs, Pt/ZIF-8 loaded TiO_2 NTs and ZIF-8

Figure 7-3 shows the XRD patterns of the annealed TiO_2 NTs arrays at 550°C under

ambient air for 3 h with and without ZIF-8 loading. For reference, the pattern of TiO₂ NTs on titanium metal is also illustrated on the bottom. As shown, TiO₂ NTs consist of the anatase phase (e.g. denoted as A in the pattern). The XRD pattern of all ZIF-8 loaded TiO₂ NTs contains three very weak rutile peaks (i.e. denoted as R in the pattern) that can be neglected in terms of the influence of photo degradation activity of TiO₂ NTs.

By means of diffuse reflectance UV-vis spectroscopy (see Figure 7-4), it was observed that all the Pt/ZIF-8 loaded TiO₂ samples have an onset of absorption band significantly red shifted comparing to the Pt/TiO₂ NTs. This observation reveals that the Pt/ZIF-8 loaded TiO₂ nanotube arrays were more sensitive to the visible light than the parent nanotube arrays.

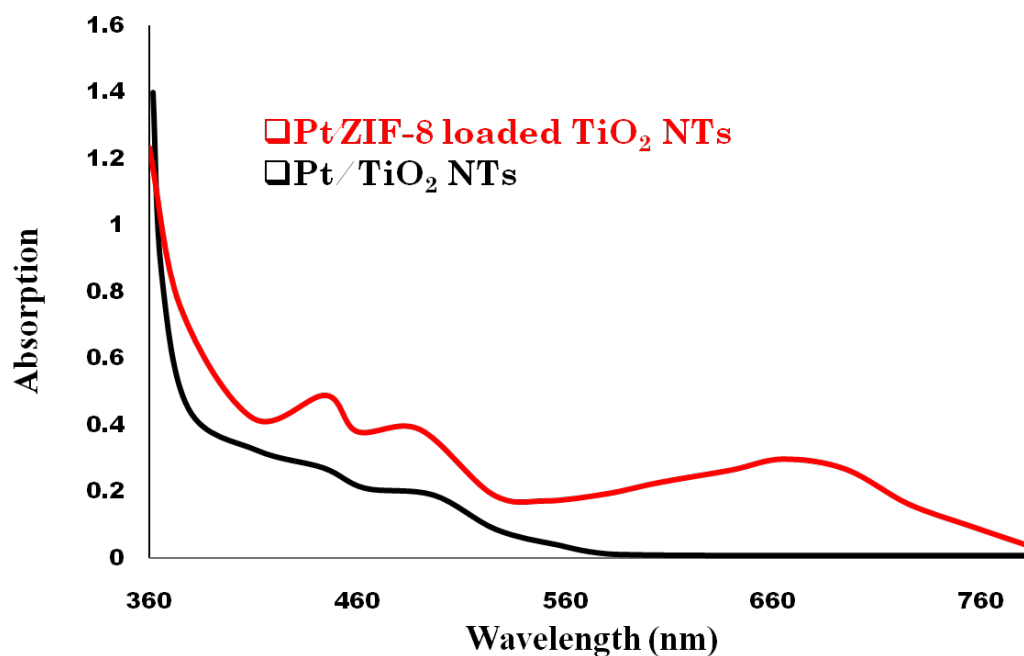


Figure 7-4: UV absorption spectra of Pt/ZIF loaded TiO₂ NTs and Pt/TiO₂ NTs

Band gap of the Pt/ZIF-8 loaded TiO_2 NTs was measured to be 2.65 eV, according to a method developed by Barton et al.²⁵ (see Figure 7-5). They pointed out that UV-vis reflectance data cannot be used directly to measure absorption coefficients (R) because of scattering contributions to the reflectance spectra. Considering the weak dependency between scattering coefficients and energy, the Kubelka-Munk function (F(R)) can be assumed to be proportional to the absorption coefficient within the narrow range of energy containing the absorption edge features. Then, a plot of $(F(R) \times E)^{1/2}$ (SQRD(F(R)*E) vs. E can be used to determine the absorption edge energy²⁵. Therefore, a strong photo catalytic activity of the ZIF-8 loaded TiO_2 NTs under visible light is assumed.

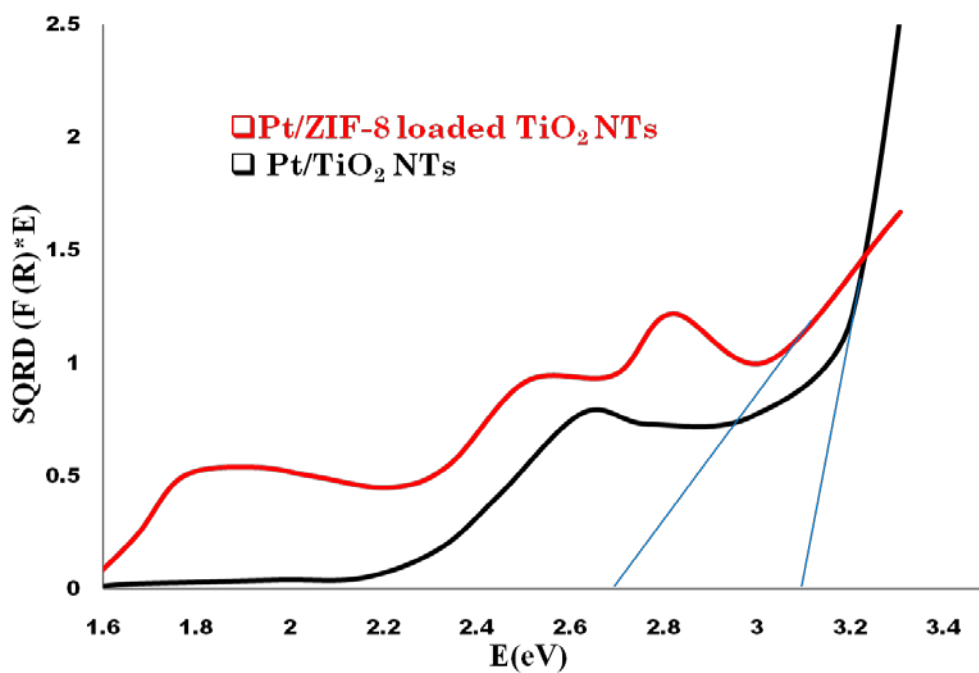


Figure 7-5: Band gap measurement of Pt/ZIF loaded TiO_2 NTs and Pt/ TiO_2 NTs

The photo catalytic oxidation mechanism is shown in Figure 7-6. During the photo catalytic oxidation process, the semi conductor (TiO_2) is activated by exciting with UV light. This excitation causes the electrons to jump from the valance band to the conduction band, resulting in the generation of high energy electrons and holes. Both the electrons and the holes eventually generate hydroxyl radicals, which are responsible for the oxidation of the organics. Pt improves catalytic performance of TiO_2 semiconductor due to its electron trapping characteristic. Pt is used to drive the equilibrium in favor of activation that causes suppressing recombination, thus the electron-hole induces photo catalytic process with higher efficiency²⁶. Pratsinis et al.²⁷ also pointed out that Pt/ TiO_2 photo catalysts favored a reductive pathway which was faster than the pathway followed by unloaded TiO_2 .

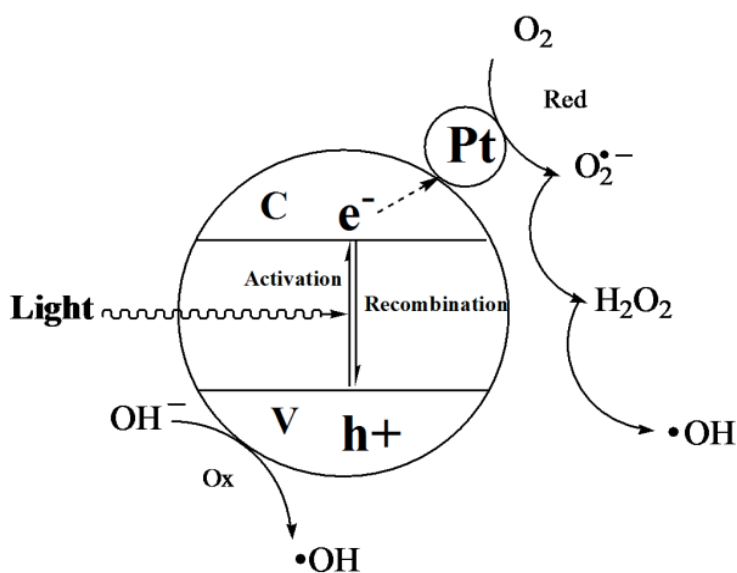
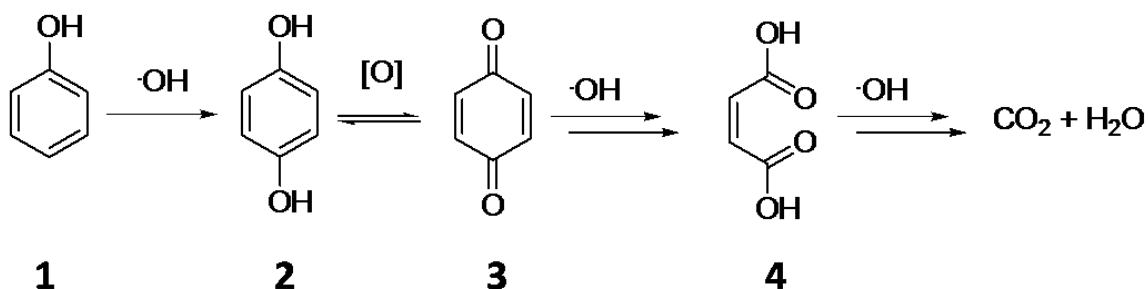


Figure 7-6: Schematic illustration of photo oxidation mechanism of Pt promoted TiO_2 semiconductors

The general mechanism of phenol degradation is shown in Scheme 7-1. The highly active hydroxyl radicals are generated by Pt/ZIF loaded TiO₂ NTs under visible light and then the hydroxyl radicals oxidize phenol (1) to hydroquinone (2) and then quinone (3) which is further oxidized to maleic acid (4). Finally, the (4) is oxidized to carbon dioxide and water²⁸.



Scheme 7-1: Photo degradation of phenol

Since the rate determining step is generation of hydroxyl radicals and the rest of oxidation steps are very fast, no intermediate was observed. Photocatalytic activity of all samples was evaluated by measuring the decomposition rate of phenol under the irradiation of artificial solar light (1.5AM, 100 mW/cm²).

Figure 7-7 shows the degradation of phenol in the presence of Pt/ZIF-8 loaded TiO₂ NTs for duration of 2 h of irradiation. Under the visible light, the maximum photodegradation efficiency of Pt/ZIF-8 loaded TiO₂ NTs is 18.6 % (see the Appendix D), which can be accounted by the lower band gap (i.e. 2.65 eV) of the developed composite. Around 3% photodegradation was observed in the presence of neat Pt/TiO₂ NTs during

the same irradiation time which may be due to the combination of the presence of trace UV light and an oxidation effect by dissolved oxygen in the suspension.

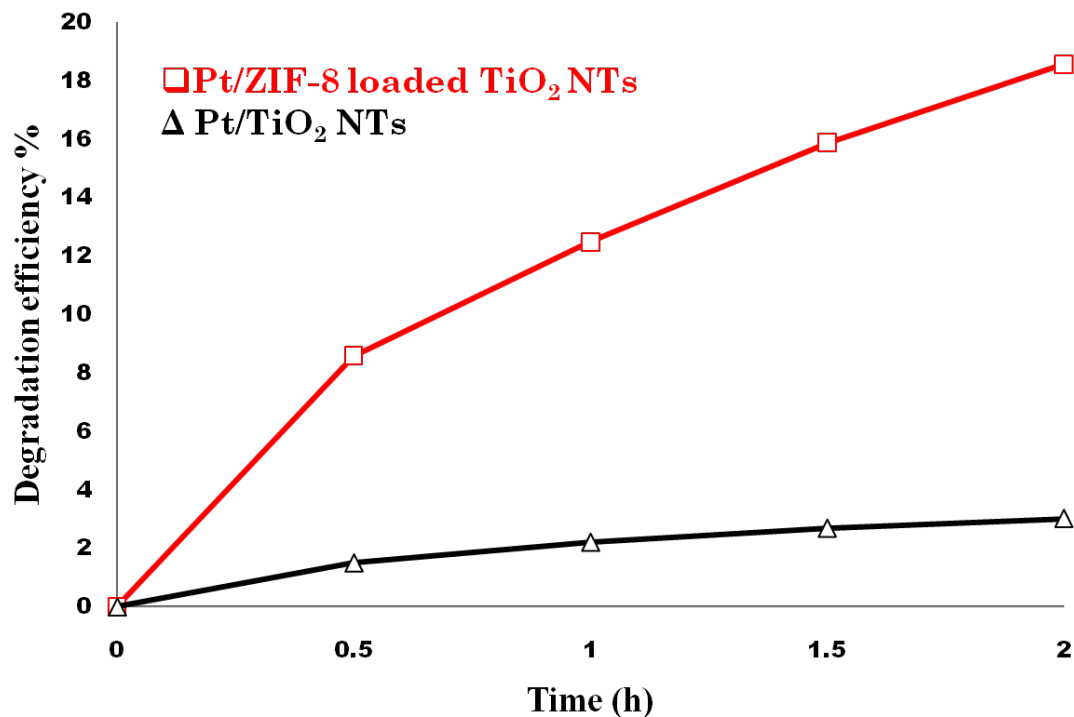


Figure 7-7: Photo degradation of Pt/ZIF loaded TiO₂ NTs, Pt/TiO₂ NTs and control

7.5 Conclusions

We have demonstrated a remarkable improvement for photo degradation of phenol by using Pt/ZIF-8 loaded TiO₂ NTs. The phenol degradation efficiency of Pt/ZIF-8 loaded TiO₂ NTs and Pt/TiO₂ NTs photo catalysts after 2 h of irradiation under visible light were 18.6% and 3.0, respectively. The unique architecture of the composite material was achieved by adding the microporous ZIF-8 nano crystallites on the surface of TiO₂ NTs and then coating by Pt nanoparticles. We combined large surface area as well as strong adsorbent properties of ZIF-8 with reducing charge recombination property of Pt/TiO₂

NTs to produce highly visible light responsive materials. The high efficiency (18.1%) of ZIF-8 loaded TiO_2 NTs surface exhibited a strong degradation of phenol. The ZIF-8 loaded TiO_2 NTs surface has a potential of serving as an effective photocatalyst for water purification.

7.6 References

- (1) Macak, J.M.; Zlamal, M.; Krysa J.; and Schmuki, P. *Small* **2007**, *3*, 300- 3004
- (2) Wang, J.; Lin, Z. *Chemistry of Materials* **2010**, *22*, 579-584.
- (3) Xu, C.; Shin, P. H.; Cao, L.; Wu, J.; Gao, D. *Chemistry of Materials* **2010**, *22*, 143-148.
- (4) Xu, H.; Tao, X.; Wang, D.; Zheng, Y.; Chen, J. *Electrochim. Acta* **2010**, *55*, 2280-2285.
- (5) Zhang, J.; Bang, J. H.; Tang, C.; Kamat, P. V. *ACS Nano* **2010**, *4*, 387-395.
- (6) Song, Y.; Schmuki, P. *Electrochemistry Communications* **2010**, *12*, 579-582.
- (7) Hsu, Y. ; Hsiung, T.; Paul Wang, H.; Fukushima, Y.; Wei, Y.; Chang, J. *Mar. Pollut. Bull.* **2008**, *57*, 873-876.
- (8) Oh, H.; Lee, J.; Kim, Y.; Suh, S.; Lee, J.; Chi, C. *Applied Catalysis B: Environmental* **2008**, *84*, 142-147.
- (9) Aresipathi, C.; Feldhoff, A.; Wark, M. *J. Mater. Sci.* **2010**, *45*, 1179-1188.
- (10) Chen, X.; Mao, S. S. *Chem. Rev.* **2007**, *107*, 2891-2959.
- (11) Gao, B.; Chen, G. Z.; Li Puma, G. *Applied Catalysis B: Environmental* **2009**, *89*, 503-509.
- (12) Paramasivam, I.; Avhale, A.; Inayat, A.; Bosmann, A.; Schmuki, P.; Schwieger, W. *Nanotechnology* **2009**, *20*, 225607.
- (13) Park, K. S.; Ni, Z.; Côté, A. P.; Choi, J. Y.; Huang, R.; Uribe-Romo, F. J.; Chae, H. K.; O'Keeffe, M.; Yaghi, O. M. *Proc. Natl. Acad. Sci. U. S. A.* **2006**, *103*, 10186-10191.

- (14) Wang, B.; Côté, A. P.; Furukawa, H.; O'Keeffe, M.; Yaghi, O. M. *Nature* **2008**, *453*, 207-211.
- (15) Hong, S.; Oh, M.; Park, M.; Yoon, J. W.; Chang, J.; Lah, M. S. *Chemical Communications* **2009**, 5397-5399.
- (16) Hu, Y.; Xiang, S.; Zhang, W.; Zhang, Z.; Wang, L.; Bai, J.; Chen, B. *Chemical Communications* **2009**, 7551-7553.
- (17) Jiang, H. -.; Liu, B.; Akita, T.; Haruta, M.; Sakurai, H.; Xu, Q. *J. Am. Chem. Soc.* **2009**, *131*, 11302-11303.
- (18) Tachikawa, T.; Choi, J. R.; Fujitsuka, M.; Majima, T. *Journal of Physical Chemistry C* **2008**, *112*, 14090-14101.
- (19) Banerjee, R.; Phan, A.; Wang, B.; Knobler, C.; Furukawa, H.; O'Keeffe, M.; Yaghi, O. *M. Science* **2008**, *319*, 939-943.
- (20) Emilio, C. A.; Litter, M. I.; Kunst, M.; Bouchard, M.; Colbeau-Justin, C. *Langmuir* **2006**, *22*, 3606-3613.
- (21) Isimjan, T. T.; Ruby, A. E.; Rohani, S.; Ray, A. K. *Nanotechnology* **2010**, *21*, 055706.
- (22) Isimjan, T. T.; Yang, D.-Q.; Rohani, S.; Ray, A. K. *Journal of Nanoscience and Nanotechnology* **2010**, *10*, 1-5.
- (23) Cravillon, J.; Münzer, S.; Lohmeier, S.; Feldhoff, A.; Huber, K.; Wiebcke, M. *Chemistry of Materials* **2009**, *21*, 1410-1412.
- (24) Bavykin, D. V.; Lapkin, A. A.; Plucinski, P. K.; Torrente-Murciano, L.; Friedrich, J. M.; Walsh, F. C. *Top Catal* **2006**, *39*, 151-160.

- (25) <http://www.osha.gov/dts/sltc/methods/organic/org032/org032.html>. 04-05-2010.
- (26) Barton, D. G.; Shtein, M.; Wilson, R. D.; Soled, S. L.; Iglesia, E. *J Phys Chem B* **1999**, *103*, 630-640.
- (27) Hiehata¹, K.; Sasahara, A.; Onishi¹, H. *Nanotechnology* **2007**, *18*, 084007.
- (28) Height, M. J.; Pratsinis, S. E.; Mekasuwandumrong, O.; Praserthdam, P. *Applied Catalysis B: Environmental* **2006**, *63*, 305–312.
- (29) Santos, A.; Yustos, P.; Quintanilla, A.; Rodríguez, S.; García-Ochoa, F. *Applied Catalysis B: Environmental* **2002**, *39*, 97-113.

Chapter 8

A new approach of tailoring wetting properties of TiO₂ nanotubular surfaces

A paper based on the chapter has been submitted to the following journal: Material Science and Engineering B

8.1 Abstract

TiO₂ nanotube layers were grown on a Ti surface by electrochemical anodization. As prepared, these layers showed a superhydrophilic wetting behavior. Modified with 1H,1H,2H,2H-perfluorooctyltriethoxysilane (PTES), the layers showed a superhydrophobic behavior. We demonstrate how to change the surface characteristics of the TiO₂ nanotube layers in order to achieve any desirable degree of hydrophobicity between 100° to 170°. The treated superhydrophobic TiO₂ nanotube layers have an advanced contact angle exceeding 165°, a receding angle more than 155° and a slide angle less than 5°. It is found that the surface morphology of the film which depends on anodization time among other variables, has a great influence on the superhydrophobic properties of the surface after PTES treatment. The hydrodynamic properties of the surface are discussed in terms of both Cassie and Wenzel mechanisms. The layers are characterized with dynamic contact angle measurements, SEM, and XPS analyses.

Keyword: TiO₂ Nanotubes, Anodization, Contact angle and Superhydrophobic surface

8.2 Introduction

Recently, significant progress has been made in improving wettability of semiconducting surfaces¹. Superhydrophobic semiconducting surfaces with water contact angle (CA) more than 150° attract much interest due to the many useful applications they offer in our daily life. Among the various superhydrophobic surfaces, the surfaces that are made either by TiO₂ nanoparticles² or nanotubes³ have controllable hydrophobicity leading to many potential applications, such as self-cleaning surfaces⁴, antibacterial surfaces⁵ and sticky tapes⁶.

Superhydrophobic properties of a surface can be controlled by both the chemical composition of the surface and surface morphology. Chemical composition can be modified by applying low free energy fluoroalkylsilane compounds on the surface⁷. A rough surface morphology can be created by using many different methods for example: plasma etching⁸, microwave-plasma enhanced chemical vapor deposition⁹, and anodic oxidation¹⁰.

Since titanium is considered as one of the most important materials in many industries, the surface engineering of titanium and its alloys is drawing lots of attention. Specially, the surface wettability study is one of the main concerns. Large degree of stable surface wettability can be achieved by attachment of ordered self-assembled monolayers (SAMs) of organic molecules such as fluorphosphate and fluoroalkylsilanes. This often is carried out by an attachment of phosphonates or silanes to OH-groups on the TiO₂ surface¹¹. Recently, Wang et al.¹² reported approaches to engineering titanium surfaces with superoleophobicity toward a broad range of oil liquids, based on anodization and laser micromachining. Lai et al designed different types of TiO₂

nanostructures which can be transformed to superhydrophobic surfaces after treating with fluoroalkylsilane. Although, both of these contributions mentioned that the surface roughness can be tuned by changing the anodization time, no systematic study has been reported in terms of roughness changes with the anodization time and its mechanism.

In this paper, we describe a simple process of generating super-hydrophobic surfaces by self-assembling the fluoroalkylsilane (PTES) compound on different TiO₂ surfaces. The surfaces formed by three different nanostructures include: nanopore array (NPA), nanotube array (NTA) and nanovesuvianite (NVS). The formation of these vertically oriented nano structures is achieved by a simple one-step electrochemical self-assembly process. By adjusting the anodization time, the morphology of the surfaces is changed from NPA to NTA and then NVS. A series of superhydrophobic surfaces with both large contact angle and small slide angle are achieved. The XRD, XPS, SEM and contact angle measurements are used to investigate the mechanism of hydrophobic behavior.

8.3 Materials and methods

The Ti foil (0.8 mm thickness, 99.6 % purity) and all chemicals were purchased from Alfa-Aser (Ward Hill, MA, USA). Prior to anodization, the titanium foil was cleaned by using distilled water and acetone. It was then dried off in air, etched in (3.4 M HF and 5M HNO₃) for 20 s, rinsed with deionized water, dried with air and used immediately.

The polished Ti foil was anodized in an ethylene glycol solution containing NH₄F (0.38 wt%) and H₂O (1.79 wt%), and placed in a well-insulated bath for several hours at 30 V and at room temperature using a DC power supply. After the anodization, the samples were washed with distilled water and acetone and then dried off with air¹³.

The electrochemical anodization experiments were performed in a conventional two-electrode cell. A platinum foil (10mm×20mm) was used as a counter electrode (cathode) and a titanium sheet served as the working electrode (anode). A Ti sheet of size 1 cm × 1 cm was pressed between a set of O-rings in the Teflon sample holder. The Pt wire was located on the back side of the sample as the electrical contact, and then fixed in the electrochemical cell with an active anode area of 0.9 cm² exposed to the electrolyte. During processing, the anode and cathode were parallel with a separation distance of 2 cm. All anodization experiments were performed potentiostatically, under constant applied voltage, at room temperature. The electrochemical anodization was carried out by using a source meter (Keithley 2602, MetricTest, Hayward, CA, USA) interfaced to a computer. The microstructural morphological features of all samples were examined with a field emission scanning electron microscope (FE-SEM, Hitachi S-5000, Tokyo, Japan). The crystalline phases were recorded by X-ray diffraction using a powder X-ray diffractometer (Rigaku RINT 2500, Tokyo, Japan) with Cu K α radiation ($\lambda= 1.54\text{\AA}$) at 40 kV and 50 mA with a scan rate of 0.05 °/s and a scan speed of 1°/min over a 2 θ range from 20° to 90°.

The contact angle measurements were performed on the modified TiO₂ nanotubes surfaces using a model 100 goniometer system (Rame-hart Inc., USA). For all systems, the images of the drops were recorded every 10 s, which allowed the drops to adjust their shape. The contact angle values were determined with a precision of 0.5°.

The results in the elemental compositions were determined by X-ray photoelectron spectroscopy (XPS, Perkin Elmer, Waltham, MA, USA) and EDXA. The XPS analyses were carried out with a Kratos Axis Ultra spectrometer using a monochromatic Al K(alpha) source (15mA, 14kV). XPS can detect all elements except hydrogen and helium,

probes the surface of the sample to a depth of 5-7 nanometres, and has detection limits ranging from 0.1 to 0.5 atomic percent depending on the element. The instrument work function was calibrated to give a binding energy (BE) of 83.96 eV for the Au 4f_{7/2} line for metallic gold and the spectrometer dispersion was adjusted to give a BE of 932.62 eV for the Cu 2p_{3/2} line of metallic copper. The Kratos charge neutralizer system was used on all specimens. Survey scan analyses were carried out with an analysis area of 300 x 700 microns and pass energy of 160 eV. High resolution analyses were carried out with an analysis area of 300 x 700 microns and pass energy of 20 eV. Spectra have been charge corrected to the main line of the carbon 1s spectrum (adventitious carbon) set to 284.8 eV. Spectra were analysed using CasaXPS software (version 2.3.14).

Before surface modification with self-assembled monolayers (SAMs) the samples were washed in acetone, ethanol and ultrapure water, each for 10 min, under sonication for cleaning purposes. Attachment of fluorine compound to TiO₂ nanotubes was achieved by soaking the samples for 12 hours in 0.1 g/mL solution of PTES in methanol. The samples were then removed, washed with methanol and ultrapure water, and dried at 140°C for 1 hour⁷. Wettability of the different surfaces was characterized by contact angle measurements under equilibrium conditions.

8.4 Results and Discussion

8.4.1 XRD Results

Due to the amorphous nature of as prepared TiO₂ NTs, the peaks in Figure 8-1 belong to the titanium substrate. To form anatase, the as-prepared amorphous porous

layers were annealed at 550 °C for 3hours. After annealing the diffraction pattern confirmed successful conversion to anatase¹³.

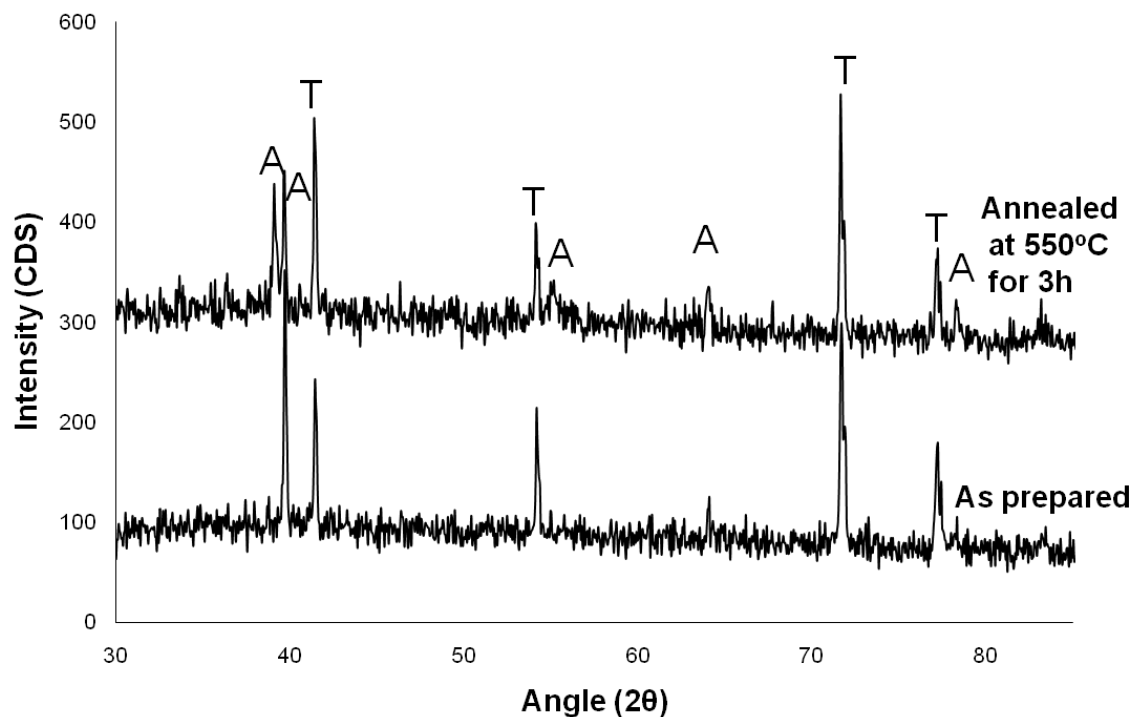


Figure 8-1: XRD patterns for TiO₂ nanotube surface at 25°C and after annealing for 3hours at 550°C.

8.4.2 SEM Results

Figure 8-2 shows the top view SEM image of the typical TiO₂ film by anodizing the Ti sheet for different duration time from 0.3 hours to 20 hours.

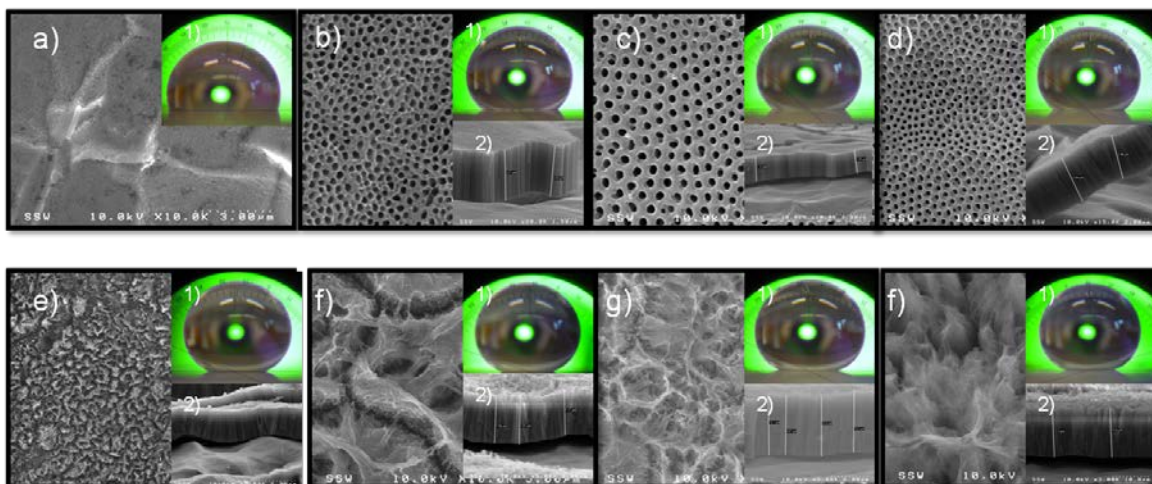


Figure 8-2: SEM images of TiO_2 nanotube surfaces, tube length and water contact angle after different anodization time: a) 0 hour, b) 0.5 hour, c) 1.0 hour, d) 1.5 hour, e) 3.0 hours, f) 5.0 hours, g) 7.0 hours, h) 20 hours.

The scanning electron images show small papillae hills starting at 5 hours anodization time. It shows that the special nanostructure surface comprises of TiO_2 nanotubes with average thickness ranging from $2.0 \mu\text{m}$ to $13.4 \mu\text{m}$. The highly ordered TiO_2 nanotube surface was formed after 2.5 hours anodization time. Subsequently the nanotubes started to collapse and the surface became non-uniform NVS surface. However, the thickness of the TiO_2 nanotubes layer still increased with the anodization time (Figure 8-3).

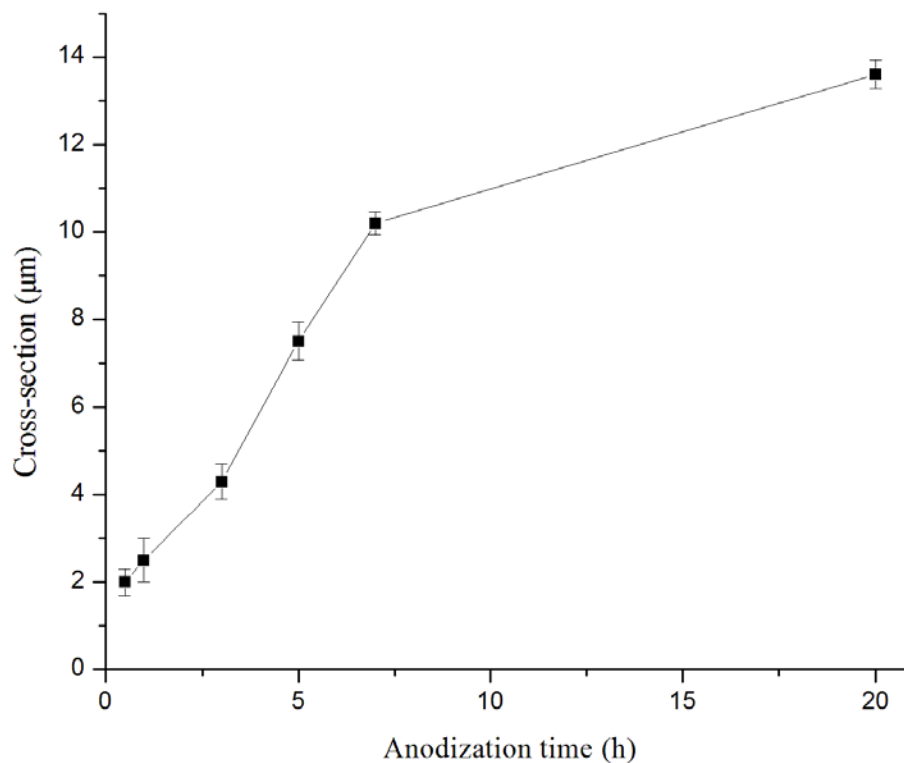


Figure 8-3: The cross-section of TiO₂ nanotube surface as a function of the anodization time.

Water droplets quickly spread and wet the aligned TiO₂ nanotube film due to side penetration of the liquid by capillary forces in the special tubular structure, indicating that such TiO₂ nanotube film is superhydrophilic before treating with PTES.

8.4.3 XPS Results

XPS was used to analyze the composition of the TiO₂ surface after fluorination, as shown in Figure 8-4. XPS analysis confirmed the presence of the fluorine and carbon on the surface of nanotubes (Figure 8-4a).

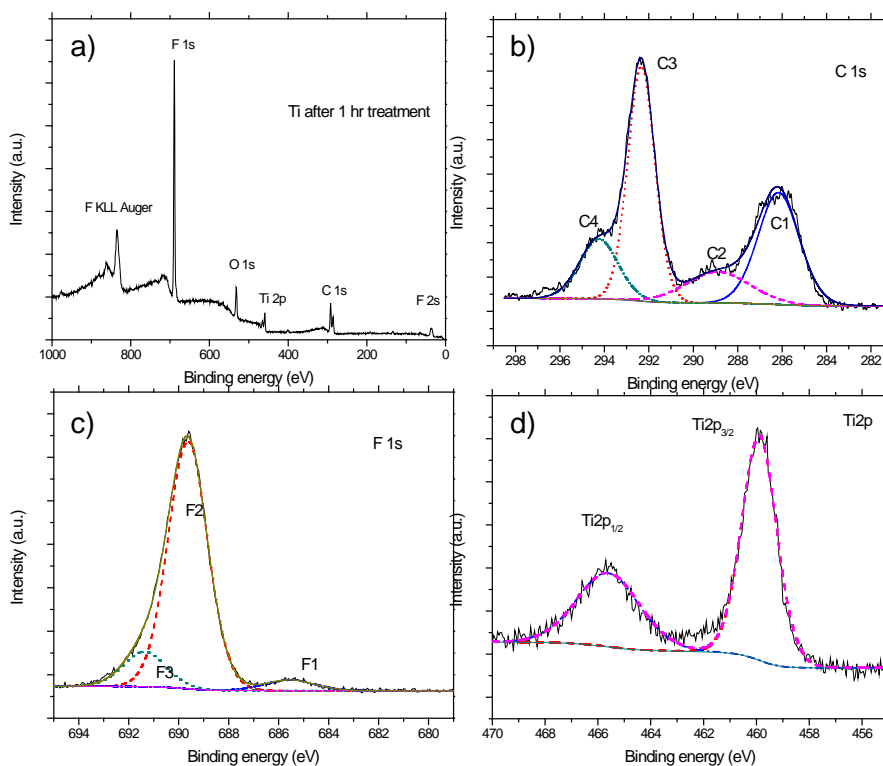


Figure 8-4: XPS results of PTES functionalized TiO_2 nanotube surface a) wide-scan spectrum b) C 1s spectrum c) F 1s spectrum d) Ti 2p spectrum

The broad C 1s peaks ranging from 280 to 300 eV in the XP spectra are contributed by several types of functional groups that have different binding energies.

In order to alter the surface properties, PFTS molecules were attached to the TiO_2 surface. All different components and their binding energies are shown in Figure 4a. The binding energy of C1s peaks can be distinguished (Fig. 8-5b) as CF_3 at 294.7 eV, CF_2 - CF_2 - CH_2 at 292.1 eV, CF_2 - CF_2 - CH_2 at 289.2 eV, and C - C at 285.6 eV¹⁴. The three F1 peaks (Figure 4c) represent CF_3 (691.1 eV), CF_2 - CF_2 (690.3 eV) and CH_2 - CF (686.5 eV), respectively. An increase of about 2 eV of Ti 2p to high binding energy indicates TiO_2 has been besieged by high electronegative $[\text{CF}_n]$ compounds (Figure 8-4d). Interestingly,

the fluorine content increases up to 5 hours anodization time (57.5%) and then slightly decrease to 57.0% (Figure 8-5).

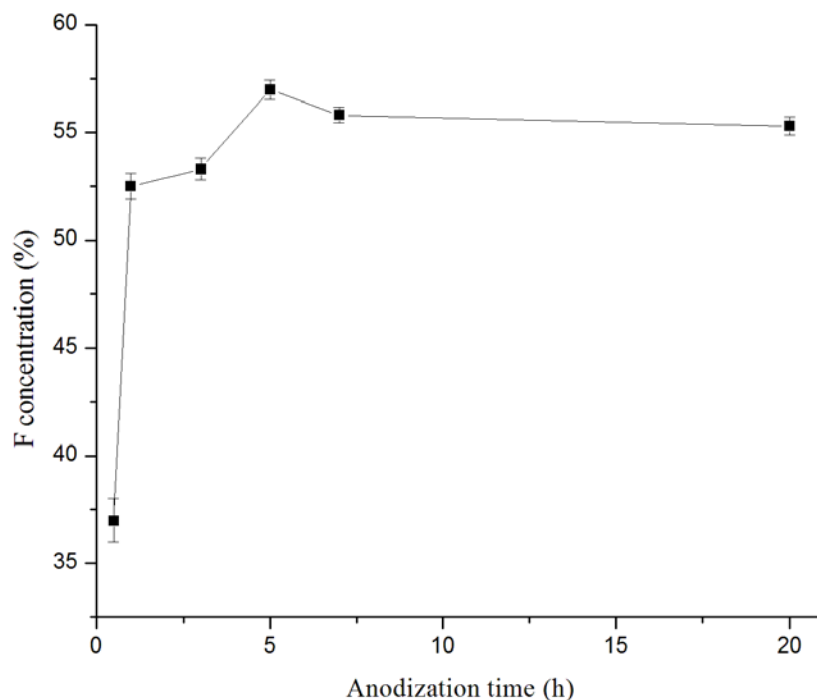


Figure 8-5: Fluorine content of super hydrophobic TiO_2 nanotube surfaces versus different annealing times

However, 5 h anodization time is not the optimum level in terms of superhydrophobicity due to the small receding angle as well as higher slide angle (Figure 8-6). The fluorine content does not change after 7 hours. It reveals that the surface properties remain the same after 7 hours which was also proven by contact angle measurements (Figure 8-6).

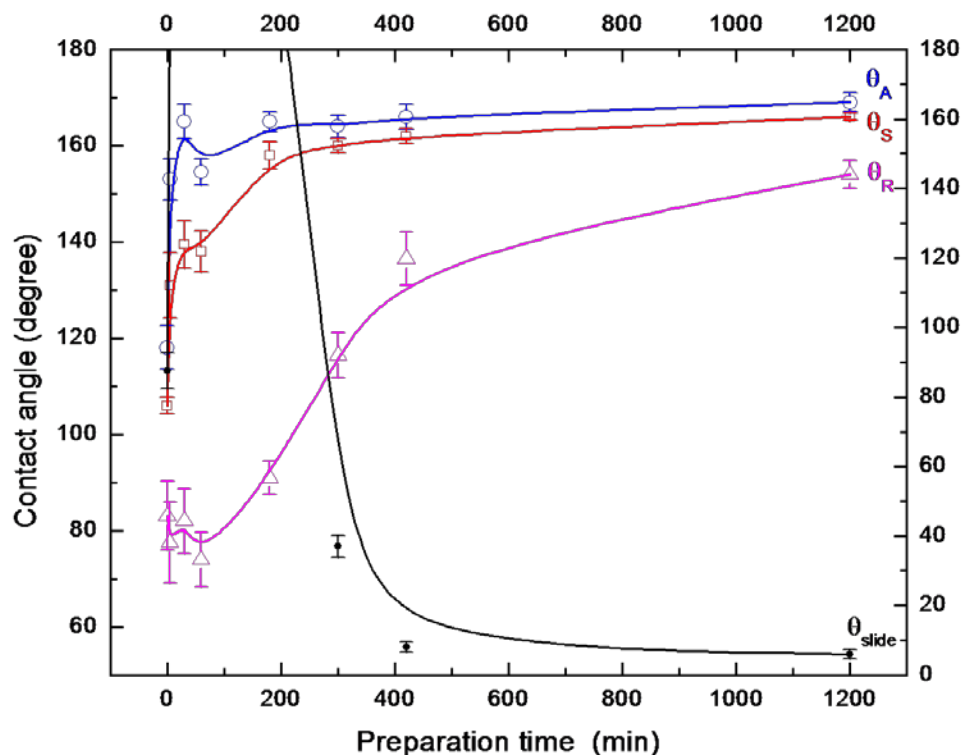


Figure 8-6: Water contact angles measured of the TiO_2 nanotube surface after modification with PTES advancing (circles), static (squares), receding (triangles) and slide (black squares) water contact angles are plotted as a function of the anodization time of Ti foil in ethylene glycol solution

For example, the advanced, receding and slide angles were almost the same after 7 hours.

The superhydrophobic surface started to form after 7 hours anodization time. Therefore, 7 hours anodization time appears to be enough to make superhydrophobic surface.

8.4.4 Contact angle

Contact angle measurement is one of the most important indicators of surface properties. The contact angle of flat surfaces can be determined by three-face-free energy interfaces by Young's equations ¹⁵

$$\cos \theta = (\gamma_{SV} - \gamma_{SL})/\gamma_{LV} \quad (8-1)$$

where γ_{SL} , γ_{SV} and γ_{LV} are the solid/liquid, solid/vapor and liquid/vapor surface tensions, respectively. For a none-flat surface the modified version of Young's equation is Wenzel's equation¹⁶ in the form of:

$$\cos \theta_w = r \cos \theta \quad (8-2)$$

where the roughness factor, $r > 1$, is defined as the ratio of the actual area of the rough surface to the geometric projected area. The contact angles of a rough and a smooth surface are represented by θ_w and θ , respectively. It is proven that after a certain critical value of r , the contact angle continues to increase while hysteresis starts to decrease¹⁷ due to the surface transfer from Wenzel to Cassie-Baxter regime. The hysteresis is defined in terms of the difference of the advancing (θ_a) and receding (θ_r) angles (i.e., $\theta_H = \theta_a - \theta_r$).

However, in the case of highly ordered and uniform TiO₂ nanotube arrays (NTA), the water droplets rest on the TiO₂ NTA surface. There is a top flat solid surface and a flat air gap between the TiO₂ NTs (Figure 8-7(a)).

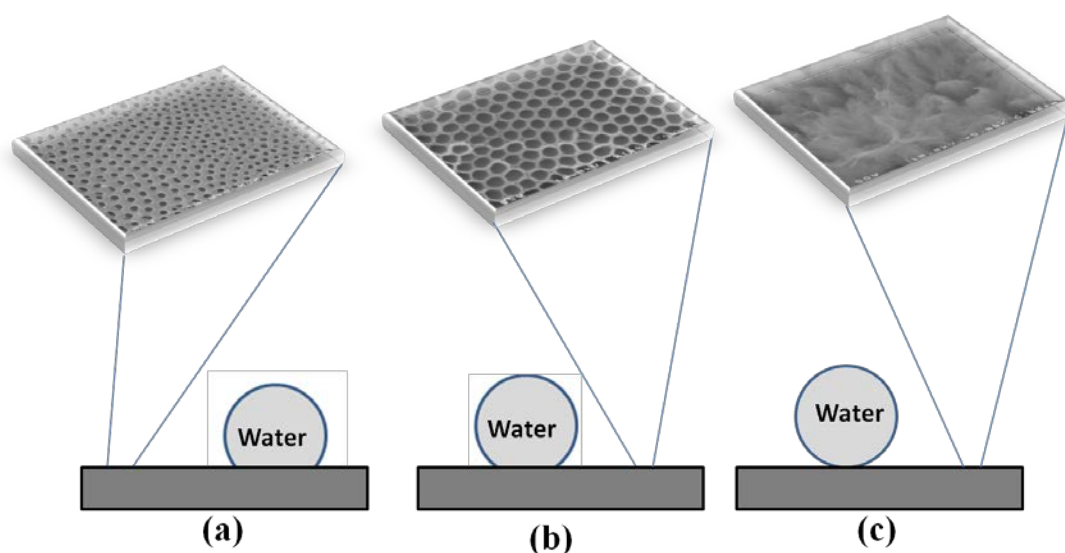


Figure 8-7: Wetting states of TiO₂ layers: (a) Wenzler (b) Cassie-Baxter (c) Combined

This phenomenon can be described by Cassie-Baxter equation ¹⁸.

$$\text{Cos } \theta_w = \varphi_s \text{ Cos } \theta + (1 - \varphi_s) \text{ Cos } \theta_x \quad (8-3)$$

where, $\varphi_s < 1$ is the fraction of the top solid surface of the protrusions, and $(1 - \varphi_s)$ is the fraction of the air gaps. θ_x is the contact angle on the gas in the gaps which is about 180° . Therefore, equation (8-3) can be simplified to equation (8-4). Although, the contact angle increases with the increase of anodization time according to Cassie-Baxter regime, the slide angle of the surface can remain high (Figure 8-7(b)).

$$\text{Cos } \theta_w = -1 + \varphi_s (\text{Cos } \theta + 1) \quad (8-4)$$

The contact surface area decreases and the flat air gaps increase along with increasing of the anodization time; therefore, the net result is an increase in the contact angle. However, after certain period of time the TiO_2 NTAs are no more capable of vertical growth and they collapse. Therefore, the surface is not uniform. The two equations can be combined to give a more general equation (8-5) that can be applied to non-flat contacting areas ¹⁹ (Figure 8-7(c)).

$$\text{Cos } \theta_w = -1 + \varphi_s (r \text{ Cos } \theta + 1) \quad (8-5)$$

Therefore, in titanium nanostructures, the surface adhesive forces can be tuned effectively by changing the interactions at nanoscale between the solid surface and the air-pocket ratio. In the cases of nanopore array (NPA) and nanotube array (NTA), capillary adhesive forces play a dominant role, while nano vesuvianite structure (NVS) has extremely low adhesion capacity for water. This indicates that the roughness factor 'r' reaches the critical value during the surface transfer from NPA to NTA. Over all, the NVS surface satisfied all requirements of being a superhydrophobic surface such as high water contact angle, small slide angle and small hysteresis.

Water rapidly spreads and wets the as-anodized TiO₂ porous film without PTES modification due to side penetration of the liquid by capillary forces. Under these conditions the water contact angle is close to 0° (superhydrophilic). However, the surface can be modified with organic monolayers using functional groups such as carboxylates, phosphates, or silanes to obtain a superhydrophobic surface. To make the top part of the tubes superhydrophobic, PTES was grafted to the outer tube layer after the anodization step. As shown in Figure 6, the surface wettability with PTES monolayer grafting changes from superhydrophilic to superhydrophobic with a contact angle $\theta = 165^\circ$.

The droplets with spherical shapes slide spontaneously and hardly come to rest even when they are placed gently onto the PTES modified TiO₂ surface. The water contact angle on such a TiO₂ porous film was as high as 160° (Figure 8-6), while that of a regular superhydrophilic flat TiO₂ surface modified by PTES was around 115° (Figure 8-6). This is in good agreement with the results of coating fluorocarbon hydrophobic layers on smooth surfaces by self-assembly.

Seven different TiO₂ NTs samples were prepared. Each sample was anodized with different anodization time (0, 30, 60, 90, 180, 300, 420, and 1200 min) and then fluorinated. The advancing angle (θ_A), static angle (θ_S) receding angle (θ_R) and slide angle (θ_{slide}) were all measured at each point. As the anodization time increased, θ_A and θ_S both increased, while θ_R decreased slightly for the first 90 min, and then increased. The slide angle (θ_{slide}), however, displayed a much different pattern. At time zero (original titanium surface) θ_{slide} was approximately 83°. At 30 min, θ_{slide} reached to the maximum point and it remained at the maximum until 180 min of anodization. θ_{slide} then decreased for the remainder of the experiment.

These results indicate that at the beginning, the PTES modified surface was in Wenzler regime, after one hour annealing, the surface reached Cassie-Baxter and had a high contact angle and a high slide angle. Finally, after 7 hours of annealing the surface demonstrated high contact angle but low slide angle. The surface becomes superhydrophobic when it is in combined regime.

8.5 Conclusions

By using a facile electrochemical oxidation mechanism any degree of wettability of a TiO_2 surface i.e. a contact angle between 100° and 170° can be obtained by two steps, which are anodization and modification with PTES. It reveals that the superhydrophobic surfaces can be achieved after 7 hours of anodization in the ethylene glycol based electrolyte applying the following experimental conditions: 2cm separation distance between anode and cathode, under constant voltage of 30V at room temperature followed by PTES treatment. The results provide new insights vary the wettability of superhydrophobic surfaces. These types of materials may have potential applications in coating and gene delivery ¹⁹.

8.6 References

- (1) Kim, T. ; Tahk, D.; Lee, H. H. *Langmuir* **2009**, *25*, 6576-6579.
- (2) C. Takei, M. Nonogi, A. Hibara, T. Kitamori, H.B. Kim, *Lab on Chip* **2007**, *7*, 596-602
- (1) E. Balaur, J.M. Macak, L. Taveira, P. Schmuki, *Electrochem. Commun.* **2005**, *7*, 1066-1070.
- (2) Yamashita, H.; Nakao, H.; Takeuchi, M.; Nakatani, Y.; Anpo, M. *Nucl Instrum Methods Phys Res Sect B* **2003**, *206*, 898-901.
- (3) Kangwansupamonkon, W.; Lauruengtana, V.; Surassmo, S.; Ruktanonchai, U. *Nanomed. Nanotechnol. Biol. Med.* **2009**, *5*, 240-249.
- (4) Wade, D. C. *J. Forensic Identif.* **2002**, *52*, 551-559.
- (5) Lai, Y. K.; Gao, X. F.; Zhuang, H. F.; Huang, J. Y.; Lin, C. J.; Jiang, L. *Adv Mater.* **2009**, *21*, 3799-3803.
- (6) (a) Le Guéhenec, L.; Soueidan, A.; Layrolle, P.; Amouriq, Y. *Dent. Mater.* **2007**, *23*, 844-854. (b) Di Mundo, R.; Palumbo, F.; D'Agostino, R. *Langmuir* **2010**, *26*, 5196-5201. (c) Pearton, S. J.; Lee, J. W.; Lambers, E. S.; Abernathy, C. R.; Ren, F.; Hobson, W. S.; Shul, R. J. *J. Electrochem. Soc.* **1996**, *143*, 752-758.
- (7) (a) Shimizu, K.; Einaga, Y.; Ohnishi, K.; Fujishima, A.; Habazaki, H.; Skeldon, P.; Thompson, G. E. *Surf Interface Anal* **2002**, *33*, 35-40. (b) Michalikova, L.; Rezek, B.; Kromka, A.; Kalbacova, M. *Vacuum* **2009**, *84*, 61-64.
- (8) (a) Kim, K.; Ramaswamy, N. *Dent. Mater. J.* **2009**, *28*, 20-36. (b) Lim, J. H.; Choi, J. *Small* **2007**, *3*, 1504-1507.
- (9) Ghicov, A.; Schmuki, P. *Chem. Commun.* **2009**, 2791-2793.

- (10) (a) D. Wang, X-L. Wang, X-J. Liu, F. Zhou, J. Phys. Chem. C 114 (2010) 9938.
(b) Y. Yang, Y-K. Lai, Q-Q. Zhang, K. Wu, L-H. Zhang, C-J. Lin, P-F. Tang, Colloids and Surfaces B: Biointerfaces 79 (2010) 309.
- (11) (a) Isimjan, T. T.; Ruby, A. E.; Rohani, S.; Ray, A. K. *Nanotechnology* **2010**, *21*, 055706. (b) Isimjan, T. T.; Yang, D.-Q; Rohani, S.; Ray, A. K. *Journal of Nanoscience and Nanotechnology* **2011**, *11*, 1079-1083.
- (12) (a) Hsieh, C.T.; Lai, M.H.; Cheng, Y.S. *Journal of Colloid and Interface Science* **2009**, *340*, 237–242. (b) Girardeaux, C.; Idrissi, Y.; Pireaux, J. J.; Caudano, R. *Applied Surface Science* 1996, *96-98*, 586-590.
- (13) Young, T. *Phil. Trans. R. Soc. Lond.* **1805**, *95*, 65–87.
- (14) Wenzel, R.N. *Ind. Eng. Chem.* **1936**, *28*, 988-994.
- (15) (a) Vourdas, N.; Tserepi, A.; Gogolides, E. *Nanotechnology* **2007**, *18*, 125304. (b) Liu, B.; Lange, F.F. *Langmuir* **2010**, *26*, 3637-3641.
- (16) Cassie, A. B. D.; Baxter, S. *Trans. Faraday Soc.* **1944**, *40*, 546-551.
- (17) Roach, P.; Shirtcliffe, N. J.; Newton, M. I. *Soft Matter*. **2008**, *4*, 224–240.

Chapter 9

Conclusions and Recommendations

9.1 Fabrication of highly ordered TiO₂ nanotubes

The investigation of fabricating well-ordered, reproducible and economical TiO₂ nanotubes is the primary and important prerequisite for large scale production of TiO₂ nanotubes. In this thesis, at first, the sonication-assisted fabrication process was investigated in detail and then titanium metal was used as a cathode to replace expensive platinum. The method included 1) Finding proper annealing time so that the TiO₂ nanotubes layer will not fall off from the surface after sonication, 2) characterization using SEM and XRD.

9.1.1 Conclusions

The present work was accomplished by two steps. In the step one, we were able to form highly ordered TiO₂ nanostructures by anodizing Ti foil in NH₄F electrolytes. The wall thickness and tube diameter as well as tube length were ranging from 10 nm to 25 nm, 60 nm to 100 nm and 5 μm to 7 μm respectively after sonication. The as prepared Ti surface has two layers: the top layer is TiO₂ nanowire and underneath is a highly ordered TiO₂ nanotubes array. The top layer can be completely removed by annealing and a mild sonication process to expose the highly ordered nanotube layer. The length of the retained uniform and highly ordered nanotubes is independent of the treatment time. The dimensions of the retained TiO₂ nanotubes can be well controlled. The process may be extended to other nanotubes preparation. In the second steps, we have used Ti as a cathode material during the electrochemical fabrication of TiO₂ nanotube arrays in

non-aqueous electrolytes. Ti showed promising results to replace the conventionally used and comparatively expensive Pt cathode. In terms of photo conversion efficiency, the highest PCE was achieved using Ti-cathode. Ti showed excellent stability in the EG electrolytes. The structure, morphology, and photoelectrochemical properties were studied in comparison to the nanotube arrays fabricated under different conditions such as: applied potential (20 V – 40 V) and distance between two electrodes (1 cm to 3 cm) with the same anodization time of 3 h. We show that highly ordered and strong photochemical responsive TiO₂ nanotubes can be fabricated simply by changing the distance between two electrodes and applied potential during the anodization. The highest PCE observed was 29% which is one of the highest PCE reported so far. This work not only opens a new way to engineer titanium dioxide nanostructures but also offers a big step towards producing cheap TiO₂ nanotubes in large area.

9.1.2 Limitations

- Although, the samples are reproducible, it is always difficult to get identical results due to the sensitivity of nanostructure to the tiny changes in the experimental conditions.
- Since nano level polishing of the surface is almost impossible, the various level of polishing will make a big difference on the surface morphology of the titanium plates.

9.1.3 Further Work

- A thorough study should be conducted to investigate the large area fabrication of TiO₂ nanotubes
- Fabrication of TiO₂ nanotubes on various shape titanium surfaces can be investigated.
- A more comprehensive investigation is required to study the fabrication mechanism.

9.2 Modification of highly ordered TiO₂ nanotubes

Development of an efficient process to increase the visible light response of TiO₂ nanotubes relies on the modifications either by doping other elements such as N, C, S, Fe, and Cr or loading various nano-composites on the surface of TiO₂ nanotubes. In the thesis, we examined two different types of doping such as solution doping and gas phase doping. In the solution doping, we dissolved K₃Fe(CN)₆ in the electrolyte solution and use that solution to fabricate Fe-C-N codoped TiO₂ nanotubes. In case of gas phase doping, we annealed as prepared TiO₂ nanotubes under nitrogen. The results were evaluated by measuring PCE and the maximum PCE was estimated by DOE study. In the other study, we loaded ZIF-8 on the surface and the photo-degradation efficiencies were measure after certain time frame. The results were characterized by SEM, EDX, XRD, UV-vis and XPS.

9.2.1 Conclusions

9.2.1.1 Fe-C-N codoped TiO₂ nanotubes

A new and simple modified anodization method was utilized to fabricate Fe–N–C doped and highly ordered TiO₂ nanotubes array which exhibits the maximum photo-conversion efficiency of around 2.7% in 1 M KOH. The enhancement of photo-activity can be attributed to not only the accessible surface area of TiO₂ nanotubes but also to lower band gap ($E = 2.7$ eV) created by the addition of Fe, N and C into the TiO₂ nanotube lattice during the anodization process.

9.2.1.2 PCE optimization of N-doped TiO₂ nanotubes

We prepared N₂ doped, highly smooth and ordered TiO₂ NTs by two-step process and then annealed under N₂ atmosphere. The photo-electrochemical water splitting efficiencies (PCE) of the N₂ doped TiO₂ nanotubes under visible light were measured and used as the response for DOE optimization. The PCE was optimized with respect to annealing temperature, heating rate and annealing time. The optimal result was validated by performing real experiments using the formulation obtained from the statistical optimization and the average optimal PCE obtained was 7.42%, which is within 95% confidence interval of the modeling result (7.26%).

9.2.1.3 Pt/ZIF-8-loaded TiO₂ nanotube composite

We have demonstrated a potential photo-catalysis for water purification by using Pt/ZIF-8 loaded TiO₂ NTs. The unique architecture was achieved in situ growth of the

microporous ZIF-8 nano crystallites on the surface of TiO₂ NTs and then coating by Pt nanoparticles. The combination of large surface area and strong adsorbent properties of ZIF-8 with reducing charge recombination property of Pt/TiO₂ NTs, produced highly visible light responsive material. The phenol degradation efficiency of Pt/ZIF-8 loaded TiO₂ NTs photo catalysts after 2 h of irradiation under visible light was 18.6%.

9.2.2 Limitations

- The solution doping of Fe-C-N should be studied systematically in order to obtain optimized efficiency. The quantities of Fe inside lattice requires stronger verification because EDX only showed that there was Fe in the material but it did not say how much was it and whether it was inside lattice.
- Determining the actual amounts of nitrogen inside the lattice was difficult due to the similar binding energy of surface absorbed nitrogen to doped nitrogen.
- The relationship between band gap and PCE should be studied in more detail.
- Stability of Pt/ZIF-8 loaded TiO₂ nanotube composite after reaction is questionable.

9.2.3 Future work

- The Fe-C-N co-doping can be optimized by changing the voltage, concentration of K₃Fe₃(CN)₆ and even the electrolyte in order to obtain the highest PCE.
- The optimized condition may applicable to the N-doping of TiO₂ nanoparticles as

well as larger area of TiO₂ nanotubes. The N-doped materials can be used as photo-catalysis for water purification.

- Different metal organic frame works (MOF) with the surface area larger than ZIF-8 can be replaced ZIF-8 which may results better catalytic response.

9.3 Application of TiO₂ nanotubes

TiO₂ nanotube arrays have been found to possess outstanding charge transport and carrier lifetime properties enabling a variety of advanced applications, including their use in sensors, dye sensitized solar cells, hydrogen generation by water photo-electrolysis, photocatalytic reduction of CO₂ under outdoor sunlight, and super-capacitors. In this part of the thesis, a novel method was developed for changing surface wettability of TiO₂ nanotube surface using two-step process including anodization and solution based self-assembly.

9.3.1 Conclusions

We used a facile electrochemical oxidation mechanism to obtain superhydrophobic surface just by simply changing the anodization time followed by functionalization of fluorine compound. Surface wettability of a TiO₂ surface i.e. a contact angle between 100° and 170° can be obtained by this process, It reveals that the superhydrophobic surfaces can be achieved after 7 hours of anodization in the ethylene glycol based electrolyte applying the following experimental conditions: 2cm separation distance

between anode and cathode, under constant voltage of 30V at room temperature followed by PTES treatment. The results provide new insights of changing the wettability of superhydrophobic surfaces.

9.3.2 Limitations

- The super-hydrophobicity of the TiO₂ nanotubes based surface is not uniform. The contact angle of different parts of the surface may vary a little bit which may be due to the not consistence surface roughness.
- The superhydrophobic surfaces are very diligent and can be destroyed easily by gentle scratching.

9.3.3 Future works

- This kind of process can be extending to larger surface areas and various types of surfaces.
- The superhydrophobic TiO₂ nanotube surface may have potential applications of corrosion protection of Ti based materials such as tubes and rods.
- Other applications such as solar cell, hydrogen generation and sensor should be investigated.

Appendices

Appendix A for Chapter 3

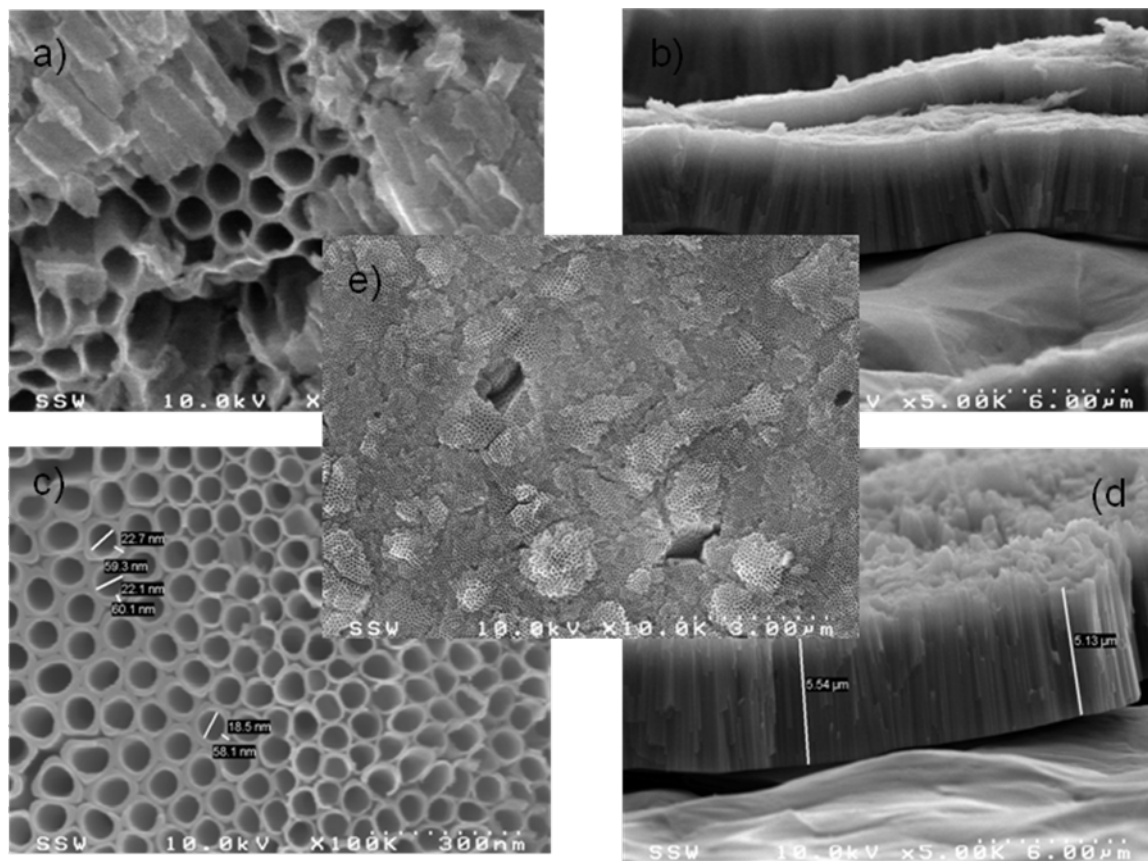


Figure A-1: FE SEM images of the surfaces of Ti samples anodized in glycerol - 5% water - 3% NH_4F solution at 30V at 3 hrs. (a) top view of as-prepared, (b) cross-section of as-prepared, (c) top view of annealed and sonicated, (d) cross-section of annealed and sonicated, and (e) lower magnification of top view of annealed and sonicated sample

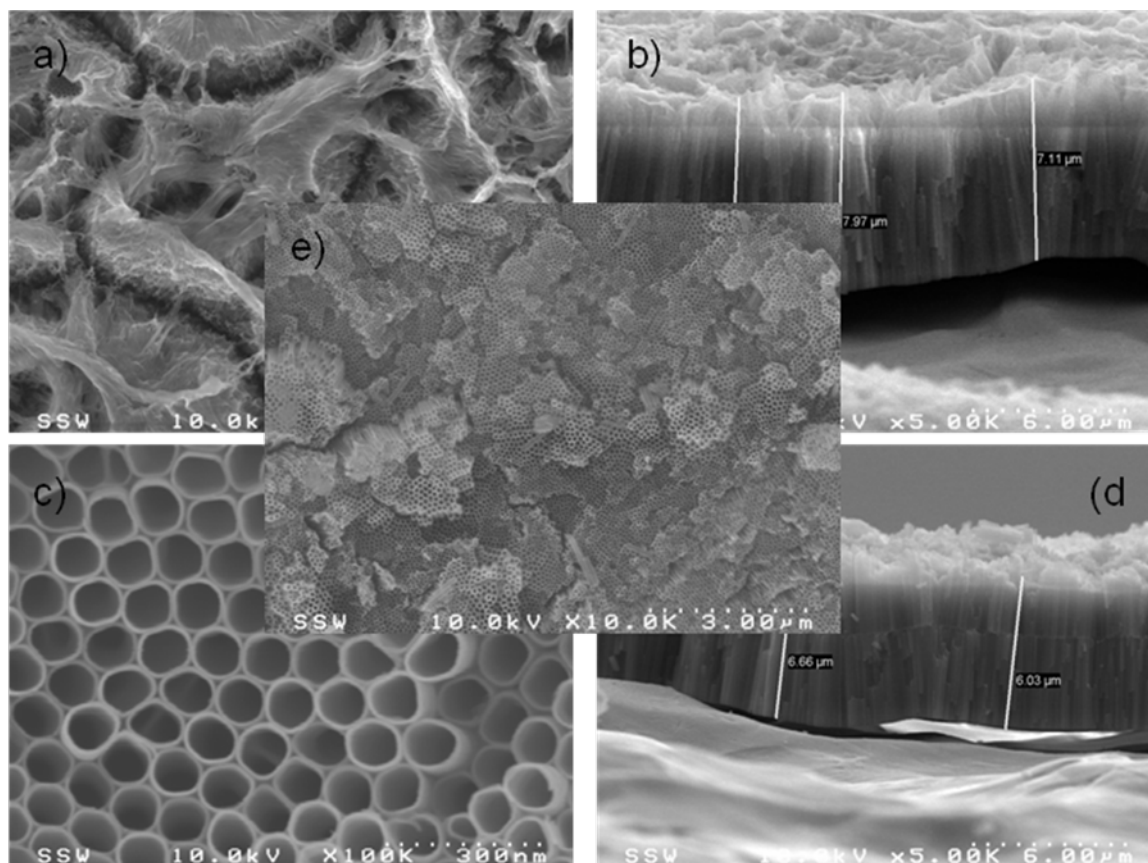


Figure A-2: FE SEM images of the surfaces of Ti samples anodized in glycerol - 5% water - 3% NH_4F solution at 30V at 5 hrs. (a) top view of as-prepared, (b) cross-section of as-prepared, (c) top view of annealed and sonicated, (d) cross-section of annealed and sonicated, and (e) lower magnification of top view of annealed and sonicated sample

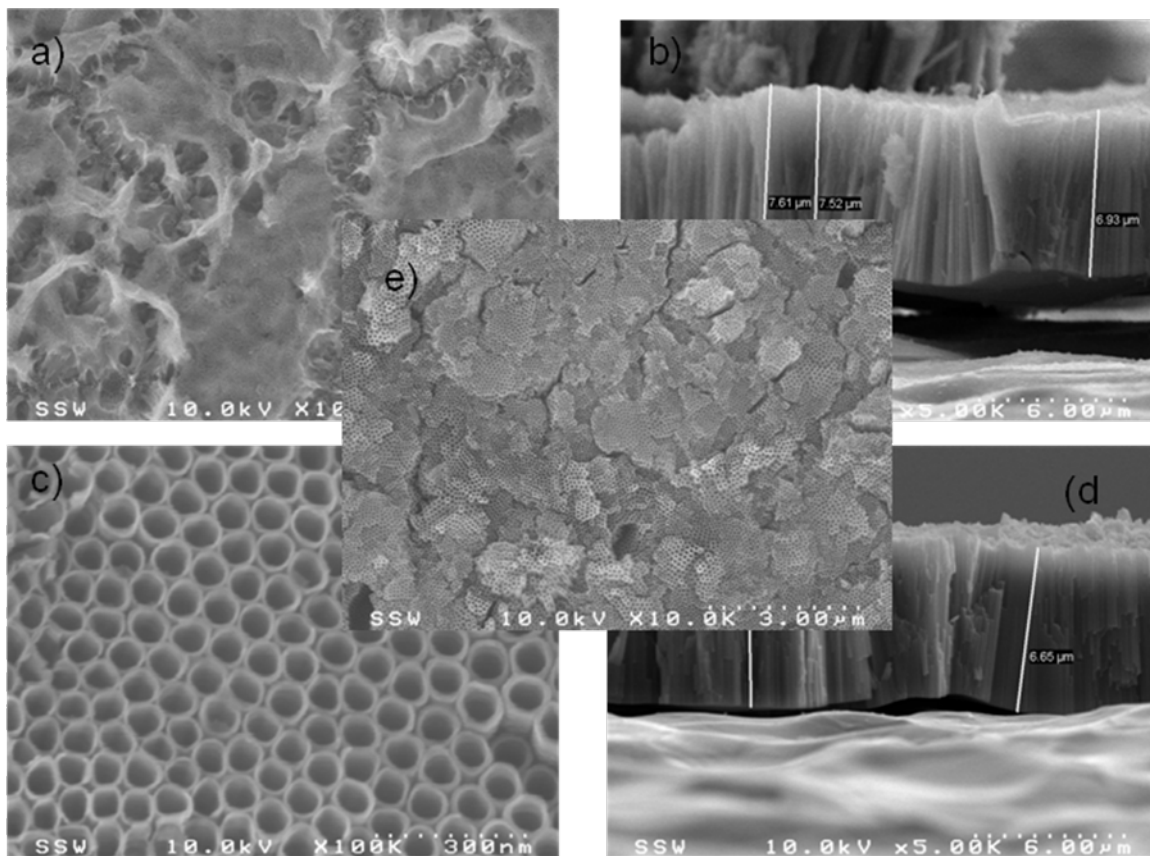


Figure A-3: FE SEM images of the surfaces of Ti samples anodized in glycerol - 5% water - 3% NH_4F solution at 30V at 6 hrs. (a) top view of as-prepared, (b) cross-section of as-prepared, (c) top view of annealed and sonicated, (d) cross-section of annealed and sonicated, and (e) lower magnification of top view of annealed and sonicated sample

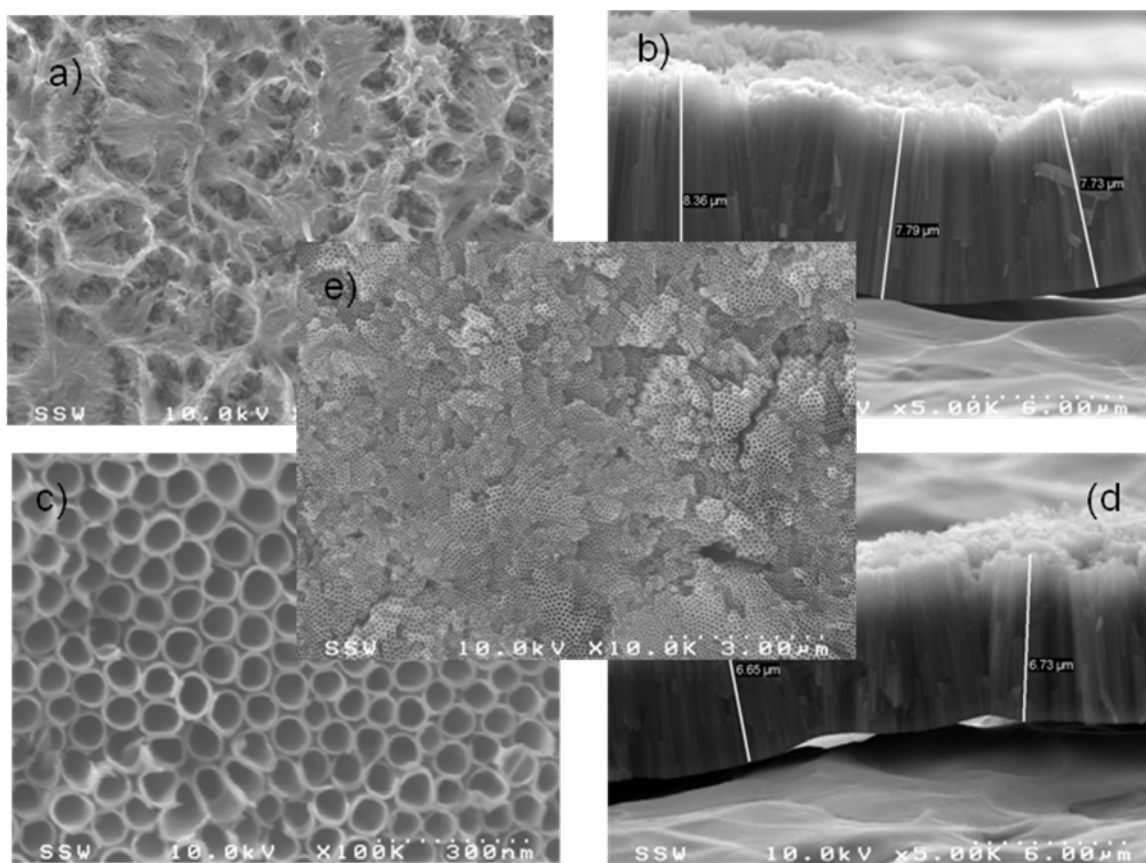


Figure A-4: FE SEM images of the surfaces of Ti samples anodized in glycerol - 5% water - 3% NH_4F solution at 30V at 7 hrs. (a) top view of as-prepared, (b) cross-section of as-prepared, (c) top view of annealed and sonicated, (d) cross-section of annealed and sonicated, and (e) lower magnification of top view of annealed and sonicated sample

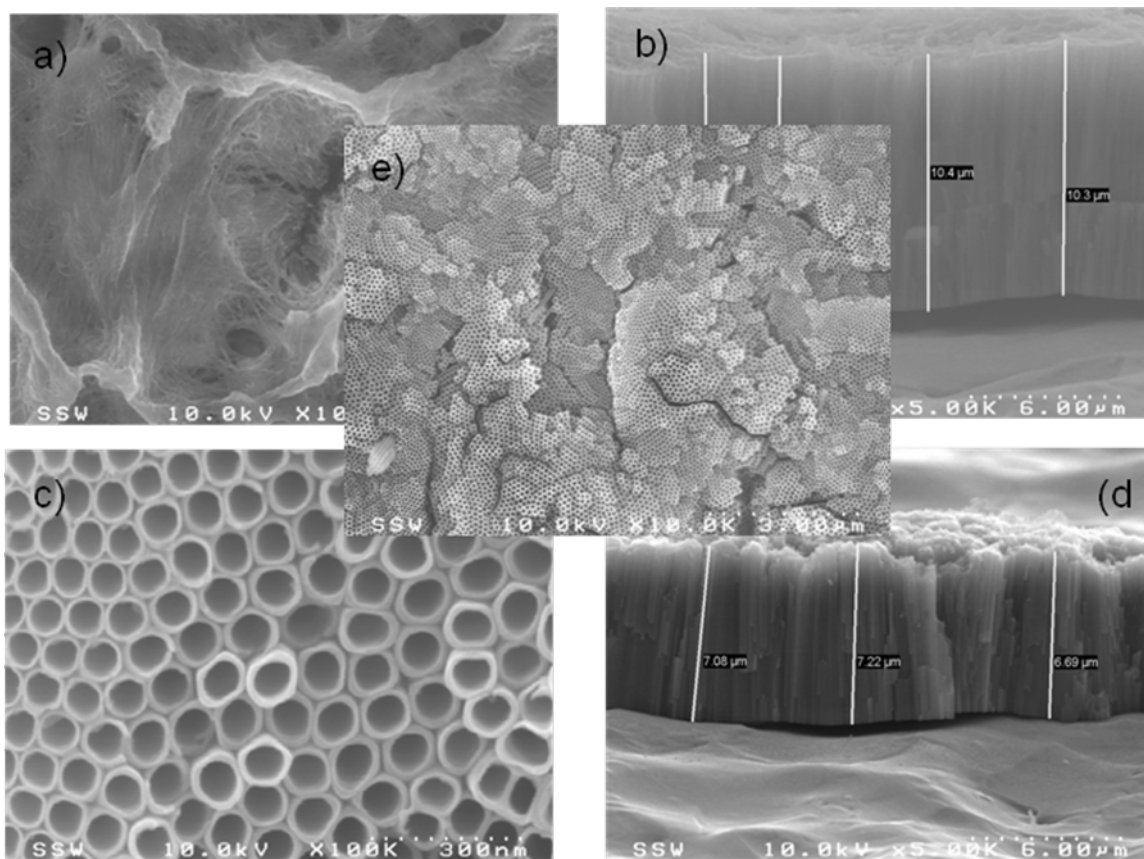


Figure A-5: FE SEM images of the surfaces of Ti samples anodized in glycerol - 5% water - 3% NH_4F solution at 30V at 13 hrs. (a) top view of as-prepared, (b) cross-section of as-prepared, (c) top view of annealed and sonicated, (d) cross-section of annealed and sonicated, and (e) Lower magnification of top view of annealed and sonicated sample

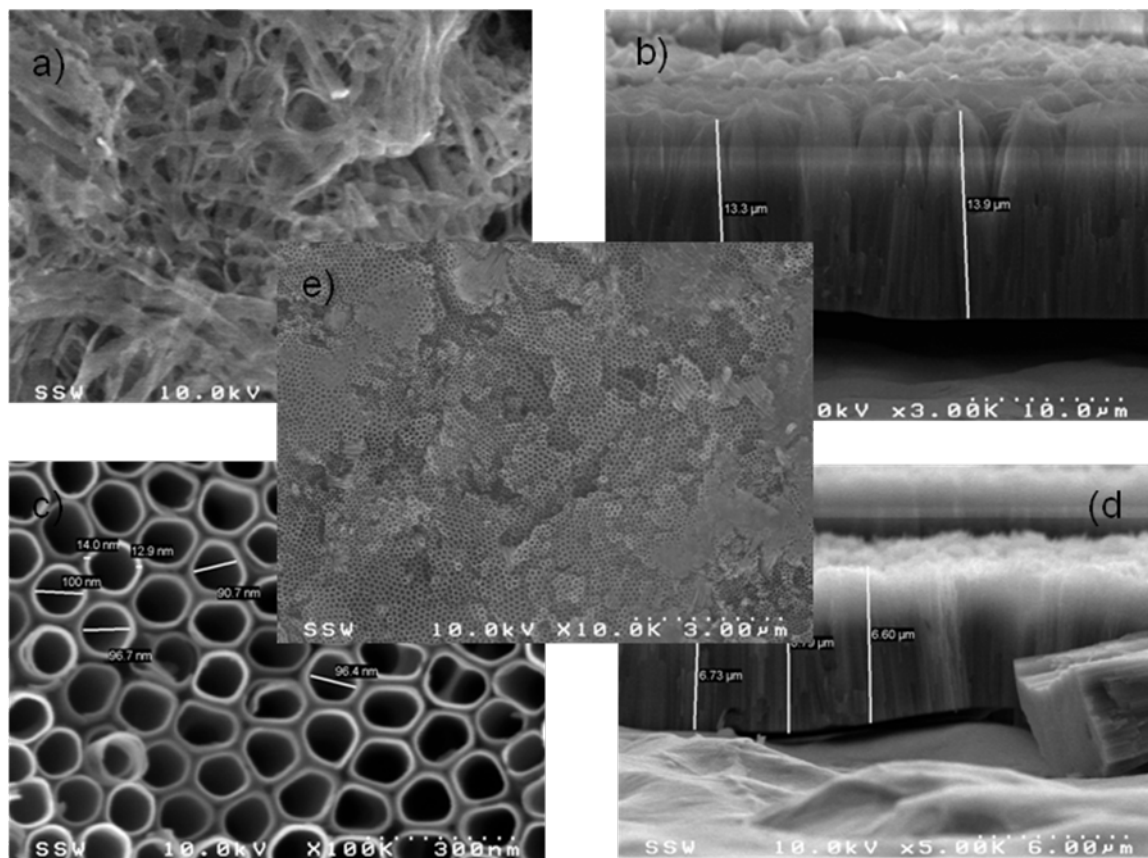


Figure A-6: FE SEM images of the surfaces of Ti samples anodized in glycerol - 5% water - 3% NH_4F solution at 30V at 20 hrs. (a) top view of as-prepared, (b) cross-section of as-prepared, (c) top view of annealed and sonicated, (d) cross-section of annealed and sonicated, and (e) lower magnification of top view of annealed and sonicated sample

Appendix B for Chapter 4

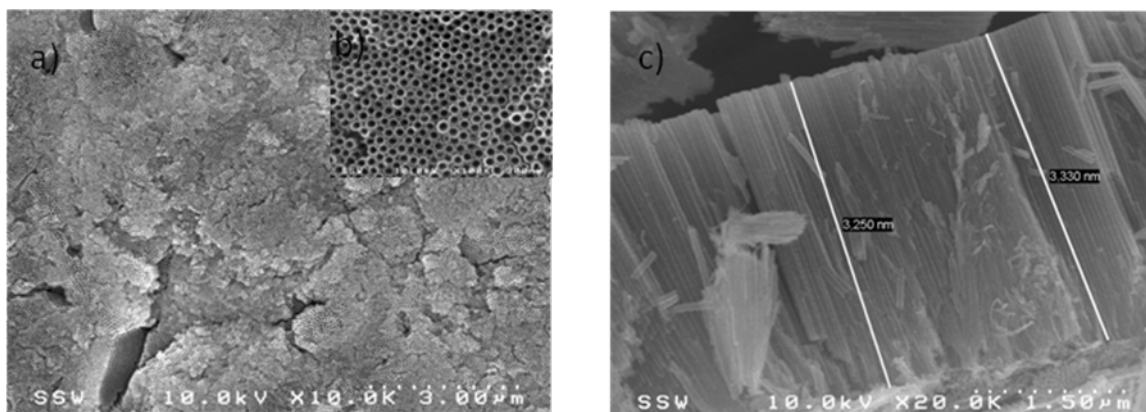


Figure B-1: SEM images of TiO_2 nanotubes fabricated under condition of 1cm between cathode and anode, 20 V constant voltage and 3 h anodization time. (a) top view of lower magnitude image (b) top view of higher magnitude image (c) cross-section.

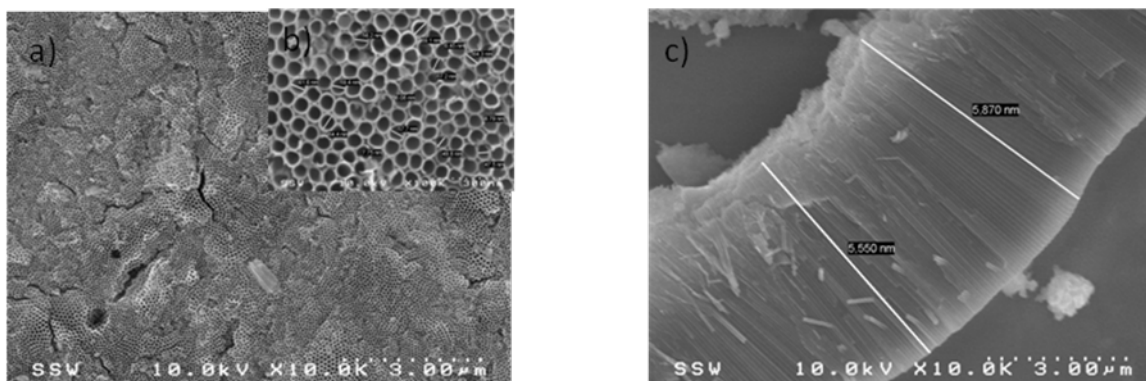


Figure B-2: SEM images of TiO_2 nanotubes fabricated under condition of 1cm between cathode and anode, 30 V constant voltage and 3 h anodization time. (a) top view of lower magnitude image (b) top view of higher magnitude image (c) cross-section.

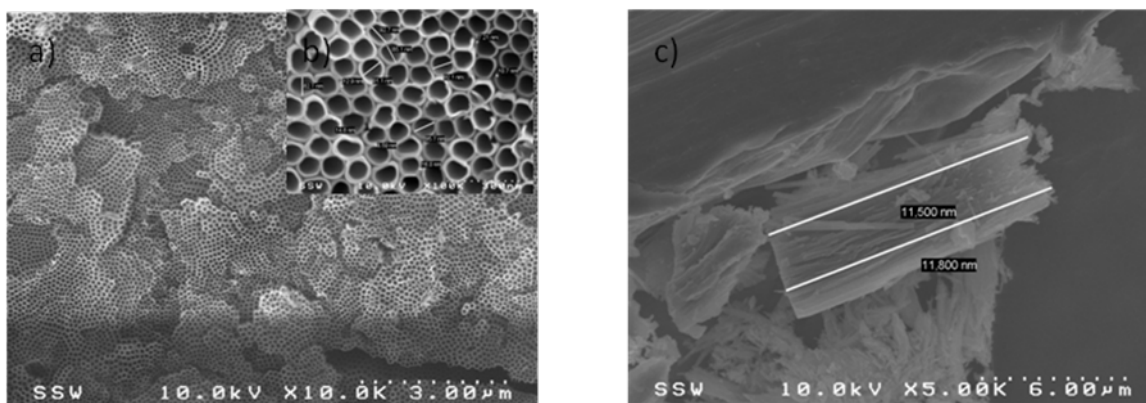


Figure B-3: SEM images of TiO_2 nanotubes fabricated under condition of 1cm between cathode and anode, 40 V constant voltage and 3 h anodization time. (a) top view of lower magnitude image (b) top view of higher magnitude image (c) cross-section.

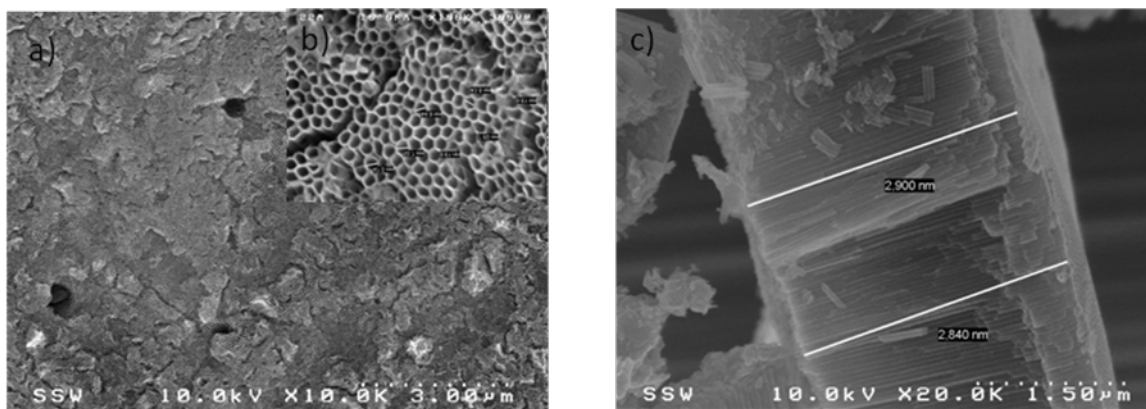


Figure B-4: SEM images of TiO₂ nanotubes fabricated under condition of 2cm between cathode and anode, 20 V constant voltage and 3 h anodization time (a) top view of lower magnitude image (b) top view of higher magnitude image (c) cross-section.

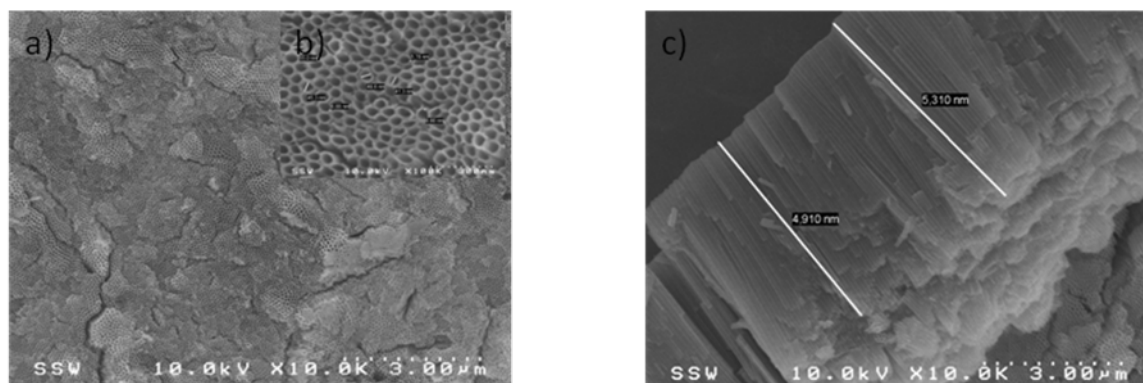


Figure B-5: SEM images of TiO₂ nanotubes fabricated under condition of 2cm between cathode and anode, 30 V constant voltage and 3 h anodization time. (a) top view of lower magnitude image (b) top view of higher magnitude image (c) cross-section.

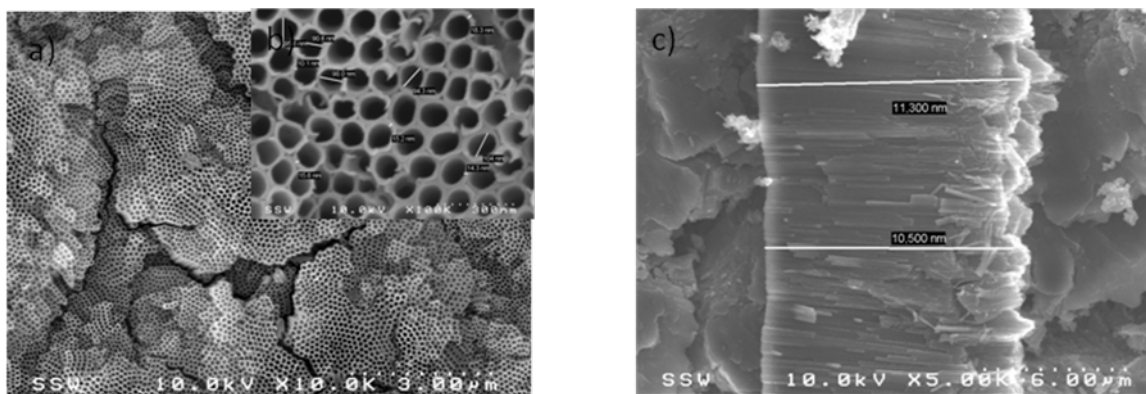


Figure B-6: SEM images of TiO_2 nanotubes fabricated under condition of 2cm between cathode and anode, 40 V constant voltage and 3 h anodization time (a) top view of lower magnitude image (b) top view of higher magnitude image (c) cross-section

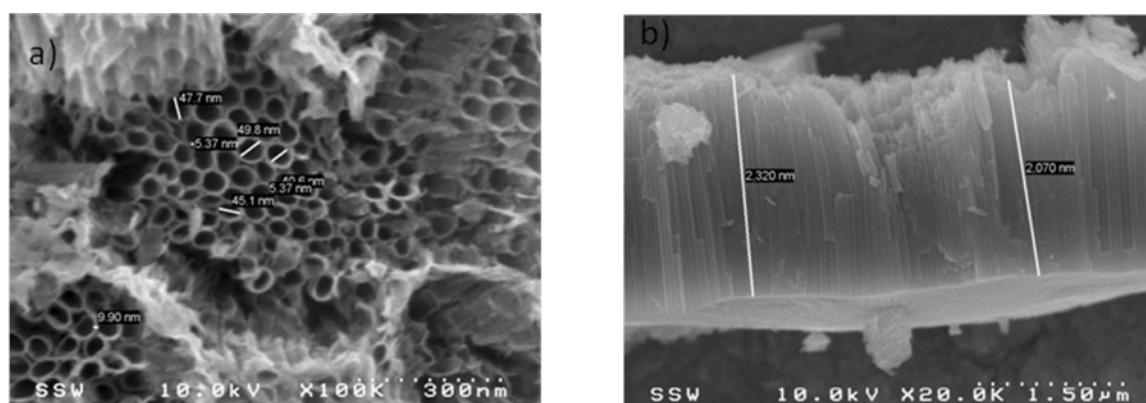


Figure B-7: SEM images of TiO_2 nanotubes fabricated under condition of 3cm between cathode and anode, 20 V constant voltage and 3 h anodization time (a) top view of lower magnitude image (b) top view of higher magnitude image (c) cross-section

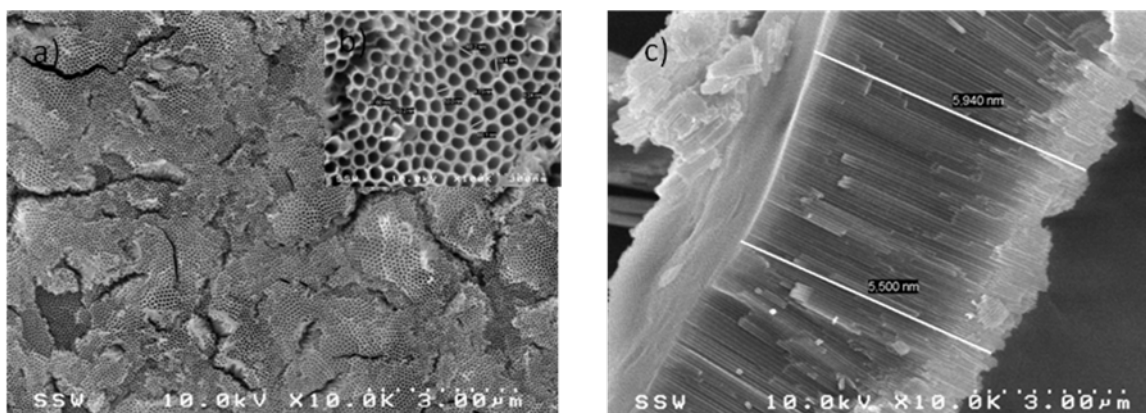


Figure B-8: SEM images of TiO_2 nanotubes fabricated under condition of 3cm between cathode and anode, 30 V constant voltage and 3 h anodization time (a) top view of lower magnitude image (b) top view of higher magnitude image (c) cross-section

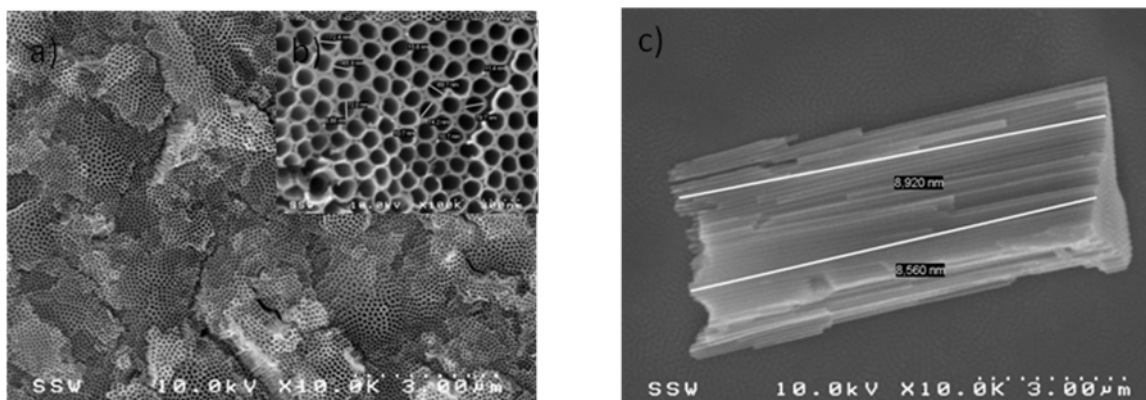


Figure B-9: SEM images of TiO_2 nanotubes fabricated under condition of 3cm between cathode and anode, 40 V constant voltage and 3 h anodization time (a) top view of lower magnitude image (b) top view of higher magnitude image (c) cross-section

Appendix C for chapter 6

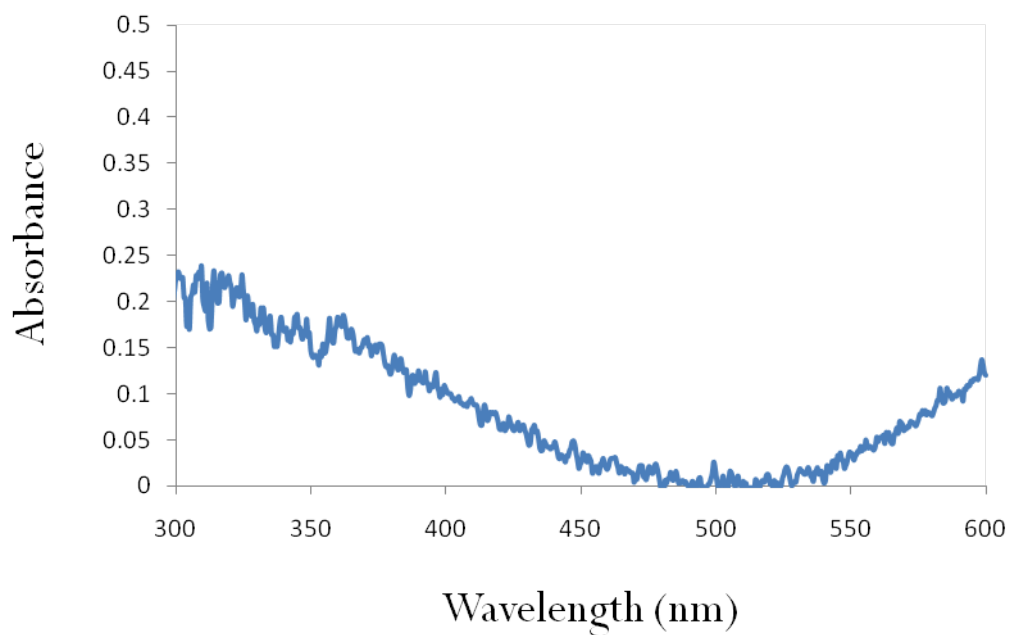


Figure C-1: UV-vis of sample 2

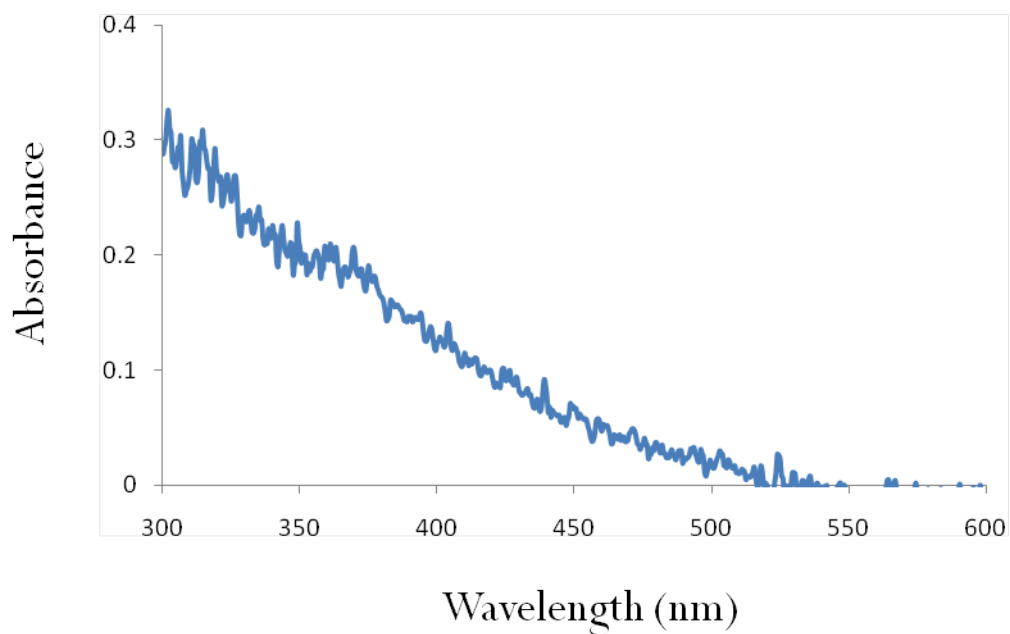


Figure C-2: UV-vis of sample 3

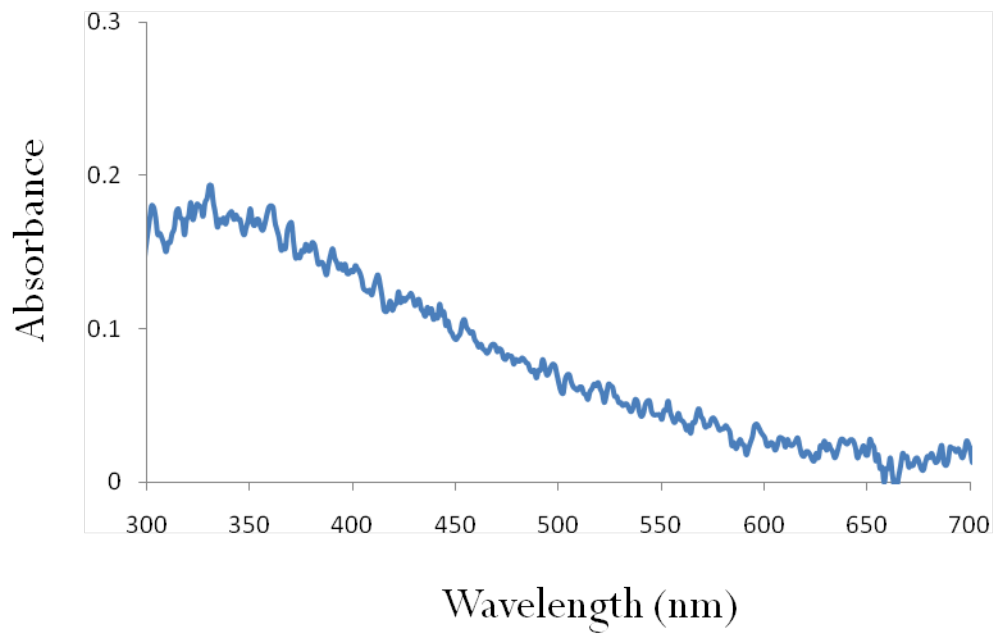


Figure C-3: UV-vis of sample 4

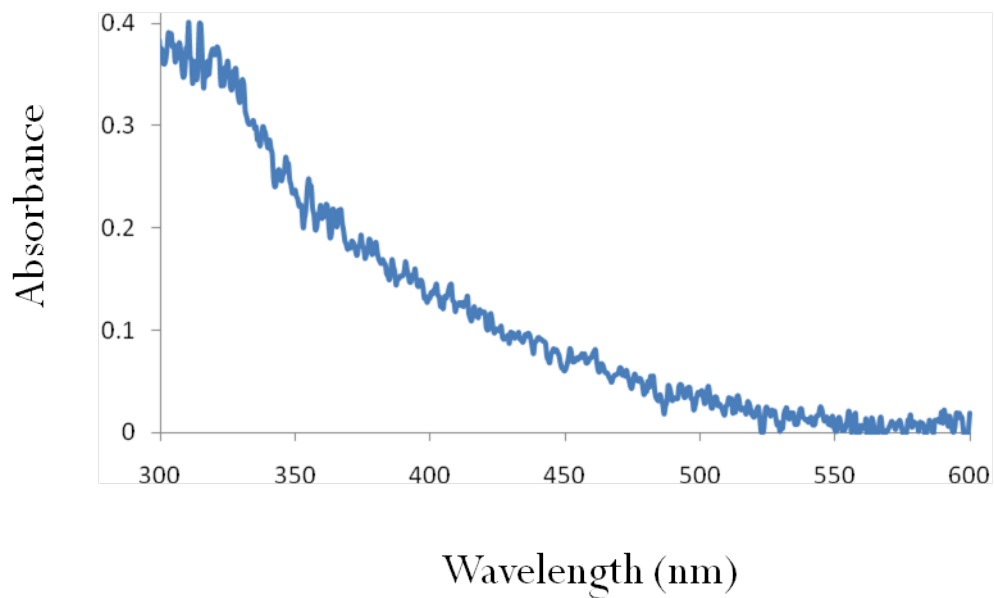


Figure C-4: UV-vis of sample 5

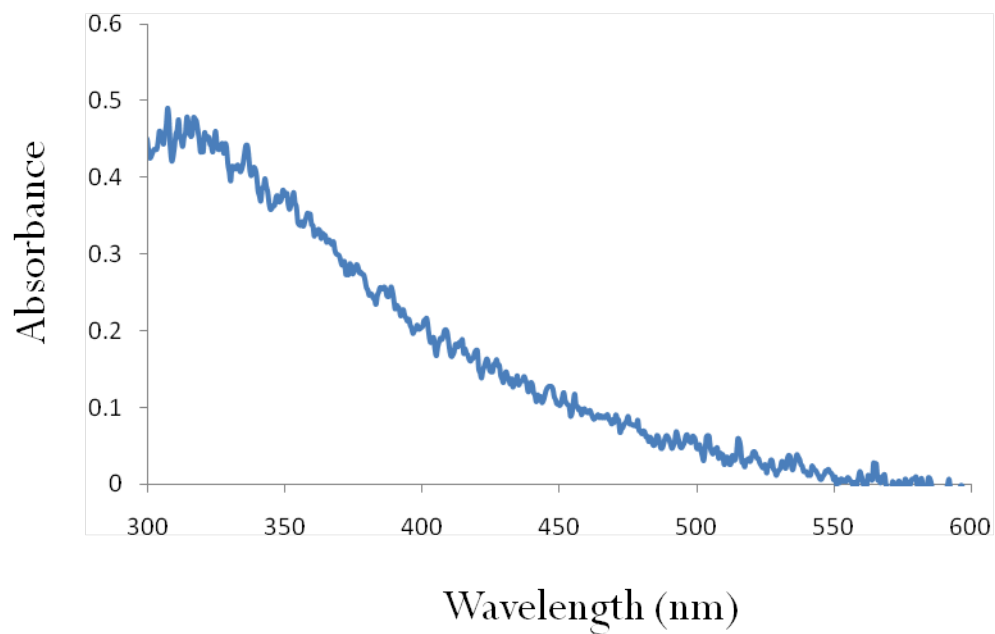


Figure C-5: UV-vis of sample 6

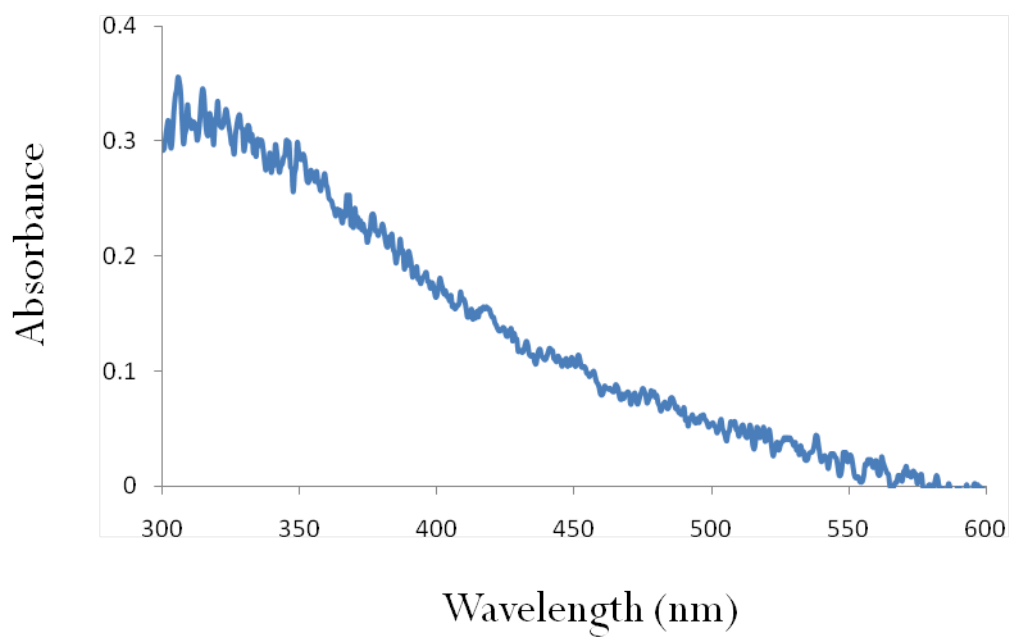


Figure C-6: UV-vis of sample 7

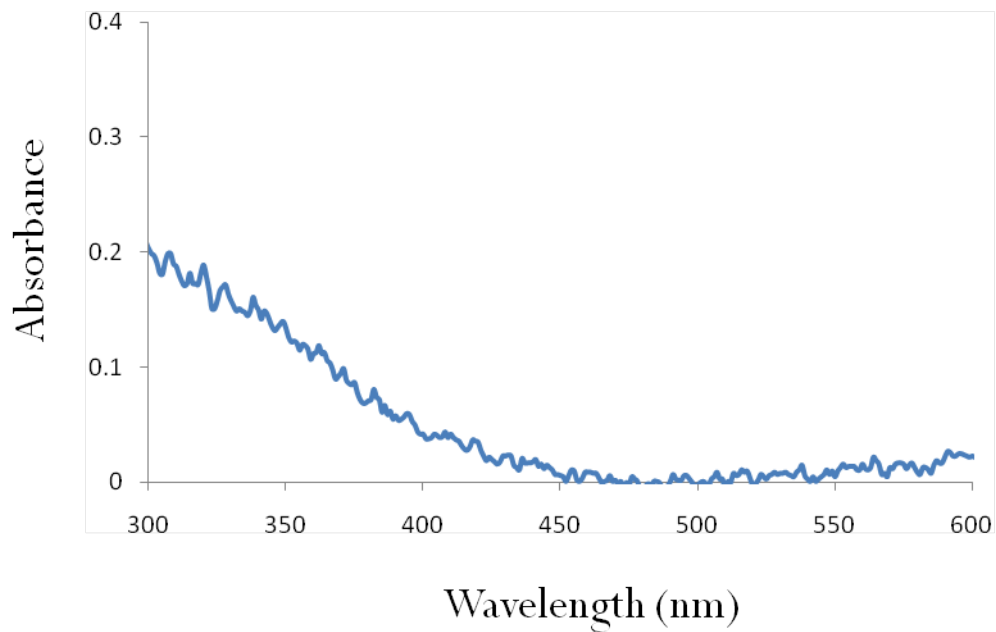


Figure C-7: UV-vis of sample 8

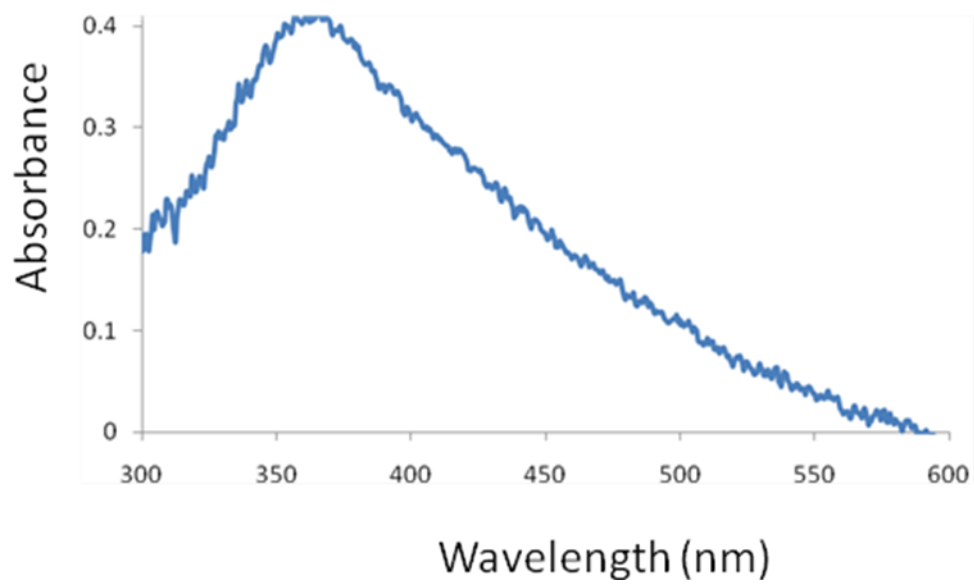


Figure C-8: UV-vis of sample 9

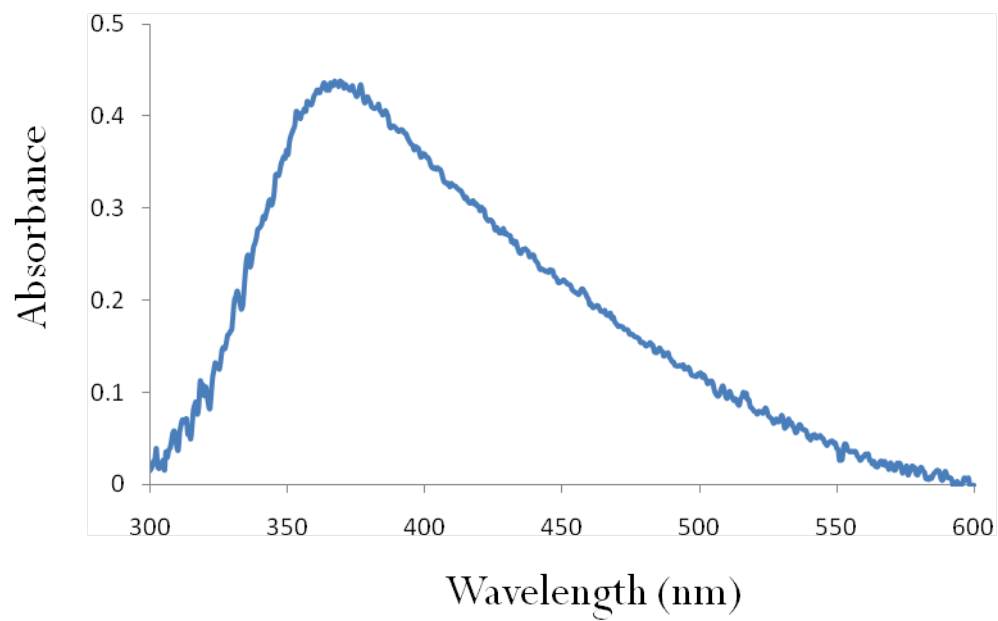


Figure C-9: UV-vis of sample 10

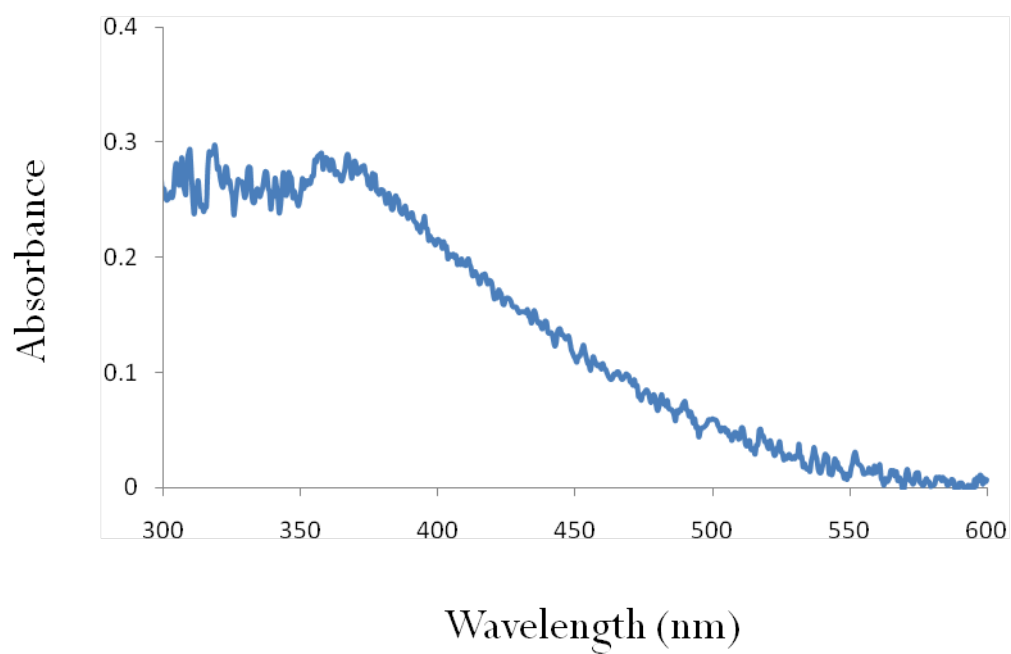


Figure C-10: UV-vis of sample 11

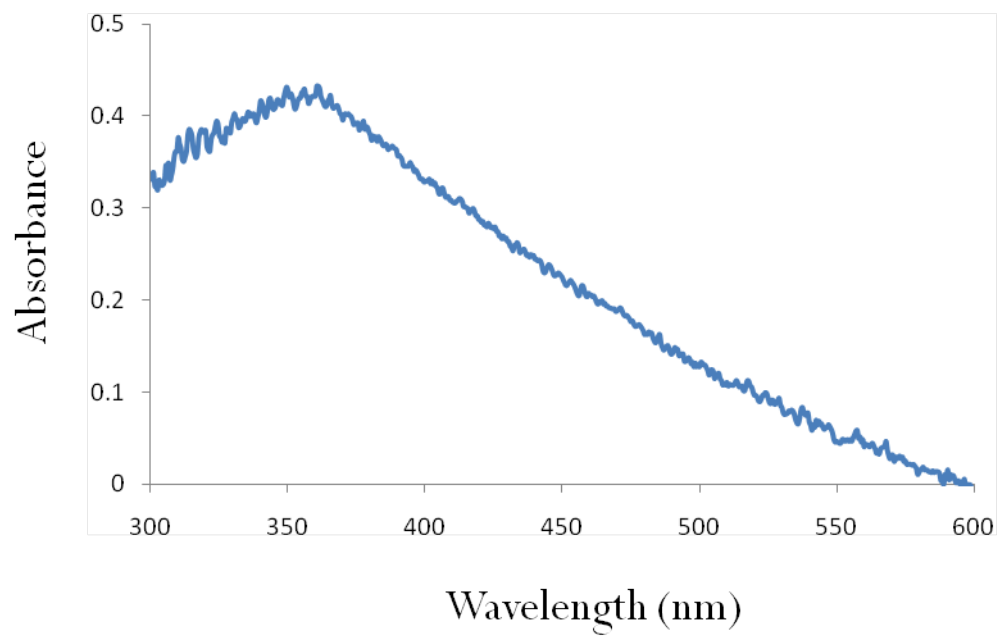


Figure C-11: UV-vis of sample 12

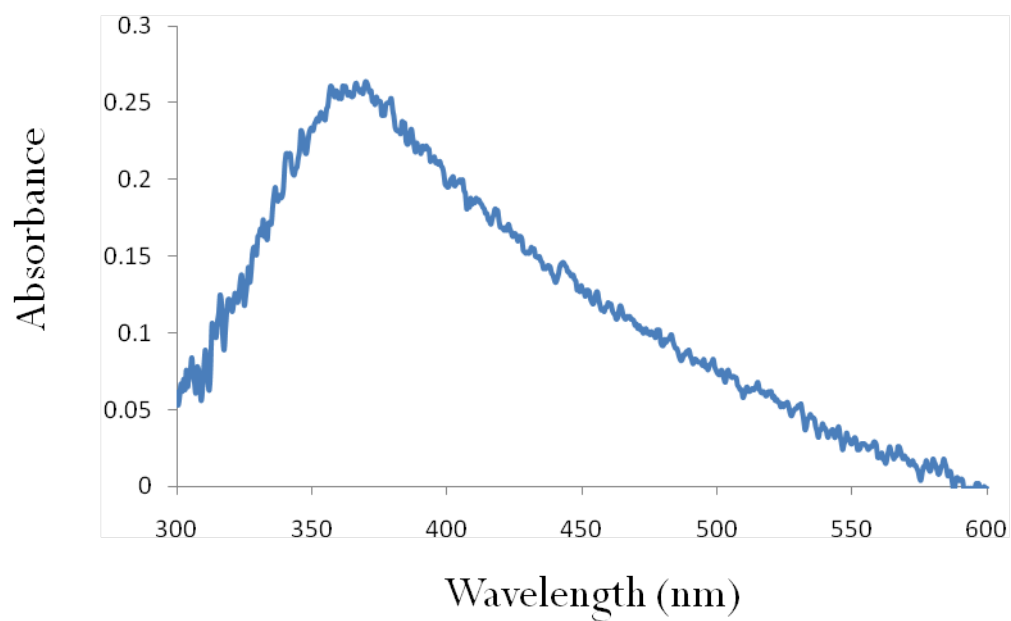


Figure C-12: UV-vis of sample 13

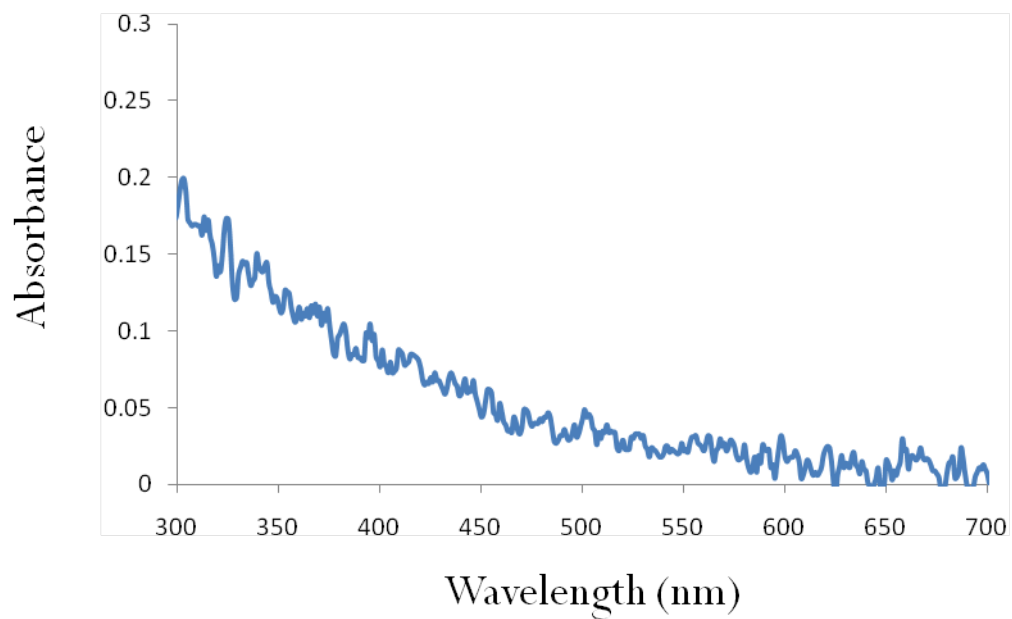


Figure C-13: UV-vis of sample 14

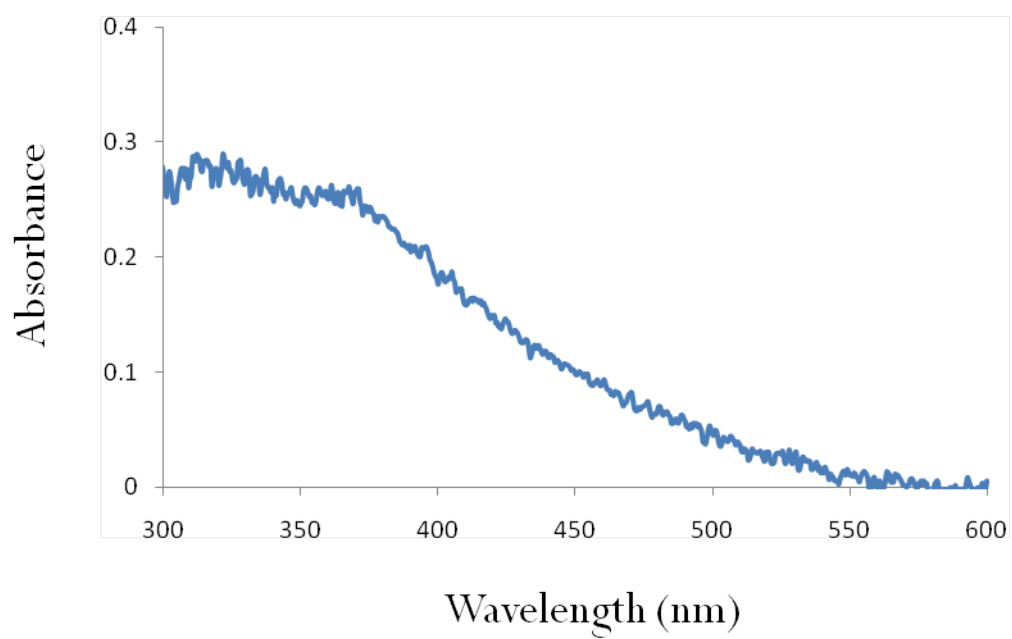


Figure C-14: UV-vis of sample 15

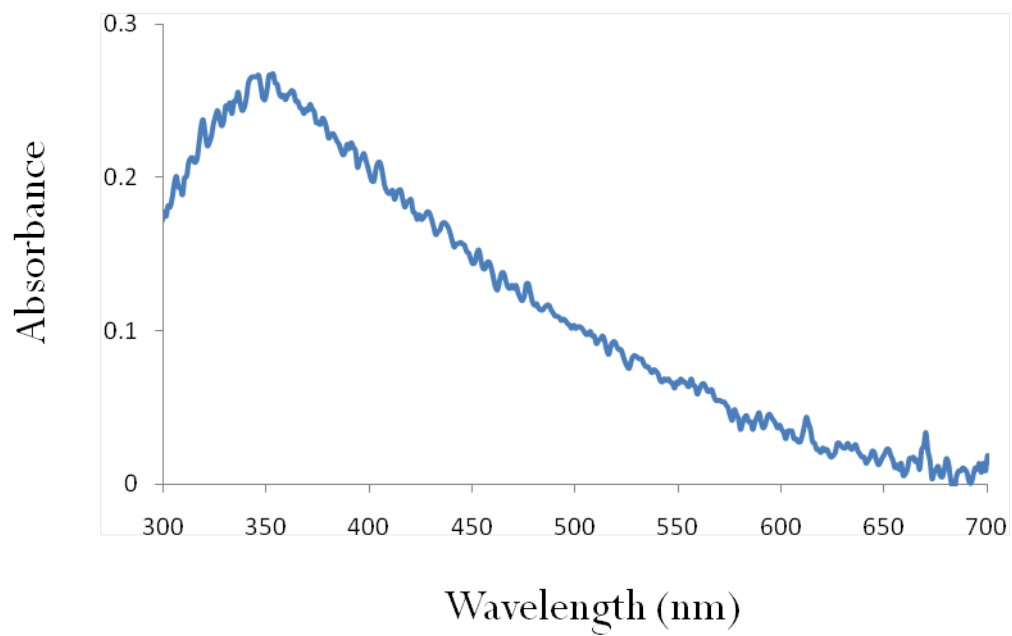


Figure C15: UV-vis of sample 16

Appendix D for chapter 7

Synthesis of ZIF-8:

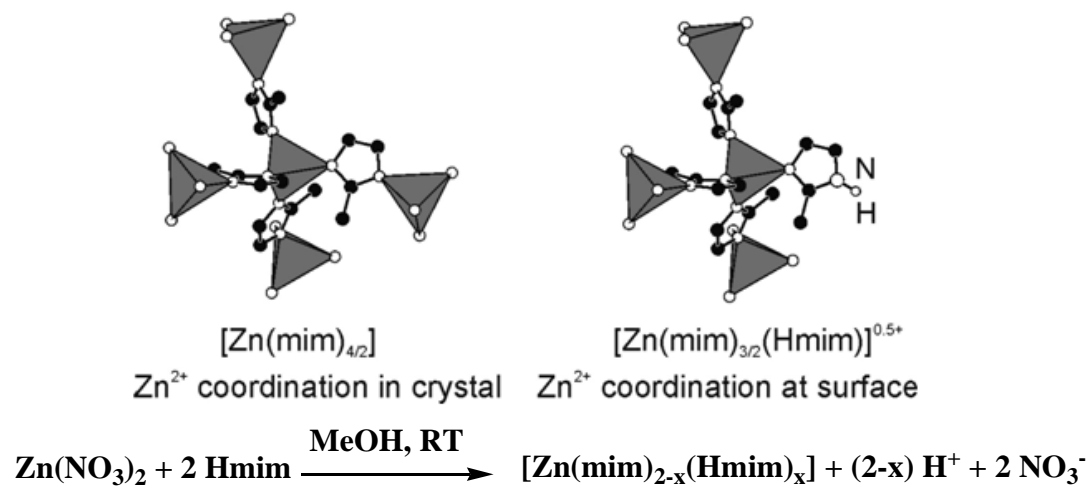


Figure D-1: Synthesis of ZIF-8 Nanocrystals Capped with Neutral 2-Methylimidazole

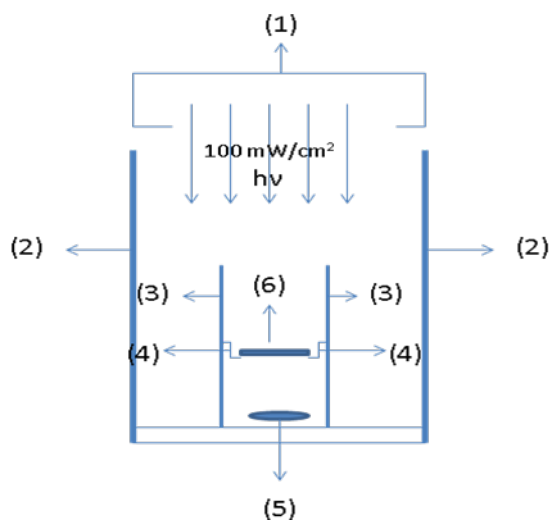
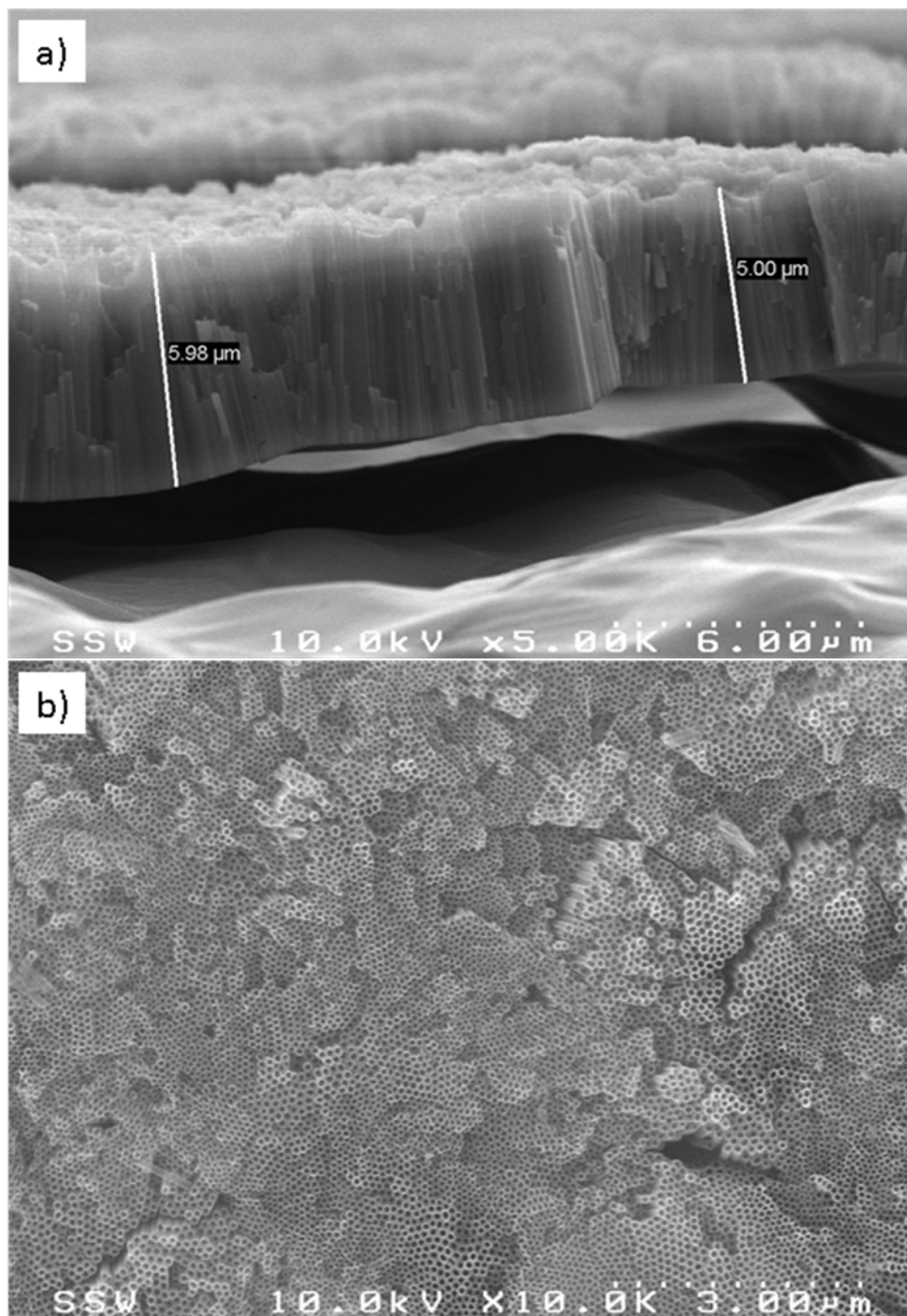
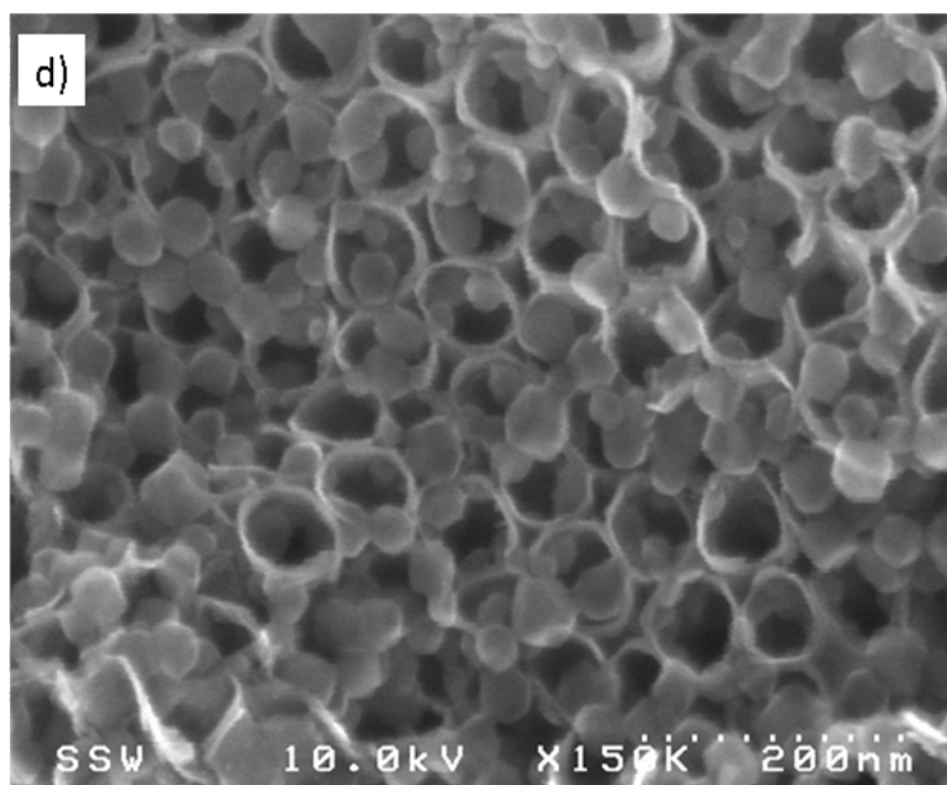
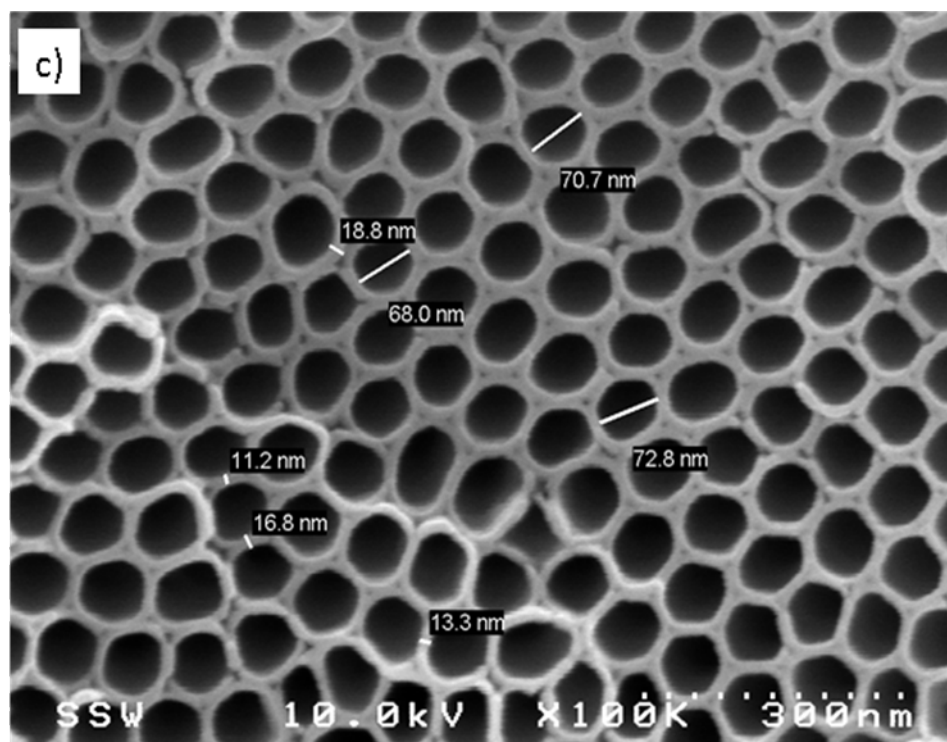
Schematic illustration of catalytic setup:

Figure D-2: Cross section of the set-up used for photocatalytic tests: (1) Solar simulator; (2) Black box; (3) Reactor ; (4) Sample holder; (5) Stirrer bar; (6) Sample

SEM micrographs of the TiO₂ NT samples:



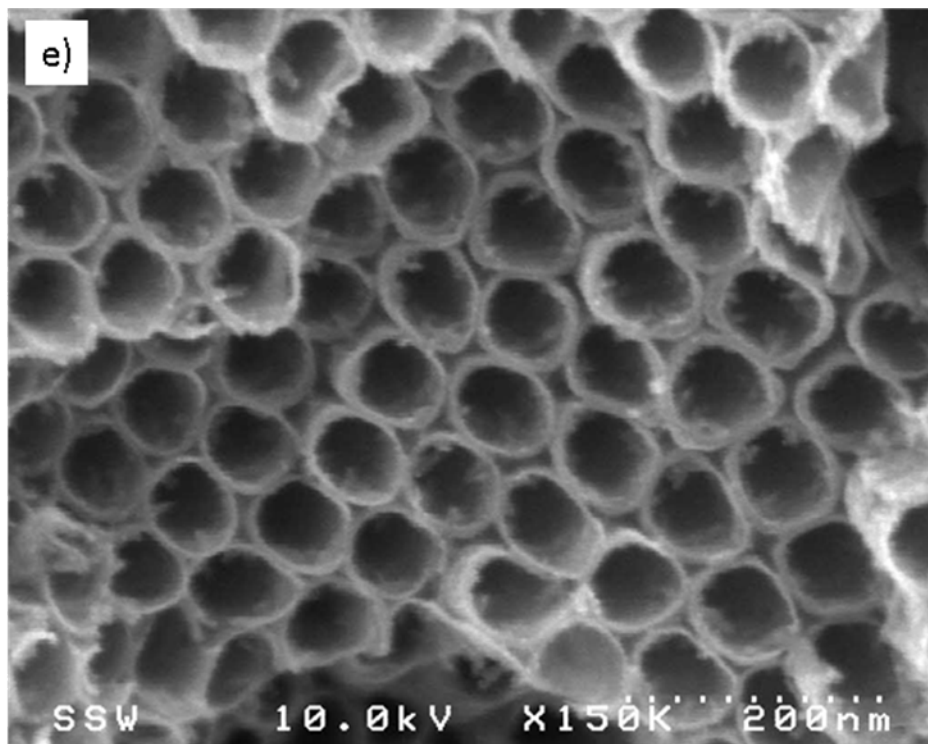
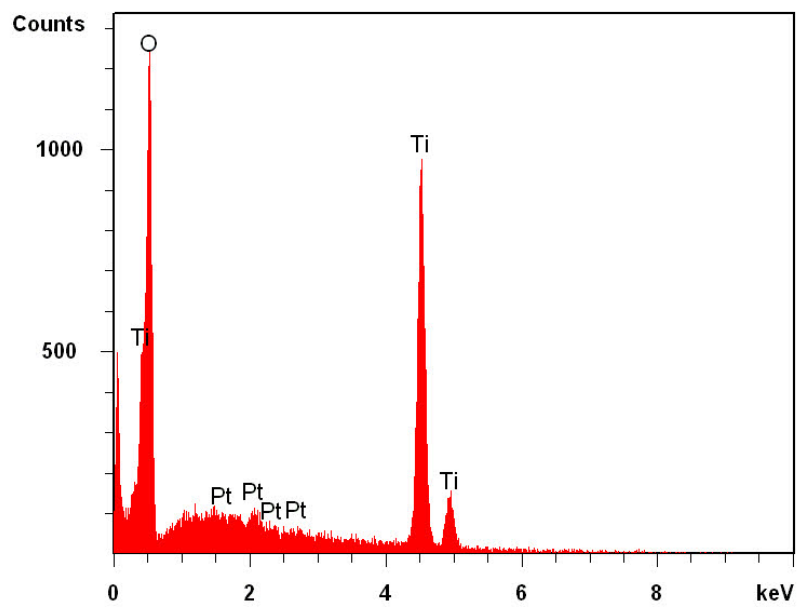


Figure D-3: SEM micrographs of TiO_2 NT samples: (a) Cross-section of unloaded TiO_2 NTs, (b) top view of unloaded TiO_2 NTs at larger magnitude, (c) pore size and wall thickness of unloaded TiO_2 NTs, (d) Pt/ZIF-8 loaded TiO_2 NTs, (e) Pt loaded TiO_2 NTs

EDX results:Figure D-4: EDX results of Pt loaded TiO₂ NTs

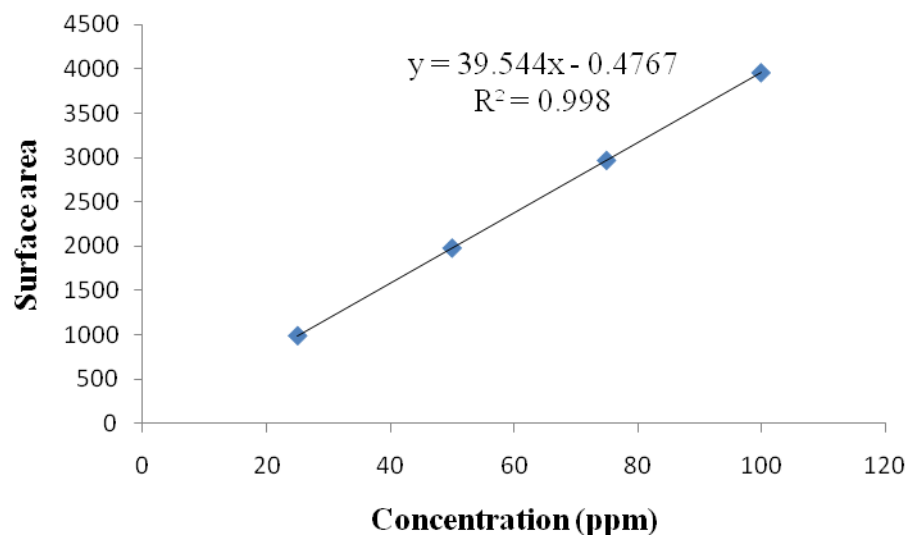
Calibration curve

Figure D-5: Calibration curve for phenol

Band gap calculation:

1) Wavelength (λ) was converted into Energy (E) according to equation (1)

$$E = h\nu = \frac{hc}{\lambda} \quad (1)$$

Where, h is Planck's constant (6.626×10^{-34} J.s), C is speed of light (3.0×10^8 m.s⁻¹) and λ is wavelength of light.

2) F(R) vs λ was measured by UV-vis

3) Band gap measurement curve was made by $\sqrt{F(R) \times E}$ vs. E

ZIF-8 loading calculation:

The chemical composition of ZIF-8 is Zn (mIm)₂ (i.e. Zn(2-methylimidazole)₂) with molecular mass of 227.6 g.mol⁻¹. Each molecular unit contains one Zn (65.4 g.mol⁻¹). According to EDX results, the Zn concentration was 5.2%, therefore the ZIF-8 loading can be calculated as following:

$$\text{ZIF-8\%} = (227.6/65.4) \times 5.2\% = 18.1\%$$

Appendix E for copy rights permission of figures used

Rightslink Printable License

Page 1 of 5

AMERICAN CHEMICAL SOCIETY LICENSE TERMS AND CONDITIONS

Apr 08, 2011

This is a License Agreement between Tayirjan Isimjan ("You") and American Chemical Society ("American Chemical Society") provided by Copyright Clearance Center ("CCC"). The license consists of your order details, the terms and conditions provided by American Chemical Society, and the payment terms and conditions.

All payments must be made in full to CCC. For payment instructions, please see information listed at the bottom of this form.

License Number	2644260983098
License Date	Apr 08, 2011
Licensed content publisher	American Chemical Society
Licensed content publication	The Journal of Physical Chemistry C
Licensed content title	Anodization Fabrication of Highly Ordered TiO ₂ Nanotubes
Licensed content author	Shiqi Li et al.
Licensed content date	Jul 1, 2009
Volume number	113
Issue number	29
Type of Use	Thesis/Dissertation
Requestor type	Not specified
Format	Print and Electronic
Portion	Table/Figure/Micrograph
Number of Table/Figure/Micrographs	10
Author of this ACS article	No
Order reference number	
Title of the thesis / dissertation	Fabrication, Modification and Application of Visible Light Responsive TiO ₂ Nanotubes
Expected completion date	Apr 2011
Estimated size(pages)	200
Billing Type	Invoice
Billing Address	1481 limberlost unit 156
	London, ON N6G 2C7
	Canada
Customer reference info	
Total	0.00 USD
Terms and Conditions	

Thesis/Dissertation

ACS / RIGHTS LINK TERMS & CONDITIONS THESIS/DISSERTATION

INTRODUCTION

The publisher for this copyrighted material is the American Chemical Society. By clicking "accept" in connection with completing this licensing transaction, you agree that the following terms and conditions apply to this transaction (along with the Billing and Payment terms and conditions established by Copyright Clearance Center, Inc. ("CCC"), at the time that you opened your Rightslink account and that are available at any time at <<http://myaccount.copyright.com>>).

LIMITED LICENSE

Publisher hereby grants to you a non-exclusive license to use this material. Licenses are for one-time use only with a maximum distribution equal to the number that you identified in the licensing process.

GEOGRAPHIC RIGHTS: SCOPE

Licenses may be exercised anywhere in the world.

RESERVATION OF RIGHTS

Publisher reserves all rights not specifically granted in the combination of (i) the license details provided by you and accepted in the course of this licensing transaction, (ii) these terms and conditions and (iii) CCC's Billing and Payment terms and conditions.

PORTION RIGHTS STATEMENT: DISCLAIMER

If you seek to reuse a portion from an ACS publication, it is your responsibility to examine each portion as published to determine whether a credit to, or copyright notice of, a third party owner was published adjacent to the item. You may only obtain permission via Rightslink to use material owned by ACS. Permission to use any material published in an ACS publication, journal, or article which is reprinted with permission of a third party must be obtained from the third party owner. ACS disclaims any responsibility for any use you make of items owned by third parties without their permission.

REVOCACTION

The American Chemical Society reserves the right to revoke a license for any reason, including but not limited to advertising and promotional uses of ACS content, third party usage, and incorrect figure source attribution.

LICENSE CONTINGENT ON PAYMENT

While you may exercise the rights licensed immediately upon issuance of the license at the end of the licensing process for the transaction, provided that you have disclosed complete and accurate details of your proposed use, no license is finally effective unless and until full payment is received from you (by CCC) as provided in CCC's Billing and Payment terms and conditions. If full payment is not received on a timely basis, then any license preliminarily granted shall be deemed automatically revoked and shall be void as if never granted. Further, in the event that you breach any of these terms and conditions or any of CCC's Billing and Payment terms and conditions, the license is automatically revoked and shall be void as if never granted. Use of materials as described in a revoked license, as well as any use of the materials beyond the scope of an unrevoked license, may constitute copyright infringement and publisher reserves the right to take any and all action to protect its copyright in the materials.

COPYRIGHT NOTICE: DISCLAIMER

You must include the following copyright and permission notice in connection with any

reproduction of the licensed material: "Reprinted ("Adapted" or "in part") with permission from REFERENCE CITATION. Copyright YEAR American Chemical Society."

WARRANTIES: NONE

Publisher makes no representations or warranties with respect to the licensed material.

INDEMNITY

You hereby indemnify and agree to hold harmless publisher and CCC, and their respective officers, directors, employees and agents, from and against any and all claims arising out of your use of the licensed material other than as specifically authorized pursuant to this license.

NO TRANSFER OF LICENSE

This license is personal to you or your publisher and may not be sublicensed, assigned, or transferred by you to any other person without publisher's written permission.

NO AMENDMENT EXCEPT IN WRITING

This license may not be amended except in a writing signed by both parties (or, in the case of publisher, by CCC on publisher's behalf).

OBJECTION TO CONTRARY TERMS

Publisher hereby objects to any terms contained in any purchase order, acknowledgment, check endorsement or other writing prepared by you, which terms are inconsistent with these terms and conditions or CCC's Billing and Payment terms and conditions. These terms and conditions, together with CCC's Billing and Payment terms and conditions (which are incorporated herein), comprise the entire agreement between you and publisher (and CCC) concerning this licensing transaction. In the event of any conflict between your obligations established by these terms and conditions and those established by CCC's Billing and Payment terms and conditions, these terms and conditions shall control.

JURISDICTION

This license transaction shall be governed by and construed in accordance with the laws of the District of Columbia. You hereby agree to submit to the jurisdiction of the courts located in the District of Columbia for purposes of resolving any disputes that may arise in connection with this licensing transaction.

THESES/DISSERTATION TERMS

Regarding your request for permission to include your paper(s) or portions of text from your paper(s) in your thesis/dissertation, permission is now automatically granted; please pay special attention to the **implications** paragraph below. The Copyright Subcommittee of the Joint Board/Council Committees on Publications approved the following:

Copyright permission for published and submitted material from theses and dissertations ACS extends blanket permission to students to include in their theses and dissertations their own articles, or portions thereof, that have been published in ACS journals or submitted to ACS journals for publication, provided that the ACS copyright credit line is noted on the appropriate page(s).

Publishing implications of electronic publication of theses and dissertation material

Students and their mentors should be aware that posting of theses and dissertation material on the Web prior to submission of material from that thesis or dissertation to an ACS journal may affect publication in that journal. Whether Web posting is considered prior publication may be evaluated on a case-by-case basis by the journal's editor. If an ACS journal editor considers Web posting to be "prior publication", the paper will not be accepted for

publication in that journal. If you intend to submit your unpublished paper to ACS for publication, check with the appropriate editor prior to posting your manuscript electronically.

Reuse/Republication of the Entire Work in Theses or Collections: Authors may reuse all or part of the Submitted, Accepted or Published Work in a thesis or dissertation that the author writes and is required to submit to satisfy the criteria of degree-granting institutions. Such reuse is permitted subject to the ACS' "Ethical Guidelines to Publication of Chemical Research" (<http://pubs.acs.org/page/policy/ethics/index.html>); the author should secure written confirmation (via letter or email) from the respective ACS journal editor(s) to avoid potential conflicts with journal prior publication*/embargo policies. Appropriate citation of the Published Work must be made. If the thesis or dissertation to be published is in electronic format, a direct link to the Published Work must also be included using the ACS Articles on Request author-directed link - see

<http://pubs.acs.org/page/policy/articlesonrequest/index.html>

* Prior publication policies of ACS journals are posted on the ACS website at

<http://pubs.acs.org/page/policy/prior/index.html>

If your paper has not yet been published by ACS, please print the following credit line on the first page of your article: "Reproduced (or 'Reproduced in part') with permission from [JOURNAL NAME], in press (or 'submitted for publication'). Unpublished work copyright [CURRENT YEAR] American Chemical Society." Include appropriate information.

If your paper has already been published by ACS and you want to include the text or portions of the text in your thesis/dissertation in **print or microfilm** formats, please print the ACS copyright credit line on the first page of your article: "Reproduced (or 'Reproduced in part') with permission from [FULL REFERENCE CITATION.] Copyright [YEAR] American Chemical Society." Include appropriate information.

Submission to a Dissertation Distributor: If you plan to submit your thesis to UMI or to another dissertation distributor, you should not include the unpublished ACS paper in your thesis if the thesis will be disseminated electronically, until ACS has published your paper. After publication of the paper by ACS, you may release the entire thesis (not the individual ACS article by itself) for electronic dissemination through the distributor; ACS's copyright credit line should be printed on the first page of the ACS paper.

v1.2

Gratis licenses (referencing \$0 in the Total field) are free. Please retain this printable license for your reference. No payment is required.

If you would like to pay for this license now, please remit this license along with your payment made payable to "COPYRIGHT CLEARANCE CENTER" otherwise you will be invoiced within 48 hours of the license date. Payment should be in the form of a check or money order referencing your account number and this invoice number RLNK10966079.

Once you receive your invoice for this order, you may pay your invoice by credit card. Please follow instructions provided at that time.

Make Payment To:
Copyright Clearance Center
Dept 001
P.O. Box 843006
Boston, MA 02284-3006

For suggestions or comments regarding this order, contact Rightslink Customer Support: customercare@copyright.com or +1-877-622-5543 (toll free in the US) or +1-978-646-2777.

**AMERICAN CHEMICAL SOCIETY LICENSE
TERMS AND CONDITIONS**

Apr 12, 2011

This is a License Agreement between Tayirjan Isimjan ("You") and American Chemical Society ("American Chemical Society") provided by Copyright Clearance Center ("CCC"). The license consists of your order details, the terms and conditions provided by American Chemical Society, and the payment terms and conditions.

All payments must be made in full to CCC. For payment instructions, please see information listed at the bottom of this form.

License Number	2646600911459
License Date	Apr 12, 2011
Licensed content publisher	American Chemical Society
Licensed content publication	Nano Letters
Licensed content title	Self-Organized Regular Arrays of Anodic TiO ₂ Nanotubes
Licensed content author	Yeonmi Shin et al.
Licensed content date	Oct 1, 2008
Volume number	8
Issue number	10
Type of Use	Thesis/Dissertation
Requestor type	Not specified
Format	Print and Electronic
Portion	Table/Figure/Micrograph
Number of Table/Figure/Micrographs	10
Author of this ACS article	No
Order reference number	
Title of the thesis / dissertation	Fabrication, Modification and Application of Visible Light Responsive TiO ₂ Nanotubes
Expected completion date	Apr 2011
Estimated size(pages)	200
Billing Type	Invoice
Billing Address	1481 limberlost unit 156
	London, ON N6G 2C7
	Canada
Customer reference info	
Total	0.00 USD
Terms and Conditions	

Thesis/Dissertation

**AMERICAN CHEMICAL SOCIETY LICENSE
TERMS AND CONDITIONS**

Apr 12, 2011

This is a License Agreement between Tayirjan Isimjan ("You") and American Chemical Society ("American Chemical Society") provided by Copyright Clearance Center ("CCC"). The license consists of your order details, the terms and conditions provided by American Chemical Society, and the payment terms and conditions.

All payments must be made in full to CCC. For payment instructions, please see information listed at the bottom of this form.

License Number	2646601209663
License Date	Apr 12, 2011
Licensed content publisher	American Chemical Society
Licensed content publication	Chemical Reviews
Licensed content title	Titanium Dioxide Nanomaterials: Synthesis, Properties, Modifications, and Applications
Licensed content author	Xiaobo Chen et al.
Licensed content date	Jul 1, 2007
Volume number	107
Issue number	7
Type of Use	Thesis/Dissertation
Requestor type	Not specified
Format	Print and Electronic
Portion	Table/Figure/Micrograph
Number of Table/Figure/Micrographs	10
Author of this ACS article	No
Order reference number	
Title of the thesis / dissertation	Fabrication, Modification and Application of Visible Light Responsive TiO ₂ Nanotubes
Expected completion date	Apr 2011
Estimated size(pages)	200
Billing Type	Invoice
Billing Address	1481 limberlost unit 156
	London, ON N6G 2C7
	Canada
Customer reference info	
Total	0.00 USD
Terms and Conditions	

Thesis/Dissertation

**AMERICAN CHEMICAL SOCIETY LICENSE
TERMS AND CONDITIONS**

Apr 12, 2011

This is a License Agreement between Tayirjan Isimjan ("You") and American Chemical Society ("American Chemical Society") provided by Copyright Clearance Center ("CCC"). The license consists of your order details, the terms and conditions provided by American Chemical Society, and the payment terms and conditions.

All payments must be made in full to CCC. For payment instructions, please see information listed at the bottom of this form.

License Number	2646650982959
License Date	Apr 12, 2011
Licensed content publisher	American Chemical Society
Licensed content publication	Journal of the American Chemical Society
Licensed content title	Tetrachelate Porphyrin Chromophores for Metal Oxide Semiconductor Sensitization: Effect of the Spacer Length and Anchoring Group Position
Licensed content author	Jonathan Rochford et al.
Licensed content date	Apr 1, 2007
Volume number	129
Issue number	15
Type of Use	Thesis/Dissertation
Requestor type	Not specified
Format	Print and Electronic
Portion	Table/Figure/Micrograph
Number of Table/Figure/Micrographs	10
Author of this ACS article	No
Order reference number	
Title of the thesis / dissertation	Fabrication, Modification and Application of Visible Light Responsive TiO ₂ Nanotubes
Expected completion date	Apr 2011
Estimated size(pages)	200
Billing Type	Invoice
Billing Address	1481 limberlost unit 156 London, ON N6G 2C7 Canada
Customer reference info	
Total	0.00 USD
Terms and Conditions	

**THE AMERICAN ASSOCIATION FOR THE ADVANCEMENT OF SCIENCE LICENSE
TERMS AND CONDITIONS**

Apr 13, 2011

This is a License Agreement between Tayirjan Isimjan ("You") and The American Association for the Advancement of Science ("The American Association for the Advancement of Science") provided by Copyright Clearance Center ("CCC"). The license consists of your order details, the terms and conditions provided by The American Association for the Advancement of Science, and the payment terms and conditions.

All payments must be made in full to CCC. For payment instructions, please see information listed at the bottom of this form.

License Number	2647120851670
License date	Apr 13, 2011
Licensed content publisher	The American Association for the Advancement of Science
Licensed content publication	Science
Licensed content title	High-Throughput Synthesis of Zeolitic Imidazolate Frameworks and Application to CO ₂ Capture
Licensed content author	Rahul Banerjee, Anh Phan, Bo Wang, Carolyn Knobler, Hiroyasu Furukawa, Michael O'Keeffe, Omar M. Yaghi
Licensed content date	Feb 15, 2008
Volume number	319
Issue number	5865
Type of Use	Thesis / Dissertation
Requestor type	Other Individual
Format	Print and electronic
Portion	Figure
Number of figures/tables	10
Order reference number	
Title of your thesis / dissertation	Fabrication, Modification and Application of Visible Light Responsive TiO ₂ Nanotubes
Expected completion date	Apr 2011
Estimated size(pages)	200
Total	0.00 USD

Terms and Conditions

American Association for the Advancement of Science TERMS AND CONDITIONS

Regarding your request, we are pleased to grant you non-exclusive, non-transferable permission, to republish the AAAS material identified above in your work identified above, subject to the terms and conditions herein. We must be contacted for permission for any uses other than those specifically identified in your request above.

The following credit line must be printed along with the AAAS material: "From [Full Reference Citation]. Reprinted with permission from AAAS."

All required credit lines and notices must be visible any time a user accesses any part of the AAAS material and must appear on any printed copies and authorized user might make.

This permission does not apply to figures / photos / artwork or any other content or materials included in your work that are credited to non-AAAS sources. If the requested material is sourced to or references non-AAAS sources, you must obtain authorization from that source as well before using that material. You agree to hold harmless and indemnify AAAS against any claims arising from your use of any content in your work that is credited to non-AAAS sources.

If the AAAS material covered by this permission was published in Science during the years 1974 - 1994, you must also obtain permission from the author, who may grant or withhold permission, and who may or may not charge a fee if permission is granted. See original article for author's address. This condition does not apply to news articles.

The AAAS material may not be modified or altered except that figures and tables may be modified with permission from the author. Author permission for any such changes must be secured prior to your use.

Whenever possible, we ask that electronic uses of the AAAS material permitted herein include a hyperlink to the original work on AAAS's website (hyperlink may be embedded in the reference citation).

AAAS material reproduced in your work identified herein must not account for more than 30% of the total contents of that work.

AAAS must publish the full paper prior to use of any text.

AAAS material must not imply any endorsement by the American Association for the Advancement of Science.

This permission is not valid for the use of the AAAS and/or Science logos.

AAAS makes no representations or warranties as to the accuracy of any information contained in the AAAS material covered by this permission, including any warranties of merchantability or fitness for a particular purpose.

If permission fees for this use are waived, please note that AAAS reserves the right to charge for reproduction of this material in the future.

Permission is not valid unless payment is received within sixty (60) days of the issuance of this permission. If payment is not received within this time period then all rights granted herein shall be revoked and this permission will be considered null and void.

In the event of breach of any of the terms and conditions herein or any of CCC's Billing and Payment terms and conditions, all rights granted herein shall be revoked and this permission will be considered null and void.

AAAS reserves the right to terminate this permission and all rights granted herein at its discretion, for any purpose, at any time. In the event that AAAS elects to terminate this permission, you will have no further right to publish, publicly perform, publicly display, distribute or otherwise use any matter in which the AAAS content had been included, and all

fees paid hereunder shall be fully refunded to you. Notification of termination will be sent to the contact information as supplied by you during the request process and termination shall be immediate upon sending the notice. Neither AAAS nor CCC shall be liable for any costs, expenses, or damages you may incur as a result of the termination of this permission, beyond the refund noted above.

This Permission may not be amended except by written document signed by both parties.

The terms above are applicable to all permissions granted for the use of AAAS material. Below you will find additional conditions that apply to your particular type of use.

FOR A THESIS OR DISSERTATION

If you are using figure(s)/table(s), permission is granted for use in print and electronic versions of your dissertation or thesis. A full text article may be used in print versions only of a dissertation or thesis.

Permission covers the distribution of your dissertation or thesis on demand by ProQuest / UMI, provided the AAAS material covered by this permission remains in situ.

If you are an Original Author on the AAAS article being reproduced, please refer to your License to Publish for rules on reproducing your paper in a dissertation or thesis.

FOR JOURNALS:

Permission covers both print and electronic versions of your journal article, however the AAAS material may not be used in any manner other than within the context of your article.

FOR BOOKS/TEXTBOOKS:

If this license is to reuse figures/tables, then permission is granted for non-exclusive world rights in all languages in both print and electronic formats (electronic formats are defined below).

If this license is to reuse a text excerpt or a full text article, then permission is granted for non-exclusive world rights in English only. You have the option of securing either print or electronic rights or both, but electronic rights are not automatically granted and do garner additional fees. Permission for translations of text excerpts or full text articles into other languages must be obtained separately.

Licenses granted for use of AAAS material in electronic format books/textbooks are valid only in cases where the electronic version is equivalent to or substitutes for the print version of the book/textbook. The AAAS material reproduced as permitted herein must remain in situ and must not be exploited separately (for example, if permission covers the use of a full text article, the article may not be offered for access or for purchase as a stand-alone unit), except in the case of permitted textbook companions as noted below.

You must include the following notice in any electronic versions, either adjacent to the reprinted AAAS material or in the terms and conditions for use of your electronic products: "Readers may view, browse, and/or download material for temporary copying purposes only, provided these uses are for noncommercial personal purposes. Except as provided by law, this material may not be further reproduced, distributed, transmitted, modified, adapted, performed, displayed, published, or sold in whole or in part, without prior written permission from the publisher."

If your book is an academic textbook, permission covers the following companions to your textbook, provided such companions are distributed only in conjunction with your textbook

at no additional cost to the user:

- Password-protected website
- Instructor's image CD/DVD and/or PowerPoint resource
- Student CD/DVD

All companions must contain instructions to users that the AAAS material may be used for non-commercial, classroom purposes only. Any other uses require the prior written permission from AAAS.

Rights also extend to copies/files of your Work (as described above) that you are required to provide for use by the visually and/or print disabled in compliance with state and federal laws.

This permission only covers a single edition of your work as identified in your request.

FOR NEWSLETTERS:

Permission covers print and/or electronic versions, provided the AAAS material reproduced as permitted herein remains in situ and is not exploited separately (for example, if permission covers the use of a full text article, the article may not be offered for access or for purchase as a stand-alone unit)

FOR ANNUAL REPORTS:

Permission covers print and electronic versions provided the AAAS material reproduced as permitted herein remains in situ and is not exploited separately (for example, if permission covers the use of a full text article, the article may not be offered for access or for purchase as a stand-alone unit)

FOR PROMOTIONAL/MARKETING USES:

Permission covers the use of AAAS material in promotional or marketing pieces such as information packets, media kits, product slide kits, brochures, or flyers limited to a single print run. The AAAS Material may not be used in any manner which implies endorsement or promotion by the American Association for the Advancement of Science (AAAS) or Science of any product or service. AAAS does not permit the reproduction of its name, logo or text on promotional literature.

If permission to use a full text article is permitted, The Science article covered by this permission must not be altered in any way. No additional printing may be set onto an article copy other than the copyright credit line required above. Any alterations must be approved in advance and in writing by AAAS. This includes, but is not limited to, the placement of sponsorship identifiers, trademarks, logos, rubber stamping or self-adhesive stickers onto the article copies.

Additionally, article copies must be a freestanding part of any information package (i.e. media kit) into which they are inserted. They may not be physically attached to anything, such as an advertising insert, or have anything attached to them, such as a sample product. Article copies must be easily removable from any kits or informational packages in which they are used. The only exception is that article copies may be inserted into three-ring binders.

FOR CORPORATE INTERNAL USE:

The AAAS material covered by this permission may not be altered in any way. No additional printing may be set onto an article copy other than the required credit line. Any

alterations must be approved in advance and in writing by AAAS. This includes, but is not limited to the placement of sponsorship identifiers, trademarks, logos, rubber stamping or self-adhesive stickers onto article copies.

If you are making article copies, copies are restricted to the number indicated in your request and must be distributed only to internal employees for internal use.

If you are using AAAS Material in Presentation Slides, the required credit line must be visible on the slide where the AAAS material will be reprinted

If you are using AAAS Material on a CD, DVD, Flash Drive, or the World Wide Web, you must include the following notice in any electronic versions, either adjacent to the reprinted AAAS material or in the terms and conditions for use of your electronic products: "Readers may view, browse, and/or download material for temporary copying purposes only, provided these uses are for noncommercial personal purposes. Except as provided by law, this material may not be further reproduced, distributed, transmitted, modified, adapted, performed, displayed, published, or sold in whole or in part, without prior written permission from the publisher." Access to any such CD, DVD, Flash Drive or Web page must be restricted to your organization's employees only.

FOR CME COURSE and SCIENTIFIC SOCIETY MEETINGS:

Permission is restricted to the particular Course, Seminar, Conference, or Meeting indicated in your request. If this license covers a text excerpt or a Full Text Article, access to the reprinted AAAS material must be restricted to attendees of your event only (if you have been granted electronic rights for use of a full text article on your website, your website must be password protected, or access restricted so that only attendees can access the content on your site).

If you are using AAAS Material on a CD, DVD, Flash Drive, or the World Wide Web, you must include the following notice in any electronic versions, either adjacent to the reprinted AAAS material or in the terms and conditions for use of your electronic products: "Readers may view, browse, and/or download material for temporary copying purposes only, provided these uses are for noncommercial personal purposes. Except as provided by law, this material may not be further reproduced, distributed, transmitted, modified, adapted, performed, displayed, published, or sold in whole or in part, without prior written permission from the publisher."

FOR POLICY REPORTS:

These rights are granted only to non-profit organizations and/or government agencies. Permission covers print and electronic versions of a report, provided the required credit line appears in both versions and provided the AAAS material reproduced as permitted herein remains in situ and is not exploited separately.

FOR CLASSROOM PHOTOCOPIES:

Permission covers distribution in print copy format only. Article copies must be freestanding and not part of a course pack. They may not be physically attached to anything or have anything attached to them.

FOR COURSEPACKS OR COURSE WEBSITES:

These rights cover use of the AAAS material in one class at one institution. Permission is valid only for a single semester after which the AAAS material must be removed from the Electronic Course website, unless new permission is obtained for an additional semester. If the material is to be distributed online, access must be restricted to students and instructors enrolled in that particular course by some means of password or access control.

FOR WEBSITES:

You must include the following notice in any electronic versions, either adjacent to the reprinted AAAS material or in the terms and conditions for use of your electronic products: "Readers may view, browse, and/or download material for temporary copying purposes only, provided these uses are for noncommercial personal purposes. Except as provided by law, this material may not be further reproduced, distributed, transmitted, modified, adapted, performed, displayed, published, or sold in whole or in part, without prior written permission from the publisher."

Permissions for the use of Full Text articles on third party websites are granted on a case by case basis and only in cases where access to the AAAS Material is restricted by some means of password or access control. Alternately, an E-Print may be purchased through our reprints department (brocheleau@rockwaterinc.com).

REGARDING FULL TEXT ARTICLE USE ON THE WORLD WIDE WEB IF YOU ARE AN 'ORIGINAL AUTHOR' OF A SCIENCE PAPER

If you chose "Original Author" as the Requestor Type, you are warranting that you are one of authors listed on the License Agreement as a "Licensed content author" or that you are acting on that author's behalf to use the Licensed content in a new work that one of the authors listed on the License Agreement as a "Licensed content author" has written.

Original Authors may post the 'Accepted Version' of their full text article on their personal or on their University website and not on any other website. The 'Accepted Version' is the version of the paper accepted for publication by AAAS including changes resulting from peer review but prior to AAAS's copy editing and production (in other words not the AAAS published version).

FOR MOVIES / FILM / TELEVISION:

Permission is granted to use, record, film, photograph, and/or tape the AAAS material in connection with your program/film and in any medium your program/film may be shown or heard, including but not limited to broadcast and cable television, radio, print, world wide web, and videocassette.

The required credit line should run in the program/film's end credits.

FOR MUSEUM EXHIBITIONS:

Permission is granted to use the AAAS material as part of a single exhibition for the duration of that exhibit. Permission for use of the material in promotional materials for the exhibit must be cleared separately with AAAS (please contact us at permissions@aaas.org).

FOR TRANSLATIONS:

Translation rights apply only to the language identified in your request summary above.

The following disclaimer must appear with your translation, on the first page of the article, after the credit line: "This translation is not an official translation by AAAS staff, nor is it endorsed by AAAS as accurate. In crucial matters, please refer to the official English-language version originally published by AAAS."

FOR USE ON A COVER:

Permission is granted to use the AAAS material on the cover of a journal issue, newsletter issue, book, textbook, or annual report in print and electronic formats provided the AAAS material reproduced as permitted herein remains in situ and is not exploited separately

By using the AAAS Material identified in your request, you agree to abide by all the terms and conditions herein.

Questions about these terms can be directed to the AAAS Permissions department permissions@aaas.org.

v 2

Gratis licenses (referencing \$0 in the Total field) are free. Please retain this printable license for your reference. No payment is required.

If you would like to pay for this license now, please remit this license along with your payment made payable to "COPYRIGHT CLEARANCE CENTER" otherwise you will be invoiced within 48 hours of the license date. Payment should be in the form of a check or money order referencing your account number and this invoice number RLNK10969133.

Once you receive your invoice for this order, you may pay your invoice by credit card. Please follow instructions provided at that time.

**Make Payment To:
Copyright Clearance Center
Dept 001
P.O. Box 843006
Boston, MA 02284-3006**

For suggestions or comments regarding this order, contact Rightslink Customer Support: customercare@copyright.com or +1-877-622-5543 (toll free in the US) or +1-978-646-2777.

ELSEVIER ORDER DETAILS

Apr 12, 2011

Order Number	500607285
Order Date	Apr 12, 2011
Licensed content publisher	Elsevier
Licensed content publication	International Journal of Hydrogen Energy
Licensed content title	Hydrogen generation under sunlight by self ordered TiO ₂ nanotube arrays
Licensed content author	Zhaoyue Liu, Batric Pesic, Krishnan S. Raja, Raghu R. Rangaraju, Mano Misra
Licensed content date	May 2009
Licensed content volume number	34
Licensed content issue number	8
Number of pages	8
Start Page	3250
End Page	3257
Type of Use	reuse in a thesis/dissertation
Intended publisher of new work	other
Portion	figures/tables/illustrations
Number of figures/tables/illustrations	>10
Actual number of figures/tables/illustrations	11
Format	both print and electronic
Are you the author of this Elsevier article?	No
Will you be translating?	No
Order reference number	
Title of your thesis/dissertation	Fabrication, Modification and Application of Visible Light Responsive TiO ₂ Nanotubes
Expected completion date	Apr 2011
Estimated size (number of pages)	200
Elsevier VAT number	GB 494 6272 12
Permissions price	Not Available
VAT/Local Sales Tax	Not Available
Total	Not Available

**ELSEVIER LICENSE
TERMS AND CONDITIONS**

Apr 12, 2011

This is a License Agreement between Tayirjan Isimjan ("You") and Elsevier ("Elsevier") provided by Copyright Clearance Center ("CCC"). The license consists of your order details, the terms and conditions provided by Elsevier, and the payment terms and conditions.

All payments must be made in full to CCC. For payment instructions, please see information listed at the bottom of this form.

Supplier	Elsevier Limited The Boulevard, Langford Lane Kidlington, Oxford, OX5 1GB, UK
Registered Company Number	1982084
Customer name	Tayirjan Isimjan
Customer address	
License number	2646621158288
License date	Apr 12, 2011
Licensed content publisher	Elsevier
Licensed content publication	Coordination Chemistry Reviews
Licensed content title	Porphyrins as light harvesters in the dye-sensitised TiO ₂ solar cell
Licensed content author	Wayne M. Campbell, Anthony K. Burrell, David L. Officer, Kenneth W. Jolley
Licensed content date	July 2004
Licensed content volume number	248
Licensed content issue number	13-14
Number of pages	17
Start Page	1363
End Page	1379
Type of Use	reuse in a thesis/dissertation
Intended publisher of new work	other
Portion	figures/tables/illustrations
Number of figures/tables/illustrations	10
Format	both print and electronic
Are you the author of this Elsevier article?	No
Will you be translating?	No
Order reference number	

Thesis/Dissertation

ACS / RIGHTS LINK TERMS & CONDITIONS THESIS/DISSERTATION

INTRODUCTION

The publisher for this copyrighted material is the American Chemical Society. By clicking "accept" in connection with completing this licensing transaction, you agree that the following terms and conditions apply to this transaction (along with the Billing and Payment terms and conditions established by Copyright Clearance Center, Inc. ("CCC"), at the time that you opened your Rightslink account and that are available at any time at <<http://myaccount.copyright.com>>).

LIMITED LICENSE

Publisher hereby grants to you a non-exclusive license to use this material. Licenses are for one-time use only with a maximum distribution equal to the number that you identified in the licensing process.

GEOGRAPHIC RIGHTS: SCOPE

Licenses may be exercised anywhere in the world.

RESERVATION OF RIGHTS

Publisher reserves all rights not specifically granted in the combination of (i) the license details provided by you and accepted in the course of this licensing transaction, (ii) these terms and conditions and (iii) CCC's Billing and Payment terms and conditions.

PORTION RIGHTS STATEMENT: DISCLAIMER

If you seek to reuse a portion from an ACS publication, it is your responsibility to examine each portion as published to determine whether a credit to, or copyright notice of, a third party owner was published adjacent to the item. You may only obtain permission via Rightslink to use material owned by ACS. Permission to use any material published in an ACS publication, journal, or article which is reprinted with permission of a third party must be obtained from the third party owner. ACS disclaims any responsibility for any use you make of items owned by third parties without their permission.

REVOCATION

The American Chemical Society reserves the right to revoke a license for any reason, including but not limited to advertising and promotional uses of ACS content, third party usage, and incorrect figure source attribution.

LICENSE CONTINGENT ON PAYMENT

While you may exercise the rights licensed immediately upon issuance of the license at the end of the licensing process for the transaction, provided that you have disclosed complete and accurate details of your proposed use, no license is finally effective unless and until full payment is received from you (by CCC) as provided in CCC's Billing and Payment terms and conditions. If full payment is not received on a timely basis, then any license preliminarily granted shall be deemed automatically revoked and shall be void as if never granted. Further, in the event that you breach any of these terms and conditions or any of CCC's Billing and Payment terms and conditions, the license is automatically revoked and shall be void as if never granted. Use of materials as described in a revoked license, as well as any use of the materials beyond the scope of an unrevoked license, may constitute copyright infringement and publisher reserves the right to take any and all action to protect its copyright in the materials.

COPYRIGHT NOTICE: DISCLAIMER

You must include the following copyright and permission notice in connection with any reproduction of the licensed material: "Reprinted ("Adapted" or "in part") with permission from REFERENCE CITATION. Copyright YEAR American Chemical Society."

WARRANTIES: NONE

Publisher makes no representations or warranties with respect to the licensed material.

INDEMNITY

You hereby indemnify and agree to hold harmless publisher and CCC, and their respective officers, directors, employees and agents, from and against any and all claims arising out of your use of the licensed material other than as specifically authorized pursuant to this license.

NO TRANSFER OF LICENSE

This license is personal to you or your publisher and may not be sublicensed, assigned, or transferred by you to any other person without publisher's written permission.

NO AMENDMENT EXCEPT IN WRITING

This license may not be amended except in a writing signed by both parties (or, in the case of publisher, by CCC on publisher's behalf).

OBJECTION TO CONTRARY TERMS

Publisher hereby objects to any terms contained in any purchase order, acknowledgment, check endorsement or other writing prepared by you, which terms are inconsistent with these terms and conditions or CCC's Billing and Payment terms and conditions. These terms and conditions, together with CCC's Billing and Payment terms and conditions (which are incorporated herein), comprise the entire agreement between you and publisher (and CCC) concerning this licensing transaction. In the event of any conflict between your obligations established by these terms and conditions and those established by CCC's Billing and Payment terms and conditions, these terms and conditions shall control.

JURISDICTION

This license transaction shall be governed by and construed in accordance with the laws of the District of Columbia. You hereby agree to submit to the jurisdiction of the courts located in the District of Columbia for purposes of resolving any disputes that may arise in connection with this licensing transaction.

THESES/DISSERTATION TERMS

Regarding your request for permission to include **your** paper(s) or portions of text from **your** paper(s) in your thesis/dissertation, permission is now automatically granted; please pay special attention to the **implications** paragraph below. The Copyright Subcommittee of the Joint Board/Council Committees on Publications approved the following:

Copyright permission for published and submitted material from theses and dissertations ACS extends blanket permission to students to include in their theses and dissertations their own articles, or portions thereof, that have been published in ACS journals or submitted to ACS journals for publication, provided that the ACS copyright credit line is noted on the appropriate page(s).

Publishing implications of electronic publication of theses and dissertation material

Students and their mentors should be aware that posting of theses and dissertation material on the Web prior to submission of material from that thesis or dissertation to an ACS journal may affect publication in that journal. Whether Web posting is considered prior publication

may be evaluated on a case-by-case basis by the journal's editor. If an ACS journal editor considers Web posting to be "prior publication", the paper will not be accepted for publication in that journal. If you intend to submit your unpublished paper to ACS for publication, check with the appropriate editor prior to posting your manuscript electronically.

Reuse/Republishment of the Entire Work in Theses or Collections: Authors may reuse all or part of the Submitted, Accepted or Published Work in a thesis or dissertation that the author writes and is required to submit to satisfy the criteria of degree-granting institutions. Such reuse is permitted subject to the ACS' "Ethical Guidelines to Publication of Chemical Research" (<http://pubs.acs.org/page/policy/ethics/index.html>); the author should secure written confirmation (via letter or email) from the respective ACS journal editor(s) to avoid potential conflicts with journal prior publication*/embargo policies. Appropriate citation of the Published Work must be made. If the thesis or dissertation to be published is in electronic format, a direct link to the Published Work must also be included using the ACS Articles on Request author-directed link - see <http://pubs.acs.org/page/policy/articlesonrequest/index.html>

* Prior publication policies of ACS journals are posted on the ACS website at <http://pubs.acs.org/page/policy/prior/index.html>

If your paper has not yet been published by ACS, please print the following credit line on the first page of your article: "Reproduced (or 'Reproduced in part') with permission from [JOURNAL NAME], in press (or 'submitted for publication'). Unpublished work copyright [CURRENT YEAR] American Chemical Society." Include appropriate information.

If your paper has already been published by ACS and you want to include the text or portions of the text in your thesis/dissertation in **print or microfilm formats**, please print the ACS copyright credit line on the first page of your article: "Reproduced (or 'Reproduced in part') with permission from [FULL REFERENCE CITATION.] Copyright [YEAR] American Chemical Society." Include appropriate information.

Submission to a Dissertation Distributor: If you plan to submit your thesis to UMI or to another dissertation distributor, you should not include the unpublished ACS paper in your thesis if the thesis will be disseminated electronically, until ACS has published your paper. After publication of the paper by ACS, you may release the entire thesis (**not the individual ACS article by itself**) for electronic dissemination through the distributor; ACS's copyright credit line should be printed on the first page of the ACS paper.

v1.2

Gratis licenses (referencing \$0 in the Total field) are free. Please retain this printable license for your reference. No payment is required.

If you would like to pay for this license now, please remit this license along with your payment made payable to "COPYRIGHT CLEARANCE CENTER" otherwise you will be invoiced within 48 hours of the license date. Payment should be in the form of a check or money order referencing your account number and this invoice number RLNK10968461.

Once you receive your invoice for this order, you may pay your invoice by credit card. Please follow instructions provided at that time.

**Make Payment To:
Copyright Clearance Center
Dept 001
P.O. Box 843006**

Boston, MA 02284-3006

For suggestions or comments regarding this order, contact Rightslink Customer Support: customercare@copyright.com or +1-877-622-5543 (toll free in the US) or +1-978-646-2777.

Curriculum Vitae

Name: Tayirjan T. Isimjan

Current work

-
- | | |
|--|--------------|
| Graduate Student, UWO, and London, Ontario | 2008-present |
|--|--------------|
- Focus: Fabrications, characterizations and applications of light sensitive TiO₂ nanotubes
- Synthesis of supramolacular polymers
 - Fabricate TiO₂ nanotubes by anodization
 - Characterize TiO₂ nanotubes by SEM, XRD and UV-vis
 - Activate TiO₂ nanotubes by doping and dye sensitization
 - Design solar cell and water purification reactors
 - Functionalized TiO₂ nanoparticles coating
 - Photochemical purification of water using 172 nm UV
 - V₂O₅ coating on TiO₂ nanotubes
 - Superhydrophobic surface and applications
 - Oil/Water purification

Practical Experience

-
- | | |
|--|---------------------|
| Research Scientist, Trojan UV, London, Ontario | June, 2010-Oct 2010 |
|--|---------------------|
- Focus: MITACS internship on advanced oxidation
- Research Scientist, NAEJA Pharmaceutical Inc., Edmonton, Alberta
2006-2007
Focus: Contract research in medicinal chemistry for library synthesis
 - Research in organic chemistry, McMaster University, Hamilton, Ontario 2004-2006
Focus: Pramanicin and quantitative structure-activity correlation
 - Research associate and lecturer, Xinjiang University, Urumqi, China 1996-2004
Focus: Natural product isolation and structure modification

Education

-
- McMaster University (with Prof. Paul Harrison), Canada, M.Sc. graduate, Organic Synthesis, 2004-2006
 - Xinjiang University (with Prof. Ling Hua Sao), China, M.Sc. graduate, Natural Organic Chemistry, 2000-2003
 - Dalian University of Technology, China, B.Eng. Undergraduate, Polymer Materials, 1992-1996

Publication

- **Tayirjan T. Isimjan**, Hossein Kazemian, Sohrab Rohani*, Ajay K. Ray, “Photo catalytic activities of Pt/ZIF-8 loaded highly ordered TiO₂ nanotubes” *Journal of Material Chemistry* in press.
- **Tayirjan T. Isimjan**, Gillies, Elizabeth “Self-Assembly of Supramolecular Polymers from β -Strand Peptidomimetic-Poly(ethylene oxide) Hybrids” *Macromolecules* **2010**, 43 (10), 4453-4459.
- **Tayirjan T. Isimjan**, Ahmed El Ruby, Sohrab Rohani*, Ajay K. Ray* “Fabrication of highly-ordered and visible-light responsive Fe-C-N-codoped TiO₂ nanotubes” *Nanotechnology* **2010**, 21.
- **Tayirjan T. Isimjan**, D.-Q Yang, Sohrab Rohani*, Ajay K. Ray “An Innovative Approach to Synthesize Highly-Ordered TiO₂ Nanotubes” *Journal of Nanoscience and Nanotechnology* **2010**, 10, 1–5.
- Tao ye, **Tayirjan T. Isimjan**, Sohrab Rohani “Superhydrophobic transparent glass” *Nanotechnology*. (in press)
- **Tayirjan T. Isimjan**, Haishaer Turebieke, “Study on the Degradation and Residual of Endosulfan in soil using High effective liquid Chromatography” *Journal of Xinjiang university*, **2003**, 3(4), 45-47.
- Malik, M. P. Yuldashev, A. Obid, **T Ismoil**, L. Ya. Ping “Flavonoids of Aerial part of lycopus lucidus” *Chemistry of natural compounds*, **2002**, 6, 612-613.
- Haishaer Turebieke, **Tayirjan T. Isimjan**, “Chromatographic behaviors of fat soluble vitamins is reversed phase liquid chromatography with water-isopropanol mobile phase” *Chinese journal of Spectroscopy and Spectrology*, **2002**, 22(4), 95-97.
- Haishaer Turebieke, **Tayirjan T. Isimjan** “Separation of four kinds of water-soluble vitamins using ion-pair reagent by HPLC” *Chinese journal of analytical chemistry*, **2002**, 30(7), 56-58.
- Haishaer Turebieke, **Tayirjan T. Isimjan** “Determination of the pigments in siyadan oil” *Xinjiang Journal of Traditional Chinese Medicine*, **2001**, 4, 32-34.
- Jiang, Yuan yun cheng, **Tayirjan T. Isimjan** “Microwave induced tranfer hydrodehalogenation of haloaromatics over raney- neckel-palladium on carbon” *Dalian University of Technology Press* **1995**, 493-496.

Manuscripts submitted for publications

- **Tayirjan T. Isimjan**, D.-Q Yang, Sohrab Rohani*, Ajay K. Ray “A new approach of tailoring wetting properties of TiO₂ nanotubular surface” submitted to *Material and Engineering Science B*.
 - **Tayirjan T. Isimjan**, Sohrab Rohani*, Ajay K. Ray “Fabrication of TiO₂ nanotubes using Ti as cathode” submitted to *International Journal of Hydrogen Energy*.(under revision)
-

Manuscripts for publications

- **Tayirjan T. Isimjan**, Tao Ye, Sohrab Rohan, Ajay K. Ray “Anti-corrosion and Superhydrophobic Stainless steel”.
-

Dissertation

- Ph.D thesis title: Fabrication, modification and application of sunlight responsive TiO₂ nanotubes with Dr. Rohani Sohrab and Dr. Ajay Ray, UWO, Canada.
- M.Sc thesis title: Synthesis of analogues of pramanicin for bioactivity analysis with Dr. Dr. Paul Harrison, McMaster University, Canada.
- M.Sc thesis title: Purification and characterization of flavonoids from local plant *Lycopus Lucidus*. With Dr. Ling Hua Cao, Xinjiang University, China.

Non-referred publications

- P. H. M. Harrison, **T. Simayi** and J. Ferras, Ozgur Kutuk, Gozde Senel, Canan Karakaya and Huveyda Basaga “Biological Activity of Pramanicin, and Structure-Activity Relationships” Canadian Society for Chemistry Conference. May 2006, Halifax, NS, Canada
- **Tayirjan T. Isimjan**, Ahmed El Ruby, Sohrab Rohani*, Ajay K. Ray* “Fabrication of highly-ordered and visible-light responsive Fe-C-N-codoped TiO₂ nanotubes” Particle Technology Research Centre Conference of The University of Western Ontario, July, 2009, London, Ontario, Canada
- **Tayirjan T. Isimjan**, Sohrab Rohani, Ajay K. Ray* “Fabrication of highly-ordered and visible-light responsive Fe-C-N-codoped TiO₂ nanotubes” Particle Technology Research Centre Conference of The University of Western Ontario, Aug , 2010, London, Ontario, Canada